Synthesis, Properties, and Biology of Advanced H_2S-Releasing Materials

Jeffrey C. Foster

Dissertation submitted to the faculty of the Virginia Polytechnic Institute and State University in partial fulfillment of the requirements for the degree of

Doctor of Philosophy

In

Chemistry

John B. Matson, Committee Chair

Tijana Z. Grove

Louis A. Madsen

Kevin J. Edgar

March 22, 2017

Blacksburg, VA

Keywords: hydrogen sulfide (H_2S), RAFT polymerization, polymer micelles, chemotherapeutic, bottlebrush polymers

Synthesis, Properties, and Biology of Advanced H_2S-Releasing Materials

Jeffrey C. Foster

ABSTRACT

Hydrogen sulfide (H_2S) is an endogenously produced signaling gas involved in numerous cellular functions. At the appropriate concentration, exogenous administration of this gasotransmitter regulates vasodilation, promotes angiogenesis of endothelial cells, and generally exhibits beneficial effects as an anti-inflammatory and antioperoxidative agent. H_2S is also capable of acting as a gaseous chemotherapeutic agent. Therefore, the therapeutic potential of exogenous delivery of H_2S is vast.

The delivery of H_2S is complicated by its gaseous nature. Under physiologically relevant conditions, H_2S is rapidly depleted from solution by oxidation and/or degassing. Therefore, direct exogenous delivery is difficult. To date, most studies have employed Na_2S as a convenient H_2S source. However, the rapid surge in H_2S concentration upon Na_2S dissolution followed by its rapid decline poorly mimics the sustained production of low concentrations of H_2S that occurs in biological systems.

We synthesized a library of *S*-aroylthiooximes (SATOs)—H_2S-releasing compounds that more aptly mimic in vivo H_2S concentrations. SATOs are synthesized via reaction of a *S*-aroylthiohydroxylamine and an aldehyde or ketone. SATOs release H_2S in response to a thiol functionality. H_2S release from SATOs could be controlled, with H_2S release half-lives on the order of minutes to hours.

SATO chemistry was utilized to prepare H_2S-releasing polymers. Copolymers prepared using RAFT polymerization could be functionalized with SATOs with conversions > 99%, and these

polymers released H_2S on a similar timescale to our small molecule donors, confirming the viability of SATO formation as a post-polymerization modification strategy.

SATO-functionalized polymer amphiphiles were prepared that self-assembled into micelles or vesicles based on their composition. H_2S was released from these polymer assemblies more slowly than from the small molecules and statistical polymers. These H_2S-releasing micelles were employed in in vitro cytotoxicity studies. H_2S released from the micelles was found to be selectively toxic to human colon cancer cells compared with healthy fibroblasts. These polymeric micelle donors outperformed existing H_2S donors in terms of their toxicity towards cancer cells. The observed enhanced toxicity was suspected to arise from the slow and sustained release of H_2S from the micelles.

Synthesis, Properties, and Biology of Advanced H_2S-Releasing Materials

Jeffrey C. Foster

GENERAL AUDIENCE ABSTRACT

Hydrogen sulfide (H_2S) is biologically relevant gas involved in numerous cellular functions. At the appropriate concentration, administration of this gasotransmitter exhibits potentially beneficial effects in multiple biological systems. H_2S is also capable of acting as a gaseous chemotherapeutic agent. Therefore, the therapeutic potential of H_2S is vast.

The delivery of H_2S is complicated by its gaseous nature. Under physiologically relevant conditions, H_2S is rapidly depleted from solution by oxidation and/or degassing. Therefore, direct external delivery is difficult. To date, most studies have employed used sulfide salds as a convenient H_2S source. However, these poorly mimic the production of low concentrations of H_2S that occurs in biological systems.

We synthesized a library of *S*-aroylthiooximes (SATOs)—H_2S-releasing molecules that more aptly mimic H_2S concentrations in the body. SATOs can be triggered to release H_2S by biologically relevant compounds. H_2S release from SATOs could be controlled over minutes to hours.

SATO chemistry was utilized to prepare H_2S-releasing polymers. Copolymers were prepared using and functionalized with SATOs, and these polymers released H_2S on a similar timescale to our small molecule donors.

SATO-functionalized nanoparticles were also prepared. H_2S was released from these nanoparticles assemblies more slowly than from the small molecules and polymers. H_2S released from the micelles was found to be selectively toxic to human colon cancer cells compared with healthy

cells. These nanoparticle donors outperformed existing H_2S donors in terms of their toxicity towards cancer cells. The observed enhanced toxicity was suspected to arise from the slow and sustained release of H_2S from the nanoparticles.

Acknowledgements

First I would like to thank my advisor Dr. John B. Matson for his patience (it must have taken a lot) guidance, and hands-off approach to leadership. I feel very fortunate to been given freedom to explore interesting subjects within the fields of H_2S delivery and bottlebrush polymer synthesis. I would also like to thank my committee members (and alternate committee members) Dr. Tijana Grove, Dr. S. Richard Turner, Dr. Louis Madsen, and Dr. Kevin Edgar.

Thanks are also in order to Chris Winkler, Steve McCartney, Ken Knott, Geno Iannaccone, Dr. N. Murthy (all of whom were instrumental), Dr. Richard Gandour, Dr. Johan Foster, Dr. Webster Santos, Dr. Gordon Yee, and Dr. Paul Deck for a variety of reasons, all of them positive.

I thank my frequent collaborator and friend Scott Radzinski for his advice, support, and good humor throughout the 5 years of my tenure at Virginia Tech. Also, Jen, Chad, Kyle, Ming, Yun, Kuljeet, Jeff 2, Mohammed, Ryan (a.k.a. Richard), Kearsley, and all of the talented undergrads I worked with over the years.

Finally, I would like to thank my family for supporting me through my graduate career. This journey began with me asking my wife to move across the country with me (from beautiful the central California coast) and we're somehow still together, even after 5 years of life lived 2 h away from the closest Trader Joe's. And despite my best efforts to avoid the field of chemistry (my first chemistry course wasn't until my sophomore year of undergrad), I am now blissfully heading towards a career as a chemistry Professor.

Table of Contents

Attribution

Several colleagues and coworkers aided in the writing and research behind several of the chapters of this dissertation. They are listed below, along with their affiliations. In addition, a brief description of their background and their contributions are included here.

Contributors:

Dr. Jeffrey Foster (Ph.D., Department of Chemistry and Macromolecules Innovation Institute, Virginia Tech)

Dr. John Matson (Ph.D., Department of Chemistry and Macromolecules Innovation Institute, Virginia Tech)

Dr. Scott Radzinski (Ph.D. Department of Chemistry and Macromolecules Innovation Institute, Virginia Tech)

Chadwick Powell (graduate student, Department of Chemistry and Macromolecules Innovation Institute, Virginia Tech)

Xianlin Zou (graduate student, Department of Biological sciences, Virginia Tech)

Dr. Carla Finkielstein (Ph.D., Department of Biological sciences, Virginia Tech)

Chapter 3: Jeff Foster provided the primary writing for this chapter as well as the majority of the SATO synthesis and characterization and obtained the majority of the data. Chad Powell and Scott Radzinski contributed some of the data in the manuscript, including H_2S release kinetics. John Matson is the advisor and committee chair. Professor Matson provided guidance, hydrolysis data, writing, and editing of this chapter.

Chapter 4: Jeff Foster synthesized the polymers, conducted the solution analysis, and provided the primary writing for this chapter. John Matson provided guidance, hydrolysis data, writing, and editing of this chapter.

Chapter 5: Jeff Foster conducted small molecule synthesis, solution characterization of the polymer micelles, H_2S release experiments, and provided the primary writing for this chapter. Scott Radzinski synthesized the polymers analyzed in this chapter. Xianlin Zou and Carla Finkielstein conducted the in vitro cell assays in this manuscript. John Matson provided guidance, writing, and editing of this chapter.

Chapter 6: Jeff Foster provided the primary writing for this chapter. Scott Radzinski contributed to the writing of this chapter. John Matson provided guidance, writing, and editing of this chapter.

Chapter 7: Scott Radzinski synthesized and characterized some of the polymers analyzed in this chapter, conducted kinetic experiments, and contributed to the writing of this chapter. Jeff Foster had a similar role in this chapter. John Matson provided guidance, writing, and editing of this chapter.

Chapter 8: Jeff Foster synthesized and characterized some of the polymers analyzed in this chapter, conducted kinetic experiments, and contributed to the writing of this chapter. Scott

Radzinski had a similar role in this chapter. John Matson provided guidance, writing, and editing of this chapter.

Chapter 9: Scott Radzinski synthesized and characterized some of the polymers analyzed in this chapter, conducted kinetic experiments, and contributed to the writing of this chapter. Jeff Foster had a similar role in this chapter. John Matson provided guidance, writing, and editing of this chapter.

Chapter 1. Introduction to Dissertation

Hydrogen sulfide (H_2S) is one of three currently identified gaseous signaling molecules known as gasotransmitters. Gasotransmitters, which also include nitric oxide (NO) and carbon monoxide (CO), are interesting to study due to their extensive involvement in cellular signaling. H_2S has been shown to regulate vasodilation, promote angiogenesis, and generally exhibit beneficial effects as an anti-inflammatory agent. The biological activities of all three gasotransmitters are reviewed in more detail in Chapter 2. New chemical tools have been developed over the past ~5 years to support biological studies of H_2S. For example, H_2S sensors have been developed which report on H_2S concentrations in vivo and in vitro, and compounds have been prepared that can be triggered to release H_2S (H_2S donors) in response to various stimuli.

The short in vivo half-life of H_2S makes delivering the gas a difficult challenge. The vast majority of H_2S biological studies have been conducted using sulfide salts (Na_2S and NaSH). These inorganic sulfide sources generate H_2S instantaneously upon dissolution, resulting in a rapid surge in H_2S concentration followed by a rapid decline. These sulfide salts are convenient; however, their rapid release poorly mimics the in vivo biosynthesis of H_2S. Therefore, challenges in H_2S biology may be resolved by developing advanced delivery vehicles that produce well-defined quantities of H_2S over controllable timescales.

The field of H_2S biology has expanded immensely over the past few years, with multiple reports of small molecule H_2S donors that more aptly mimic the sustained endogenous production of the gas in vivo. Our foray into the field of small molecule H_2S donors is covered in Chapter 3. Despite this progress, many small molecule H_2S donors suffer from limitations such as ill-defined release mechanisms, poor water solubility, and inherent (or latent) toxicity. These small molecule donors

are not capable of targeting specific tissues, making targeted delivery nearly impossible. Therefore, a more advanced solution is required to meet the growing demands in the field of H_2S biology.

To address these challenges, a handful of polymers that release H_2S have been reported that address some shortcomings of small molecule H_2S donors. We prepared H_2S releasing homo- and statistical copolymers and these vehicles are discussed in detail in Chapter 4. However, these polymeric delivery vehicles also have limitations—linear polymers are typically too small to avoid rapid renal clearance in the bloodstream and have limited capacity for targeting a specific site in the body. In contrast, block copolymer amphiphiles self-assembled into micelles are an ideal solution due to the fact that they are typically of ideal size (20-100 nm) for long bloodstream circulation and can target specific sites in the body (e.g., a solid tumor) through either passive or active mechanisms. Polymer micelles that combine controlled H_2S release with the capacity for in vivo targeting and long bloodstream circulation are therefore needed to advance the field of H_2S biology and to develop novel therapeutics. To meet these challenges, we prepared H_2S releasing micelles, and this work is discussed in Chapter 5.

Through our efforts to develop polymer micelles that deliver H_2S, we discovered a marked dependence of the release kinetics of H_2S on the topology of the polymer utilized (i.e., statistical linear copolymer vs block copolymer vs polymer assembly). We wondered if more complex topologies such as star or bottlebrush polymers could further enhance H_2S release profiles. Therefore, we were interested in developing H_2S-releasing bottlebrush polymers that might have specific advantages over linear polymer and block copolymer assemblies.

Bottlebrush polymers can be prepared via one of four approaches: (1) the grafting-from strategy, whereby polymer side chains are grown from a polymeric backbone decorated with initiating

functionalities; (2) the grafting-to methodology involving the attachment of pre-formed polymers to reactive sites on a polymer backbone; (3) the grafting-through or macromonomer (MM) approach, in which polymers fitted with a polymerizable moiety are utilized as MMs in an subsequent polymerization; and, (4) the transfer-to strategy. The transfer-to method is a hybrid of the grafting-from and grafting-to strategies that is specific to reversible addition-fragmentation chain transfer (RAFT) polymerization. Like grafting-from, transfer-to involves the use of a polymeric chain transfer agent (CTA). During transfer-to, polymeric radicals detach from the bottlebrush backbone, propagate freely in solution, and return to the backbone through a chain-transfer reaction with a pendant CTA. Mechanistic details of the transfer-to strategy are reviewed in Chapter 6.

To conduct bottlebrush polymer synthesis via RAFT-transfer-to, the CTA must be attached to the polymer backbone through the Z-group. Therefore, RAFT transfer-to polymerization requires the use of Z-functional CTAs. To date, few strategies have been developed to prepare RAFT CTAs with functional Z-groups. We prepared CTAs with norbornene imide and amine Z-groups that could be directly polymerized by ring-opening metathesis polymerization (ROMP) to produce poly(CTAs). These CTAs could be utilized to prepare bottlebrush polymers by both the RAFT transfer-to and ROMP grafting through strategies. This work is summarized in Chapters 7 and 8.

Due to the nature of the polymerization mechanism, wherein polymer radicals propagate in solution, “dead” linear polymer can arise from termination reactions between detached polymer radicals. Under optimized conditions, these “dead” polymer impurities can be minimized. A study on the factors affecting the quality of bottlebrush polymer synthesis by RAFT transfer-to is presented in Chapter 9.

Transfer-to overcomes some of the disadvantages inherent in grafting-from such as bottlebrush coupling, which leads to the formation of high molecular weight impurities, and intramolecular coupling between side-chain polymers, forming imperfections in the bottlebrush polymer structure (loops). These imperfections and impurities could alter the biological activity of the bottlebrush polymers. Therefore, we feel that transfer-to is the ideal approach to synthesize H_2S-releasing bottlebrush polymers.

Chapter 2: Preparation of Gasotransmitter Releasing Materials for Therapeutic Applications

2.1. Introduction

Cellular signaling is a vital component of a complex communication system that governs cell activities and cellular coordination. Information is transmitted between cells via signaling molecules released into the extracellular space (paracrine or endocrine signaling), or via direct contact between cellular protrusions (juxtacrine signaling). Signaling molecules are generally subdivided into classes based on the system in which they principally act—hormones in the endocrine system, neurotransmitters in the nervous systems, cytokines in the immune system—or according to their chemical nature—lipids, phospholipids, amino acids, proteins, or gasses. The participation of gasses in intracellular communication is a relatively new idea,[1] and has overturned conventional understanding of how signaling molecules are produced, regulated, and transported.[2] Nitric oxide (NO) was the first so-called gasotransmitter identified,[3,4] its discovery garnering a Nobel Prize for Ignarro, Furchgott, and Murad. Since then, carbon monoxide (CO) and hydrogen sulfide (H_2S) have also been found to have physiological relevance. Due to their involvement in a number of signaling pathways, the therapeutic potential of these gaseous signaling molecules is vast. While all gasotransmitters have unique and important physiological activities, NO has been most extensively studied. Herein, the current understanding and applications of NO as a therapeutic agent will be reviewed, and parallels will be drawn to the other gasotransmitters, specifically H_2S, to substantiate them as molecules worthy of further study.

2.2. Nitric Oxide

NO is a gaseous radical present in the atmosphere as a natural product of electrical discharges of lightning and as a byproduct of combustion. In biological systems, NO is produced endogenously and functions as a signaling molecule.

2.2.1. Endogenous Production

NO is produced endogenously from l-arginine via the enzymatic action of nitric oxide synthases (NOS)s. In mammals, this process is mediated by the calcium/calmodulin controlled isoenzymes endothelial NOS and neuronal NOS.[2,5,6] A third inducible isoform of NOS (iNOS) produces NO as an immune defense mechanism.[6] The catalytic production of NO proceeds as a sequence of two monooxygenation steps (Scheme 2.1). First, l-arginine is hydroxylated by O_2 and NADPH to form *N*-ω-hydroxy-l-arginine in a mechanism similar to the action of amino acid hydrolases.[2,5,6] In the second step, *N*-ω-hyroxy-l-arginine is oxidized to give l-citrulline, H_2O, and NO.[2,5,6]

Scheme 2.1. Synthesis of NO by NOS.

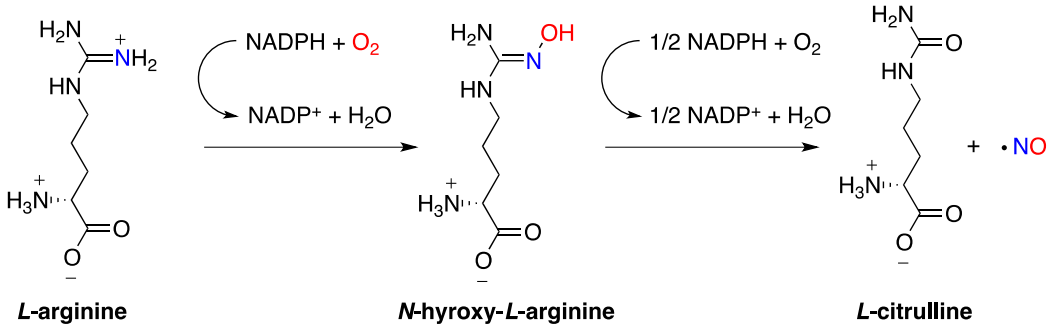

2.2.2. Physiology

Unlike other signaling molecules, gasotransmitters are relatively short lived, with a half-lives in the timescale of seconds under physiological conditions.[5] Typical intracellular signaling

compounds are synthesized and stored in vesicular structures for later extracellular release.[2] In contrast, NO must be synthesized as needed. As such, the generation/release of NO is not regulated by exocytosis but rather via the modulation of its biosynthetic enzymes.[2]

A second fundamental difference between gaseous and traditional signaling compounds is the mechanism of action. NO does not bind to plasma membrane receptors to amplify cellular signaling cascades. Rather, because of its size, NO can diffuse through the cell membrane and chemically modify molecular targets as in the S-nitrosylation of the NMDA-type glutamate receptor in the brain.[7] Given its radical nature, NO can be inactivated by reaction with biological substrates such as glutathione.[2,5] The inherent reactivity of NO has led to disfavor of the idea of a random diffusion mechanism. Instead, various NO shuttles have been identified such as the scaffold protein carboxy-terminal PDZ ligand of neuronal NO synthase protein that deliver NO to its target.[8] Additionally, NO's biosynthetic enzymes have been found to bind directly to protein targets.[9]

The primary mechanism of action of NO involves the binding and subsequent activation of soluble guanylyl cyclase, resulting in the up-regulation of cyclic guanosine monophosphate (cGMP)—a secondary messenger for NO. The NO signaling cascade typically progresses via the cGMP-mediated activation of protein kinase G; however, cGMP can also be converted to its precursor guanosine triphosphate and effectively block further production of NO (Figure 2.1).[10]

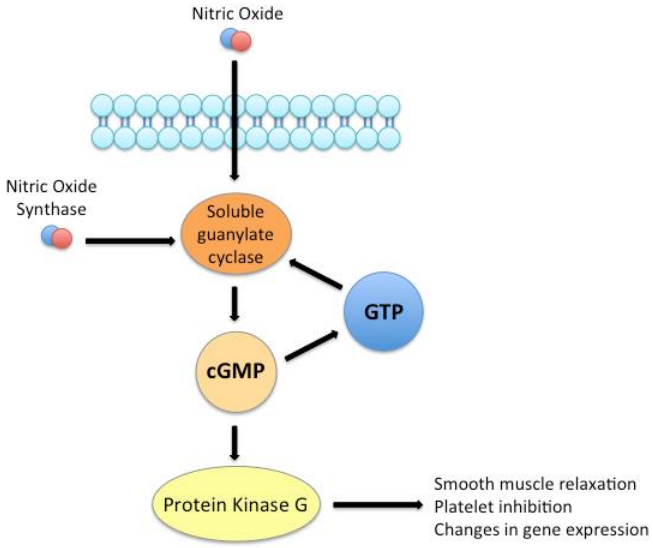

Figure 2.1. Generalized NO signaling pathway.

2.2.3. Importance of [NO]

The effect of concentration on the action of NO is dramatic. For example, at picomolar and nanomolar concentrations, NO has been shown to have protective and/or therapeutic (i.e. anti-apoptotic) effects, whereas concentrations of NO ≥ 400 nM can result in apoptosis and full cell cycle arrest.[11] This concept can be represented graphically for a number of systems as a bell-shaped dose response curve (Figure 2.2).[12,13]

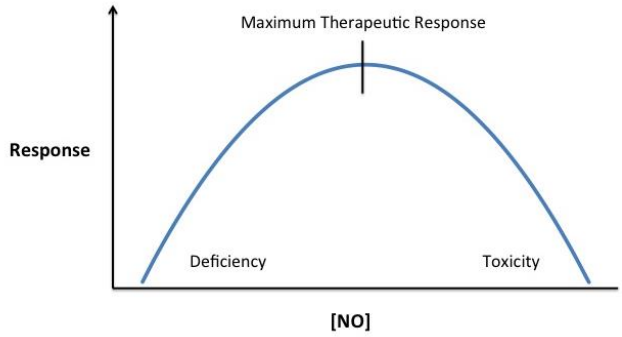

Figure 2.2. Generalized bell-shaped dose response curve for NO.

As we shall see, the ability to control the release profile of exogenous NO donors is critical to the preparation of NO-releasing materials for therapeutic applications.

2.2.4. Therapeutic Applications of NO

The involvement of NO in a vast array of intracellular signaling pathways opens the door for a number of therapeutic avenues simply by affecting local concentrations of NO. For example, NO deficiency induced via inhibition of NOSs has been found to be detrimental in a number of biological systems such as the regulation of blood pressure as well as lipid and glucose homeostasis.[11] Indeed, the function of NO is ubiquitous, and inhibition of its production alters virtually all known regulatory systems. As the role of NO deficiency in a number of diseases—pulmonary hypertension,[14] chronic kidney disease,[15] inflammation-rooted problems including cancer[6,16] and dementia[17]—is elucidated, the value of NO-based therapeutics becomes increasingly obvious. Currently, two strategies are employed in therapeutic applications of NO: the creation of drugs that (1) alter the in vivo enzymatic production of NO or (2) that actively release it.[5] In vitro and in vivo studies involving active NO donors have yielded promising results in the relaxation of smooth endothelial muscle,[14,18,19] the reduction of inflammation,[20] the protection against

ischemia/reperfusion injury,[21,22] the suppression of cancerous tumor growth,[6,16,23] and the facilitation of wound healing.[24]

2.2.5. Detection of NO

The detection of NO is typically accomplished through colorimetric or electrochemical methods. Common assays are discussed below.

2.2.5.1. The Griess Assay

The Griess assay is a popular method for the determination of NO concentration due to its low cost, simplicity, and applicability to a number of systems.[25] This spectrophotometric method indirectly measures [NO] as nitrite (NO_2^-), an autooxidation product of NO and O_2.[26] As shown in Figure 2.3, NO_2^- reacts with sulfanilamide to form a diazonium salt intermediate. In a subsequent step, the diazonium salt combines with N-1-diapthylethylenediamine, yielding an azo dye (N-alpha-naphthyl-ethylenediamine).

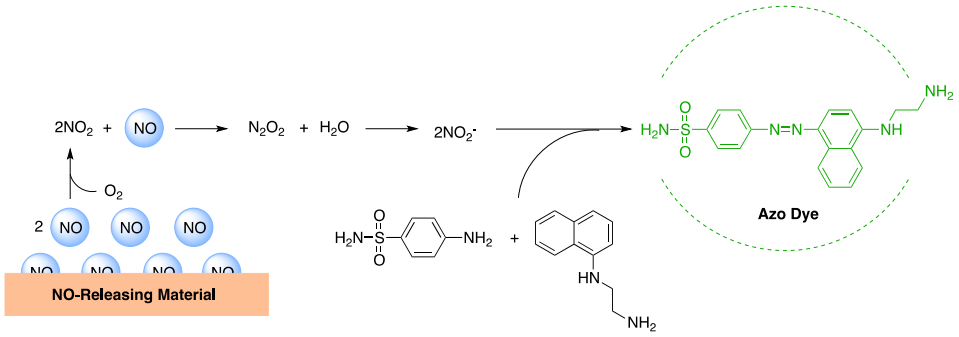

Figure 2.3. Spectrophotometric determination of [NO] via the Griess assay.

The azo dye exhibits an absorbance maximum in the visible range (λ_{max} = 540 nm) that can be followed by spectrophotometry.[25]

2.2.5.2. Chemiluminescence

While the Griess assay represents a simple, low cost method to measure [NO], chemiluminescence provides a direct measurement of this value via reaction of NO with O_3 generated in situ in the chemiluminescence instrument (Figure 2.4).[27]

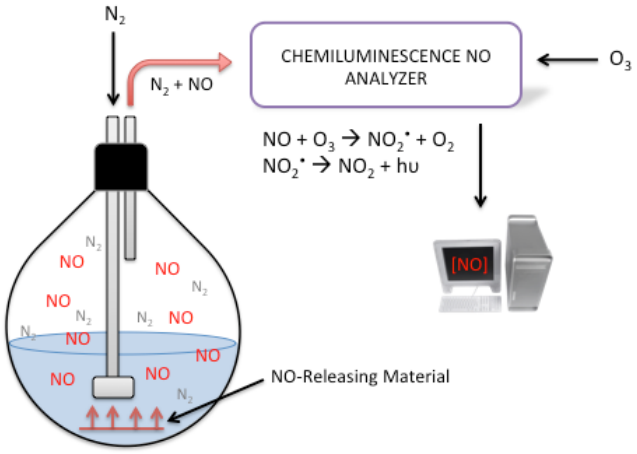

Figure 2.4. Determination of [NO] using a chemiluminescence method.

In this type of experiment, NO generated from an NO-releasing compound is carried to a reaction cell within the instrument by a continuous N_2 stream. The NO then reacts with O_3 to produce $NO_2^{\bullet}$ that subsequently decomposes to NO_2 and light. A photomultiplier tube (PMT) detects this emission (between 600-875 nm).[27]

2.2.5.3. Electrochemical Methods

The concentration of NO can be measured directly via potentiometry utilizing a NO-selective electrode. In contrast to chemiluminescence, electrochemical determination of [NO] is more cost efficient, the related technology is more easily scaled, and experiments may be conducted in situ.[28]

The electrochemical determination of [NO] typically involves either (1) a 2 electron reduction of NO to $N_2O_2^{2-}$ (Equation 2.1), or (2) a 3 electron oxidation of NO to NO_3^- (Equations 2.2.1-2.2.3).[28]

$$NO + 2e^- \rightarrow N_2O_2^{2-} \quad (2.1)$$

$$NO \rightarrow NO^+ + 2e^- \quad (2.2.1)$$

$$NO^+ + OH^- \rightarrow HNO_2 \quad (2.2.2)$$

$$HNO_2 + 2H_2O \rightarrow NO_3^- + 3H^+ + e^- \quad (2.2.3)$$

2.2.6. NO-Releasing Materials

Having established the importance of the concentration of NO on cellular function, and having enumerated a number of therapeutic applications of the gas, it is clear that compounds and/or materials that could release the gas in a targeted and controlled way are desirable. A number of NO-donating materials have been prepared, from small molecules donors to synthetic polymeric scaffolds to NO-releasing peptides, most of which inherit their NO-generating capacity from one of two moieties: S-nitrosothiols and diazeniumdiolates.

2.2.6.1. NO-Releasing Moieties

While a number of NO-releasing moieties have been reported—organic nitrates and nitrites, metal-NO complexes and nitrosamines—*S*-nitrosothiols (RSNOs) and diaziniumdiolates (NONOates) have garnered attention in the literature due to their ease of installation and their ability to generate NO spontaneously in physiological media. RSNOs are endogenous NO donors of the general structure R-S-N=O, thought to play a role in the physiological transport of NO in vivo.[29] Compounds of this type are prepared exogenously via the reaction of a thiol and a nitrosating agent (i.e. alkyl nitrile, dinitrogen trioxide, and nitrous acid from $NaNO_2$ under acidic conditions) (Scheme 2.2).[30] RSNOs are characterized by their yellow to green color and distinctive

absorbances in the visible (550-600 nm) and UV (225-261 nm) regions of the electromagnetic spectrum.[30] In contrast to NONOates, RSNOs release NO in response to multiple triggers (Scheme 2.2).[30]

Scheme 2.2. Preparation and decomposition of RSNOs.

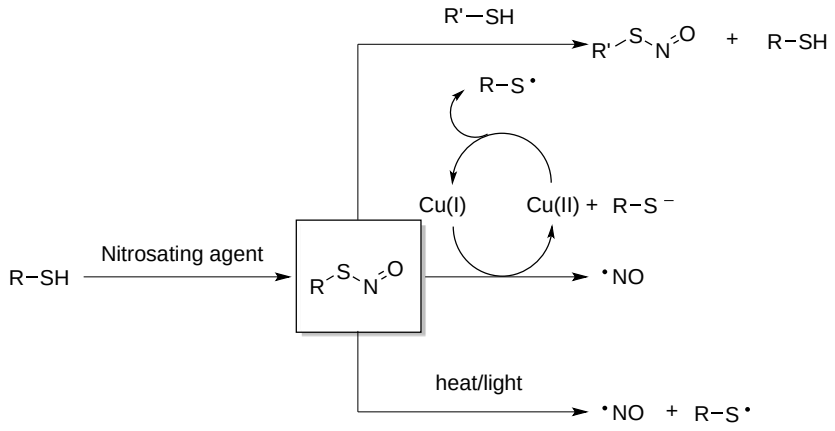

Thermal and photoinitiated mechanisms result in hemolytic cleavage of the S-N bond.[30] A thiyl radical generated in this process can react with a second RSNO to yield a second equivalent of NO.[30] Trace amounts of copper can also trigger NO release, whereby Cu(I), itself reduced from Cu(II) by free thiolate, can react to reduce the RSNO in a catalytic process.[30] Finally, the nitroso functionality can be directly transferred to another thiol via a transnitrosation process.[30]

In contrast to RSNOs, NONOates are not generated endogenously but are prepared in the lab from secondary amines and high pressure NO(g).[31] As shown in Scheme 2.3, these reactions are typically conducted in the presence of a base such as NaOMe to deprotonate the resulting N-diazeniumdiolate, as amine NONOates are unstable in the protonated form.[31] The counter ion associated with the base (i.e. Na+ in the case of NaOMe) stabilizes the product anion, thereby driving the equilibrium of the reaction toward the products.[31]

Scheme 2.3. Preparation and decomposition of NONOates from secondary amines.

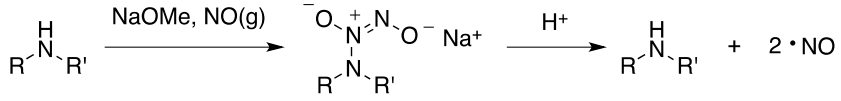

NONOates generate NO in response to changes in pH. NO release half-lives can range from as long as 20 h in the case of certain NONOates derived from polyamines to as little as 1.8 s for the N-diazeniumdiolate of proline.[31] Under physiological conditions (37°C, pH = 7.4), NONOates decompose spontaneously to regenerate the original amine plus two equivalents of NO.[31]

2.2.6.2. Direct Encapsulation of NO

Encapsulation of NO in polymeric vesicles has been reported.[32] This method has the advantage of delivering the therapeutic agent (NO) directly to the desired target in contrast to delivering a prodrug that needs to be triggered in order to generate NO and could potentially decompose to undesirable byproducts such as reactive nitrogen species. Cavalieri et al. prepared poly(vinyl alcohol) (PVA) microbubbles for NO delivery (Figure 2.5). The microbubbles were synthesized using a reaction commonly employed in carbohydrate chemistry. Head-to-head linkages that inevitably arise during the polymerization of vinyl monomers, in this case PVA, were cleaved by periodates (i.e. KIO_4) in a post polymerization modification reaction to produce a small percentage of telechelic PVA chains with aldehyde end groups. Under acidic conditions (i.e. pH < 5), these end groups were acetalated by the hydroxyl side groups of another PVA chain, effectively causing the telechilic PVA to act as a crosslinking reagent. High sheer was employed during the crosslinking reaction to entrap air. The reaction was terminated by neutralization, and the formation of microbubbles was verified by electron paramagnetic resonance spectroscopy.

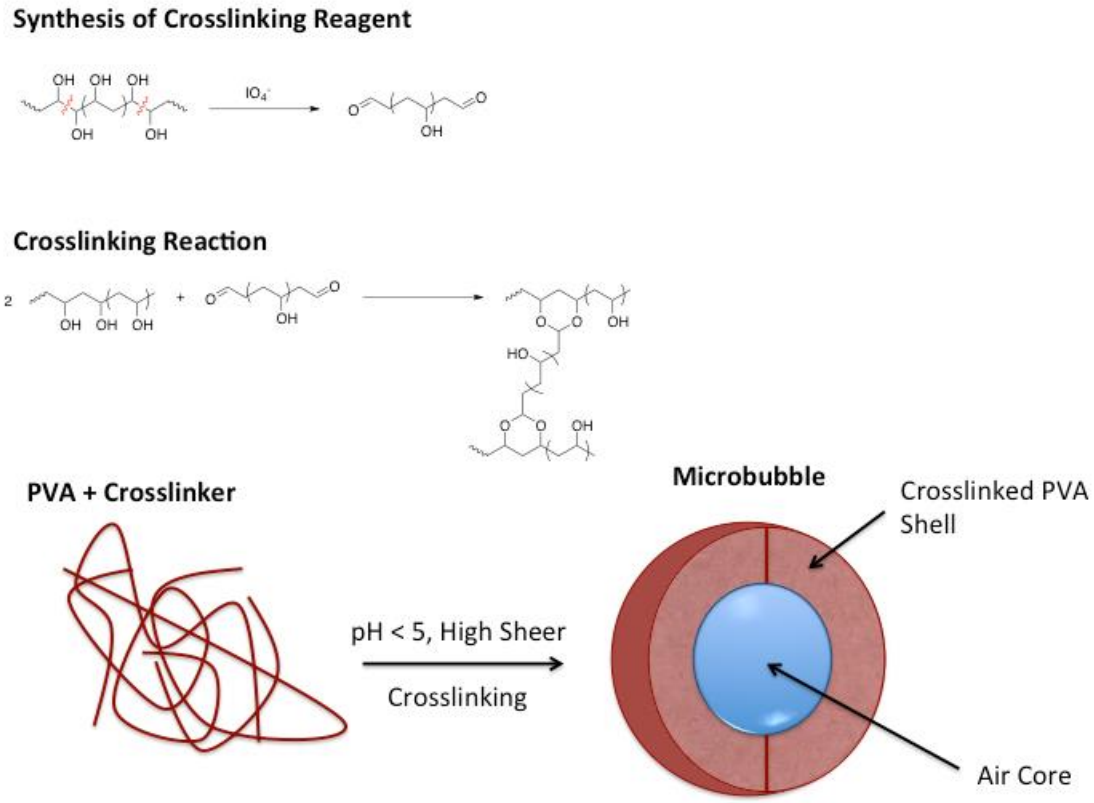

Figure 2.5. Synthesis of Cross-linked PVA microbubbles.

NO loading was accomplished via subjection of the microbubbles to NO(g) at 1.5 bar in a sealed container for 2 h. The Griess assay was employed to assess NO loading and release rate. It was found that on average, the microbubbles contained 3.6 μmol of NO per bubble. Additionally, the microbubbles were reported to release the gas over a period of 2 h.

While the direct encapsulation of NO is advantageous because of its capability to directly deliver NO to the target area and the inherent biocompatibility of both the cross-linked PVA microbubble and the reagents utilized to prepare it, this method suffers from the disadvantage of an observed NO loss to diffusion. Hypothetically, improvement of NO retention could be accomplished in a number of ways, such as increasing the crosslinking density, thereby reducing pore size, or by decreasing the polarity of the inner surface of the capsule to hinder NO diffusion.

2.2.6.3. Bio-Based NO Donors

In contrast to a number of synthetic NO delivery vehicles, bio-based alternatives have the advantage of their inherent biocompatibility. In addition, the incredible specificity of proteins makes them ideal candidates for modification to achieve targeted NO delivery. For example, Hrabie et al. reported the installation of protected NO-releasing NONOates on bovine serum albumin (BSA) and human serum albumin (HSA) via a *N*-(γ-maleimido-butyryloxy)succinimide (GMBS) linker.[33] The acid-liable nature of diaziniumdiolates can complicate the preparation of compounds suitable for coupling to protein-reactive reagents. Instead, protecting groups have been employed to generate NONOate-containing precursors stable to further reaction and long-term storage. The methoxymethyl (MOM) moiety is one such protecting group. To prepare a peptide-reactive NO donor, Hrabie first generated the diazeniumdiolate of monoprotected piperazine.[33] Reaction of this compound with chloromethyl methyl ether yielded the MOM-protected derivative. Following hydrolysis of the carbamate, a Michael-type reaction with GMBS yielded the carboxy terminated protected NO moiety.[33] In the final step, DCC coupling chemistry was employed to generate a protein-reactive *N*-hydroxysuccinimide ester.[33]

Scheme 2.4. Preparation of protein-reactive NO-generating moiety.

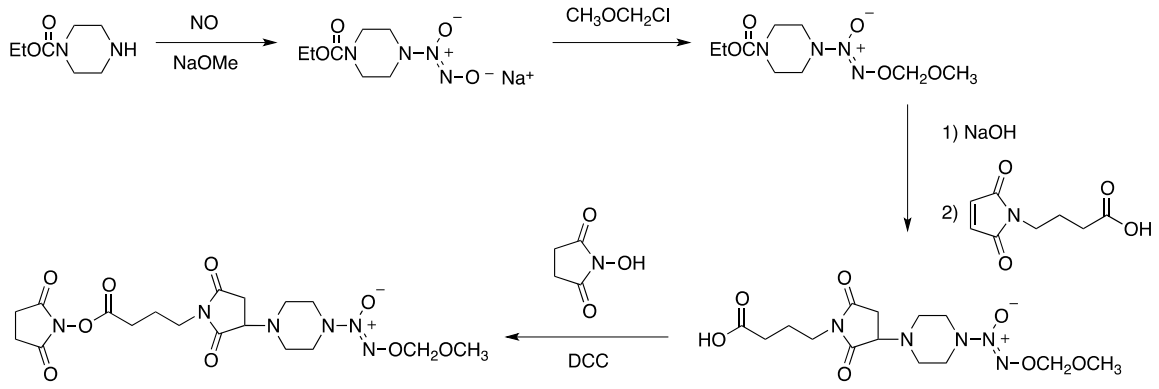

Matrix-assisted laser desorption ionization time-of-flight mass spectrometry was used to evaluate the degree of incorporation of the NO-releasing moiety into the BSA and HSA proteins.[33] Of the 59 lysine residues available for reaction, it was found that ~22 and ~19 NO groups were incorporated into BSA and HSA respectively.[33] The resulting protein-borne protected NONOates were found to hydrolyze slowly in aqueous solution at physiological temperature and pH. A release half-life on the order of 20 d was determined using the chemiluminescence method.[33]

The nitrosation of proteins has been studied extensively as a route to NO-releasing materials due in part to the ubiquity of the *S*-nitrosothiol group. Various attempts to nitrosate BSA directly have been attempted, either by reaction of the single cysteine residue with a nitrosating agent, or by reducing the 17 disulfide linkages present in BSA to expose additional thiol functionality.[34] As one could imagine, the latter approach led to disruption of protein tertiary structure and function.[34] A different approach involved the conversion of amine and alcohol functionalities present in BSA to thiol groups using *N*-acetylhomocysteine thiolactone, however protein oligomerization was observed, likely the result of intermolecular disulfide bond formation.[35] In light of this work, Katsumi et. al. modified BSA with polyethylene glycol (PEG).[36] PEGylation was accomplished using an *N*-hydroxysuccinimide-activated PEG.[36] The BSA-PEG conjugate was further modified by reaction with *N*-succinimidyl-*S*-acetylthiolate.[36] Following deacylation with hydroxylamine, the exposed thiol was nitrosated by sodium nitrate under acidic conditions.[36] PEGylation was found to increase the stability of the RSNO group via the cage effect while simultaneously reducing protein aggregation.[36] It was found that an average of ~10 mol of NO was incorporated per mol of protein, and the PEG-BSA conjugate released NO with a half-life of ~150 h.[36] Although peptides have the innate advantage of biocompatibility, their limited NO payloads ultimately lead to restricted utility.

2.2.6.4. Polymeric Organic Scaffolds

Synthetic polymers provide a scaffold for the incorporation of NO-releasing functionality into a variety of delivery vehicles. Homopolymers, block copolymers, brush polymers, and dendrimers are a few of the topologies that have been explored for the purpose of NO delivery. Precise control over the degree of NO incorporation, polymer molecular weight (MW), topology, morphology, and the kinetics of NO release can be achieved by changing one or more of a number of experimental parameters including the monomer(s) used, the polymerization mechanism, or the processing conditions of the synthesized material. Polymers can be prepared with secondary amine or thiol functionality that can be later modified to imbue NO-releasing capability (i.e. via the formation of a RSNO or NONOate).

The first tunable NO-releasing microparticles were reported by Meyerhoff et. al. in 2002.[37] Methacrylate monomers were prepared with linear aliphatic and heterocyclic secondary amine pendant groups. The amines were protected with t-butoxycarbonyl (boc) to prevent intermolecular Michael addition reactions between the amines and the vinyl groups of other monomers during polymerization (Scheme 2.5).

Scheme 2.5. Representative synthesis of secondary amine-bearing monomer (A) and polymerization and post polymerization reactions (B) to achieve NO-releasing homopolymer.

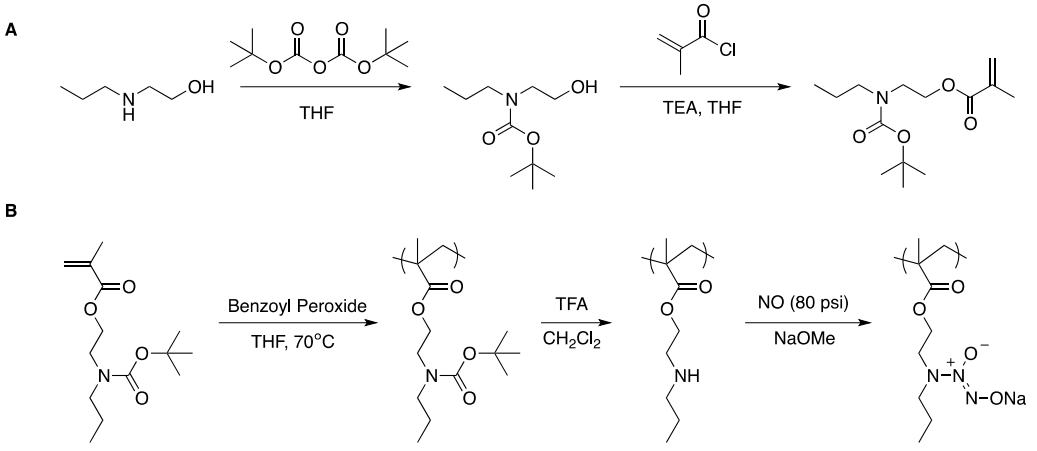

The monomers were polymerized via a benzoyl peroxide initiated radical polymerization. Following deprotection of the amines using trifluoroacetic acid (TFA), the resulting amino-functionalized polymer was exposed to high pressure NO in a 25% v/v solution of NaOMe in MeOH. The NO-releasing polymers were found to have a payload of 1.99 μmol per mg of polymer by the chemiluminescence method. The apparent $t_{1/2}$ of NO release ranged from 30 to 60 min. The secondary-amine bearing methacrylates were copolymerized with methyl methacrylate to investigate the effect of polymer composition on the maximum NO loading as well as fundamental properties such as the glass transition temperature. Copolymers with higher secondary amine content were found to have higher NO payloads but lower glass transition temperatures. Given that homopolymers of the amine-containing monomers exhibited glass transition temperatures near room temperature, this finding is in accordance with the Fox-Flory relationship. Finally, microbeads were prepared via a suspension process. Various methacrylate amines were suspended in a poly(vinyl alcohol) solution and cross-linked with the divinyl compound 1,6-hexanedioldimethacrylate. The resulting microbeads were determined to be on the order of 100-200 μm in size by scanning electron microscopy (SEM) and released NO at a rate similar to that of the linear polymers and copolymers.

Micelles are a well-studied vehicle for drug delivery.[38] Their amphiphilic nature makes them ideal for facilitating the solubilization of hydrophobic drugs. Micelles are typically prepared via the self-assembly of amphiphilic block copolymers. The morphology of the micelle can be manipulated to yield a number of interesting shapes including spheres and cylinders by tuning the hydrophobic/hydrophilic volume fraction. The micelle diameter and core/shell volume ratio can be influenced by varying the block copolymer length (molecular weight) and block ratio

respectively. Importantly, the diameter of micelles can affect their cellular uptake and accumulation.[39]

Jo et al. prepared micelles for the delivery of NO from vinyl monomers bearing pendant secondary amines. Well-defined block copolymers of poly(N-acryloyl-2,5-dimethylpiperazine) (PAZd) and poly(N-acryloylmorpholine) (PAM) were synthesized by reversible addition fragmentation chain transfer (RAFT) polymerization using a carboxyl-functionalized chain transfer agent (Scheme 2.6).

Scheme 2.6. Preparation of well-defined, amine-bearing amphiphilic copolymers.

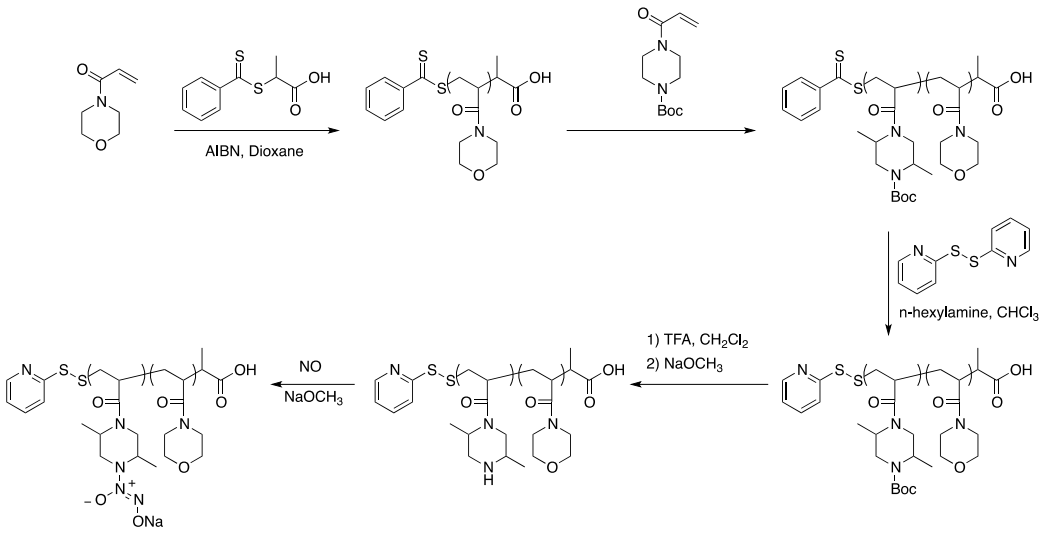

The PAM block was polymerized first and purified via precipitation. The resulting macro chain transfer agent was utilized in a subsequent step to polymerize tert-butoxycarbonyl-protected N-acryloyl-2,5-dimethylpiperazine. Aminolysis by 2,2'-dithiopyridine exchanged the dithioester with a stable pyridyl disulfide group presumably to prevent reversible thiol exchange reactions, as has been reported in other systems.[40] The copolymer was subjected to trifluoroacetic acid, resulting in deprotection to restore the secondary amine functionality of the pendant groups. The water-soluble, deprotected copolymer was reacted with NO in the presence of base, gradually converting

the amine groups to NONOates. Thermogravametric analysis demonstrated 84% conversion of amines to NONOates. As the NONOate groups are incorporated, the PAZd block becomes increasingly hydrophobic, resulting in segregation and eventually aggregation to form micelles. The average micelle diameter was determined to be 80 nm by DLS. *Ex vivo* infusion of a micellar solution into rabbit carotid arteries was accomplished without injury to the endothelium. The micelles were found to penetrate and accumulate in the arterial intima by fluorescence microscopy in accordance with the current understanding nanoparticle arterial interstitial penetration.[41] Additionally, the Griess assay showed the incorporation of NO to be on the order of 1.5 μmol per micelle.

Dendrimers are a class of hyperbranched synthetic polymers having well-defined structures and a multivalent surface.[42] Their morphology and properties are defined primarily by the chemical and structural nature of three components: (1) a central core, (2) an interior dendritic structure, and (3) an exterior, multivalent surface. The structural character of this class of molecules imparts a number of unique properties. For example, water solubility can be achieved by functionalizing the corona with hydrophilic groups—a feat that is typically difficult to achieve with linear polymers due to intermolecular chain entanglements. Dendrimers are prepared by one of two approaches. A divergent approach involves the outward growth of dendritic branches from a central core via a stepwise addition of AB_2 type monomers. The "B" functionality must be initially protected to prevent gelation and subsequently deprotected/activated following the reaction of "A" with the growing dendron. Conversely, a convergent method, developed by Hawker et al., begins at the periphery and grows inward. This process involves the reaction of terminal (T) units with an AB_2 monomer with protected "A" functionality. The "A" group is then deprotected/activated, and 2 equivalents of this AB_2-T_2 unit are coupled to an "A" protected AB_2 monomer as before.

To achieve NO delivery from a dendritic scaffold, Stasko et al. utilized G3 and G5 amine surface-functionalized poly(polypropylenimine) tetramaine dendrimers (DAB-Am-16 and DAB-Am-64 respectively) to prepare diazeniumdiolate-bearing NO delivery vehicles. The abundance of amines on the corona allowed for high NO loading relative to linear polymers of similar molecular weights. As shown in Figure 2.7, the amine-functionalized dendrimers were prepared via a divergent approach utilizing Michael-type chemistry followed by metal-mediated reduction of the nitrile group.

Figure 2.7. Divergent synthesis of (A) amine-functionalized DAB-Am-16 and (B) subsequent conversion of pendant amines to diaziniumdiolates.

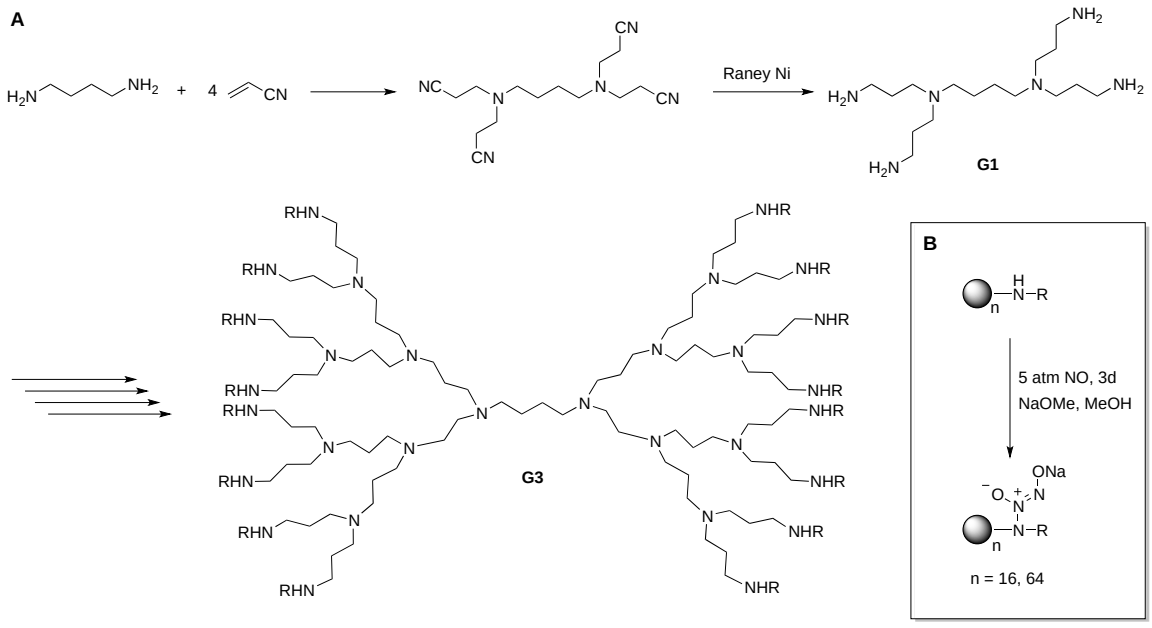

The resulting third generation dendrimer was dissolved in MeOH and exposed to high pressures of NO (5 atm) for a period of 3d. NO release from the dendrimer conjugates was evaluated by chemiluminescence. An initial burst of NO was observed following dissolution of the dendrimers in PBS, however no sustained NO generation occurred. From the data, an amine to NONOate conversion efficiency of < 1% was calculated. The conjugation reaction was repeated under basic conditions, and the conversion improved (~3% incorporation). It is known that NONOates derived

from secondary amines exhibit improved stability relative to those of primary amines. Therefore, to improve conversion, and to enhance the NO release profile of the denrimer conjugates, the pendant primary amines of DAB-Am-16 were transformed to secondary amines via a two-step process. First, reaction of the aforementioned amines with heptenoyl chloride resulted in the formation of an amide that was later reduced to the corresponding secondary amine (DAB-C7-16) with $LiAlH_4$. Chemiluminescene measurements showed conversions on the order of 35%—a drastic improvement over those obtained for the primary amine conjugates. Additionally, while NO release from the DAB-Am-16/NO occurred instantaneously, DAB-C7-16 released the gas slowly over a period of >16 h. It was theorized that an increase in local pH (i.e. lower proton concentration), occurring as a result of the regeneration of secondary amines following NO release, led to slower decomposition of remaining the NONOate groups. The NO payload of the functionalized dendrimers outclassed the materials previously discussed while maintaining a slow and sustained NO release profile. Higher generation dendrimers were produced bearing tandem hydroxyl and secondary amine coronal functionality to achieve water solubility.

2.3. CO-Releasing Materials

Similar to NO, CO is known to act in a number of signaling pathways. Produced endogenously and systemically, this gas transmitter has a number of protective roles in tissues including anti-inflammatory, anti-apoptotic, and anti-proliferative functions.[43] CO also inhibits the formation of reactive oxygen species.[43] Despite the therapeutic potential of CO, which is analogous to that of NO given the broad scope of its physiological activity, few CO-delivering materials have been reported in the literature. Hasegawa et al. developed CO-releasing micelles for targeted CO delivery.[44] The block copolymers prepared bore pendant glycine motifs in the hydrophobic block that could coordinate a CO-releasing Run complex via ligand substitution to form

poly(Run$(CO)_3$Cl(ornithinecrylamide)).[44] The block copolymers were found to self-assemble into micelles of 30-40 nm in diameter. Thiol compounds such as cysteine successfully induced CO release from the micelles.

Inspired by this work, Matson et al. prepared peptide amphiphiles (PA)s bearing CO-releasing moieties that self-assembled to form nanofibers.[45] The self-assembly process was driven by β-sheet formation between components of the individual peptides, and via hydrophobic-hydrophilic interactions arising from their amphiphilic structure.[46] The PAs were prepared under standard solid phase peptide synthesis conditions. The peptide sequence was designed to contain a β-asp residue at the c-terminus with a NH2CHRCOOH unit resembling the glycine component of Ru$(CO)_3$Cl(glycinate). The CO-releasing motif was installed via reaction of the PA with $[Ru(CO)_3Cl_2]_2$ in the presence of NaOMe. A maximum conversion of 75% was observed by LCMS.[45] The low conversion was attributed to the poor solubility of the PA in MeOH.[45] Purification of the CO-bearing PA was hindered by decomposition. TEM and SAXS were employed to characterize the self-assembly of the PAs into nanofibers, which were found to have an average diameter of 8.2 nm.[45] The kinetics of CO release was quantified using a colorimetric method. The half-life of CO release was found to be 2.16 ± 0.05 min.[45] The nanofibers formed robust, physically cross-linked gels upon dissolution in water (~1 wt% PA) and exposure to $CaCl_2$.[45] Charge screening was responsible for the observed gelation.[46] Moreover, the addition of Ca mediates the formation of ion bridges between carboxylic acid groups of the glutamic acid residues.[46] CO release from the PA gel was slow relative to the un-cross-linked fibers, with a half-life of 17.8 ± 1.4 min.[45]

2.4. Hydrogen Sulfide Releasing Materials

CO and H_2S have similar therapeutic potential to NO, owing to their participation in a number of signaling pathways in vivo. However, despite the wealth of literature that exists for NO—from the exploration of NO biology, to the preparation of small molecule prodrugs that decompose to release the gas, to materials designed for the targeted and controlled release of NO—the proportion of publications dedicated to the study of CO and H_2S is relatively small. To date, only a handful of H_2S-releasing materials have been reported. As such, an opportunity exists for the creation of such materials, and doing so could facilitate the expansion of our understanding of the biology of H_2S.

2.4.1. H_2S Physiology and Donor Compounds

The expanding field of hydrogen sulfide (H_2S)-related research has created a demand for H_2S releasing compounds capable of mimicking the slow and sustained production of H_2S in vivo. Indeed, the capability to readily incorporate H_2S-releasing moieties into a variety of substrates could catalyze the expansion of a growing library of H_2S donor compounds. To date, only a handful of such compounds exist. However, these donors either release H_2S too rapidly to mimic biological H_2S generation, or their preparation requires conditions that may not be orthogonal with existing functionality (i.e. strong base in one step and strong acid in the next). In view of these limitations, a donor with a generalized structure amenable to derivitization such that its rate of H_2S release and ease of installation are controllable by the researcher is desirable. In other words, we aspired to create an H_2S-releasing counterpart to the NONOate.

Recently, H_2S been recognized as the third gasotransmitter, along with nitric oxide (NO) and carbon monoxide (CO).[47] Within the last decade, a number of physiological and pathological functions have been proposed in the literature.[48] Like NO, endogenously produced H_2S has been

found to exhibit protective effects in a number of pathologies. For example, H_2S is known to relax smooth muscle,[49] suppress oxidative stress,[50] and protect the liver in ischemia-reperfusion events.[51] In addition, reaction of H_2S with S-nitrosothiols gives thionitrious acid (HSNO), the metabolic products of which (NO^+, $NO^\bullet$, NO^-) have proven to be physiologically relevant.[52] Similar to the other gaseous mediators, H_2S is produced endogenously through a number of pathways, primarily via the pyridoxal-5' phosphate-dependent conversion of L-cysteine by cystathionine β-synthase and cystathionine γ-lyase.[48,53]

Sulfide salts, such as sodium sulfide (Na_2S) and sodium hydrosulfide (NaSH) are typically employed to study the physiological and pathological roles of H_2S in a variety of cells, tissues, and animals. However, these donors suffer the disadvantage of rapid and uncontrolled H_2S release. Upon addition of water, Na_2S and NaSH react to generate their maximum output of H_2S within seconds. Given the importance of the relationship between H_2S concentration and in vivo function, this surge to supraphysiological levels is an imperfect analog to the steady endogenous production of the gas in biological systems. Moreover, NaSH can be oxidized in the presence of O_2. Therefore, fluctuations in the time between when the solution has been prepared and when the H_2S concentration is measured can have a drastic effect on the result.

Natural H_2S donors have been reported. Organic polysulfides such as diallyl trisulfide (DATS), a compound found in garlic, produce H_2S via the glutathione-mediated cleavage of S-S bonds.[54] For these compounds, H_2S generation is enhanced by allyl substituents and increasing polysulfide chain length.[54] In vivo studies involving DATS have been conducted. DATS induces vasodilation of rat aortas and can protect rat ischemic myocardium.[54,55] The need for allyl functionality, however, severely limits the potential applications of this donor type.

To facilitate the study of the biological roles of gaseous mediators in the research setting, a number of NO donor compounds have been devised. By contrast, the library of synthetic H_2S donors is presently limited. GYY4137, a Lawesson's reagent derivative, is one such synthetic donor. H_2S release from GYY4137 proceeds via hydrolysis, but occurs very slowly (<10% release after 7 days).[56] This slow release has been employed in the concentration dependent killing of several cancer cell lines. Increased activity relative to NaSH was observed, attributed to the capability of GYY4137 to release H_2S at a slow, sustained rate.[56]

The dithiothione moiety has drawn interest in the literature, and has been used to prepare H_2S-releasing drug hybrids such as S-diclofenac.[57-60] The mechanism of H_2S release of this class of compounds is not well understood, and the molecules themselves may have biological activities that are not related to the action of H_2S.[61]

Recently, Xian and coworkers reported the preparation of cysteine and glutathione triggered N-(Benzothiol)benzamide and perthiol H_2S donors that exhibit controlled, structure-dependent H_2S release kinetics.[61,62] These donor compounds are stable in aqueous solution, and are selective against other cellular nucleophiles such as those possessing OH and NH_2 groups. The release of H_2S is predicated on the instability of the N-S bond. These types of compounds are derived from reaction of benzoic anhydride with S-benzoylthiohydroxylamines (THA), which are formed via amination of thiobenzoic acid and its derivatives with hydroxylamine-O-sulfonic acid under basic conditions.

2.5. Next-Generation H_2S Donors

While the *N*-(benzoylthio)benzamides succeed in mimicking the slow and sustained release of H_2S in vivo, their structural character makes further derivatization difficult, requiring orthagonality with highly reactive functionalities such as anhydrides or acid chlorides to install the *N*-benzoyl

group. We propose the preparation of a novel synthetic strategy for accessing a variety of H_2S-releasing compounds via a thiooxime click reaction analogous to oxime chemistry. These thiooxime H_2S donors can be prepared in one step under mild conditions from THA and commercially available aldehydes and ketones, and could serve as robust and efficient method to couple H_2S releasing moieties to a plethora of substrates.

Given the structural similarity of the thiohydroxylamine group to the oxime, we envisioned the preparation of thiooximes from reaction of THAs with aldehydes and ketones. We supposed that these H_2S donors should be sufficiently stable in aqueous solution at physiological pH such that hydrolysis did not compete with H_2S release. Additionally, we envisioned that our donors would generate the gas in response to cysteine (and other thiols) similar to Xian's *N*-(benzoylthio)benzamides.

2.6. Conclusion

The diazeniumdiolate has revolutionized the field of NO research because of its ease of installation and applicability to a number of systems. A variety of delivery vehicles have been prepared to take advantage of this chemistry including liner polymers, micelles, and dendrimers to name a few. We envision that the thiooxime functional group can be exploited for the preparation of a similarly vast array of H_2S-releasing materials. The thiooxime might do for H_2S what the diazeniumdiolate has done for NO—advance our understanding of H_2S biology and enable the production of H_2S-releasing therapeutics for clinical applications.

2.6. References

(1) Gillman, M. A.; Lichtigfeld, F. J. *Journal of the Neurological Sciences* **1981**, *49*, 41.

(2) Mustafa, A. K.; Gadalla, M. M.; Snyder, S. H. *Science Signaling* **2009**, *2*, re2.

(3) Ignarro, L. J.; Buga, G. M.; Wood, K. S.; Byrns, R. E.; Chaudhuri, G. *Proc. Natl. Acad. Sci. U. S. A.* **1987**, *84*, 9265.

(4) Furchgott, R. F.; Zawadzki, J. V. *Nature* **1980**, *288*, 373.

(5) Carpenter, A. W.; Schoenfisch, M. H. *Chem. Soc. Rev.* **2012**, *41*, 3742.

(6) Lechner, M.; Lirk, P.; Rieder, J. *Seminars in Cancer Biology* **2005**, *15*, 277.

(7) Lipton, S. A.; Choi, Y.-B.; Pan, Z.-H.; Lei, S. Z.; Chen, H.-S. V.; Sucher, N. J.; Loscalzo, J.; Singel, D. J.; Stamler, J. S. *Nature* **1993**, *364*, 626.

(8) Jaffrey, S. R.; Snowman, A. M.; Eliasson, M. J.; Cohen, N. A.; Snyder, S. H. *Neuron* **1998**, *20*, 115.

(9) Aoyagi, M.; Arvai, A. S.; Tainer, J. A.; Getzoff, E. D. *EMBO J* **2003**, *22*, 1234.

(10) Denninger, J. W.; Marletta, M. A. *Biochimica et Biophysica Acta (BBA) - Bioenergetics* **1999**, *1411*, 334.

(11) Coneski, P. N.; Schoenfisch, M. H. *Chem. Soc. Rev.* **2012**, *41*, 3753.

(12) Manevich, Y.; Townsend, D. M.; Hutchens, S.; Tew, K. D. *PLoS One* **2010**, *5*, e14151.

(13) Ridnour La Fau - Thomas, D. D.; Thomas Dd Fau - Donzelli, S.; Donzelli S Fau - Espey, M. G.; Espey Mg Fau - Roberts, D. D.; Roberts Dd Fau - Wink, D. A.; Wink Da Fau - Isenberg, J. S.; Isenberg, J. S. *Antioxid. Redox Signal.*, *8*, 1329.

(14) Loscalzo, J.; Welch, G. *Progress in Cardiovascular Diseases* **1995**, *38*, 87.

(15) Baylis, C. *Am. J. Physiol.* **2008**, *294*, F1.

(16) Mocellin, S.; Bronte, V.; Nitti, D. *Medicinal Research Reviews* **2007**, *27*, 317.

(17) Steinert, J. R.; Chernova, T.; Forsythe, I. D. *The Neuroscientist* **2010**, *16*, 435.

(18) Welch, G.; Loscalzo, J. *J. Card. Surg.* **1994**, *9*, 361.

(19) Maragos, C. M.; Morley, D.; Wink, D. A.; Dunams, T. M.; Saavedra, J. E.; Hoffman, A.; Bove, A. A.; Isaac, L.; Hrabie, J. A.; Keefer, L. K. *J. Med. Chem.* **1991**, *34*, 3242.

(20) del Soldato, P.; Sorrentino, R.; Pinto, A. *Trends Pharmacol. Sci.* **1999**, *20*, 319.

(21) Katsumi, H.; Nishikawa, M.; Yasui, H.; Yamashita, F.; Hashida, M. *J. Controlled Release* **2009**, *140*, 12.

(22) Johnson, T. A.; Stasko, N. A.; Matthews, J. L.; Cascio, W. E.; Holmuhamedov, E. L.; Johnson, C. B.; Schoenfisch, M. H. *Nitric Oxide* **2009**, *22*, 30.

(23) Li, C.-Q.; Pang, B.; Kiziltepe, T.; Trudel, L. J.; Engelward, B. P.; Dedon, P. C.; Wogan, G. N. *Chem. Res. Toxicol.* **2006**, *19*, 399.

(24) Masters, K. S. B.; Leibovich, S. J.; Belem, P.; West, J. L.; Poole-Warren, L. A. *Wound Repair Regen* **2002**, *10*, 286.

(25) Tracey, W. R. *NeuroProtocols* **1992**, *1*, 125.

(26) Griess, P. *Deut. Chem. Ges. Ber.*, *12*, 426.

(27) Bates, J. N. *NeuroProtocols* **1992**, *1*, 141.

(28) Privett, B. J.; Shin, J. H.; Schoenfisch, M. H. *Chem. Soc. Rev.* **2010**, *39*, 1925.

(29) Williams, D. L. H. *Acc. Chem. Res.* **1999**, *32*, 869.

(30) Wang, P. G.; Xian, M.; Tang, X.; Wu, X.; Wen, Z.; Cai, T.; Janczuk, A. J. *Chem. Rev. (Washington, D. C.)* **2002**, *102*, 1091.

(31) Hrabie, J. A.; Keefer, L. K. *Chem. Rev.* **2002**, *102*, 1135.

(32) Paradossi, G.; Cavalieri, F.; Chiessi, E.; Ponassi, V.; Martorana, V. *Biomacromolecules* **2002**, *3*, 1255.

(33) Hrabie, J. A.; Saavedra, J. E.; Roller, P. P.; Southan, G. J.; Keefer, L. K. *Bioconjug. Chem.* **1999**, *10*, 838.

(34) Simon, D. I.; Mullins, M. E.; Jia, L.; Gaston, B.; Singel, D. J.; Stamler, J. S. *Proc. Natl. Acad. Sci. U. S. A.* **1996**, *93*, 4736.

(35) Ewing, J. F.; Young, D. V.; Janero, D. R.; Garvey, D. S.; Grinnell, T. A. *J. Pharmacol. Exp. Ther.* **1997**, *283*, 947.

(36) Katsumi, H.; Nishikawa, M.; Yamashita, F.; Hashida, M. *Journal of Pharmacology and Experimental Therapeutics* **2005**, *314*, 1117.

(37) Parzuchowski, P. G.; Frost, M. C.; Meyerhoff, M. E. *J. Am. Chem. Soc.* **2002**, *124*, 12182.

(38) Jo, Y. S.; van der Vlies, A. J.; Gantz, J.; Thacher, T. N.; Antonijevic, S.; Cavadini, S.; Demurtas, D.; Stergiopulos, N.; Hubbell, J. A. *J. Am. Chem. Soc.* **2009**, *131*, 14413.

(39) Yue, J.; Liu, S.; Xie, Z.; Xing, Y.; Jing, X. *J. Mater. Chem. B* **2013**, *1*, 4273.

(40) Willcock, H.; O'Reilly, R. K. *Polymer Chemistry* **2010**, *1*, 149.

(41) Westedt, U.; Kalinowski, M.; Wittmar, M.; Merdan, T.; Unger, F.; Fuchs, J.; Schäller, S.; Bakowsky, U.; Kissel, T. *J. Controlled Release* **2007**, *119*, 41.

(42) Stasko, N. A.; Schoenfisch, M. H. *J. Am. Chem. Soc.* **2006**, *128*, 8265.

(43) Motterlini, R.; Otterbein, L. E. *Nat. Rev. Drug. Discov.* **2010**, *9*, 728.

(44) Hasegawa, U.; van der Vlies, A. J.; Simeoni, E.; Wandrey, C.; Hubbell, J. A. *J. Am. Chem. Soc.* **2010**, *132*, 18273.

(45) Matson, J. B.; Webber, M. J.; Tamboli, V. K.; Weber, B.; Stupp, S. I. *Soft Matter* **2012**, *8*, 6689.

(46) Greenfield, M. A.; Hoffman, J. R.; Olvera de la Cruz, M.; Stupp, S. I. *Langmuir* **2009**, *26*, 3641.

(47) Abe, K. K., H. *J. Neurosci.* **1996**, *16*, 1066.

(48) Wang, R. *Physiol. Rev.* **2012**, *92*, 791.

(49) Hosoki, R.; Matsuki, N.; Kimura, H. *Biochem. Biophys. Res. Commun.* **1997**, *237*, 527.

(50) Kimura, Y. D., R.; Schubert, D.; Kimura, H. *Antioxid. Redox Signaling* **2006**, *8*, 661.

(51) Jha, S.; Calvert, J. W.; Duranski, M. R.; Ramachandran, A.; Lefer, D. J. *Am. J. Physiol.* **2008**, *295*, H801.

(52) Filipovic, M. R.; Miljkovic, J. L.; Nauser, T.; Royzen, M.; Klos, K.; Shubina, T.; Koppenol, W. H.; Lippard, S. J.; Ivanović-Burmazović, I. *J. Am. Chem. Soc.* **2012**, *134*, 12016.

(53) Hughes, M. N.; Centelles, M. N.; Moore, K. P. *Free Radical Biol. Med.* **2009**, *47*, 1346.

(54) Benavides, G. A.; Squadrito, G. L.; Mills, R. W.; Patel, H. D.; Isbell, T. S.; Patel, R. P.; Darley-Usmar, V. M.; Doeller, J. E.; Kraus, D. W. *Proc. Natl. Acad. Sci. U. S. A.* **2007**, *104*, 17977.

(55) Predmore, B. L.; Kondo, K.; Bhushan, S.; Zlatopolsky, M. A.; King, A. L.; Aragon, J. P.; Grinsfelder, D. B.; Condit, M. E.; Lefer, D. J. *Am. J. Physiol.* **2012**, *302*, H2410.

(56) Lee, Z. W.; Zhou, J.; Chen, C.-S.; Zhao, Y.; Tan, C.-H.; Li, L.; Moore, P. K.; Deng, L.-W. *PLoS One* **2011**, *6*, e21077.

(57) Fiorucci, S.; Orlandi, S.; Mencarelli, A.; Caliendo, G.; Santagada, V.; Distrutti, E.; Santucci, L.; Cirino, G.; Wallace, J. L. *Br. J. Pharmacol.* **2007**, *150*, 996.

(58) Wallace, J. L. *Trends Pharmacol. Sci.* **2007**, *28*, 501.

(59) Chattopadhyay, M.; Kodela, R.; Nath, N.; Barsegian, A.; Boring, D.; Kashfi, K. *Biochem. Pharmacol.* **2012**, *83*, 723.

(60) Kodela, R.; Chattopadhyay, M.; Kashfi, K. *ACS Medicinal Chemistry Letters* **2012**, *3*, 257.

(61) Zhao, Y.; Bhushan, S.; Yang, C.; Otsuka, H.; Stein, J. D.; Pacheco, A.; Peng, B.; Devarie-Baez, N. O.; Aguilar, H. C.; Lefer, D. J.; Xian, M. *ACS Chemical Biology* **2013**, *8*, 1283.

(62) Zhao, Y.; Wang, H.; Xian, M. *J. Am. Chem. Soc.* **2011**, *133*, 15.

(63) Raasch, M. S. *J. Org. Chem.* **1972**, *37*, 3820.

(64) Israelachvili, J. N.; Mitchell, D. J.; Ninham, B. W. *Journal of the Chemical Society, Faraday Transactions 2: Molecular and Chemical Physics* **1976**, *72*, 1525.

Chapter 3. S-Aroylthiooximes: A Facile Route to Hydrogen Sulfide-Releasing Compounds with Structure-Dependent Release Kinetics

3.1 Authors

Jeffrey C. Foster,[†] Chad R. Powell,[†] Scott C. Radzinski,[†] and John B. Matson[†]

[†]Department of Chemistry and Macromolecules Innovation Institute, Virginia Tech, Blacksburg, Virginia 24061, United States

3.2 Abstract

Here we report on the facile preparation of a family of H_2S donors based on *S*-aroylthiooximes, which are synthesized in a single step via a click reaction analogous to oxime chemistry between *S*-aroylthiohydroxylamines and aldehydes or ketones. Electrochemical and spectrophometric analysis of cysteine-triggered H_2S release revealed structure-dependent release kinetics with half-lives from 8–82 min by substitution of the *S*-aroylthiohydroxylamine ring. The pseudo-first-order rate constants of substituted *S*-aroylthiooximes fit standard linear free energy relationships (ρ = 1.05), demonstrating a significant sensitivity to electronic effects. A variety of ketones and aldehydes were used to form *S*-aroylthiohydroxylamines, demonstrating the versatility and wide applicability of this method.

3.3 Introduction

Gasotransmitters such as hydrogen sulfide (H_2S) are endogenous signaling gases that are enzymatically produced and have specific physiological functions,[1] and delivery of these gasotransmitters can be exploited for therapeutic applications.[2] The therapeutic potential of H_2S is vast, with promising preclinical studies conducted on several diseases and disorders. For example, H_2S exhibits cardioprotection through vasorelaxation,[3] suppresses oxidative stress,[4] reduces inflammation in the brain,[5] and protects the liver in ischemia-reperfusion events,[6] among other effects. Unfortunately, H_2S lags far behind the other gasotransmitters (NO and CO) in studies on its physiological role and translational potential. Versatile H_2S-releasing functional groups are needed to unlock this untapped potential and elevate the status of this gasotransmitter. Identifying a functional group that has a high capacity to release H_2S and can be incorporated into small and large molecules may revolutionize our understanding and

The study of H_2S physiology is accomplished through the use of various H_2S organic and electrochemical sensors7 in conjunction with H_2S-releasing compounds. Most studies on H_2S physiology and biology have been done with sulfide salts (Na_2S and NaHS). Organic H_2S donors have recently been developed, but most suffer a number of limitations including structural constraints and uncontrolled H_2S release kinetics.[8] The in vivo function of H_2S is coupled to its local concentration.[9] Therefore, precise control over the rate of H_2S release from donor compounds is paramount.

S-Aroylthiohydroxylamines (SATHAs) have been used in the synthesis of *N*-(benzoylthio)benzamides. As sulfur-containing analogs to acylhydrazides and acylhydroxylamines, thiohydroxylamines are reported to undergo condensation reactions with both aldehydes and ketones to form thiooximes, a functional group that has received little

attention in the literature.[10] We hypothesized that *S*-aroylthiooximes might react with cysteine to generate H_2S in a similar manner to previously reported compounds.[8d] Given the simplicity and robust nature of oxime and hydrazone-forming reactions, *S*-aroylthiooxime formation could provide a method for attaching an H_2S-releasing functionality to many types of compounds under mild reaction conditions. Herein, we report a synthetic strategy for accessing a variety of H_2S-releasing compounds via a thiooxime click reaction analogous to oxime formation. Additionally, we explore the reactivity and H_2S-releasing capacity of this unique functional group.

3.4. Results and Discussion

In order to evaluate our hypothesis, we synthesized a series of *S*-aroylthiooximes from substituted SATHAs and commercially available aldehydes and ketones (Scheme 3.1). SATHAs were prepared by previously described methods with a range of substituents.[11] Thiooxime formation reactions were conducted at equimolar concentrations of SATHA and aldehyde/ketone in CH_2Cl_2 in the presence of a catalytic quantity of trifluoroacetic acid and molecular sieves, which presumably removed the water, a byproduct of the reaction (see supporting information for details). Lower conversions were observed without the use of molecular sieves as measured by ^1H NMR.

Scheme 3.1. Synthesis of S-aroylthiooximes.

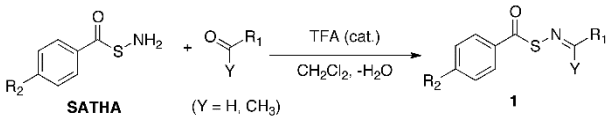

The versatility of thiooxime formation was demonstrated by mixing unsubstituted SATHA (R_2 = H) with several aldehydes and ketones (Table 3.1) to generate compounds 1a-1j. Aldehyde-derived

S-aroylthiooximes were synthesized with high conversions and high isolated yields. Additionally, thiooxime formation was not inhibited by reactive functional groups such as carboxylic acids or olefins. Most reactions required only 2 h at room temperature for full conversion. Higher temperatures reduced conversion. Ketone-derived *S*-aroylthiooximes were somewhat more difficult to make. Reactions of SATHAs with ketones typically reached a maximum conversion in 5 h at room temperature. Condensation of SATHA with a number of aliphatic aldehydes and ketones was attempted; however, only one aliphatic *S*-aroylthiooxime, derived from pivalaldehyde (1g), could be isolated due to rapid hydrolysis. We also prepared *S*-aroylthiooximes with substituents (R_2) on the SATHA ring at near complete conversion (> 99%).

Table 3.1. Conversion and hydrolysis kinetics of substituted S-aroylthiooximes.

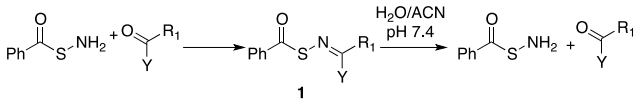

Compound	R_1, Y	% Conv[a]	$t_{1/2}$ Hydrol[b] (h)
1a	Ph, H	>99	44
1b	*p*-Ph-F, H	>99	76
1c	*p*-Ph-COOH, H	>99	58
1d	*p*-Ph-OCH_3, H	90	57
1e	Furan, H	>99	221
1f	Cinn, H	>99	118
1g	$C(CH_3)_3$, H	74	1
1h	Ph, CH_3	66	199
1i	*p*-Ph-F, CH_3	87	266
1j	*p*-Ph-OCH_3, CH_3	37	194

[a]Conversion to S-aroylthiooxime as determined by relative integration of thiooxime to aldehyde/ketone signals by ^{1}H NMR. bHydrolysis conducted in 20% (v/v) ACN in PBS (pH = 7.4) at room temperature.

For the set of ketones studied (1h-1j), conversion increases with increasing electron withdrawal. These findings are consistent with well-known linear free energy relationships.[12] This finding

agrees with kinetic data previously reported for oximes.[13] The maximum conversion attained for several substituted S-aroylthiooximes is summarized in Table 1.

Two pathways can be envisioned for generating H_2S from *S*-aroylthiooximes (Scheme 3.2). Pathway A involves addition of the cysteine thiol to the *S*-aroylthiooxime acyl group followed by rapid S→N acyl transfer in a step similar to native chemical ligation.14 In this case, the arylidenethiooxime would form, which could decompose to generate the original ketone or aldehyde along with H_2S and NH_3, as has been previously noted for similar substrates.[8d] Pathway B describes an initial hydrolysis step, which would generate the SATHA and the ketone or aldehyde used to make the *S*-aroylthiooxime. (In preliminary experiments, unsubstituted SATHA released H_2S in the presence of cysteine, leading to the same products as proposed for Pathway A.)

Scheme 3.2. Possible routes of H_2S generation.

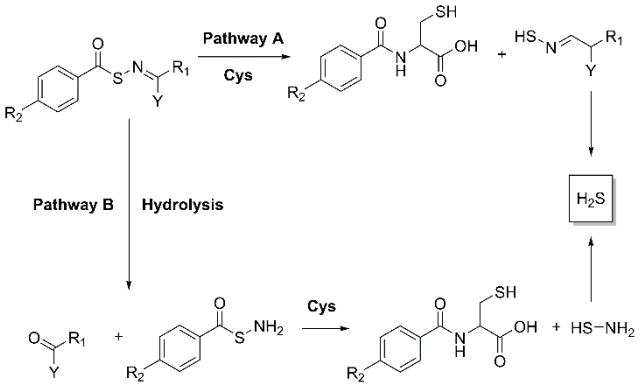

While both pathways lead to H_2S release, Pathway A would be more desirable for functionalizing substrates to make prodrugs, where H_2S would be released simultaneously with the drug. Considering the tunable hydrolysis kinetics of the analogous oxime functional group, Pathway B could be discouraged by controlling steric and electronic factors of the *S*-aroylthiooxime bond. Additionally, the rate of H_2S release could be precisely controlled by manipulating the electronics

of the SATHA ring because a likely rate-limiting step would be the breakdown or formation of a tetrahedral intermediate at the aroyl carbon.

To achieve H_2S production via Pathway A, the rate of hydrolysis (Pathway B) must to be slow relative to the rate of H_2S release from reaction with cysteine. Hydrolysis of compounds 1a-1j was evaluated via absorbance spectroscopy. In these experiments, buffered thiooxime solutions were prepared at pH 7.4, and the concentration of the S-aroylthiooximes relative to their hydrolysis products (SATHA and ketone or aldehyde) was determined over multiple half-lives. In general, *S*-aroylthiooxime hydrolyzed with half-lives in the timescale of days for compounds 1a-1j excluding 1g (Table 3.1). The *S*-aroylthiooxime prepared from pivalaldehyde (1g) exhibited poor hydrolytic stability.

The hydrolysis of *S*-aroylthiooximes followed first order kinetics but did not conform to the expected linear free energy trend.[15] The unsubstituted compound (1a) hydrolyzed faster than the F-, COOH- and OCH3-functionalized compounds (1b, 1c, and 1d). This type of behavior has been observed in other systems.[16] The ketone-derived *S*-aroylthiooximes hydrolyzed more slowly and showed a stability order of 1i > 1h > 1j. Further studies on a broader array of substrates are warranted to illuminate the mechanism(s) of hydrolysis.

To evaluate our ability to control the rate of H_2S release from *S*-aroylthiooximes, we measured H_2S release using two different methods: (1) a microelectrode-based method that gives real-time data on H_2S concentration; and (2) a colorimetric method that is better suited for longer release periods and was used to determine the half-life of H_2S release for specific compounds (Figure 3.2). Additionally, the colorimetric method allowed for the determination of the H_2S release kinetics from compounds that were insoluble in the conditions required for the microelectrode experiments (1l-1n).

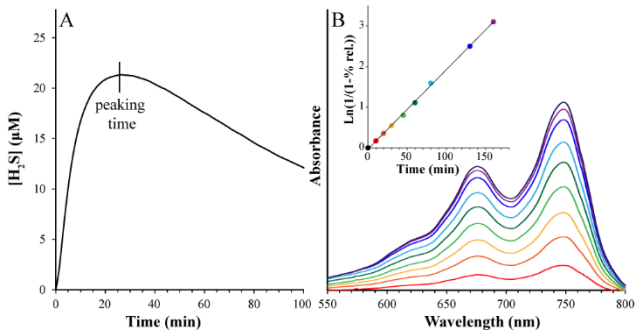

Figure 3.2. A) Representative H_2S release curve of 1a measured by the microelctrode method and B) kinetics as measured by the methylene blue spectrophotometric method. Color-coding from red through purple represents increasing time from 10 min to 200 min, respectively. Inset shows the kinetics plot derived from absorbances measured at 676 nm. Experiments were all conducted in triplicate.

For the microelectrode experiments, *S*-aroylthiooximes 1a-1j, 1k, and 1o-1p were dissolved in THF and added to buffered solutions containing an excess of cysteine. Upon addition of the *S*-aroylthiooxime, H_2S release was monitored continuously with an H_2S-selective microelectrode (Figure 3.2A). In all cases, H_2S concentration reached maximum value, which is defined as the peaking time (Tables 3.2 and 3.3), after which it began to decrease as the result of volatilization and oxidation by O2.[17]

Table 3.2. H_2S release from substituted *S*-aroylthiooximes.

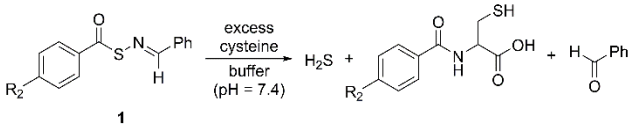

Compound	Peaking Time (min)[a]	Compound	Peaking Time (min)[a]
1a	24 ± 2	1f	26 ± 3
1b	20 ± 2	1g	27 ± 2
1c	18 ± 1	1h	34 ± 2
1d	22 ± 3	1i	34 ± 1
1e	14.8 ± 0.3	1j	33.5 ± 0.9

[a]Time after which [H_2S] reached a maximum value using an H_2S sensitive microelectrode. Studies were conducted at 40 μM *S*-aroylthiooxime in 0.1% THF in PBS buffer (pH = 7.4) at room temperature in the presence of 1 mM cysteine.

In general, substitution at the para position of the arylaldehyde ring (1a–1d) has little effect on H_2S release rate (Table 3.2). *S*-Aroylthiooximes prepared from ketones (1h–1j) generate H_2S more slowly, a phenomenon that may be attributable to the steric bulk of the CH_3 group. Although the rate of H_2S release does not exhibit a strong dependence on the electronics of the substituent on the arylaldehyde ring, the rate of hydrolysis is influenced by substitution at this position. Taken together, these data suggest that the stability of *S*-aroylthiooximes can be tuned without drastically altering the H_2S release profile.

We also tested several other molecules as triggers for H_2S release (Figure 3S2). *N*-Acetylcysteine was found to trigger H_2S generation at a slower rate. However, neither lysine nor serine triggered H_2S release, nor was H_2S generation observed in aqueous solutions of *S*-aroylthiooxime in the absence of thiol functionality.

Table 3. H_2S release from substituted *S*-aroylthiooximes.

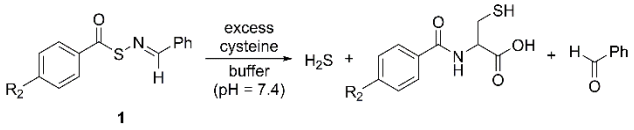

1

R_2	Peaking Time (min)[a]	$t_{1/2}$ H_2S Release (min)[b]
H (**1a**)	24 ± 2	34 ± 6
F (**1k**)	21 ± 2	29 ± 2
Cl (**1l**)	---[c]	18 ± 1
CF_3 (**1m**)	---[c]	11 ± 1
CN (**1n**)	---[c]	8 ± 1
CH_3 (**1o**)	33.7 ± 0.4	52.9 ± 1.4
OCH_3 (**1p**)	36 ± 3	82 ± 11

[a]Time after which [H_2S] reached a maximum value detected by an H_2S sensitive microelectrode. Studies were conducted at 40 μM *S*-aroylthiooxime in 0.1% THF in PBS buffer (pH = 7.4) at room temperature in the presence of 1 mM cysteine. bHalf-lives of release were measured by using the methylene blue assay at 100 μM *S*-aroylthiooxime in 30 % THF in PBS buffer (pH = 7.4) at room temperature in the presence of 1 mM cysteine. cSamples were not soluble in the media for the microelectrode probe assay.

The popular colorimetric method of measuring H_2S was first reported in 1965 and involves a reaction that converts N,N-dimethyl-p-phenylenediamine and H_2S to methylene blue,[18] which can be measured by its peak absorbance at 676 nm (Figure 3.2B). As real-time detection is not possible with the methylene blue method, time points are taken at various intervals for each compound.

Half-lives for the pseudo-first-order kinetic plots were determined (Figure 3.2B inset) and found to be on the order of 8–82 min. In general, results were similar to the electrochemical method, with H_2S release half-lives trending based on SATHA ring substituent electronics. A Hammett plot was constructed to quantify the effect of substituents on the rate of H_2S release (Figure 3.4). The Hammett plot revealed a strong dependence of the rate of H_2S release on the σ values of the SATHA substituents (ρ = 1.05). It follows from Figure 3.5 that the H_2S release kinetics of S-

aroylthiooximes can be finely tuned. The strong correlation between H_2S release rate and σ suggests that the rate of H_2S release for other S-aroylthiooximes could be predicted from the Hammett plot. These data represent an unprecedented level of control over the rate of H_2S release.

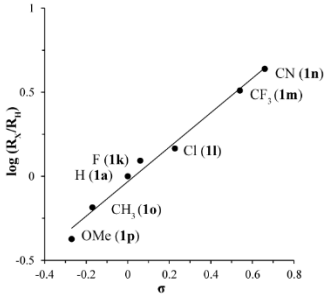

Figure 3.4. Hammett plot of the rate of H_2S release relative to 1a vs. the σ value of the p-substituent (ρ = 1.05, R2 = 0.986).

The fast reaction between *S*-aroylthiooximes and cysteine to generate H_2S ($t_{1/2}$ ~ 8–82 min) compared with their hydrolysis rate ($t_{1/2}$ ~ 45–250 h) indicates that pathway A is the primary H_2S release pathway for most *S*-aroylthiooximes under the conditions tested. To confirm the mechanism of H_2S release, the products of the reaction between 1a and cysteine were analyzed. Based on the compounds isolated by HPLC, we believe H_2S is generated according to Scheme 3.3. First, reversible thiol exchange between the *S*-aroylthiooxime and cysteine gives the arylidenethiooxime along with *N*-benzoylated cysteine after an S→N acyl transfer step. Reaction of a second equivalent of cysteine with the arylidenethiooxime generates thiocysteine, ammonia, and the original aldehyde (isolated as 2-phenylthiazolidine-4-carboxylic acid, a product of reaction with excess cysteine).[19] Thiocysteine then reacts with another equivalent of cysteine to generate cystine and H_2S.[20] This mechanism is supported by several pieces of evidence. Figure 3.3 shows the H_2S release profile of 1a in the presence of various nucleophiles. H_2S release was not observed in the absence of thiol functionality. Additionally, the rate of H_2S release is slower for the reaction of 1a with *N*-acetylcysteine compared with cysteine (peaking time of 33 min vs. 24 min). The

acetyl group of *N*-acetylcysteine prohibits S→N acyl transfer. The apparent dependence of the H_2S release rate on the ability of the *S*-benzoylcysteine byproduct to undergo S→N acyl transfer, coupled with the need of thiol reactivity to promote reversible thiol exchange, provides further evidence for the proposed mechanism.

Scheme 3.3. Proposed mechanism of H_2S release. Boxed products were either isolated from the reaction mixture or detected indirectly.

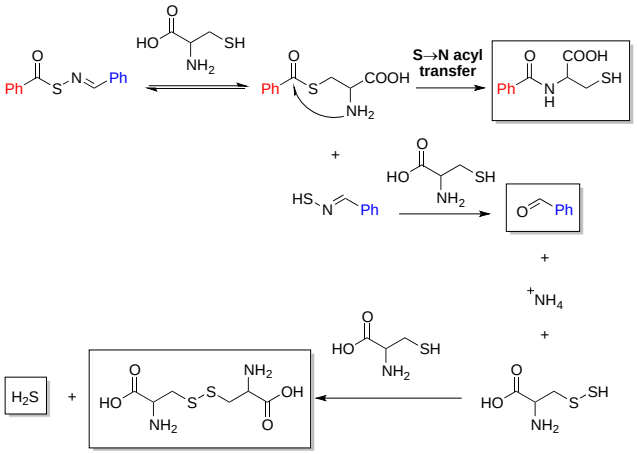

Regardless of the pathway of H_2S release, the parent aldehyde/ketone is regenerated in the process. This implies that SATHA can be conjugated to aldehyde or ketone-bearing therapeutic agents such as cinnamaldehyde (as in 1f), known to possess antimicrobial[21] and anticancer[22] properties, to impart tandem physiological activity. Existing H_2S donor-drug hybrids such as NOSH-aspirin[8a] and H_2S-releasing derivatives of diclofenac[9] fall short of this goal, as modification of the therapeutic agent to incorporate H_2S-releasing moieties can result in a loss of its original physiological activity.[9]

3.5. Conclusions

In summary, we have synthesized a series of *S*-aroylthiooximes from SATHAs and common aldehydes and ketones. The *S*-aroylthiooximes were prepared in good yields under mild conditions with little or no purification required. We showed that *S*-aroylthiooximes are relatively stable in

aqueous solution at physiological pH, and hydrolysis of these compounds can be controlled to a degree by tuning the steric and electronic factors of the *S*-aroylthiooxime bond. We demonstrated that the half-life of H_2S release could be varied between 8–82 min simply by changing the substituent on the SATHA ring. Given the ease of installation of this versatile functional group, we envision that *S*-aroylthiooximes could open new avenues for the study of H_2S biology and could enable a new generation of H_2S-releasing therapeutics and H_2S-drug conjugates.

3.6. References

1. Mustafa, A. K.; Gadalla, M. M.; Snyder, S. H., *Sci. Signal.* **2009,** *2* (68), re2.

2. (a) Motterlini, R.; Otterbein, L. E., *Nat. Rev. Drug. Discov.* **2010,** *9* (9), 728-743; (b) Carpenter, A. W.; Schoenfisch, M. H., *Chem. Soc. Rev.* **2012,** *41* (10), 3742-3752; (c) Wang, R., *Physiol. Rev.* **2012,** *92* (2), 791-896.

3. Hosoki, R.; Matsuki, N.; Kimura, H., *Biochem. Biophys. Res. Commun.* **1997,** *237* (3), 527-531.

4. Kimura, Y. D., R.; Schubert, D.; Kimura, H., *Antioxid. Redox Signaling* **2006,** *8* (4), 661-670.

5. Lee, M.; Sparatore, A.; Del Soldato, P.; McGeer, E.; McGeer, P. L., *Glia* **2010,** *58* (1), 103-113.

6. Jha, S.; Calvert, J. W.; Duranski, M. R.; Ramachandran, A.; Lefer, D. J., *Am. J. Physiol.* **2008,** *295* (2), H801-H806.

7. (a) Liu, C.; Pan, J.; Li, S.; Zhao, Y.; Wu, L. Y.; Berkman, C. E.; Whorton, A. R.; Xian, M., *Angew. Chem., Int. Ed.* **2011,** *50* (44), 10327-10329; (b) Sasakura, K.; Hanaoka, K.; Shibuya, N.;

Mikami, Y.; Kimura, Y.; Komatsu, T.; Ueno, T.; Terai, T.; Kimura, H.; Nagano, T., *J. Am. Chem. Soc.* **2011,** *133* (45), 18003-18005; (c) Peng, H.; Cheng, Y.; Dai, C.; King, A. L.; Predmore, B. L.; Lefer, D. J.; Wang, B., *Angew. Chem., Int. Ed.* **2011,** *50* (41), 9672-9675; (d) Liu, C.; Peng, B.; Li, S.; Park, C.-M.; Whorton, A. R.; Xian, M., *Organic Letters* **2012,** *14* (8), 2184-2187; (e) Lippert, A. R.; New, E. J.; Chang, C. J., *J. Am. Chem. Soc.* **2011,** *133* (26), 10078-10080.

8. (a) Kodela, R.; Chattopadhyay, M.; Kashfi, K., *ACS Med. Chem. Lett.* **2012,** *3* (3), 257-262; (b) Devarie-Baez, N. O.; Bagdon, P. E.; Peng, B.; Zhao, Y.; Park, C.-M.; Xian, M., *Organic Letters* **2013,** *15* (11), 2786-2789; (c) Lee, Z. W.; Zhou, J.; Chen, C.-S.; Zhao, Y.; Tan, C.-H.; Li, L.; Moore, P. K.; Deng, L.-W., *PLoS One* **2011,** *6*, e21077; (d) Zhao, Y.; Wang, H.; Xian, M., *J. Am. Chem. Soc.* **2011,** *133*, 15-17.

9. Wallace, J. L., *Trends Pharmacol. Sci.* **2007,** *28* (10), 501-505.

10. Barton, D. H. R.; Magnus, P. D.; Pennanen, S. I., *J. Chem. Soc., Chem. Commun.* **1974,** (23), 1007a-1007a.

11. Raasch, M. S., *J. Org. Chem.* **1972,** *37*, 3820-3.

12. Hammett, L. P., *J. Am. Chem. Soc.* **1937,** *59* (1), 96-103.

13. (a) Calzadilla, M.; Malpica, A.; Cordova, T., *J. Phys. Org. Chem.* **1999,** *12* (9), 708-712; (b) Jencks, W. P., *Progr. Phys. Org. Chem.* **1964,** *2*, 63-128; (c) Conant, J. B.; Bartlett, P. D., *J. Am. Chem. Soc.* **1932,** *54*, 2881-99.

14. Dawson, P. E., *Israel J. Chem.* **2011,** *51* (8-9), 862-867.

15. Gregory, B. J.; Moodie, R. B., *Journal of the Chemical Society B: Physical Organic* **1970,** (0), 862-866.

16. Stein, A. R.; Tencer, M.; Moffatt, E. A.; Dawe, R.; Sweet, J., *J. Org. Chem.* **1980,** *45* (17), 3539-3540.

17. Hughes, M. N.; Centelles, M. N.; Moore, K. P., *Free Radical Biol. Med.* **2009,** *47* (10), 1346-1353.

18. Siegel, L. M., *Anal. Biochem.* **1965,** *11* (1), 126-132.

19. Seki, M.; Mori, Y.; Hatsuda, M.; Yamada, S., *J. Org. Chem.* **2002,** *67* (16), 5527-5536.

20. Mueller, E. G., *Nat. Chem. Biol.* **2006,** *2* (4), 185-194.

21. Ali, S.; Khan, A.; Ahmed, I.; Musaddiq, M.; Ahmed, K.; Polasa, H.; Rao, L.; Habibullah, C.; Sechi, L.; Ahmed, N., *Ann Clin Microbiol Antimicrob* **2005,** *4* (1), 1-7.

22. Cabello, C. M.; Bair Iii, W. B.; Lamore, S. D.; Ley, S.; Bause, A. S.; Azimian, S.; Wondrak, G. T., *Free Radical Biol. Med.* **2009,** *46* (2), 220-231.

3.7. Appendix

Materials and Methods

All reagents were obtained from commercial vendors and used as received unless otherwise stated. Thiobenzoic acid was purified via vacuum distillation. All other thioacids and *S*-aroylthiohydroxylamines were prepared as previously described.[1-3] NMR spectra were measured on Agilent 400 MHz or Bruker 500 MHz spectrometers. ^{1}H and ^{13}C NMR chemical shifts are reported in ppm relative to internal solvent resonances. Yields refer to chromatographically and spectroscopically pure compounds unless otherwise stated. Infrared spectra were obtained on a Varian 670-IR spectrometer. HPLC was carried out on an Agilent 1220 system using water and CH_3CN as mobile phases with each containing 0.1% NH_4OH or 0.1% trifluoroacetic acid (TFA). Flow was maintained at 20 mL/min over gradients described for each purification on an Agilent PLRP-S column (100 Å, 10 µm, 25 x 150 mm). Fractions were analyzed by mass spectrometry (Advion Expression Compact Mass Spectrometer), and product-containing fractions were combined, rotovapped to remove CH_3CH, and lyophilized (LabConco). UV-Vis absorbance spectra were recorded on a Cary 5000 UV-Vis (Agilent) from 450 to 220 nm or on a Spectramax M2 plate reader (Molecular Devices). Reactions were performed in screw-cap scintillation vials over 3 Å molecular sieves.

Thiooxime synthesis representative procedure:

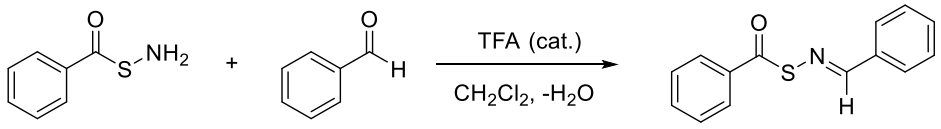

1a

S-Benzoylthiohydroxylamine (SBTHA) (200 mg, 1.3 mmol) was dissolved in 3 mL of CH_2Cl_2 in a scintillation vial charged with molecular sieves. To the vial was added benzaldehyde (135 µL, 1.3 mmol) followed by 10 µL of TFA. The vial was sealed, and the mixture was allowed to stand for 1-5 h at rt. The reaction mixture was filtered and the solvent was removed under reduced pressure to give the pure product as a white powder (309 mg, 98% yield). ^{1}H NMR ($CDCl_3$): δ 7.47 (m, 5H), 7.61 (t, 1H), 7.85 (d, 2H), 7.94 (d, 2H), 8.81 (s, 1H). ^{13}C NMR ($CDCl_3$): δ 189.12, 164.40, 135.79, 135.73, 133.92, 131.83, 129.05, 128.88, 128.49, 127.05. IR (ATR crystal) (cm^{-1}): 1673, 1203, 898, 751, 685, 641. HR-MS: $[M + H]^+$ calculated 242.0634; found 242.0640.

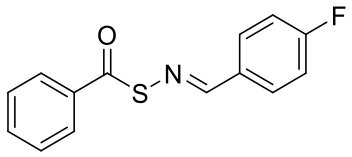

1b

Compound **1b** was prepared from SBTHA (50 mg, 0.33 mmol) and 4-fluorobenzaldehyde (35 µL, 0.33 mmol) using the same procedure as **1a**. The product was isolated as an off-white powder (81 mg, 96% yield). ^{1}H NMR ($CDCl_3$): δ 7.13 (t, 2H), 749 (t, 2H), 7.61 (t, 1H), 7.84 (t, 2H), 7.93 (d, 2H), 8.77 (s, 1H). ^{13}C NMR ($CDCl_3$): δ 189.07, 166.18, 163.73, 162.96, 135.77, 133.98, 132.21, 132.18, 130.60, 130.51, 129.08, 127.05, 116.26, 116.04. IR (ATR crystal) (cm^{-1}): 1675, 1597, 1505, 1228, 1201, 898, 767, 688, 640. HR-MS: $[M + H]^+$ calculated 260.0540; found 260.0557.

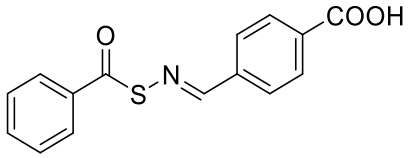

1c

Compound **1c** was prepared from SBTHA (100 mg, 0.65 mmol) and 4-formylbenzoic acid (107 mg, 0.71 mmol) using the same procedure as **1a**. The crude product was recrystallized from EtOAc to afford the pure product as a white powder (133 mg, 71.4% yield). ^{1}H NMR (DMSO-d_6): δ 7.61 (t, 2H), 7.74 (t, 1H), 7.92 (t, 4H), 8.07 (d, 2H), 9.07 (s, 1H). ^{13}C NMR (DMSO-d_6): δ 187.77, 166.92, 164.44, 138.65, 134.95, 134.39, 133.96, 129.79, 129.44, 128.00, 126.58. IR (ATR crystal) (cm^{-1}): 2950, 2811, 2657, 1677, 1284, 1198, 896, 764, 680, 638. HR-MS: $[M + H]^+$ calculated 286.0532; found 286.0531.

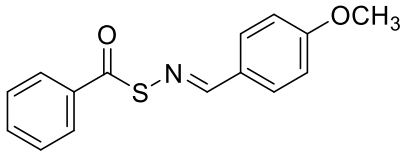

1d

Compound **1d** was prepared from SBTHA (50 mg, 0.33 mmol) and anisaldehyde (40 µL, 0.33 mmol) using the same procedure as **1a**. The product was isolated as a white powder (79 mg, 89% yield). ^{1}H NMR ($CDCl_3$): δ 3.85 (s, 3H), 6.95 (d, 2H), 7.48 (t, 3H), 7.60 (t, 1H), 7.79 (d, 2H), 7.93 (d, 2H), 8.71 (s, 1H). ^{13}C NMR ($CDCl_3$): δ 189.63, 164.42, 162.68, 135.95, 133.78, 130.35, 129.01, 128.88, 126.97, 114.32, 55.55. IR (ATR crystal) (cm^{-1}): 2930, 2834, 1674, 1592, 1556, 1590, 1251, 1202, 1169, 1024, 898, 825, 788, 684, 639. HR-MS: $[M + H]^+$ calculated 272.0740; found 272.0760.

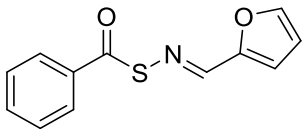

1e

Compound **1e** was prepared from SBTHA (50 mg, 0.33 mmol) and furfural (27 µL, 0.33 mmol) using the same procedure as **1a**. The product was isolated as a white powder as a mixture of cis/trans isomers (71 mg, 94% yield in a ratio of 65:35). ^{1}H NMR ($CDCl_3$): δ 6.53 (dd, 0.65H, *J* = 2Hz), 6.62 (dd, 0.35H, *J* = 2Hz), 6.94 (d, 0.65H, *J* = 4Hz), 7.10 (d, 0.35H, *J* = 4Hz), 7.49 (q, 2H, *J* = 8Hz), 7.60 (t, 1.7H, *J* = 8Hz), 7.67 (d, 0.3H, *J* = 2Hz), 7.90 (d, 1.3H, *J* = 8Hz), 8.00 (d, 0.7H, *J* = 8Hz), 8.47 (s, 0.35H), 8.62 (s, 0.65H). ^{13}C NMR ($CDCl_3$): δ 188.78, 152.48, 151.31, 149.64, 147.15, 146.26, 145.95, 135.83, 135.68, 134.04, 133.94, 129.06, 127.37, 127.03, 118.48, 116.06, 112.88, 112.36. IR (ATR crystal) (cm^{-1}): 1669, 1596, 1204, 900, 769, 747, 681, 641. HR-MS: $[M + Na]^+$ calculated 254.0246; found 254.0259.

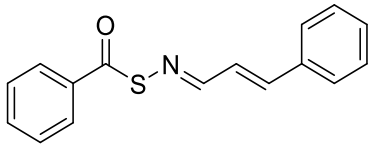

1f

Compound **1f** was prepared from SBTHA (176 mg, 1.15 mmol) and *trans*-cinnamaldehyde (145 µL, 1.15 mmol) using the same procedure as **1a**. The product was purified by HPLC (gradient of 30% to 90% CH_3CN) to afford the pure product as a light yellow powder as a mixture of cis/trans isomers (224 mg, 79% yield in a ratio of 65:35). ^{1}H NMR ($CDCl_3$): δ 6.98 (t, 0.35H), 7.02 (t, 0.65H), 7.10 (d 0.2H, *J* = 15 Hz), 7.15 (d, 0.5H, *J* = 5 Hz), 7.19 (d, 0.3H, *J* = 10 Hz), 7.39 (m, 3H), 7.49 (m, 3.6H), 7.57 (m, 0.4H), 7.62 (m, 1H), 7.93 (d, 1.5H, *J* = 5 Hz), 7.99 (d, 0.5H, *J* = 10 Hz), 8.34 (d, 0.2H, *J* = 10 Hz), 8.56 (d, 0.8H, *J* = 5 Hz). ^{13}C NMR ($CDCl_3$): δ 188.92, 165.63, 161.90, 144.96, 143.32, 135.79, 135.60, 135.24, 134.85, 133.78, 130.41, 129.80, 128.99, 128.94, 128.89, 128.87, 128.00, 127.89, 127.61, 127.14, 126.93, 121.72. IR (ATR crystal) (cm^{-1}): 1676, 1592, 1446, 1200, 899, 682, 642, HR-MS: $[M + H]^+$ calculated 268.0791; found 268.0788.

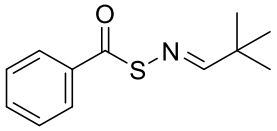

1g

Compound **1g** was prepared from SBTHA (156 mg, 1.02 mmol) and pivalaldehyde (140 µL, 1.29 mmol) using the same procedure as **1a**. The crude product was purified on a silica gel column (0.5% NEt_3 + 10% EtOAc in hexanes) to afford the pure product as an off-white powder (84 mg, 37% yield). ^{1}H NMR ($CDCl_3$): δ 1.18 (s, 9H), 7.45 (t, 2H), 7.57 (t, 1H), 7.86 (d, 2H), 8.14 (s, 1H). ^{13}C NMR ($CDCl_3$): δ 189.66, 179.07, 135.91, 133.68, 128.94, 126.89, 39.68, 26.57. IR (ATR crystal) (cm^{-1}): 2963, 1667, 1603, 1200, 899, 776, 688, 644. HR-MS: $[M + H]^+$ calculated 222.0947; found 222.0954.

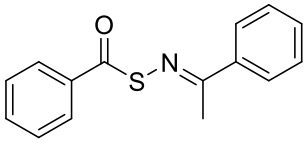

1h

Compound **1h** was prepared from SBTHA (200 mg, 1.31 mmol) and acetophenone (152 µL, 1.31 mmol) using the same procedure as **1a**. The crude product was dried under vacuum overnight and then purified on a silica gel column (0.5% NEt_3 in CH_2Cl_2) to afford the pure product as an off-white white powder (180 mg, 54% yield). ^{1}H NMR ($CDCl_3$): δ 2.54 (s, 3H), 7.43 (d, 2H), 7.50 (t, 2H), 7.62 (t, 1H), 7.94 (m, 2H), 7.99 (d, 2H). ^{13}C NMR ($CDCl_3$) δ 188.13, 167.41, 139.05, 136.29, 133.76, 130.56, 129.02, 128.58, 127.27, 127.08, 77.16, 21.57. IR (ATR crystal) (cm^{-1}): 1679, 1563, 1446, 1369, 1201, 896, 754, 677, 637. HR-MS: $[M + H]^+$ calculated 256.0791; found 256.0803.

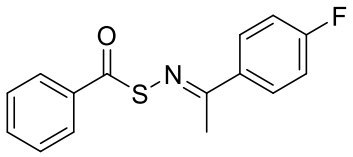

1i

Compound **1i** was prepared from SBTHA (200 mg, 1.31 mmol) and 4-fluoroacetophenone (158 µL, 1.31 mmol) using the same procedure as **1a.** The crude product was purified via recrystallization from hexanes to afford the pure product as a white powder (188 mg, 53% yield). ^{1}H NMR ($CDCl_3$): δ 2.51 (s, 3H), 7.09 (t, 2H), 7.50 (t, 2H), 7.61 (t, 1H), 7.94 (m, 2H), 7.96 (d, 2H). ^{13}C NMR ($CDCl_3$) δ 188.03, 166.03, 165.61, 163.11, 136.17, 135.30, 135.27, 133.81, 129.23, 129.14, 129.02, 127.23, 115.65, 115.43, 21.47. IR (ATR crystal) (cm^{-1}): 1683, 1592, 1562, 1501, 1203, 896, 830, 768, 683, 641. HR-MS: $[M + H]^+$ calculated 274.0696; found 274.0714.

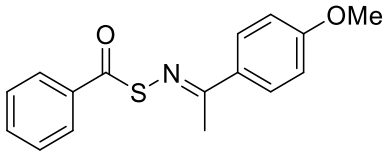

1j

Compound **1j** was prepared from SBTHA (100 mg, 0.65 mmol) and 4-methoxyacetophenone (98 mg, 0.65 mmol) using the same procedure as **1a**. The crude product was purified via HPLC (30% to 90% CH_3CN with 0.1% NH_4OH) to afford the pure product as an off-white white powder (40 mg, 22% yield). ^{1}H NMR ($CDCl_3$): δ 2.50 (s, 3H), 3.85 (s, 3H), 6.92 (d, 2H), 7.49 (t, 2H), 7.60 (t, 1H), 7.92 (d, 2H), 7.99 (d, 2H). ^{13}C NMR ($CDCl_3$) δ 188.53, 166.88, 161.65, 136.35, 133.66, 131.90, 128.97, 128.78, 127.18, 113.81, 55.50, 21.28. IR (ATR crystal) (cm^{-1}): 1672, 1582, 1554, 1506, 1254, 1200, 1172, 900, 683, 645. HR-MS: $[M + H]^+$ calculated 286.0896; found 286.0910.

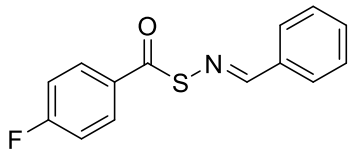

1k

Compound **1k** was prepared from *S*-(4-fluorobenzoyl)thiohydroxylamine (105 mg, 0.61 mmol) and benzaldehyde (63 µL, 0.61 mmol) using the same procedure as **1a**. The product was isolated as an off-white powder (78 mg, 91% yield). ^{1}H NMR ($CDCl_3$): δ 7.17 (t, 2H), 7.47 (m, 3H), 7.84 (d, 2H), 7.97 (d, 2H), 8.80 (s, 1H). ^{13}C NMR ($CDCl_3$): δ 187.75, 167.49, 164.98, 164.64, 135.71, 132.18, 132.15, 131.93, 129.71, 129.62, 128.93, 128.52, 116.42, 116.20. IR (ATR crystal) (cm^{-1}): 1676, 1593, 1196, 904, 833, 752, 693, 630. HR-MS: $[M + H]^+$ calculated 260.0540; found 260.0564.

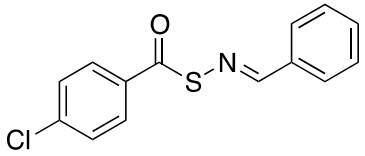

1l

Compound **1l** was prepared from *S*-(4-clorobenzoyl)thiohydroxylamine (100 mg, 0.53 mmol) and benzaldehyde (55 µL, 0.53 mmol) using the same procedure as **1a**. The product was isolated as a white powder (142 mg, 97% yield). ^{1}H NMR ($CDCl_3$): δ 7.47 (m, 5H), 7.84 (d, 2H), 7.88 (d, 2H), 8.80 (s, 1H). ^{13}C NMR ($CDCl_3$): δ 188.07, 164.80, 140.32, 135.70, 134.17, 131.99, 129.43, 128.95, 128.56, 128.44. IR (ATR crystal) (cm^{-1}): 1674, 1586, 1481, 1395, 1195, 1081, 893, 858, 829, 751, 692, 629. HR-MS: $[M + H]^+$ calculated 276.0244; found 276.0249.

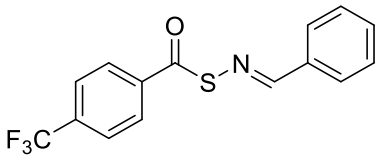

1m

Compound **1m** was prepared from *S*-(4-trifluoromethylbenzoyl)thiohydroxylamine (75 mg, 0.34 mmol) and benzaldehyde (35 µL, 0.34 mmol) using the same procedure as **1a**. The crude product was purified on a silica gel column (10% EtOAc + 0.5% NEt_3 in hexanes) to give the pure product as a white powder (78 mg, 74.4% yield). ^{1}H NMR ($CDCl_3$): δ 7.48 (m, 3H), 7.76 (d, 2H), 7.85 (d, 2H), 8.04 (d, 2H), 8.81 (s, 1H). ^{13}C NMR ($CDCl_3$): δ 188.38, 165.24, 138.66, 135.58, 135.35, 135.03, 134.70, 132.14, 128.98, 128.61, 127.47, 126.22, 126.11, 124.93, 122.21. IR (ATR crystal) (cm^{-1}): 1671, 1319, 1109, 1063, 906, 842, 750, 689, 647. HR-MS: $[M + H]^+$ calculated 310.0508; found 310.0518.

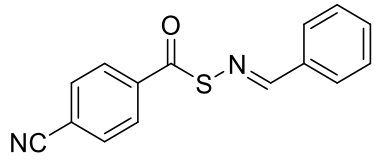

1n

Compound **1n** was prepared from 4-((aminothio)carbonyl)benzonitrile (100 mg, 0.56 mmol) and benzaldehyde (57 µL, 0.56 mmol) using the same procedure as **1a**. The product was isolated as an off-white powder (143 mg, 96% yield). ^{1}H NMR ($CDCl_3$): δ 7.47 (m, 3H), 7.79 (d, 2H), 7.83 (d, 2H), 8.01 (d, 2H), 8.79 (s, 1H). ^{13}C NMR ($CDCl_3$): δ 188.07, 165.53, 138.99, 135.46, 132.90, 132.24, 129.00, 128.62, 127.56, 117.80, 117.12. IR (ATR crystal) (cm^{-1}): 1664, 1587, 1561, 1372, 903, 761, 696, 629. HR-MS: $[M + H]^+$ calculated 267.0587; found 267.0592.

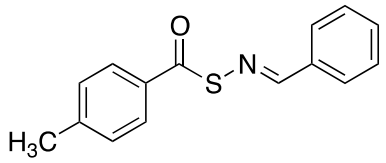

1o

Compound **1o** was prepared from *S*-(4-methylbenzoyl)thiohydroxylamine (100 mg, 0.60 mmol) and benzaldehyde (61 µL, 0.60 mmol) using the same procedure as **1a**. The product was isolated as a white powder (139 mg, 91% yield). ^{1}H NMR ($CDCl_3$): δ 2.43 (s, 3H), 7.29 (d, 2H), 7.45 (m, 3H), 7.84 (d, 4H), 8.81 (s, 1H). ^{13}C NMR ($CDCl_3$): 188.72, 164.21, 144.91, 135.87, 133.30, 131.76, 129.73, 128.89, 128.49, 127.15, 21.91. IR (ATR crystal) (cm^{-1}): 1674, 1603, 1565, 1204, 1169, 900, 815, 751, 686, 639. $[M + H]^+$ calculated 256.0791; found 256.0804.

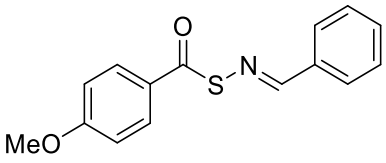

1p

Compound **1p** was prepared from *S*-(4-methoxybenzoyl)thiohydroxylamine (21 mg, 0.12 mmol) and benzaldehyde (12 µL, 0.12 mmol) using the same procedure as **1a**. The product was isolated as a white powder (29 mg, 94% yield). ^{1}H NMR ($CDCl_3$): δ 3.87 (s, 3H), 6.96 (d, 2H), 7.45 (m, 3H), 7.83 (d, 2H), 7.92 (d, 2H), 8.80 (s, 1H). ^{13}C NMR ($CDCl_3$): δ 187.58, 164.22, 163.96, 135.89, 131.68, 129.26, 128.86, 128.59, 128.43, 114.28, 55.68. IR (ATR crystal) (cm^{-1}): 1670, 1596, 1262, 1211, 1164, 900, 832, 755, 690. 641. HR-MS: $[M + H]^+$ calculated 272.0740; found 272.0750.

Calibration of H_2S Selective Probe

An EDTA solution was prepared at 154 µM by dissolving 1.43 mg of EDTA in 25 mL of DI water in a volumetric flask. The solution was purged vigorously with nitrogen for 20 min. 7.7 mg of anhydrous Na_2S was added to a vial under inert atmosphere, followed by 20 mL of the EDTA solution (to make 5 mM H_2S). A small stir bar was added to a scintillation vial containing 20 mL of 1X PBS buffer (pH = 7.4). The vial was placed on a stir plate. The H_2S sensor was immersed in the solution and the background current was allowed to stabilize for several minutes. Five aliquots of the H_2S solution were injected sequentially into the vial (20 µL, 40 µL, 60 µL, 80 µL, 100 µL). The current increased rapidly after each injection before reaching a plateau. The second aliquot was injected as soon as the current had stabilized. The other aliquots were injected similarly. The recorded data was used to construct a linear calibration curve of concentration vs. current.

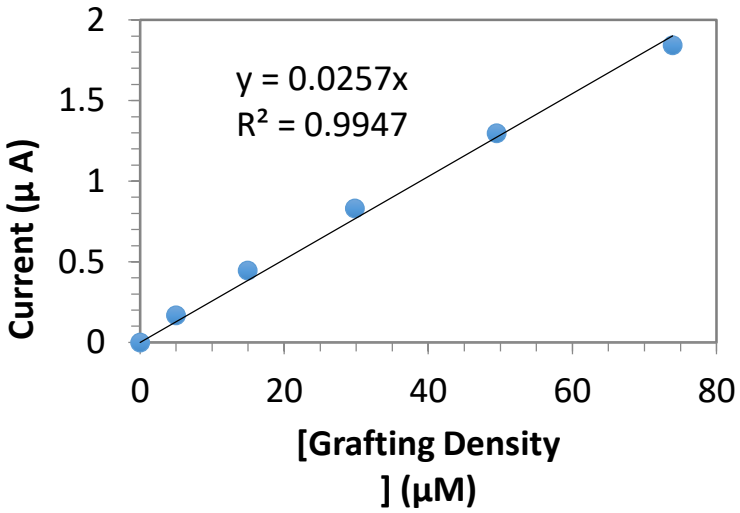

Fig 3S1. Standard curve for H_2S release in PBS buffer.

H_2S Release in the Presence of Cysteine and Other Additives

A stock solution of cysteine or other additive (lysine, *N*-acetylcysteine, serine, glutathione, or none) was prepared in PBS buffer at 400 mM. 50 µL of this solution was added to a vigorously stirred vial containing 20 mL of PBS buffer. The current was allowed to equilibrate for several minutes. Once a stable current was observed, an aliquot of *S*-aroylthiooxime stock solution (100 µL, 8 mM in THF) was added rapidly via pipette. The current was monitored over a period of approximately 1h. A plot of H_2S concentration vs. time was constructed using the calibration curve. No background subtraction was performed. H_2S release was only observed upon addition of compounds containing a thiol functionality.

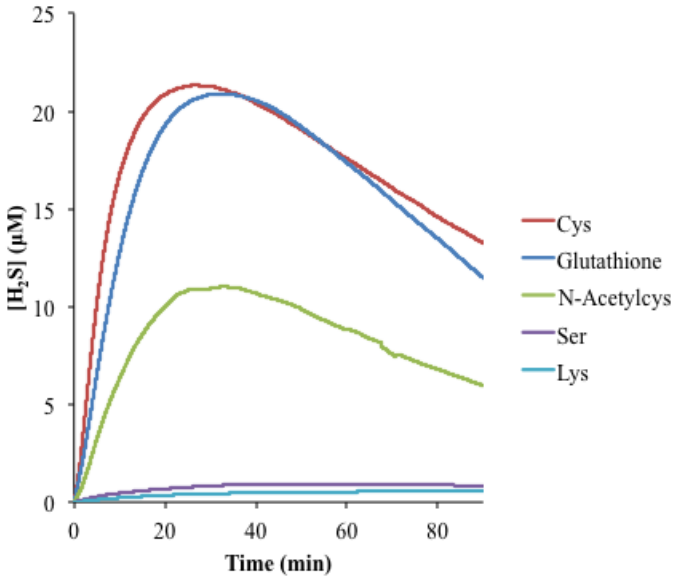

Fig 3S2. H_2S **release in the presence of various nucleophiles.**

H_2S Release as a Function of Cysteine Concentration

A stock solution of cysteine was prepared in PBS buffer at 400 mM. 12.5, 50, or 100 µL of this solution was added to a vigorously stirred vial containing 20 mL of PBS buffer. The current was

allowed to equilibrate for several minutes. Once a stable current was observed, an aliquot of a **1a** stock solution (100 µL, 8 mM in THF) was added rapidly via pipette. The current was monitored over a period of approximately 1 h. A plot of H_2S concentration vs. time was constructed using the calibration curve. No background subtraction was performed.

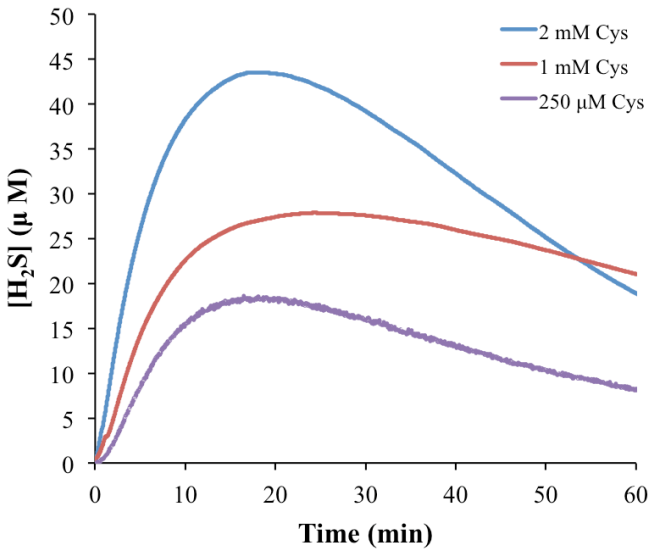

Fig 3S3. Effect of [cysteine] on H_2S release profile.

Calibration of H_2S Selective Probe in Bovine Plasma

A 100 mL of an 0.05 mg/mL EDTA solution was prepared and purged vigorously with N_2 for 20 min. Na_2S was then added to make 1 mM Na_2S. A small stir bar was added to a scintillation vial containing 15 mL of deionized water and 5 mL of bovine plasma. The vial was placed on a stir plate. The H_2S sensor was immersed in the solution and the background current was allowed to stabilize for several minutes. Three aliquots of the H_2S solution were injected sequentially into the vial (20 µL, 40 µL, 80 µL). The current increased rapidly after each injection before reaching a plateau. The second aliquot was injected as soon as the current had stabilized. The other aliquots

were injected similarly. The recorded data was used to construct a linear calibration curve of concentration vs. current.

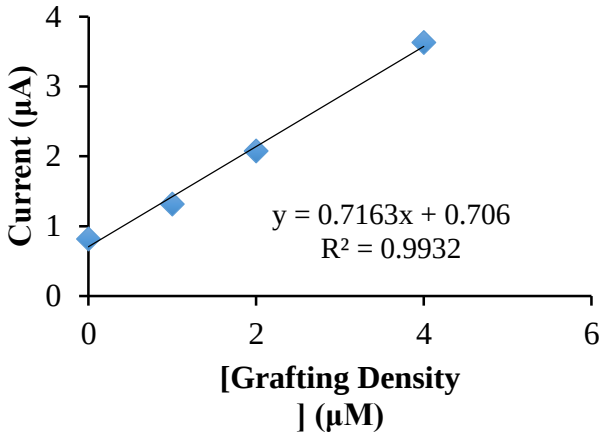

Fig 3S4. Standard curve for H_2S release in 25% v/v plasma.

H_2S release from Plasma

H_2S release from **1a** was conducted in bovine plasma. 5 µL of an 8 mM solution of **1a** in THF was added to 20 mL of a 25% v/v mixture of bovine plasma/deionized water. Thiols are known to be unstable in isolated plasma, having half-lives of disappearance on the order of minutes due to autooxidation and mixed disulfide formation reactions.[4-6] It has been reported that human plasma contains an average reduced cysteine concentration of 10 µM.[7] Therefore, we supplemented the commercial plasma with 10 µM cysteine before each run. The H_2S release profile of **1a** in plasma with 10 µM added cysteine is shown below (Fig S5 blue trace). As expected based on thiol autoxidation noted above, H_2S release was not observed in plasma in the absence of added cysteine (Fig S5 red trace). These results indicate that thiooximes would release H_2S in vivo where reduced cysteine is present.

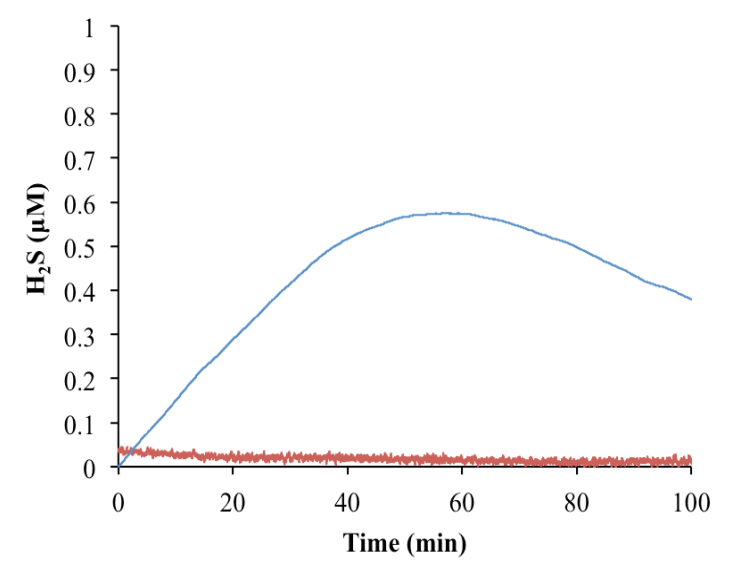

Fig 3S5. H_2S release in plasma. Blue curve shows H_2S evolution from 2 µM 1a in bovine plasma supplemented with 10 µM cysteine. Red curve shows the same experiment with no cysteine supplement.

H_2S Release Kinetics via Methylene Blue Method

Reactions for kinetics were run in triplicate, with each reaction vial containing 1.296 mL PBS, 200 µL thiooxime solution (1 mM in THF), 400 µL THF, 100 µL $Zn(OAc)_2$ solution (40 mM in H_2O), and 4 µL cysteine solution (500 mM in PBS). Final concentrations were 100 µM thiooxime, 2 mM ZnOAc, and 1 mM cysteine. A control solution was also run for each experiment using lysine in place of cysteine at the same concentration. At predetermined timepoints, 100 µL was removed from each vial. Each 100 µL aliquot was diluted with 100 µL $FeCl_3$ solution (30 mM in 1.2 M HCl) followed by 100 µL *N*,*N*-dimethyl-*p*-phenylenediamine (20 mM in 7.2 M HCl). Aliquots were stored until 3-5 h after the final aliquot had been taken. A spectrum of each aliquot was collected from 500 to 800 nm on a plate reader. A background solution was also made using THF in place of the substrate solution. Three aliquots of this background solution were diluted with $FeCl_3$ and *N*,*N*-dimethyl-*p*-phenylenediamine as described above. Kinetic analysis was done by subtracting the absorbance of the background solution from the average absorbance at each

timepoint at 676 nm. First-order half-life of H_2S release was determined by plotting time vs. ln(1/(1-% released), with $t_{1/2}$=ln(2)/slope.

Hydrolysis kinetics

Solutions for hydrolysis kinetics were prepared at 50 μM in *S*-aroylthiooxime in 20% CH_3CN in PBS. Spectra were taken at timepoints over the course of several days from 450 nm to 220 nm on a UV-Vis spectrophotometer. A background spectrum of 20% CH_3CN in PBS was subtracted from each sample spectrum, and all spectra were normalized at 450 nm, where absorbance was negligible for all samples.

Kinetic analysis was done by comparing the absorbance peak of the thiooxime (usually around 310-340 nm) to an isosbestic point for each hydrolysis experiment. The following equation was used to calculate % hydrolysis.[8]

$$\frac{A_{peak}}{A_{iso}} = \frac{\varepsilon_{SBTHApeak}[SBTHA] + \varepsilon_{spentpeak}[Spent]}{\varepsilon_{iso}([SBTHA] + [Spent])}$$

$$= \frac{\varepsilon_{SBTHApeak}}{\varepsilon_{iso}}$$

$$+ \left(\frac{[SBTHA]}{([SBTHA] + [Spent])}\right)\left(\frac{\varepsilon_{SBTHApeak} - \varepsilon_{spentpeak}}{\varepsilon_{iso}}\right)$$

Therefore,

$$\%\ hydroylsis = \frac{[SBTHA]}{([SBTHA] + [Spent])} = \left(\frac{A_{peak}}{A_{iso}} - \frac{\varepsilon_{SBTHApeak}}{\varepsilon_{iso}}\right)\left(\frac{\varepsilon_{iso}}{\varepsilon_{SBTHApeak} - \varepsilon_{spentpeak}}\right)$$

Where

$\varepsilon_{SBTHApeak}$ = extinction coefficient of thiooxime at peak absorbance

$\varepsilon_{spentpeak}$ = extinction coefficient of the SBTHA/carbonyl mixture at equilibrium

ε_{iso} = extinction coefficient at the isosbestic point

A_{peak} = absorbance at the peak maximum at a given timepoint

A_{iso} = absorbance at the isosbestic point at a given timepoint

The extinction coefficient at the peak SBTHA absorbance of the SBTHA/carbonyl mixture was determined by making a sample of each SBTHA/carbonyl mixture matching the components of each *S*-aroylthiooxime. These were prepared at 50 μM SBTHA and 50 μM carbonyl (ketone or aldehyde) in 20% CH_3CN in PBS. Samples were allowed to sit for 3 d to ensure that equilibrium had been reached before taking spectra.

Fitting to a first-order rate was accomplished by plotting time versus ln(1/(1-% hydrolysis) with with $t_{1/2}$ = ln(2)/slope.

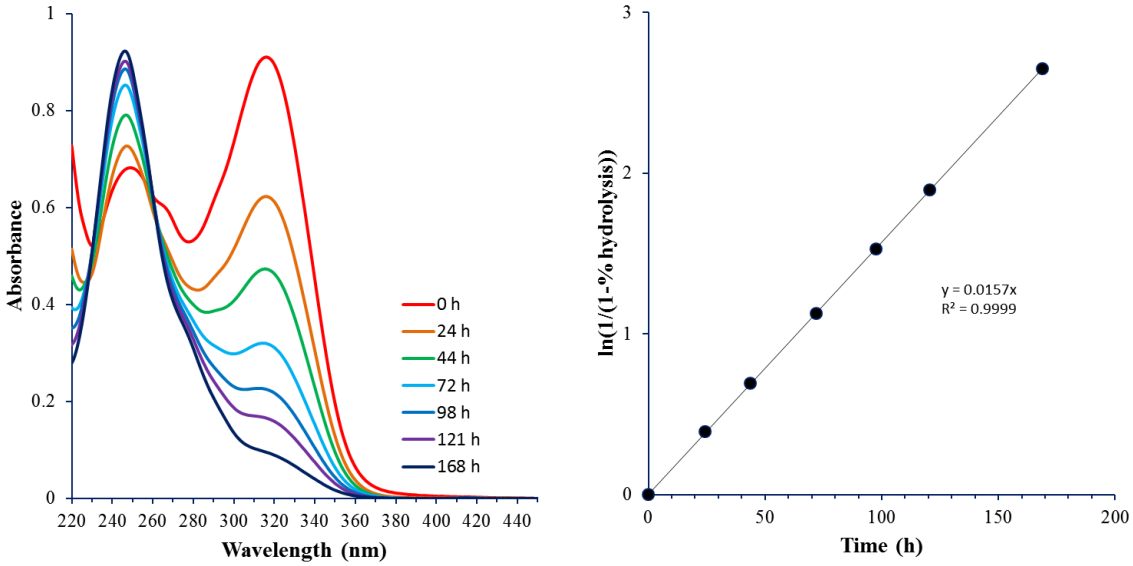

Fig 3S6. Example hydrolysis spectra and kinetic data for compound 1a. A_{peak} and A_{iso} for this compound were 316 and 262 nm, respectively.

H_2S Release Mechanism (Scheme 3.3)

The proposed mechanism is supported by several pieces of evidence. Figure 3S2 shows the H_2S release profile of **1a** in the presence of various nucleophiles. H_2S release was not observed in the absence of thiol functionality. Additionally, the rate of H_2S release is slower for the reaction of **1a** with *N*-acetylcysteine compared with cysteine (peaking time of 33 min vs. 24 min). The acetyl group of *N*-acetylcysteine prohibits S → N acyl transfer. The apparent dependence of the H_2S release rate on the ability of the *S*-benzoylcysteine byproduct to undergo S → N acyl transfer, coupled with the need of thiol reactivity to promote reversible thiol exchange, provides evidence for the proposed mechanism.

Compound **1a** (40 mg, 0.16 mmol) in 10 mL of CH_3CN was added to a stirred solution of cysteine (250 mg, 2.06 mmol) in 10 mL of PBS buffer (pH = 7.4) in a round bottom flask. The solution was stirred at room temperature overnight. The following day, the solution was filtered and concentrated to remove the organic solvent. The resulting aqueous solution was purified via preparative HPLC (gradient of 2% to 90% CH_3CN with 0.5% NH_4OH). The isolated products were characterized by NMR and HRMS as shown below.

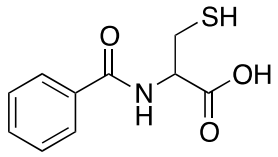

***N*-benzoylcysteine**

***N*-benzoylcysteine** was isolated by HPLC. The resulting solid was found to contain a small quantity of the disulfide dimer 3,3'-disulfanediylbis(2-benzamidopropanoic acid). ^{1}H NMR (D_2O): δ 3.10 (qd, 2H), 3.43 (dd, 0.2H), 4.66 (m, 1H), 4.76 (m, 0.2H), 7.48 (t, 0.4H), 7.58 (t, 2H), 7.86 (t,

1H), 7.76 (d, 0.4H), 7.88 (d, 2H). ^{13}C NMR (D_2O): δ 176.12, 170.36, 133.32, 132.21, 128.71, 127.15, 57.07, 26.23. $[M - H]^-$ calculated 224.0387; found 224.0396.

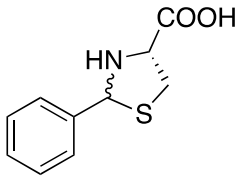

2-Phenylthiazolidine-4-carboxylic acid

2-Phenylthiazolidine-4-carboxylic acid was isolated by HPLC, a product of reaction of benzaldehyde with excess cysteine.[9] The resulting solid was a 50:50 mixture of diastereomers. ^{1}H NMR (D_2O): δ 3.02 (dd, 0.5H), 3.09 (dd, 0.5H), 3.28 (dd, 0.5H), 3.35 (dd, 0.5H), 3.78 (dd, 0.5H), 4.14 (dd, 0.5H), 5.48 (s, 0.5H), 5.70 (s, 0.5H), 7.25 (t, 0.5 H), 7.32 (m, 1.5H), 7.36 (t, 1H), 7.42 (d, 1H), 7.50 (d, 1H). ^{13}C NMR (D_2O): δ 173.22, 172.85, 141.96, 139.24, 128.50, 128.22, 128.17, 127.36, 127.22, 126.79, 72.10, 71.10, 66.65, 65.45, 59.76, 38.37, 20.78, 14.10. $[M + H]^+$ calculated 210.0583; found 210.0596.

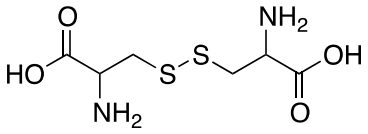

Cystine

Cystine was isolated as the HCl salt via filtration from the product analysis reaction mixture and subsequent purification by HPLC (gradient of 2% to 90% CH_3CN with 0.1% TFA). ^{1}H NMR (D_2O): δ 3.13 (m, 2H), 3.31 (dd, 2H), 4.26 (m, 1H). ^{13}C NMR (D_2O): δ 170.84, 51.93, 36.46. $[M + H]^+$ calculated 241.03; found 240.96 (LRMS).

^{1}H NMR (400 MHz, $CDCl_3$) spectrum of 1a

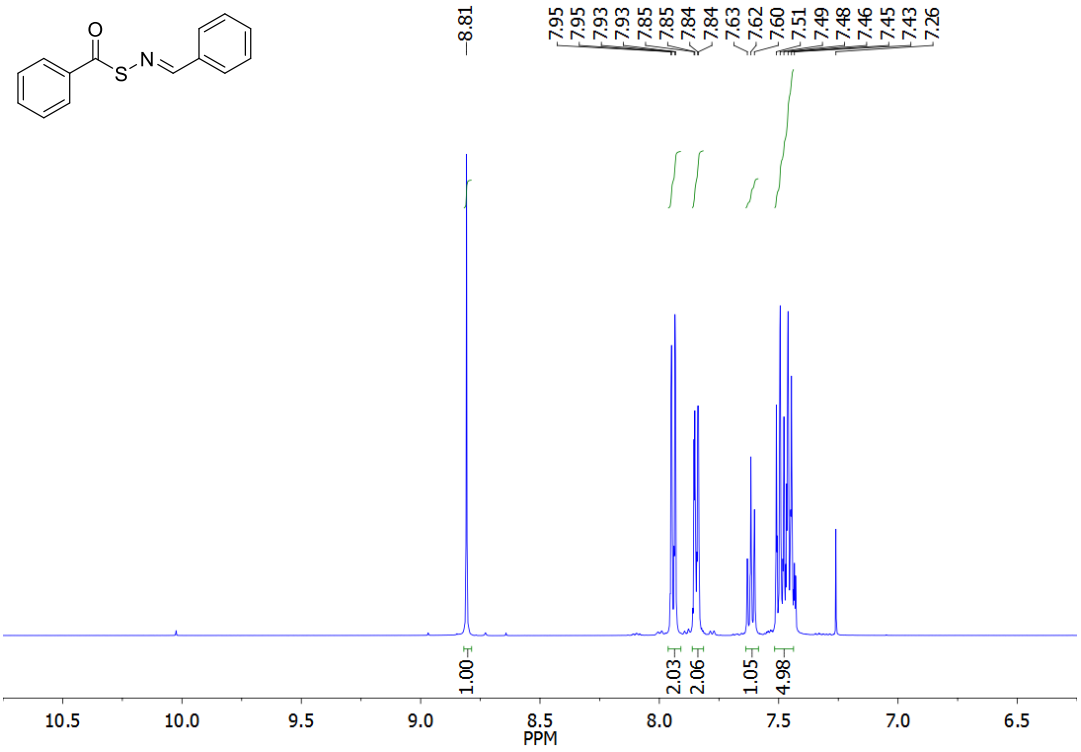

^{13}C NMR (400 MHz, $CDCl_3$) spectrum of 1a

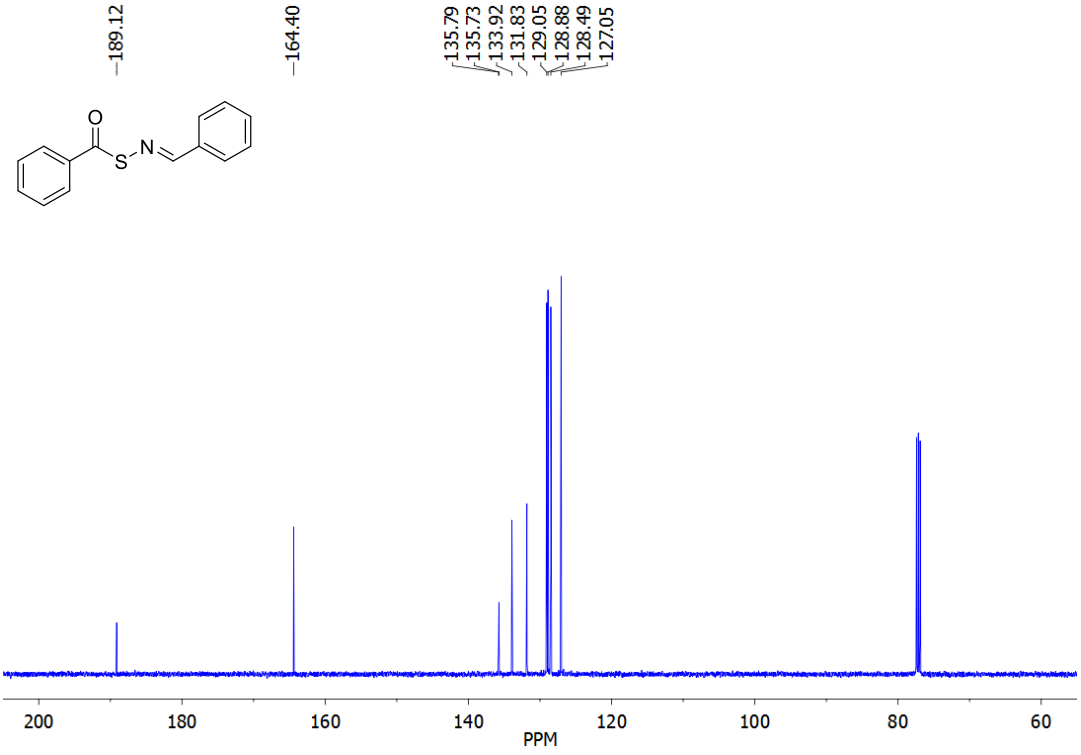

^{1}H NMR (400 MHz, $CDCl_3$) spectrum of 1b

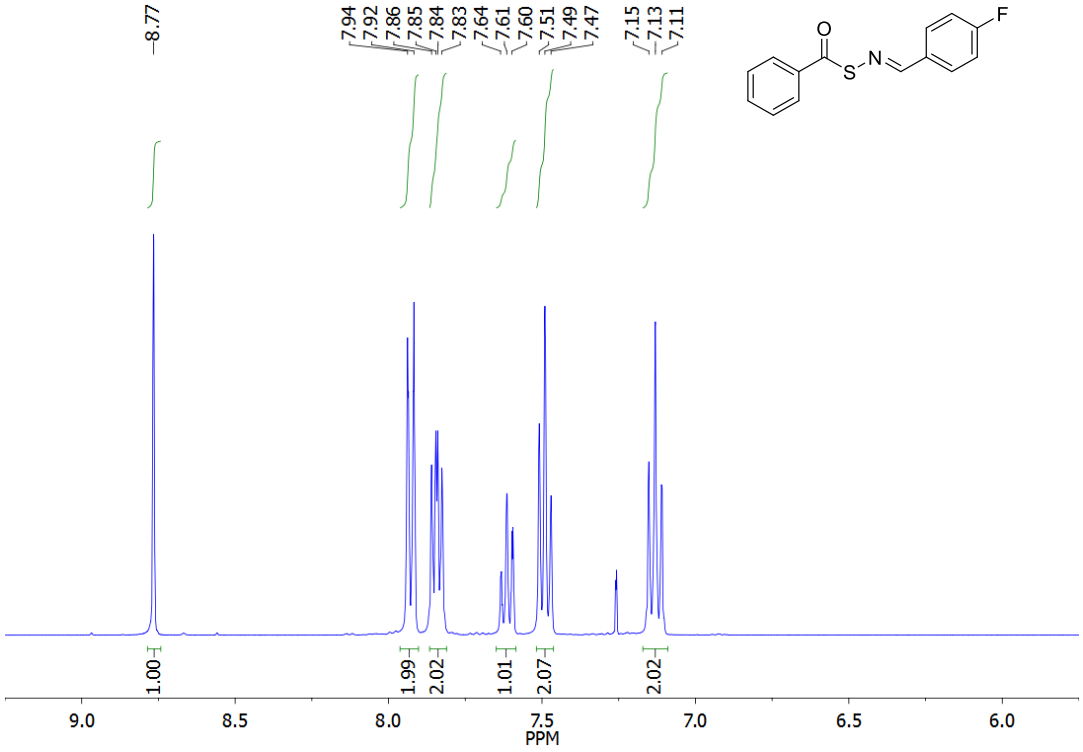

^{13}C NMR (400 MHz, $CDCl_3$) spectrum of 1b

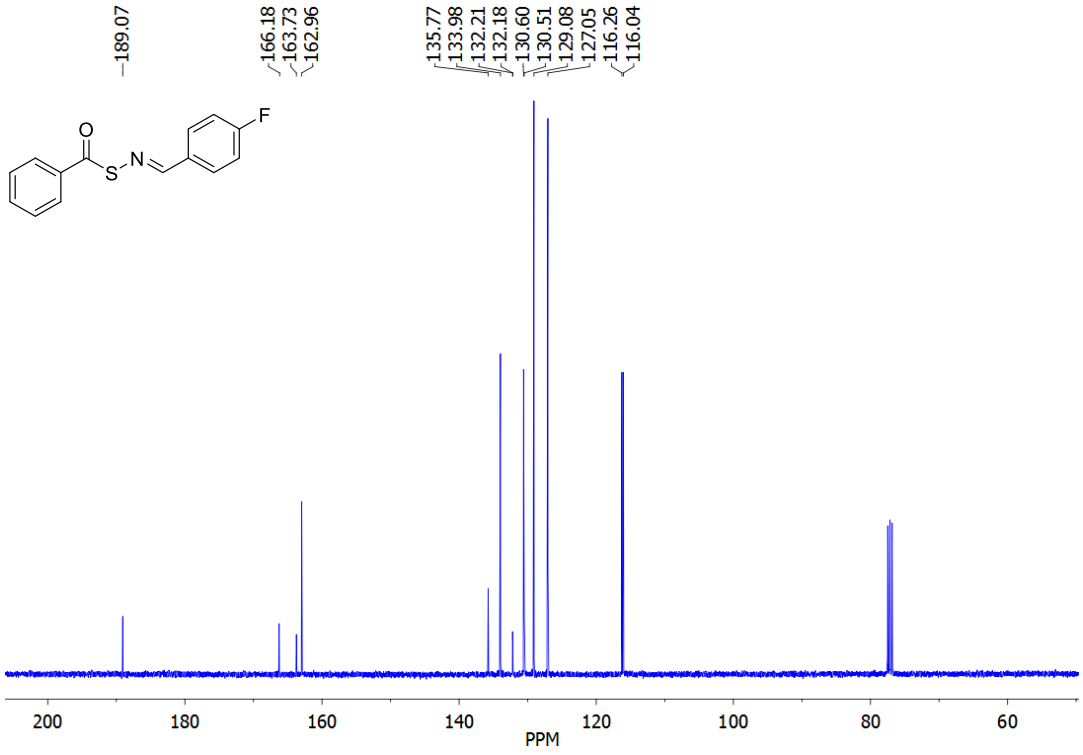

^{1}H NMR (400 MHz, DMSO-d_6) spectrum of 1c

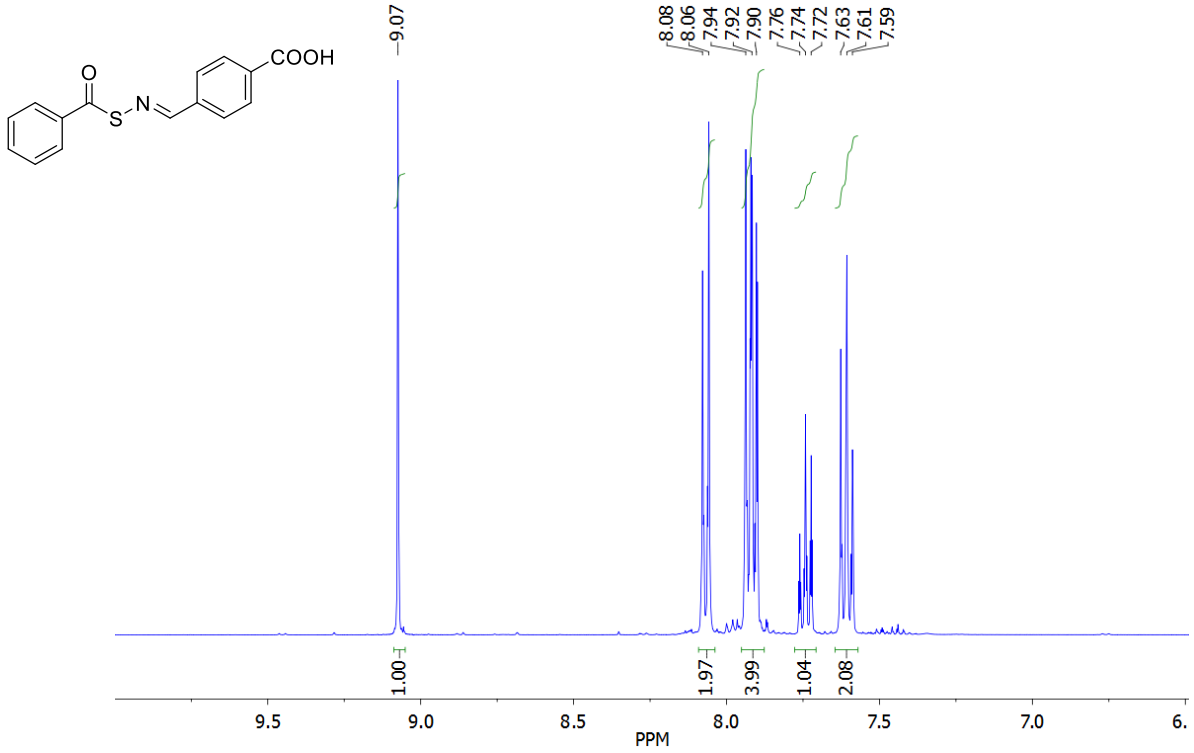

^{13}C NMR (400 MHz, DMSO-d_6) spectrum of 1c

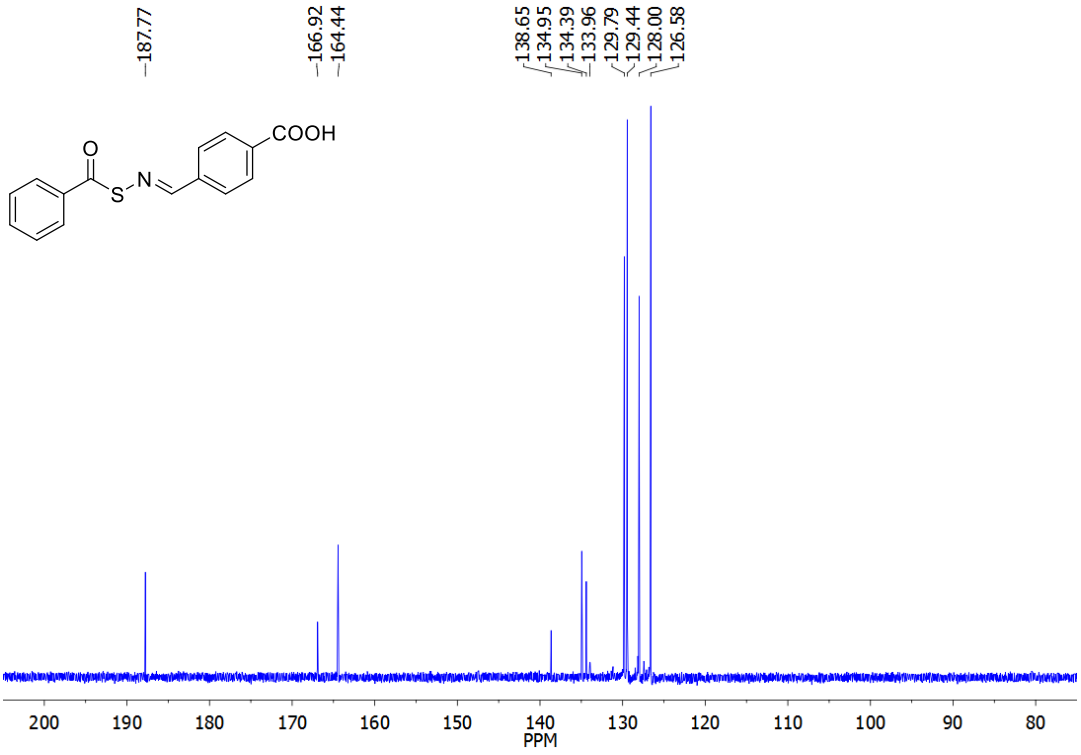

^{1}H NMR (400 MHz, $CDCl_3$) spectrum of 1d

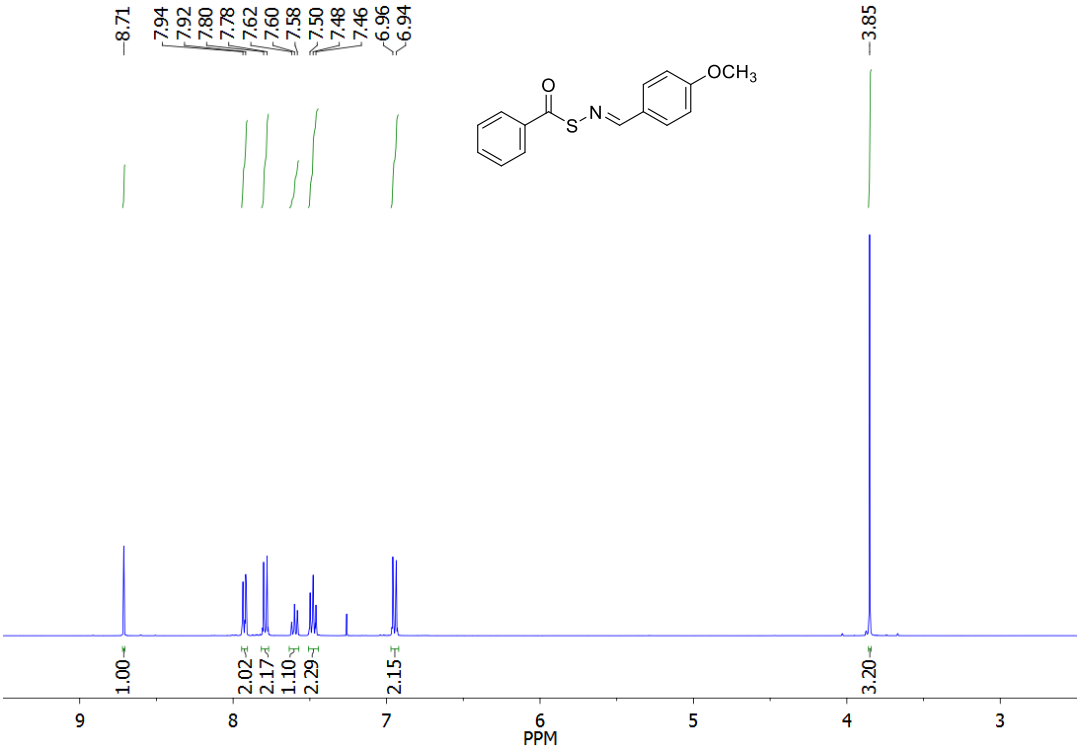

^{13}C NMR (400 MHz, $CDCl_3$) spectrum of 1d

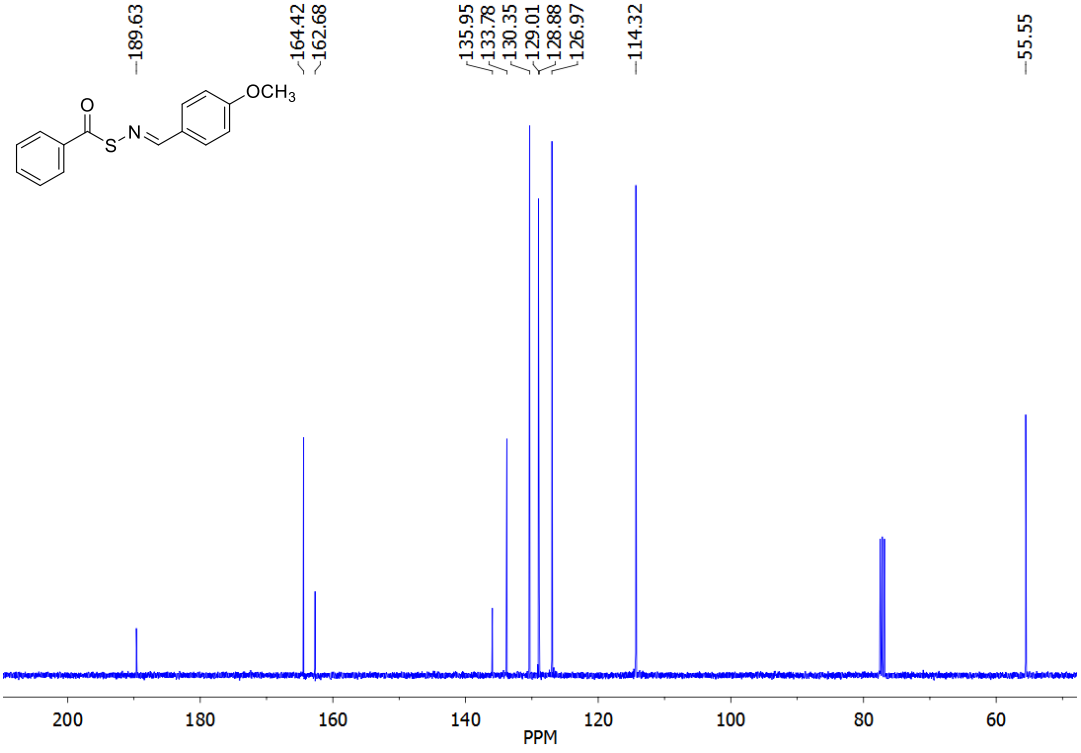

^{1}H NMR (400 MHz, $CDCl_3$) spectrum of 1e

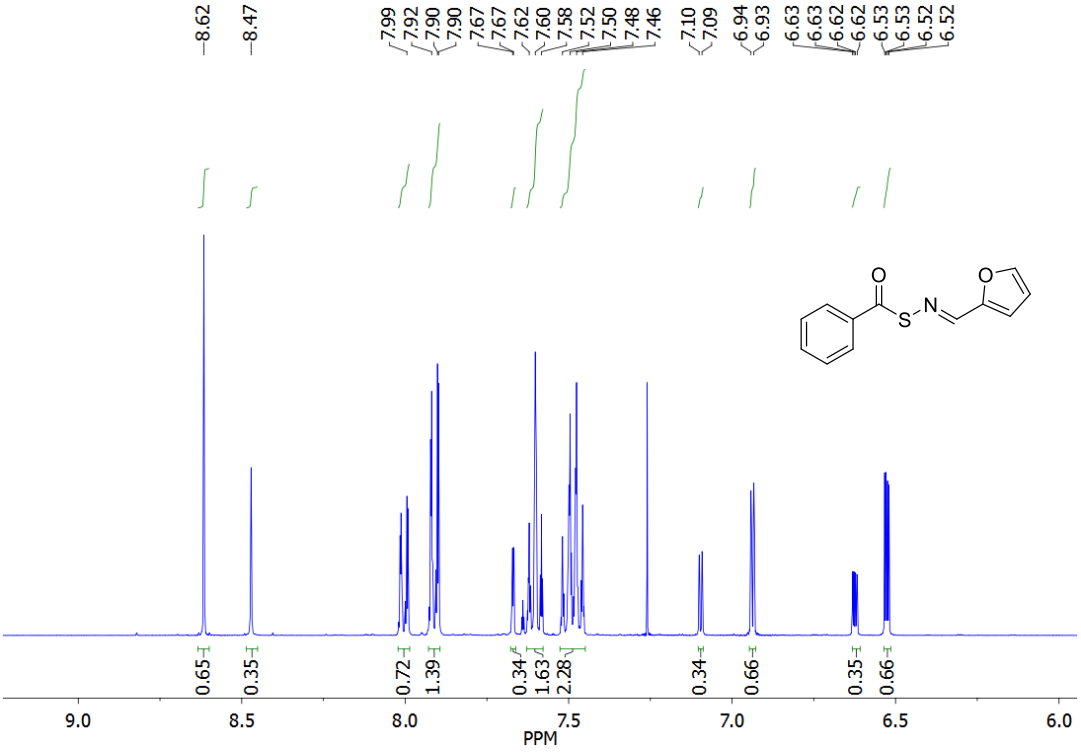

^{13}C NMR (400 MHz, $CDCl_3$) spectrum of 1e

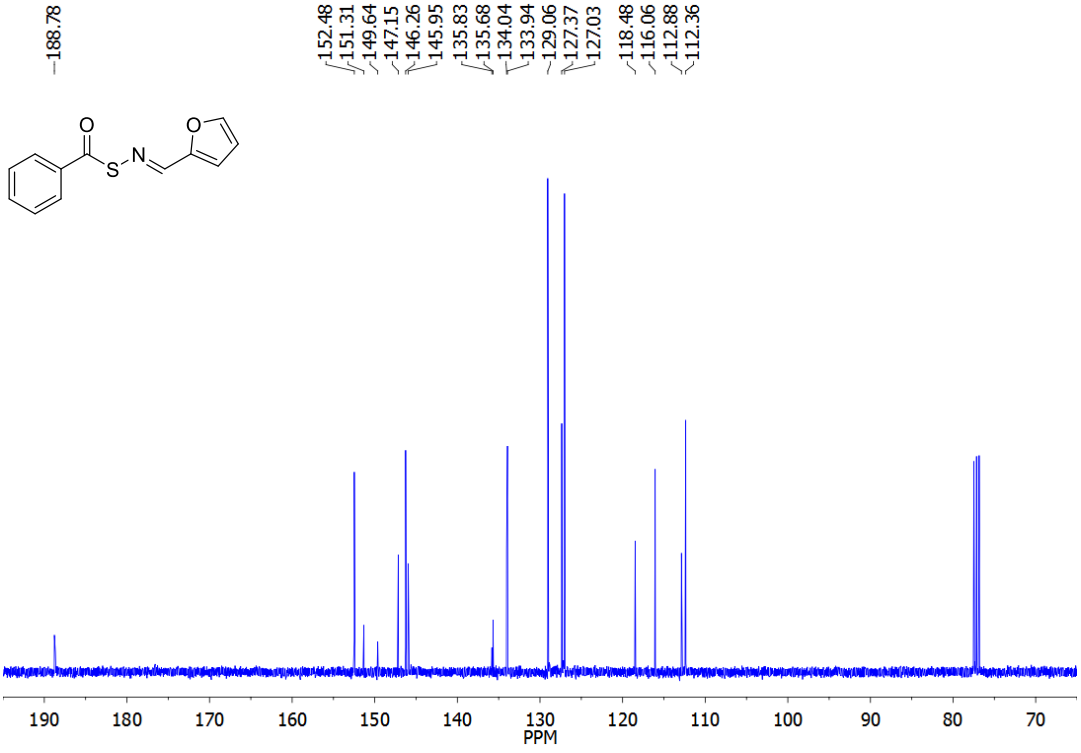

^{1}H NMR (400 MHz, $CDCl_3$) spectrum of 1f

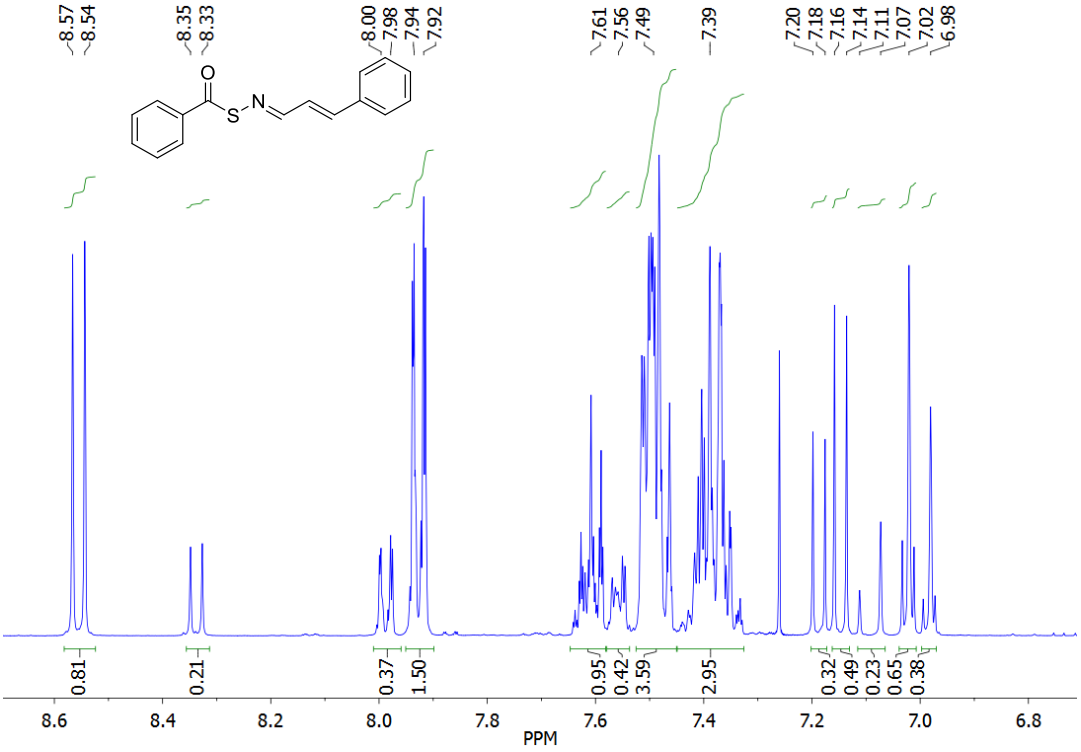

^{13}C NMR (400 MHz, $CDCl_3$) spectrum of 1f

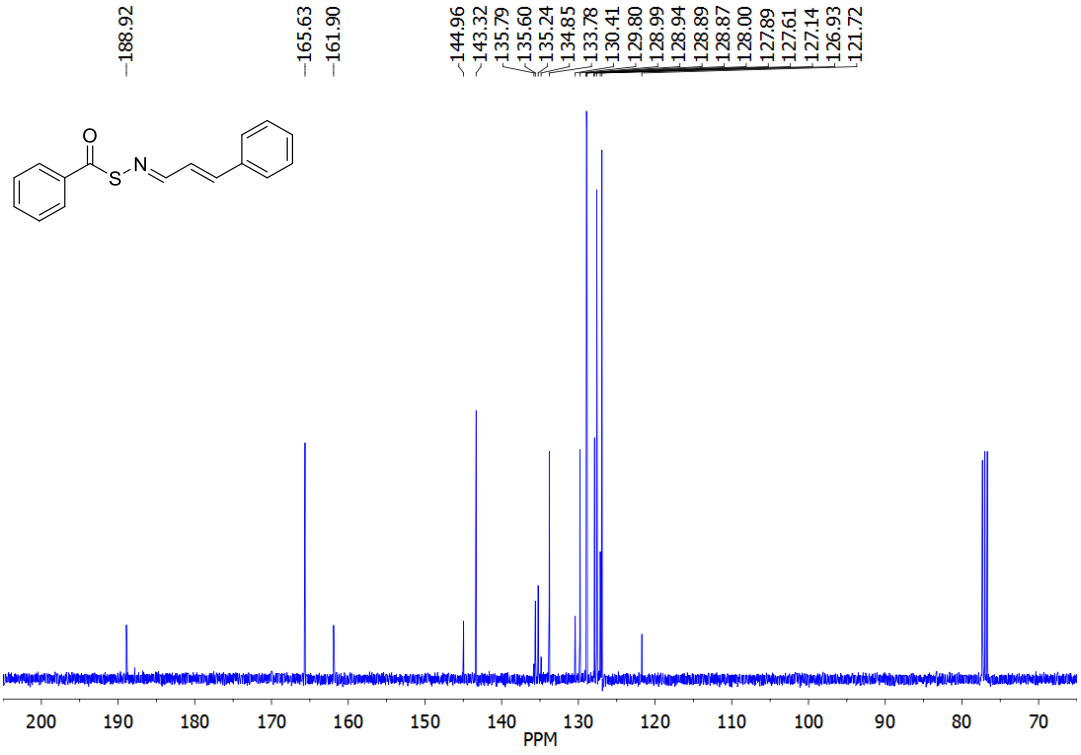

^{1}H NMR (400 MHz, $CDCl_3$) spectrum of 1g

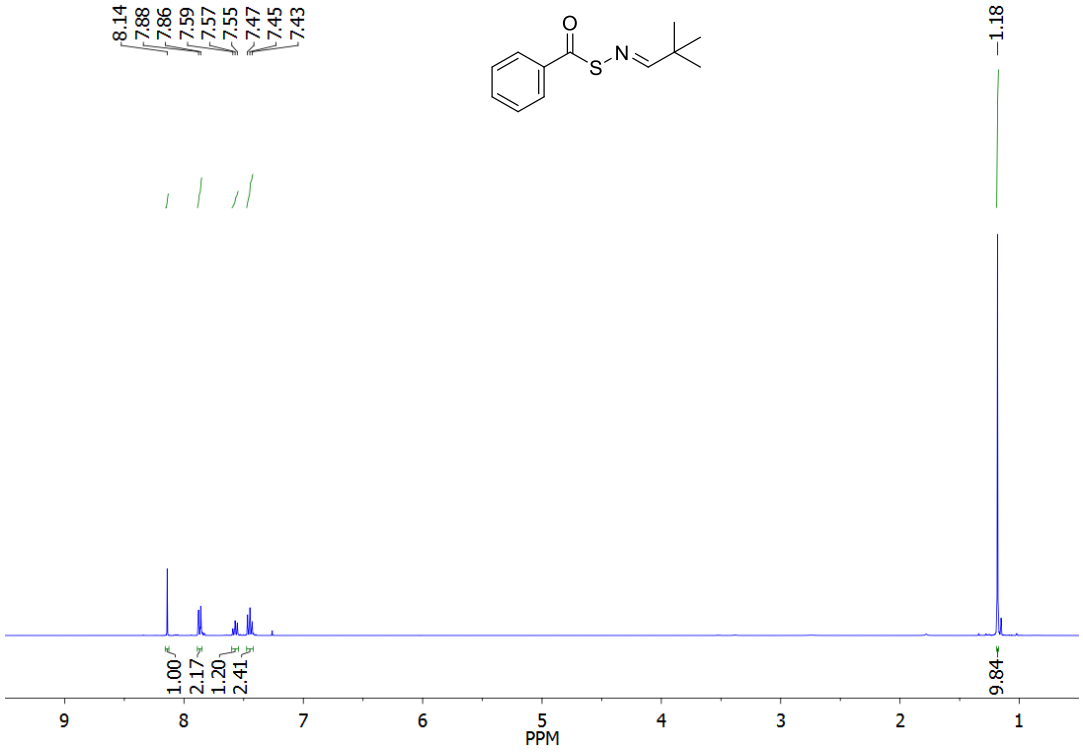

^{13}C NMR (400 MHz, $CDCl_3$) spectrum of 1g

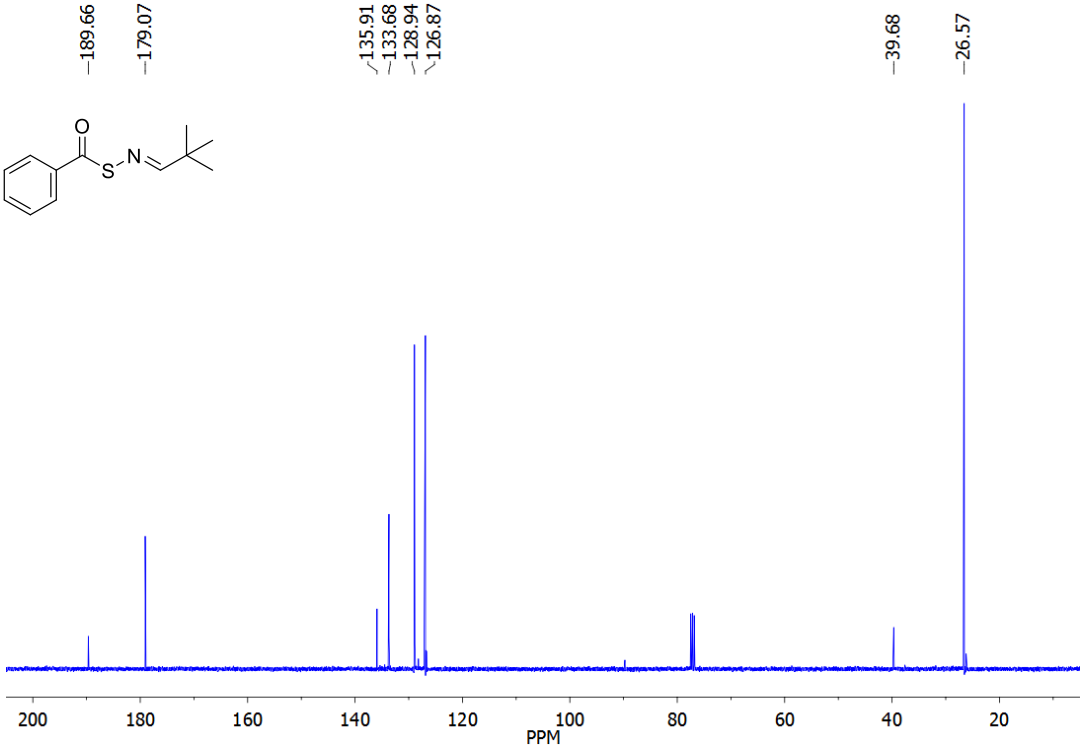

^{1}H NMR (400 MHz, $CDCl_3$) spectrum of 1h

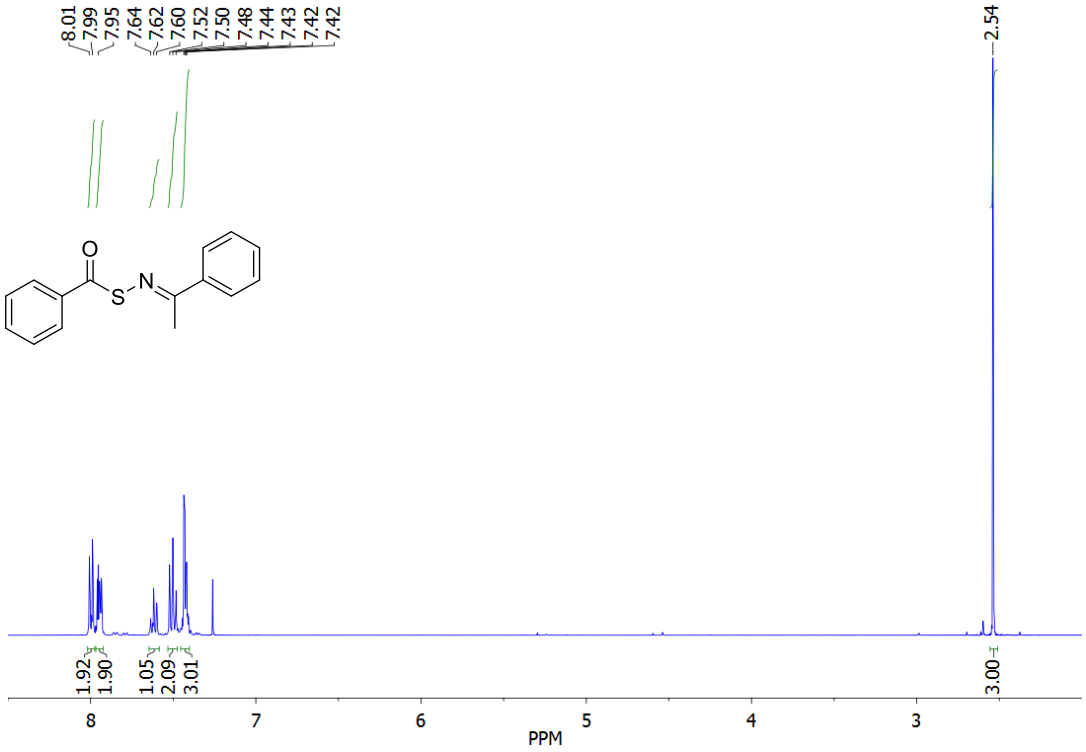

^{13}C NMR (400 MHz, $CDCl_3$) spectrum of 1h

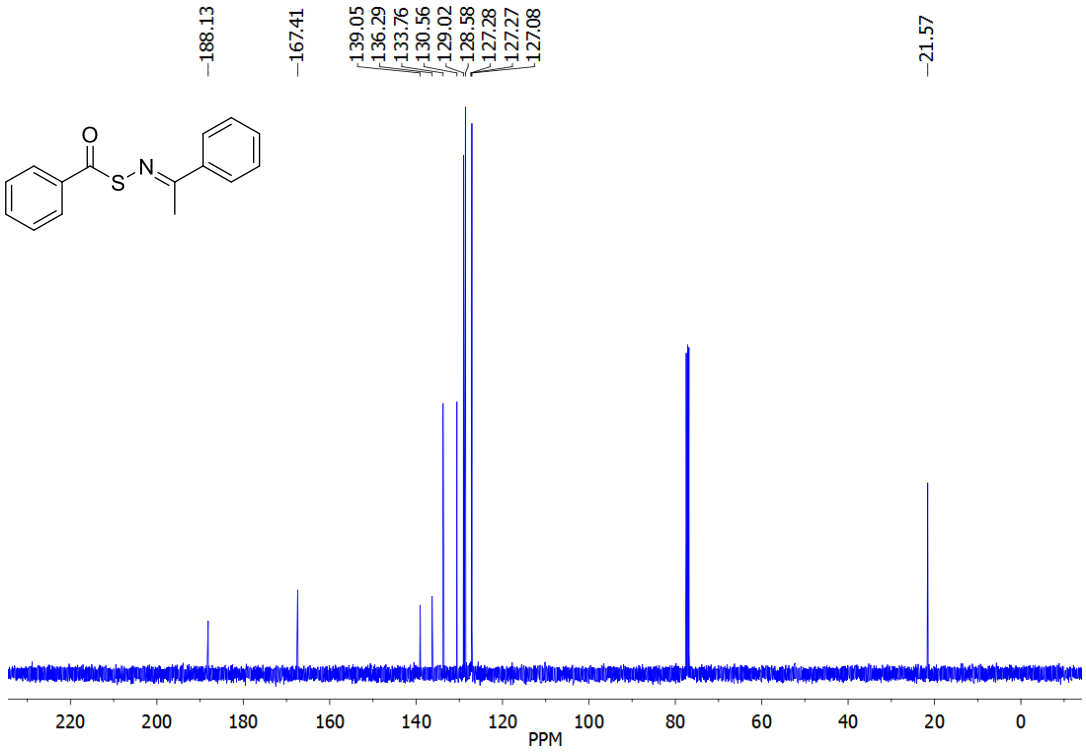

^{1}H NMR (400 MHz, $CDCl_3$) spectrum of 1i

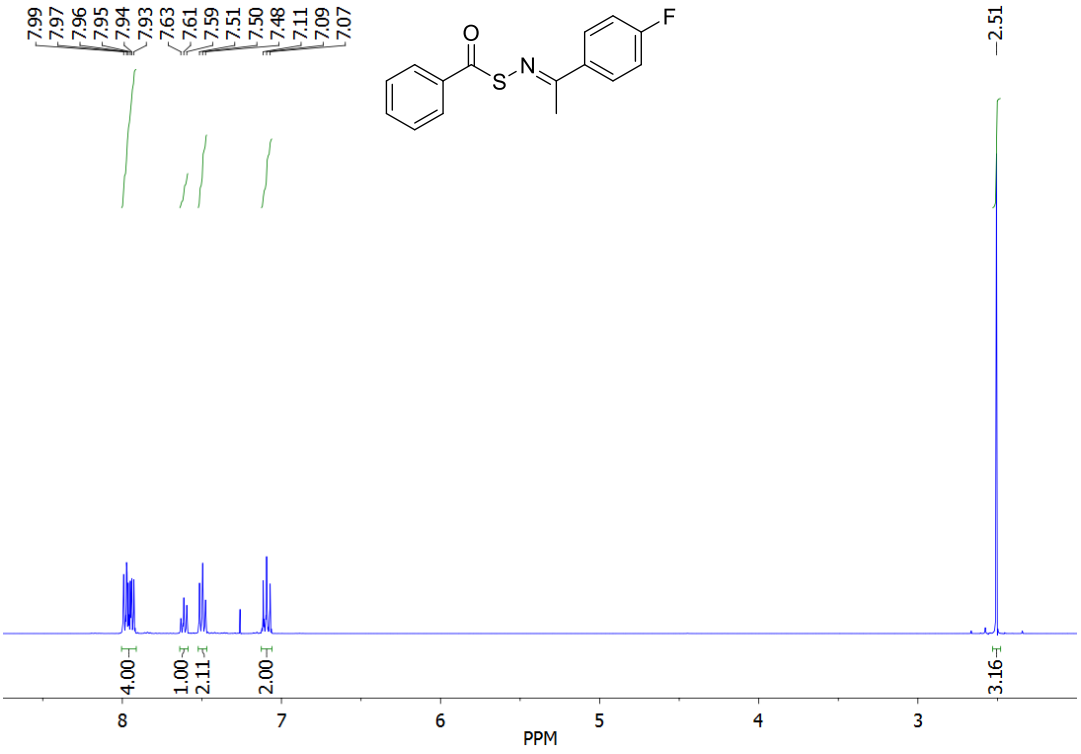

^{13}C NMR (400 MHz, $CDCl_3$) spectrum of 1i

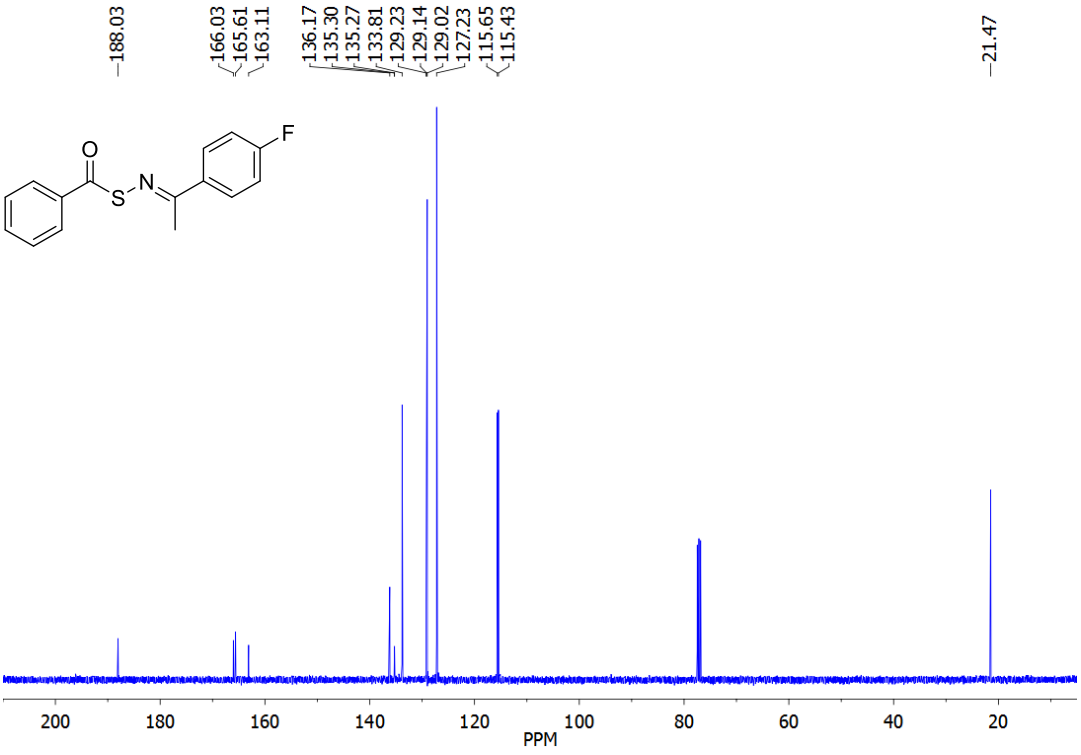

^{1}H NMR (400 MHz, $CDCl_3$) spectrum of 1j

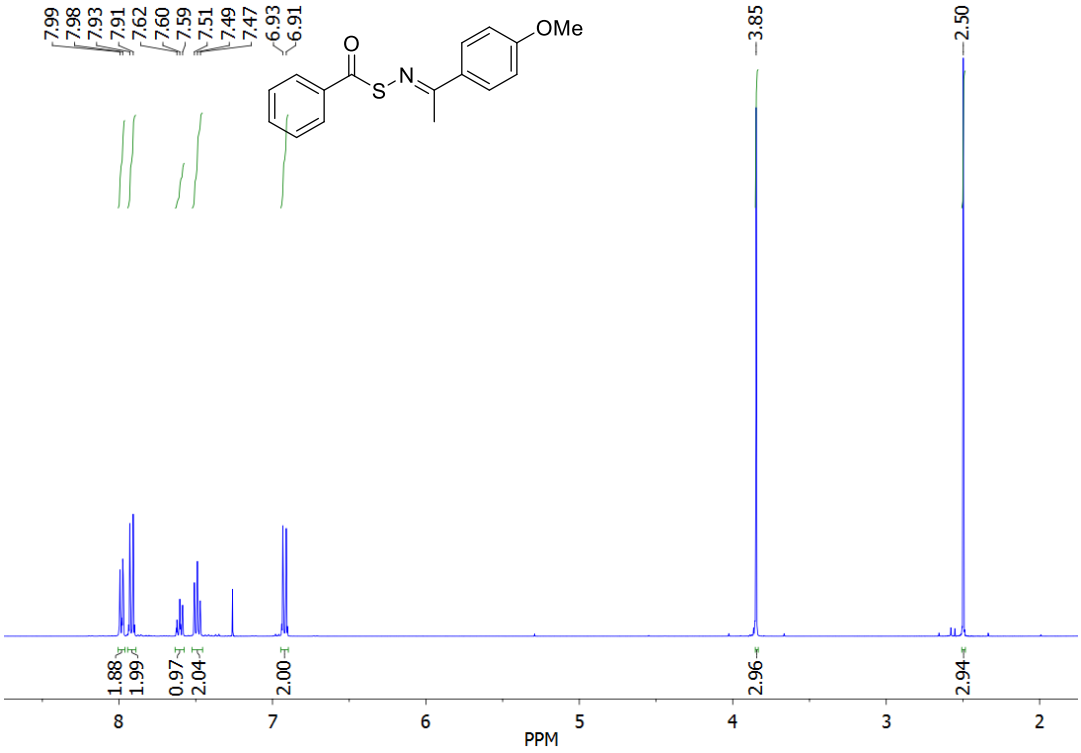

^{13}C NMR (400 MHz, $CDCl_3$) spectrum of 1j

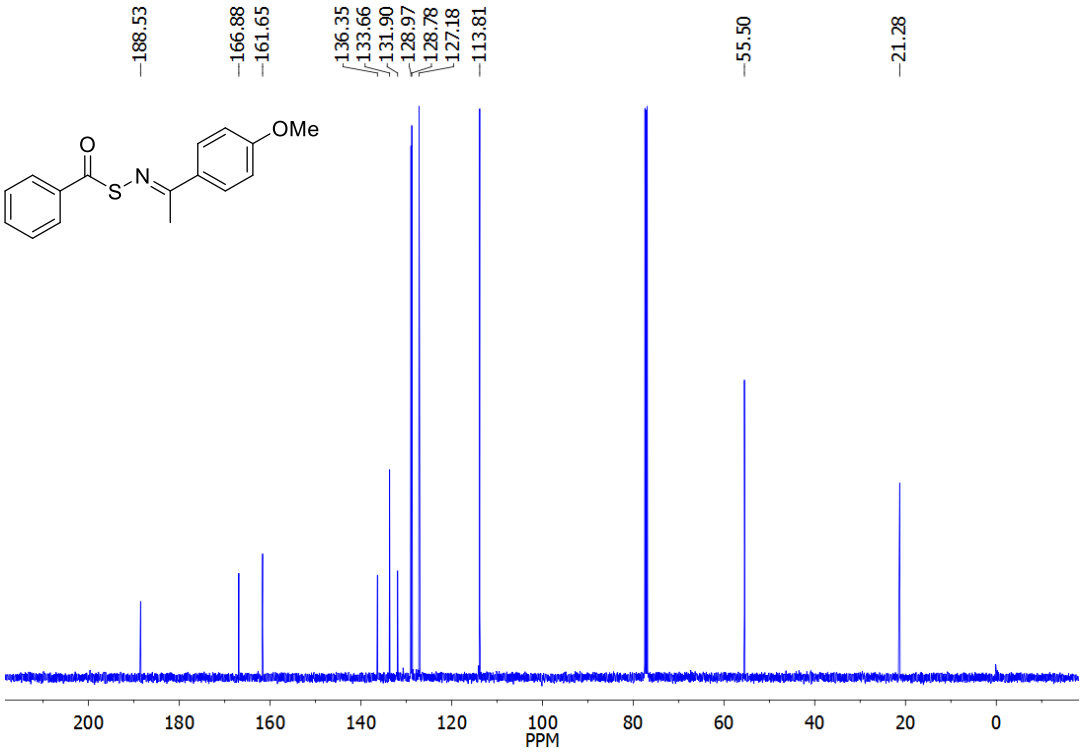

^{1}H NMR (400 MHz, $CDCl_3$) spectrum of 1k

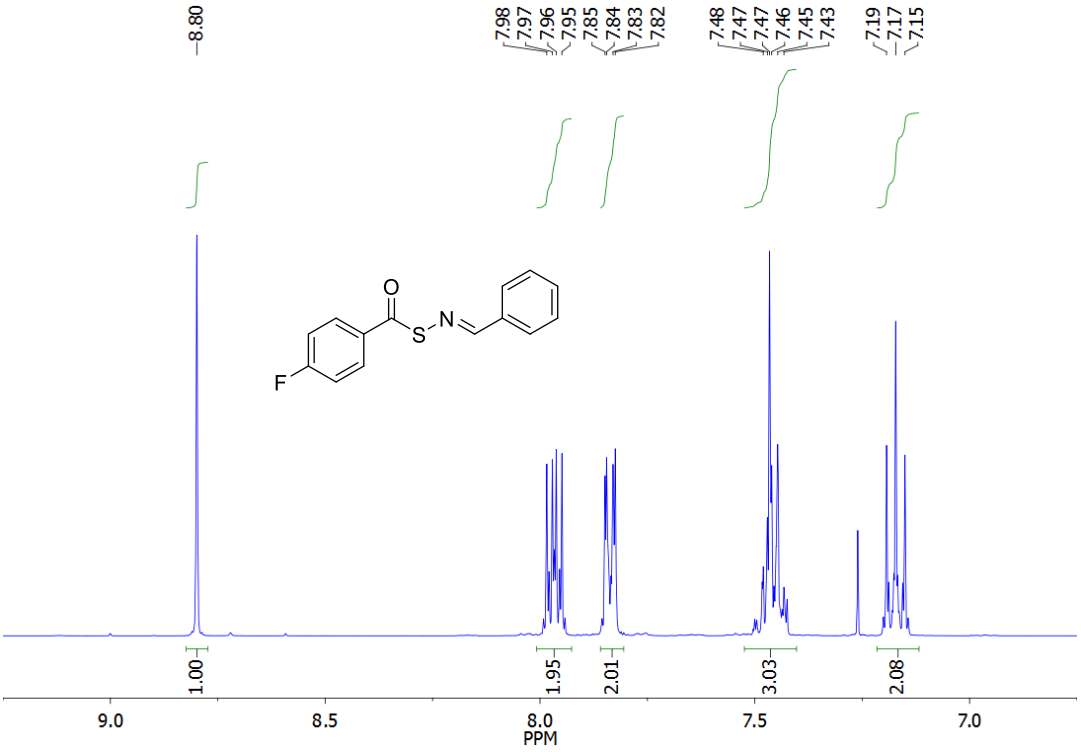

^{13}C NMR (400 MHz, $CDCl_3$) spectrum of 1k

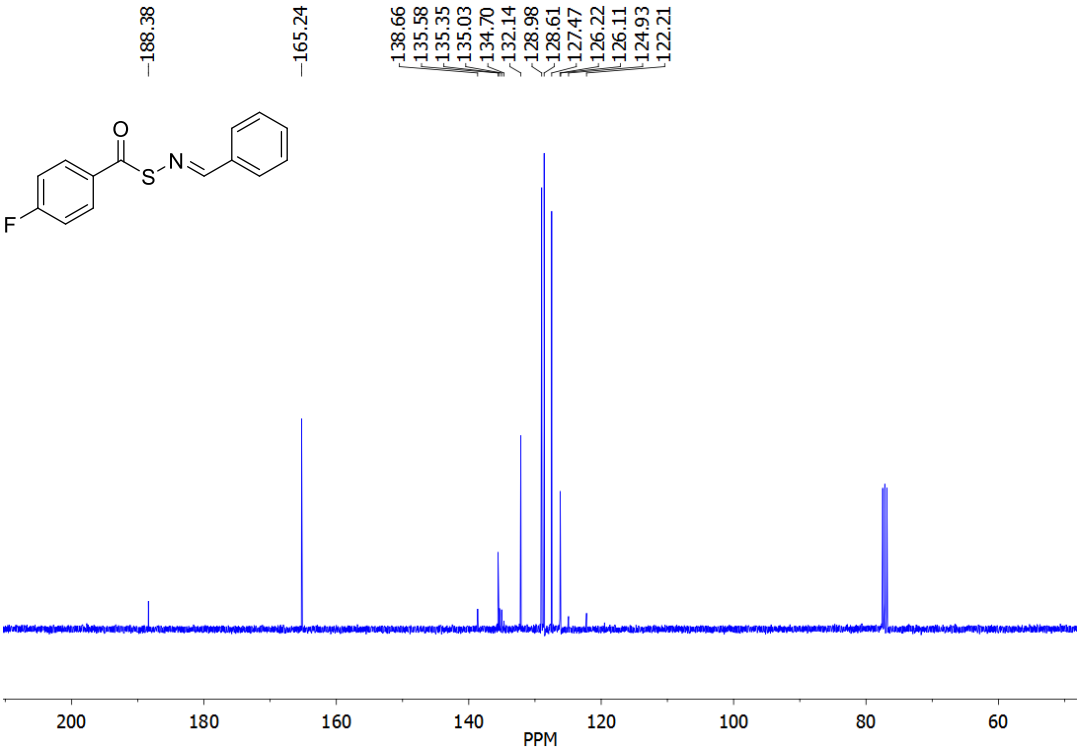

^{1}H NMR (400 MHz, $CDCl_3$) spectrum of 1l

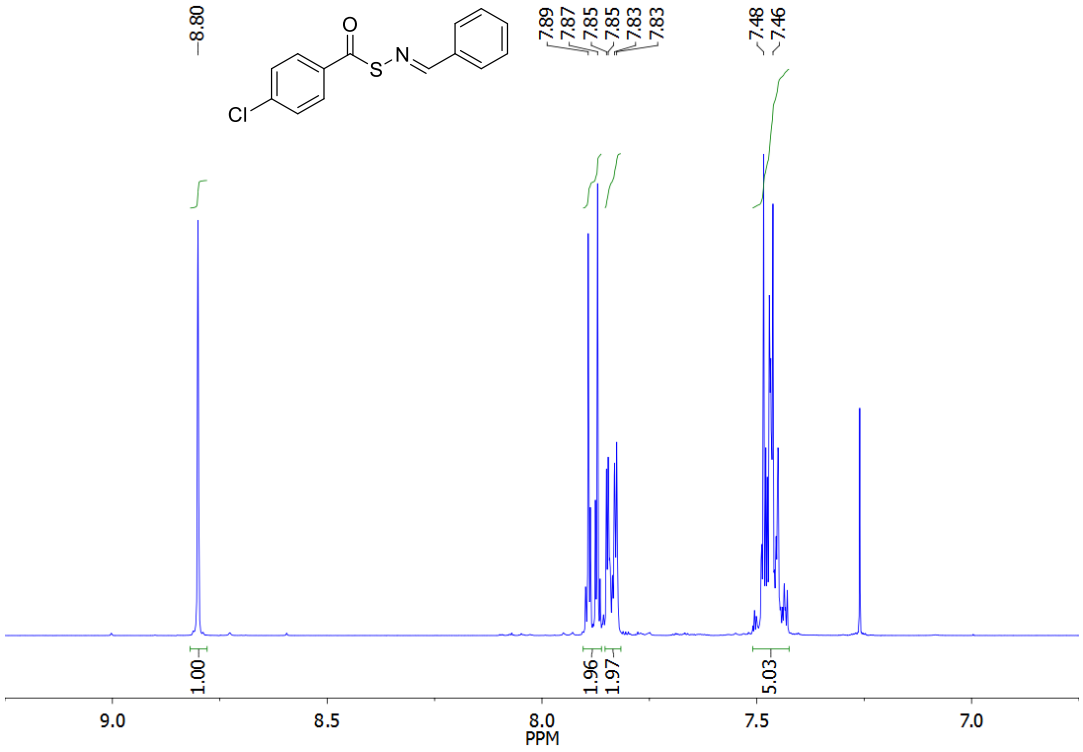

^{13}C NMR (400 MHz, $CDCl_3$) spectrum of 1l

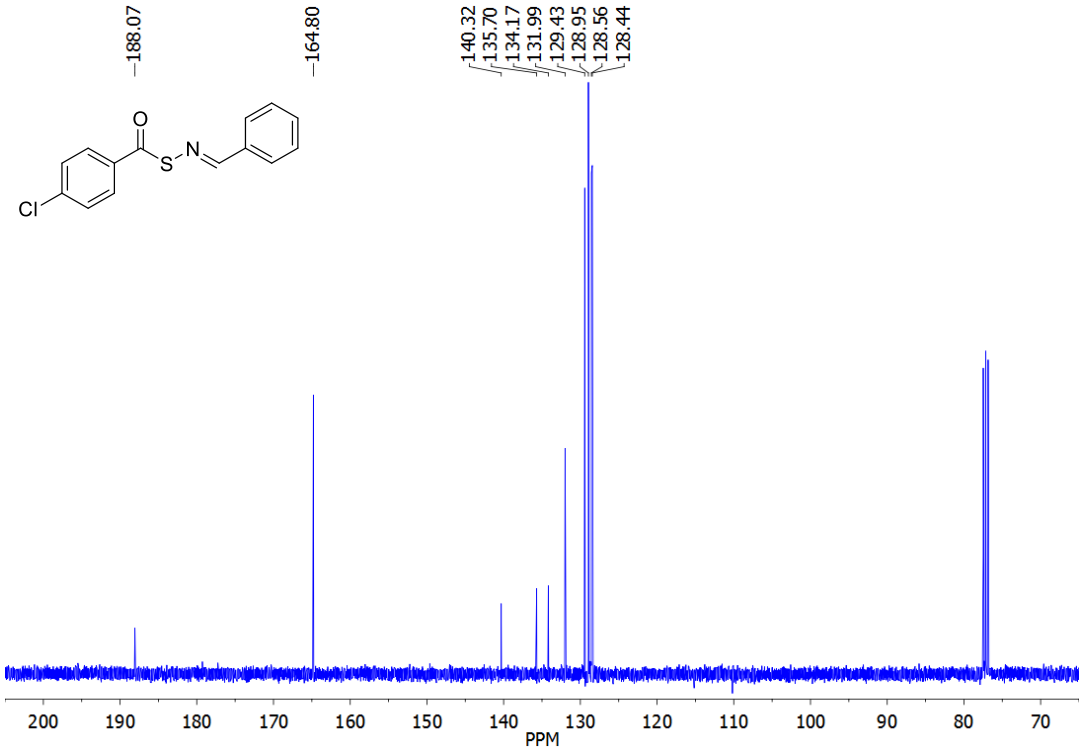

^{1}H NMR (400 MHz, $CDCl_3$) spectrum of 1m

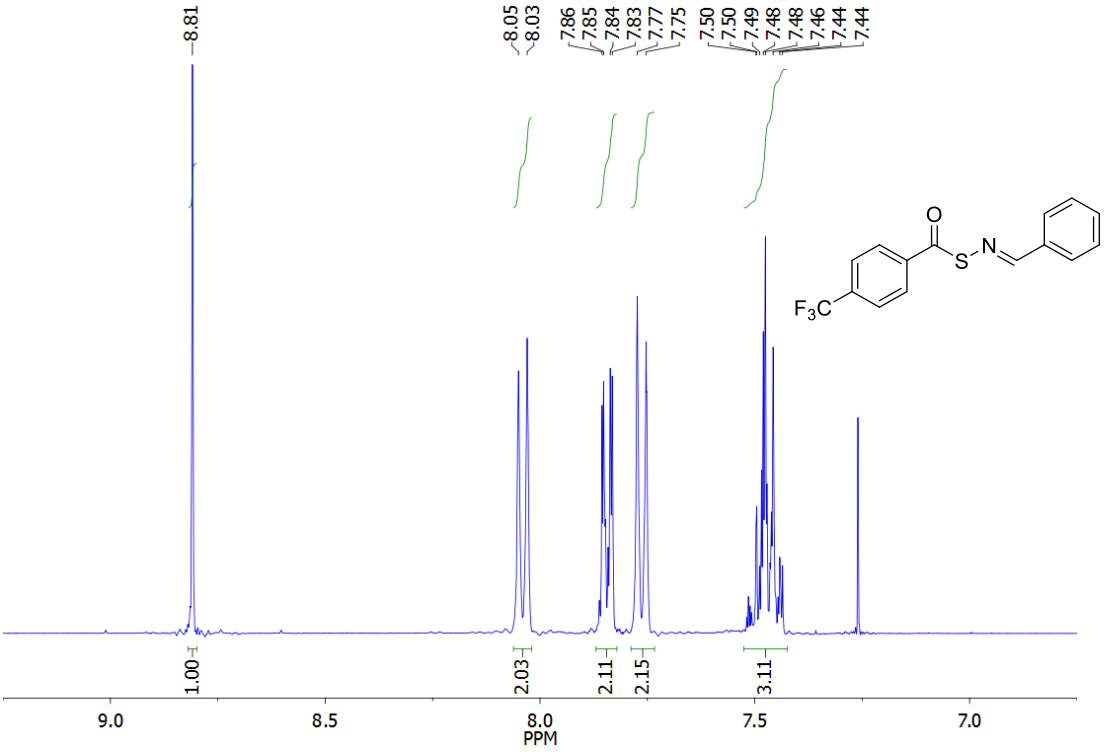

^{13}C NMR (400 MHz, $CDCl_3$) spectrum of 1m

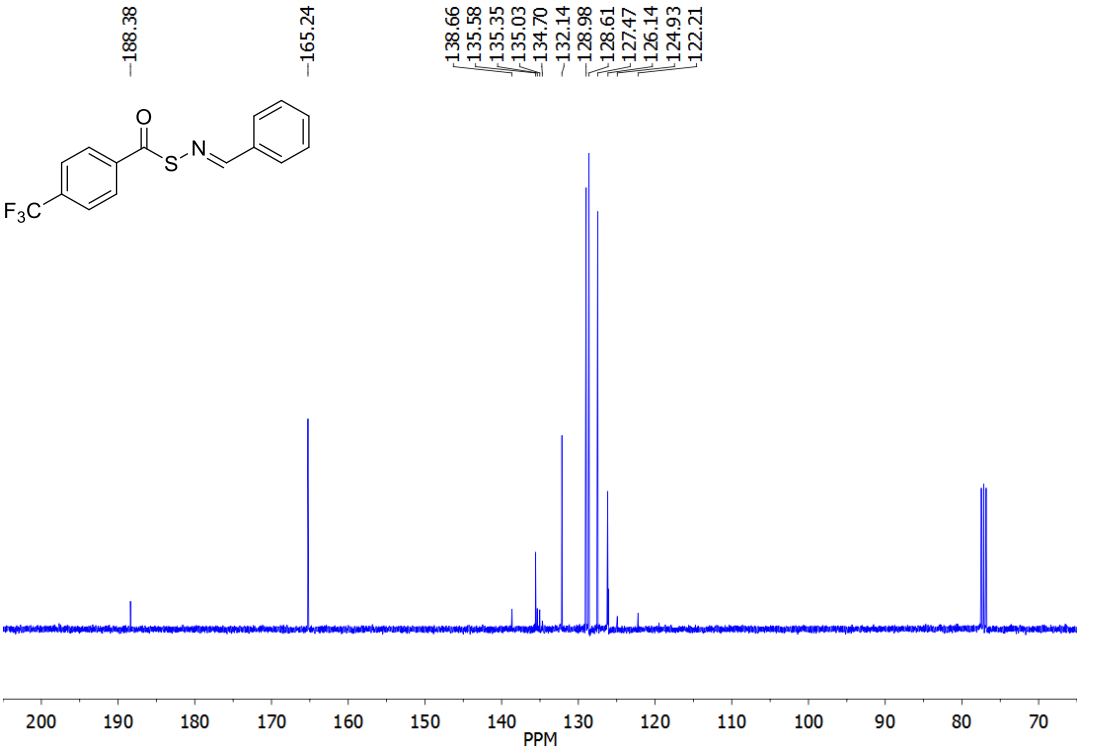

^{1}H NMR (400 MHz, $CDCl_3$) spectrum of 1n

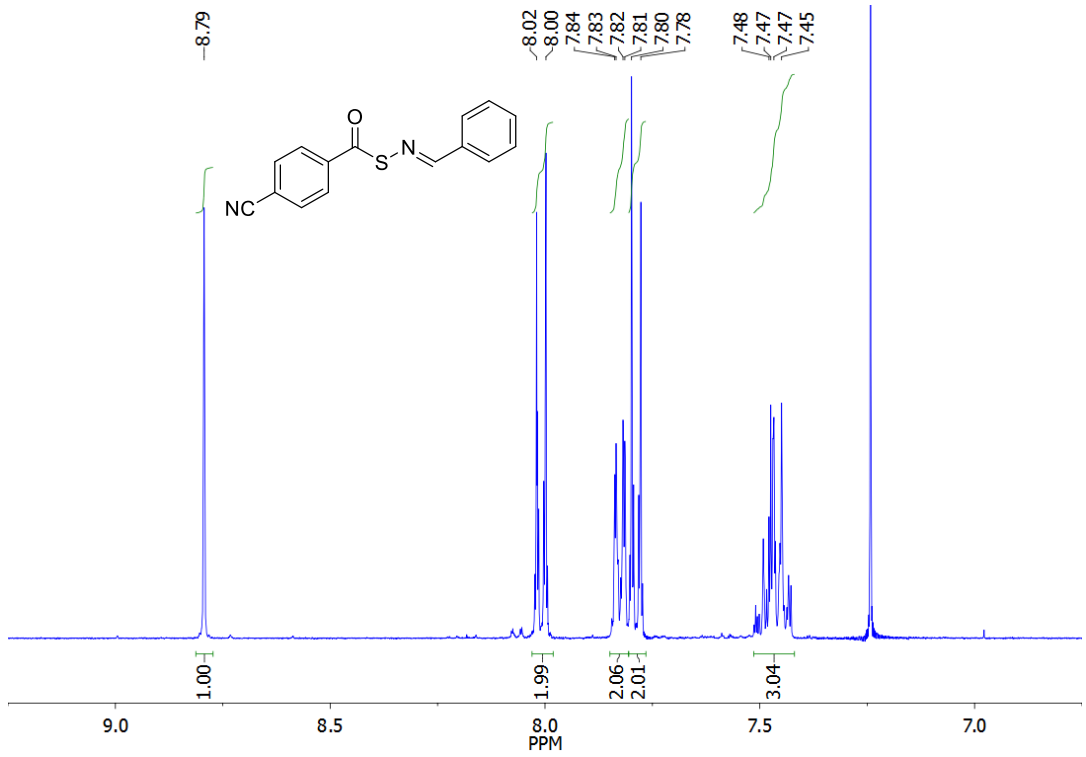

^{13}C NMR (400 MHz, $CDCl_3$) spectrum of 1n

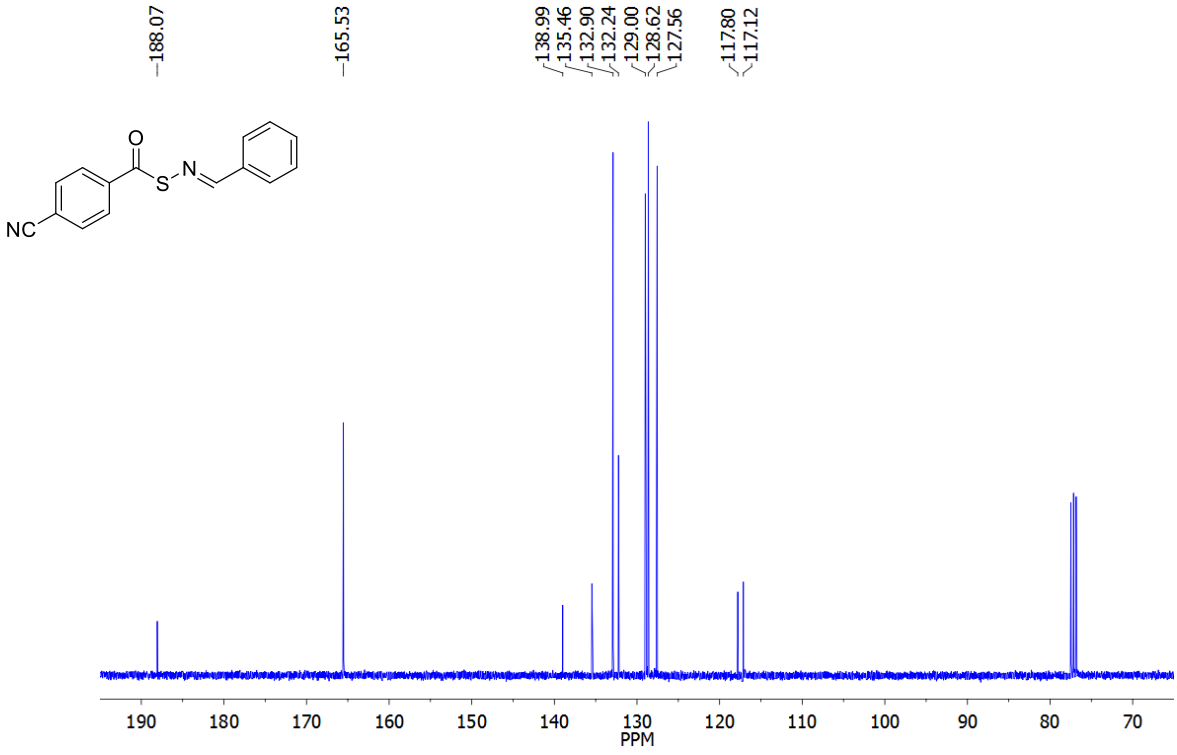

^{1}H NMR (400 MHz, $CDCl_3$) spectrum of 1o

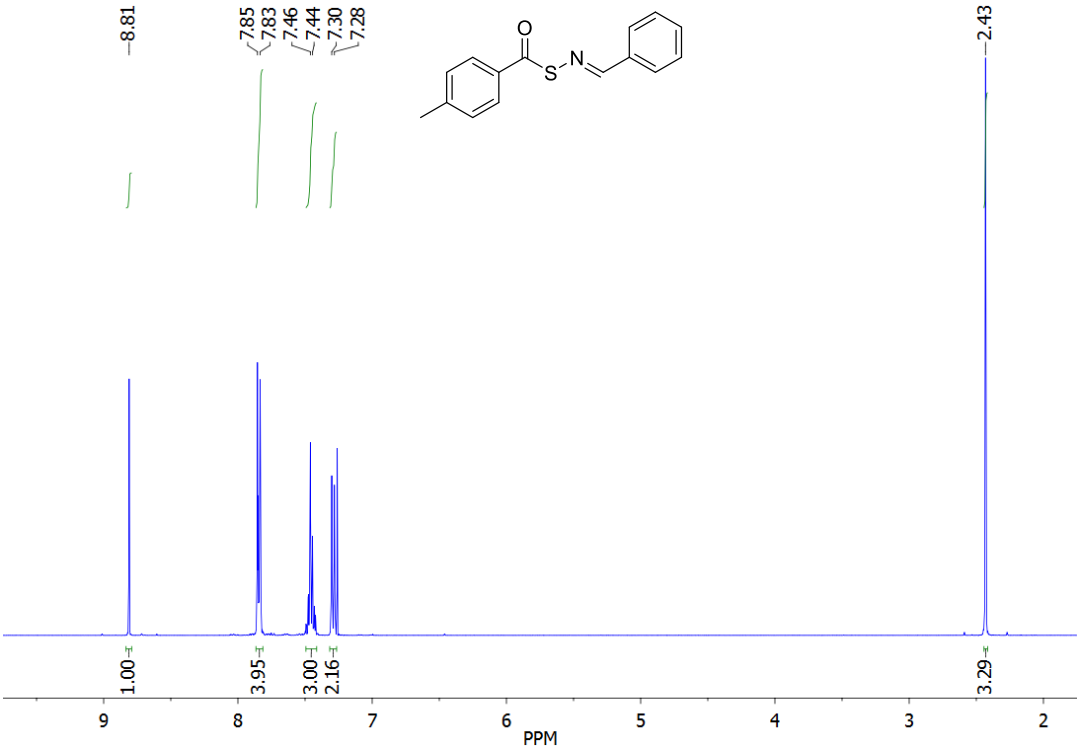

^{13}C NMR (400 MHz, $CDCl_3$) spectrum of 1o

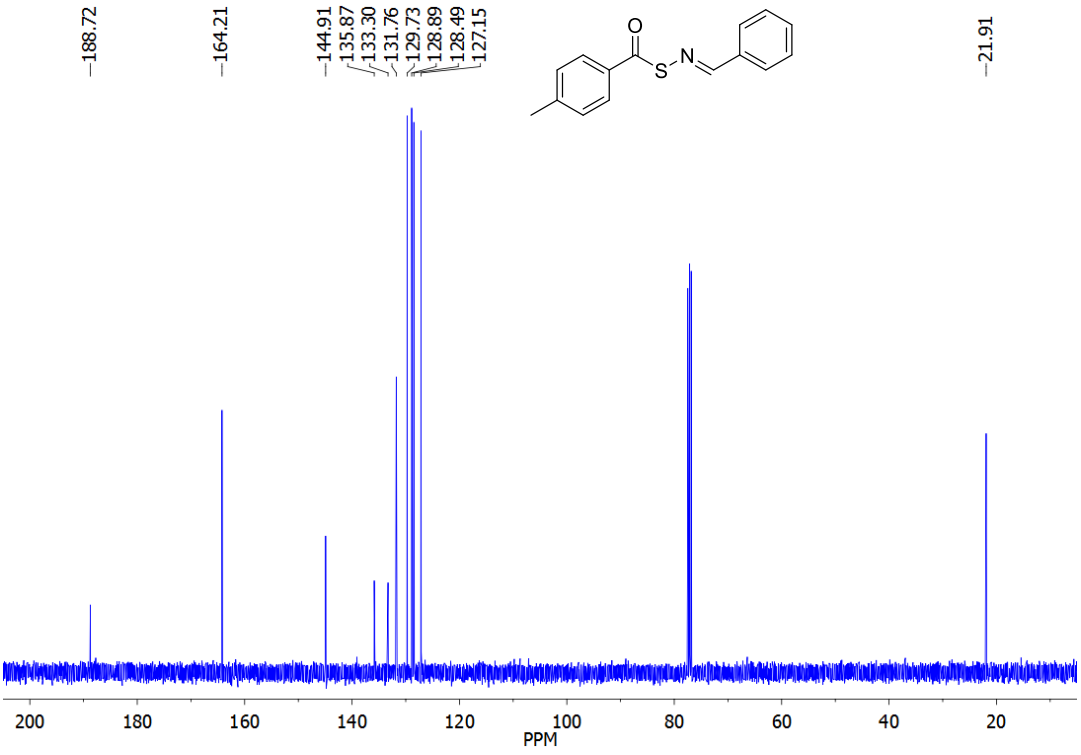

^{1}H NMR (400 MHz, $CDCl_3$) spectrum of 1p

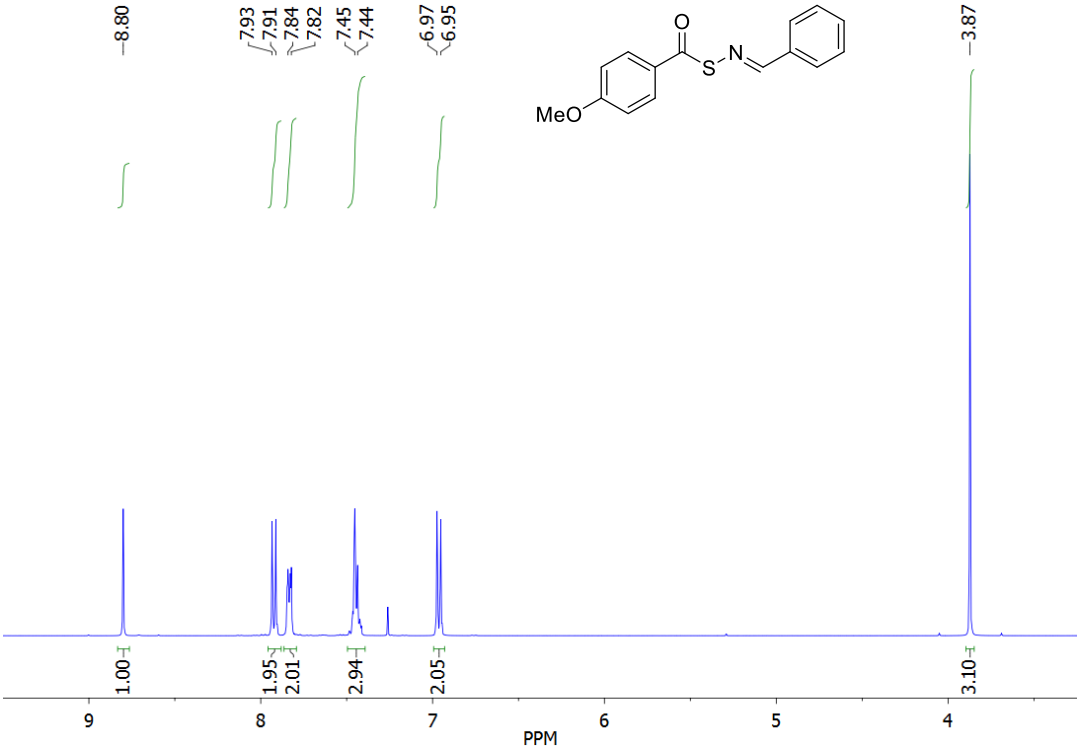

^{13}C NMR (400 MHz, $CDCl_3$) spectrum of 1p

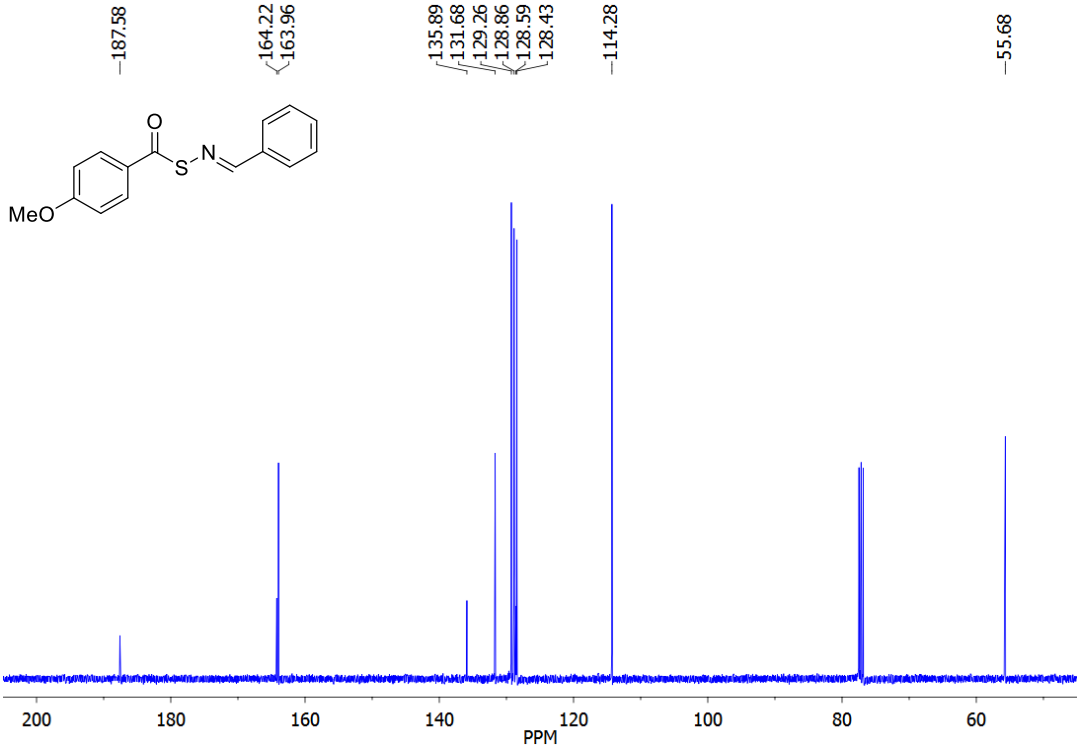

^{1}H NMR (400 MHz, D_2O) spectrum of *N*-benzoylcysteine.

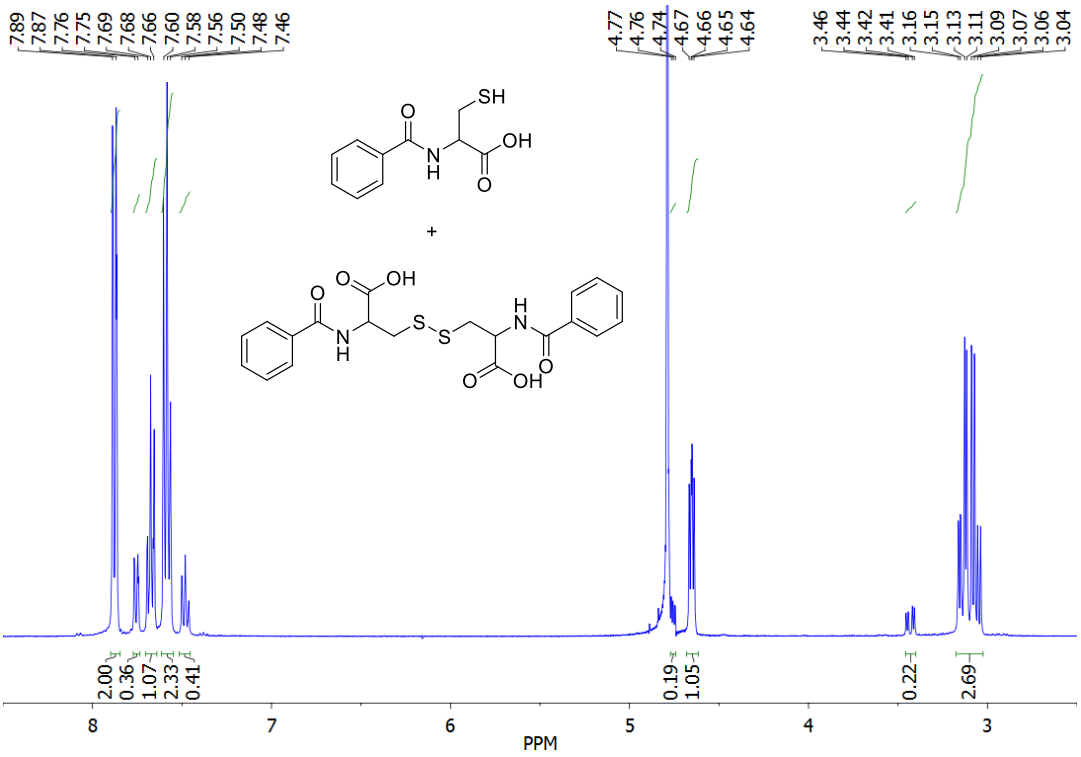

^{13}C NMR (400 MHz, D_2O) spectrum of *N*-benzoylcysteine.

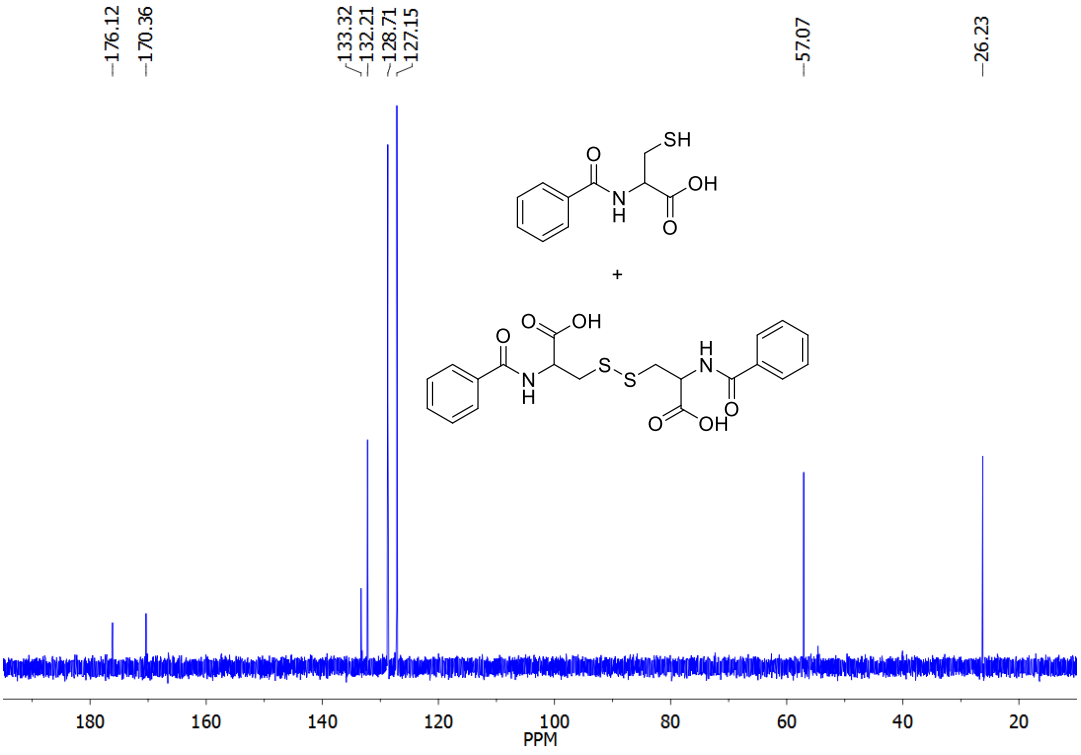

^{1}H NMR (400 MHz, DMSO-d_6) spectrum of 2-Phenylthiazolidine-4-carboxylic acid.

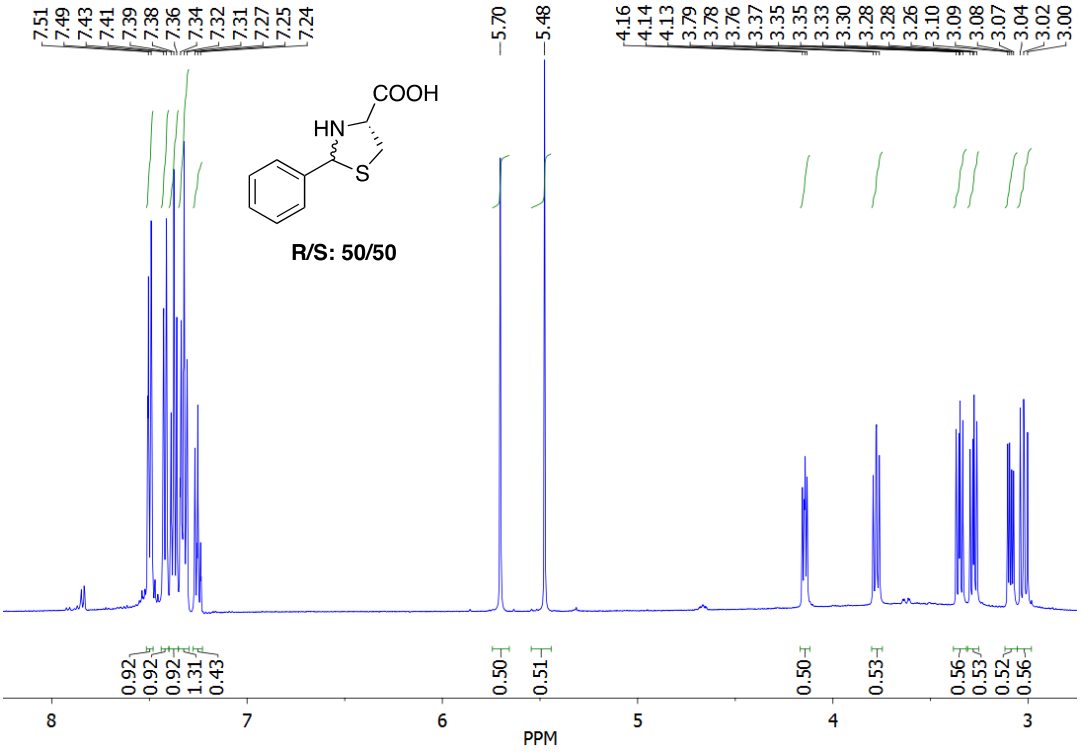

^{13}C NMR (400 MHz, DMSO-d_6) spectrum of 2-Phenylthiazolidine-4-carboxylic acid.

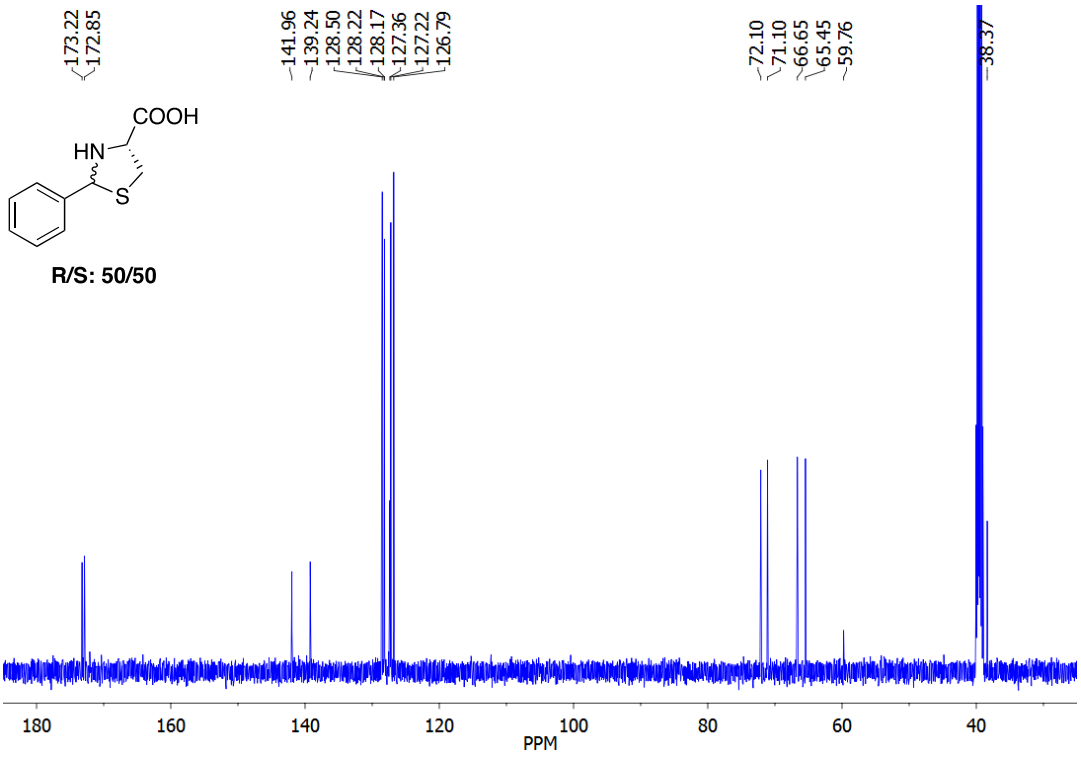

^{1}H NMR (400 MHz, D_2O) spectrum of cystine (impure).

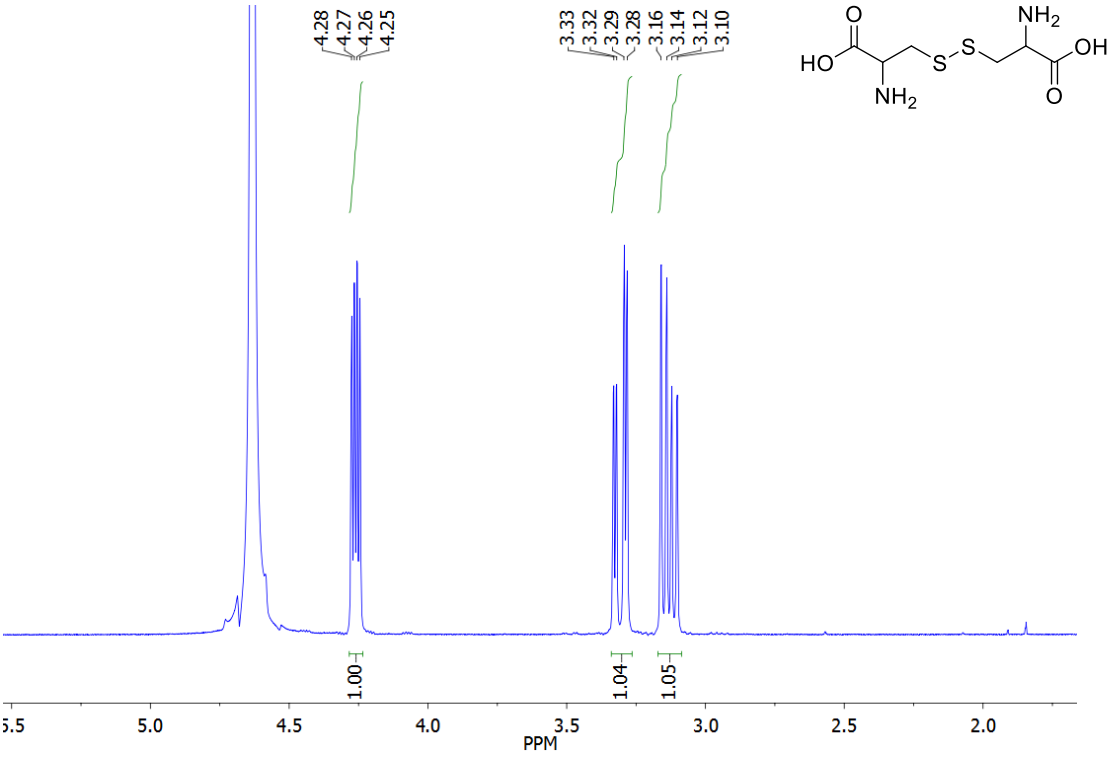

^{13}C NMR (400 MHz, D_2O) spectrum of cystine (impure).

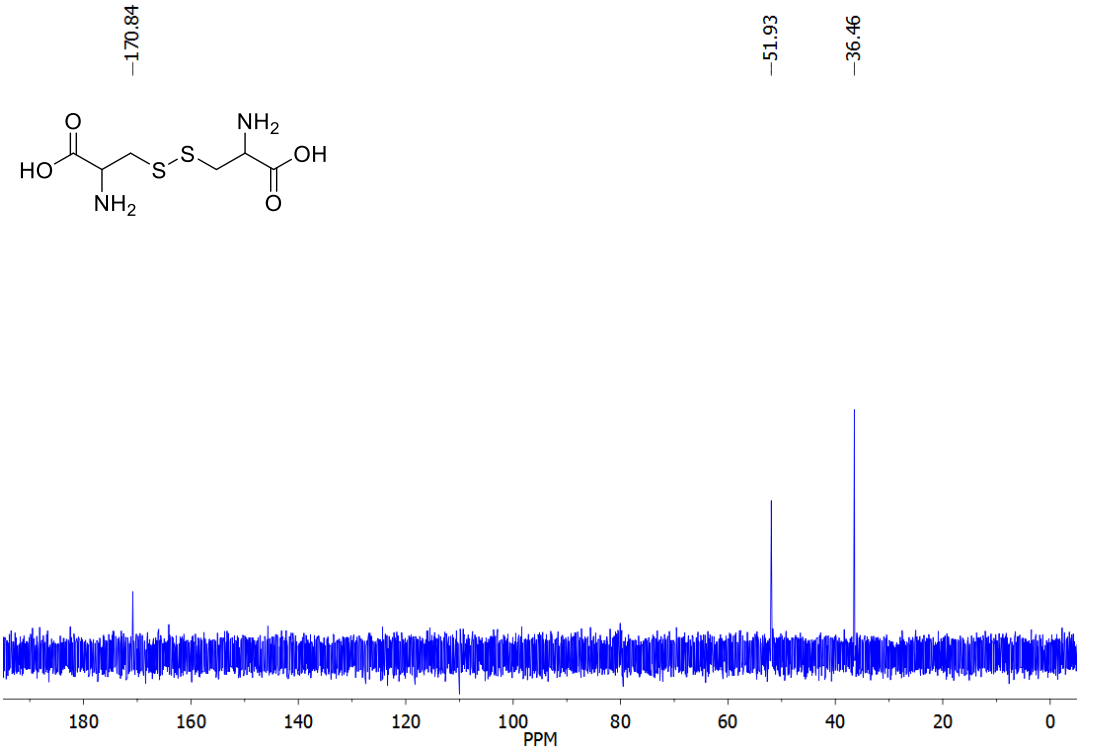

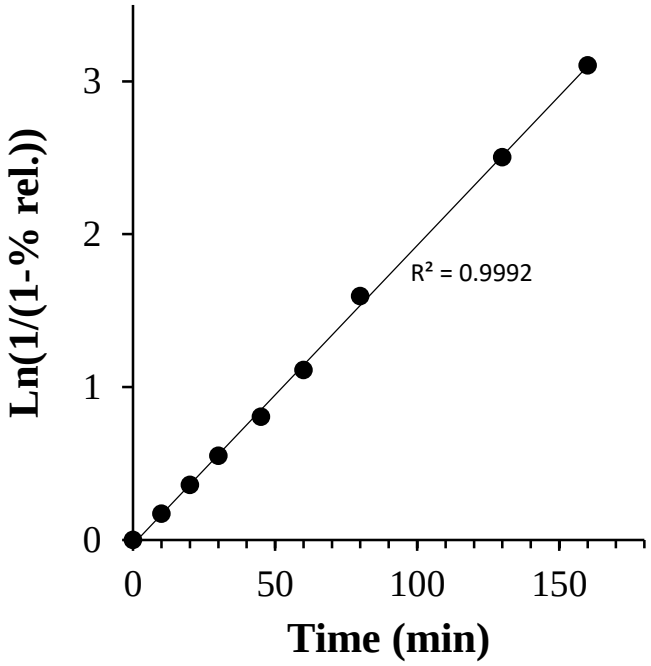

Fig 3S7. Methylene Blue Kinetics for Compound 1a (R_2 = H).

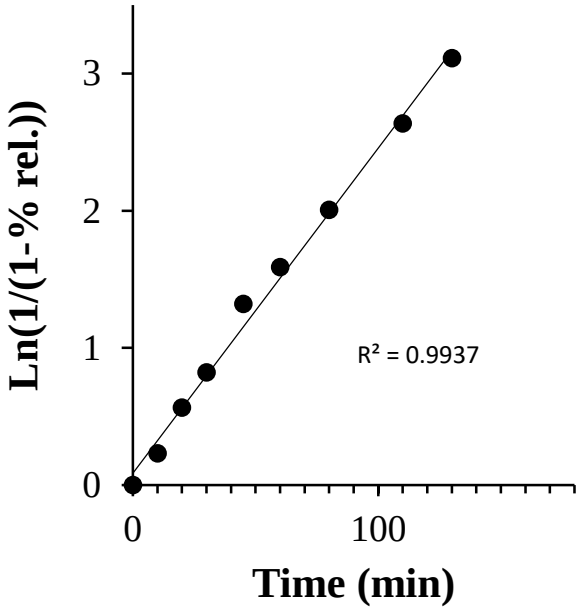

Fig 3S8. Methylene Blue Kinetics for Compound 1k (R_2 = F).

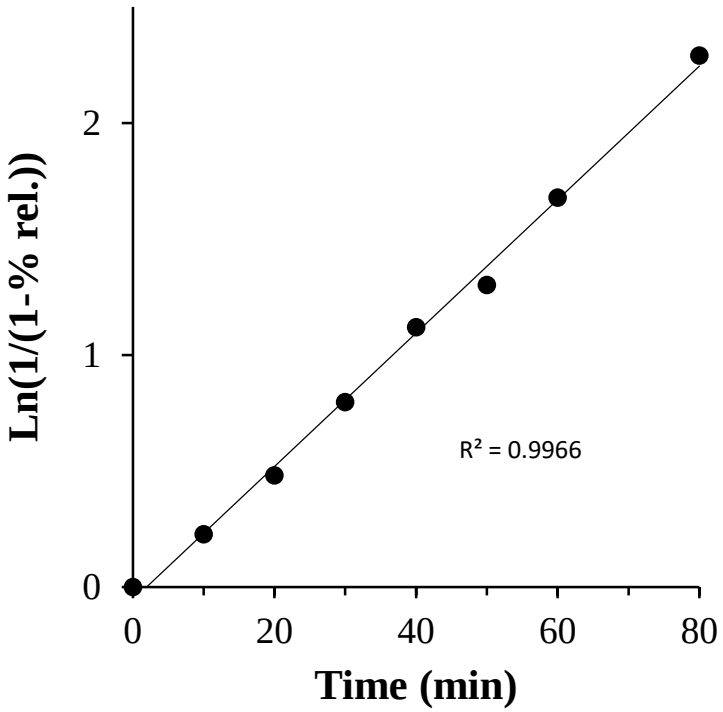

Fig 3S9. Methylene Blue Kinetics for Compound 1l (R_2 = Cl).

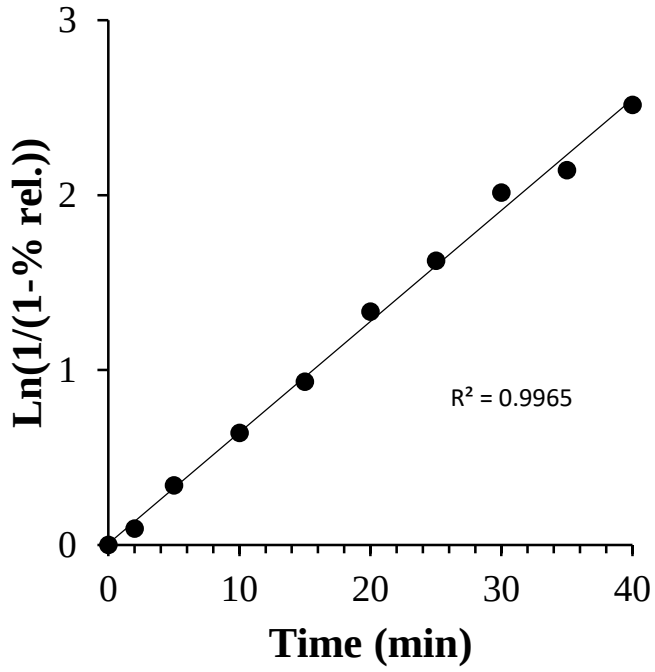

Fig 3S10. Methylene Blue Kinetics for Compound 1m (R_2 = CF_3).

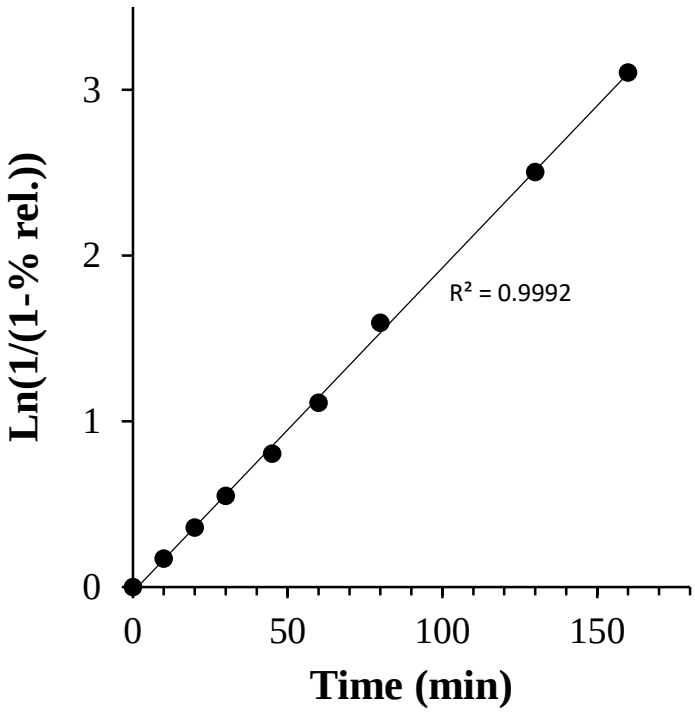

Fig 3S11. Methylene Blue Kinetics for Compound 1n (R_2 = CN).

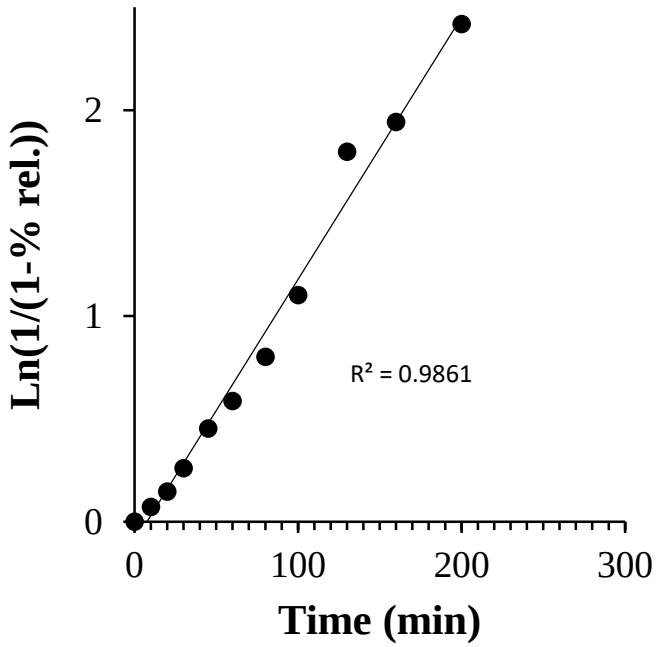

Fig 3S12. Methylene Blue Kinetics for Compound 1o (R_2 = CH_3).

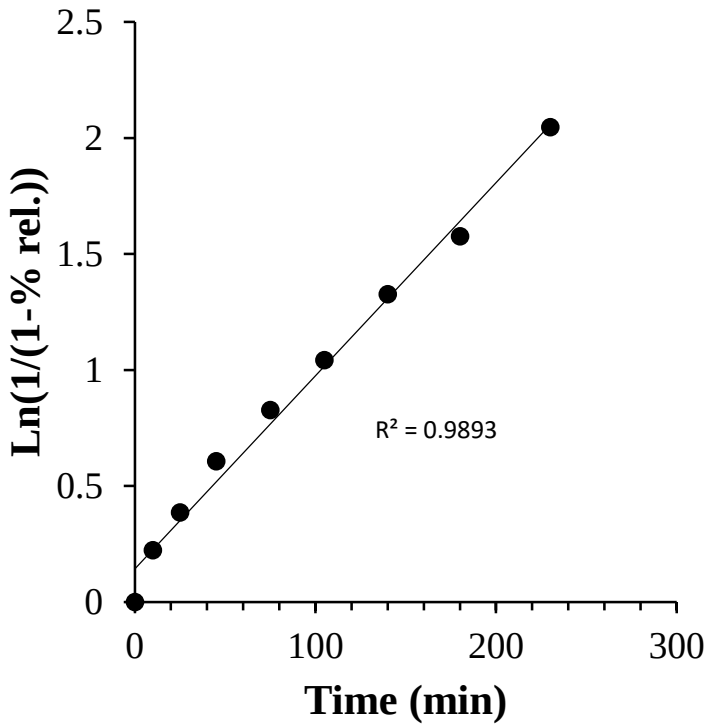

Fig 3S13. Methylene Blue Kinetics for Compound 1p ($R_2 = CH_3$).

References

(1) Raasch, M. S. *J. Org. Chem.* 1972, *37*, 3820.

(2) Toriyama, M.; Kamijo, H.; Motohashi, S.; Takido, T.; Itabashi, K. *Phosphorus, Sulfur, and Silicon and the Related Elements* 2003, *178*, 1661.

(3) Yung, T. W. K. S., M. P. *Tet. Lett.* 1990, *31*, 5935.

(4) Kleinman, W. A.; Richie, J. P. *Biochem. Pharmacol.* 2000, *60*, 19.

(5) Andersson, A.; Lindgren, A.; Hultberg, B. *Clin. Chem. (Washington, D. C.)* 1995, *41*, 361.

(6) Bald, E.; Chwatko, G.; Głowacki, R.; Kuśmierek, K. *Journal of Chromatography A* 2004, *1032*, 109.

(7) Jones, D. P.; Mody Jr, V. C.; Carlson, J. L.; Lynn, M. J.; Sternberg Jr, P. *Free Radical Biology and Medicine* 2002, *33*, 1290.

(8) Hasegawa, U.; van der Vlies, A. J.; Simeoni, E.; Wandrey, C.; Hubbell, J. A. *J. Am. Chem. Soc.* 2010, *132*, 18273.

(9) Seki, M.; Mori, Y.; Hatsuda, M.; Yamada, S. *J. Org. Chem.* 2002, *67*, 5527.

Chapter 4. Functionalization of Methacrylate Polymers with Thiooximes: A Robust Post-Polymerization Modification Reaction and a Method for the Preparation of H_2S-Releasing Polymers

4.1. Authors

Jeffrey C. Foster,[†] John B. Matson[†]

[†]Department of Chemistry and Macromolecules Innovation Institute, Virginia Tech, Blacksburg, Virginia 24061, United States

4.2. Abstract

The effectiveness of thiooxime formation as a post polymerization modification reaction was evaluated. To this end, methacrylate polymers bearing pendant aldehyde functionality were prepared via reversible addition fragmentation chain-transfer (RAFT) polymerization of 2-(4-formylbenzoyloxy)ethyl methacrylate. Polymer side-chain derivatizations with *tert*-butylhydrazide, *O*-benzylhydroxylamine, and *S*-aroylthiohydroxylamine (SATHA) were shown to be quantitative, forming the corresponding hydrazone, oxime, and thiooxime, respectively. This work represents the first example of thiooxime formation on polymers, achieving high conversions under mild conditions. In response to thiol functionality *S*-aroylthiooximes decompose to release H_2S—an endogenous signaling gas with significant therapeutic potential. H_2S release from the

resulting thiooxime-functionalized polymers was observed in the presence of cysteine and glutathione; moreover, degradation kinetics could be controlled by tuning the electronics at the *para* position of the corresponding SATHA-derived ring. In addition to generating polymers capable of controlled H_2S release, this methodology also enables thiol-triggered degradation of pendant functionalities at neutral pH.

4.3. Introduction

Recent advances in synthetic polymer chemistry allow for the construction of complex macromolecules, giving control over such parameters as topology, functionality, molecular weight (MW), and dispersity (Đ). However, many polymerization methodologies exhibit less control when sterically bulky, highly aggregating, or incompatible functional groups are incorporated into the monomer or initiator. Post-polymerization modification of polymers is a powerful tool, as it may enable the incorporation of functionalities that are incompatible with polymerization conditions.[1-4] In addition, post-polymerization modification reactions avoid the need to optimize polymerization conditions for new monomers, facilitating the comparison of differently functionalized polymers without the complication of variable backbone MW and Đ. However, careful consideration is needed to select the appropriate chemistry to modify polymers, as neighboring group effects and steric factors can hinder post-polymerization modification reactions.

Click chemistry is particularly well suited for post-polymerization modification, as this class of reactions is atom efficient, broad in scope, affords high isolated yields, and can be conducted under relatively mild conditions.[5] A number of click reactions have been applied for post polymerization modification, including copper-catalyzed azide-alkyne Huisgen cycloaddition, thiol-ene coupling, Diels-Alder cycloaddition, oxime condensation, Michael addition, and disulfide exchange via

pyridyl disulfide.[6-10] This class of robust reactions has been utilized in post-polymerization modification to couple telechelic polymers with differently functionalized chain ends (yielding di- and tri-block copolymers),[11] to prepare graft copolymers via "grafting from" and "grafting to" methodologies,[12] to conjugate synthetic polymers to biomacromolecules such as proteins and polysaccharides,[13] to crosslink polymer samples,[14] and to achieve complex topologies including core-crosslinked star polymers,[15] hyperbranched polymers,[16] and dendrimers.[17]

Thiooxime chemistry represents a novel approach for the post-polymerization modification of functional polymers. Analogous to the oxime functional group, thiooximes are prepared via the reaction of a thiohydroxylamine (R-S-NH_2) with an aldehyde/ketone.[18,19] The thiooxime formation reaction can be conducted under mild conditions and affords high isolated yields in many cases. In particular, *S*-aroylthiooximes (SATOs) exhibit high hydrolytic stability at physiological pH and decompose upon reaction with thiols.[19] In contrast to hydrazones and oximes, which can be degraded by changing pH, or other stimuli-responsive linkages that can be broken by external triggers such as irradiation or redox chemistry, *S*-aroylthiooximes may offer the possibility of thiol-driven decomposition of polymer side-chain linkages. An additional potential benefit of post-polymerization modification using SATOs is that thiol-driven decomposition of SATOs generates H_2S, which is an endogenous signaling gas with vast therapeutic potential.[20-22]

H_2S belongs to a group of signaling gases known as gasotransmitters. These endogenously produced gases (H_2S, nitric oxide, and carbon monoxide) are vital signaling molecules and possess biological activities that can be exploited in therapeutic applications. For example, H_2S acts to suppress oxidative stress,[23] reduce inflammation,[24] and protect endothelial tissue via vasodilation,[25] among other roles. These in vivo functions are intimately coupled to its local concentration.[26] Therefore, to achieve a specific therapeutic outcome, the gas must be delivered

selectively and at a controlled rate. Several H_2S-releasing functional groups have been discovered, including the versatile SATO moiety, about which we recently reported.[19,27-29] While polymeric materials have been prepared for the capture and release of H_2S formed as a byproduct in a number of industrial processes,[30] to our knowledge no H_2S-releasing synthetic polymers have been reported for potential use in biological applications. Herein, we report the first application of thiooxime formation as a polymer functionalization reaction, and we evaluate the thiol-triggered decomposition of the SATO group as a route to H_2S-releasing polymers with tunable kinetics.

4.4. Materials and Methods

Materials. All reagents were obtained from commercial vendors and used as received unless otherwise stated. The chain transfer agent 4-cyano-4-(phenylcarbonothioylthio)pentanoic acid (**CTA1**) was prepared as previously reported.[31] *S*-Aroylthiohydroxylamines (SATHAs) were prepared according to a literature procedure.[18] 2-(2-Methoxyethoxy)ethyl methacrylate and methyl methacrylate (MMA) were passed through a small column of basic alumina prior to use. Dry DMF was purified by passage through a solvent purification system.

Methods. NMR spectra were measured on Agilent 400 MHz or Bruker 500 MHz spectrometers. ^{1}H and ^{13}C NMR chemical shifts are reported in ppm relative to internal solvent resonances. Yields refer to chromatographically and spectroscopically pure compounds unless otherwise stated. Infrared spectra were obtained on a Varian 670-IR spectrometer. Gel permeation chromatography (GPC) was carried out in THF on two Agilent PLgel 10 μm MIXED-B columns connected in series with a Wyatt Dawn Helios 2 light scattering detector and a Wyatt Optilab Rex refractive index detector. No calibration standards were used, and dn/dc values were obtained by assuming 100% mass elution from the columns. Thiooxime formation reactions were performed in screw-cap 1 dram vials over 3 Å molecular sieves.

Synthesis of 2-(4-formylbenzoyloxy)ethyl methacrylate (FBEMA). A round bottom flask was charged with 4-formylbenzoic acid (4.44 g, 29.6 mmol), EDC (5.67 g, 29.6 mmol), 4-(dimethylamino)pyridinium 4-toluenesulfonate (726 mg, 2.46 mmol), and 100 mL of CH_2Cl_2. This suspension was stirred until the solids dissolved (~10 min). To the flask was added 2-hydroxyethyl methacrylate (3.21 g, 24.7 mmol) via syringe. BHT was added at ~250 ppm to inhibit polymerization. The reaction mixture was stirred at room temperature for 14 h. After this time, the solvent was removed by rotary evaporation, and the resulting oil was dissolved in diethyl ether (100 mL). 1N HCl (50 mL) was poured into the flask to dissolve the remaining residue. The liquids were transferred to a separatory funnel, the water layer was removed and discarded, and the organic layer was washed with 1N HCl (2 x 50 mL), satd. $NaHCO_3$ (3 x 50 mL), and brine (1 x 50 mL). The organic layer was dried over Na_2SO_4 and rotovapped to yield a pale yellow oil. The oil was placed in the freezer at -20 ˚C, where it solidified over 2-4 days. (5.31 g, 82% yield). ^{1}H NMR ($CDCl_3$): δ 1.94 (s, 3H), 4.50 (m, 2H), 4.61 (m, 2H), 5.59 (s, 1H), 6.14 (s, 1H), 7.95 (d, 2H), 8.19 (d, 2H), 10.10 (s, 1H). ^{13}C NMR ($CDCl_3$): δ 191.64, 167.20, 165.41, 139.44, 136.01, 134.89, 130.40, 129.65, 126.29, 63.37, 62.33, 18.38. IR (ATR crystal) (cm^{-1}): 2867, 1709, 1695, 1632, 1273, 1172, 1107, 962, 823, 759, 686, 657. HR-MS: $[2M+Na]^+$ calculated: 547.1585; found: 547.1575.

Synthesis of poly(FBEMA). A typical polymerization procedure is as follows: To an oven-dried Schlenk tube equipped with a magnetic stir bar was added **CTA1** (10.35 mg, 37.0 μmol), 2,2'-azobis(2-methylpropionitrile) (AIBN) (1.25 mg, 7.60 μmol), FBEMA (1.00 g, 3.81 mmol), and 2 mL of anhydrous DMF. The tube was deoxygenated by subjecting the contents to three freeze-pump-thaw cycles. The Schlenk tube was then back-filled with N_2 and submerged in an oil bath maintained at 75 ˚C. Samples were removed periodically by N_2-purged syringe to monitor

molecular weight evolution by GPC and conversion by ^{1}H NMR spectroscopy. The polymerization was quenched by submerging the tube into liquid N_2 and exposing the reaction solution to air. The resulting poly(FBEMA) was isolated via precipitation from a 1:1 mixture of ether and hexanes. If necessary, further precipitations from CH_2Cl_2 into hexanes were preformed to remove residual monomer.

Synthesis of poly(FBEMA-*b*-methyl methacrylate (MMA)). To an oven-dried Schlenk tube equipped with a magnetic stir bar was added AIBN (0.15 mg, 1.00 μmol), MMA (0.94 g, 9.39 mmol) and 2 mL of anhydrous DMF. Polymer **P2** (M_n = 17,300 g/mol; Đ = 1.12, 83.0 mg, 4.80 μmol) was added as a macro chain-transfer agent. The tube was deoxygenated by subjecting the contents to three freeze-pump-thaw cycles. The Schlenk tube was then back-filled with N_2 and submerged in an oil bath maintained at 75 ˚C. The polymerization was quenched after 1 h by submerging the tube into liquid N_2 and exposing the reaction solution to air. The resulting poly(FBEMA-*b*-MMA) was isolated via precipitation from a 1:1 mixture of ether and hexanes and dried under vacuum overnight. M_n = 27,200 g/mol; Đ = 1.11.

Synthesis of poly(FBEMA-*co*-MEO$_2$MA). To an oven-dried Schlenk tube equipped with a magnetic stir bar was added **CTA1** (34.0 mg, 121 μmol), AIBN (3.97 mg, 24.0 μmol), FBEMA (158 mg, 0.60 mmol), MEO$_2$MA (2.16 g, 11.5 mmol) and 2 mL of anhydrous DMF. The tube was deoxygenated by subjecting the contents to three freeze-pump-thaw cycles. The Schlenk tube was then back-filled with N_2 and submerged in an oil bath maintained at 75 ˚C. The polymerization was quenched after 1 h by submerging the tube into liquid N_2 and exposing the reaction solution to air. The resulting poly(FBEMA-*co*-MEO$_2$MA) was isolated via precipitation from a 1:1 mixture of ether and hexanes, further purified by precipitation twice from CH_2Cl_2 to hexanes, and dried under vacuum overnight. M_n = 10,400 g/mol; Đ = 1.06.

Removal of dithioester end group. A round bottom flask was charged with **P2** (1.00 g, 96.0 μmol), AIBN (316 mg, 1.90 mmol), and 30 mL of 1,4-dioxane. The flask was outfitted with a condenser, and the reaction mixture was heated at 80 ˚C for 1.5 h. The reaction mixture was allowed to cool to rt, and the polymer was recovered via precipitation from ether (861 mg, 86% yield). ^{1}H NMR analysis of the purified polymer revealed quantitative removal of the dithioester end groups. M_n = 11,900 g/mol; Đ = 1.19.

Conjugation of poly(FBEMA) to *O*-hydroxylamine/hydrazide. A general procedure for the conjugation of *O*-hydroxylamine/*tert*-butyl carbazate to poly(FBEMA) is as follows: **P2** (10.0 mg, 0.58 μmol) was dissolved in 1 mL of $CDCl_3$ in a 1 dram vial. To the vial was added either *O*-benzylhydroxylamine hydrochloride or *tert*-butyl carbazate (~16 equiv to thiooxime groups) as a solid. The reaction mixture was left to stand at rt for 24 h. ^{1}H NMR spectroscopy was conducted after this time to determine the conversion to aldoxime/hydrazone.

Conjugation of poly(FBEMA) to SATHA. A general procedure for the conjugation SATHA to poly(FBEMA) is as follows. **P2** (50.0 mg, 2.89 μmol) was dissolved in 1 mL of $CDCl_3$ in a 1 dram vial. To the vial was added SATHA (146 mg, 0.95 mmol) as a solid. Approximately 10 uL of trifluoroacetic acid (TFA) was added as a catalyst. The reaction mixture was left to stand at rt for 24 h over molecular sieves. ^{1}H NMR spectroscopy was conducted after this time to determine the conversion of aldehyde to *S*-aroylthiooxime. The modified polymer was recovered via precipitation from hexanes (67 mg, 90% yield). M_n = 29,500 g/mol; Đ = 1.12.

Calibration of H_2S **Selective Probe.** An EDTA solution was prepared at 154 μM by dissolving 1.43 mg of EDTA in 25 mL of DI water in a volumetric flask. The solution was purged vigorously with N_2 for 20 min. 7.70 mg of anhydrous Na_2S was added to a vial under inert atmosphere,

followed by 20 mL of the EDTA solution (to make 5 mM Na_2S). A small stir bar was added to a scintillation vial containing 20 mL of 1X PBS buffer (pH = 7.4). The vial was placed on a stir plate. The H_2S sensor was immersed in the solution and the background current was allowed to stabilize for several minutes. Four aliquots of the H_2S solution were injected sequentially into the vial (40 μL, 80 μL, 160 μL). The current increased rapidly after each injection before reaching a plateau. The second aliquot was injected as soon as the current had stabilized. The other aliquots were injected similarly. The recorded data were used to construct a linear calibration curve of concentration vs. current (Figure 3S22).

H_2S Release in the Presence of Cysteine or Glutathione. A stock solution of cysteine or glutathione was prepared in PBS buffer at 400 mM. 50 μL of this solution was added to a vigorously stirred vial containing 20 mL of PBS buffer. The current was allowed to equilibrate for several minutes. Once a stable current was observed, an aliquot of polymer stock solution (**P6**-**P8**) (100 μL, 2 mM in THF) was added rapidly via micropipette. The current was monitored over a period of approximately 2 h. A plot of H_2S concentration vs. time was constructed using the calibration curve. No background subtraction was performed. H_2S release was only observed upon addition of compounds containing a thiol functionality.

4.5. Results and Discussion

SATO formation involves the reaction between an aromatic aldehyde/ketone and a SATHA. Therefore, we investigated the preparation of polymers bearing pendant aldehyde functionality via the direct polymerization of an aromatic aldehyde-containing monomer by radical addition-fragmentation chain transfer (RAFT) polymerization. The RAFT process tolerates the vast majority of activated vinyl monomers and solvents,[32-34] and it has been used to prepare aldehyde-functionalized polymers, most commonly through the deprotection of pendant acetal groups,[35-37

or via the direct polymerization of aldehyde-containing monomers.[38-40] A handful of aldehyde-containing monomers have been reported in the literature, ranging from aldehyde-functionalized methacrylates,[41] to acrylates and styrenes.[42] However, we chose 2-(4-formylbenzoyloxy)ethyl methacrylate (FBEMA) due to the ease of its synthesis, fast propagation, and the enhanced reactivity of its aldehyde functionality (relative to aliphatic or more electron rich analogues). This compound was prepared in one step via the EDC-mediated condensation of 2-hydroxyethyl methacrylate with 4-carboxybenzaldehyde in 82% yield without the need for distillation or column chromatography (Scheme 4.1A). Protection of the aldehyde functional group prior to RAFT polymerization was found to be unnecessary.

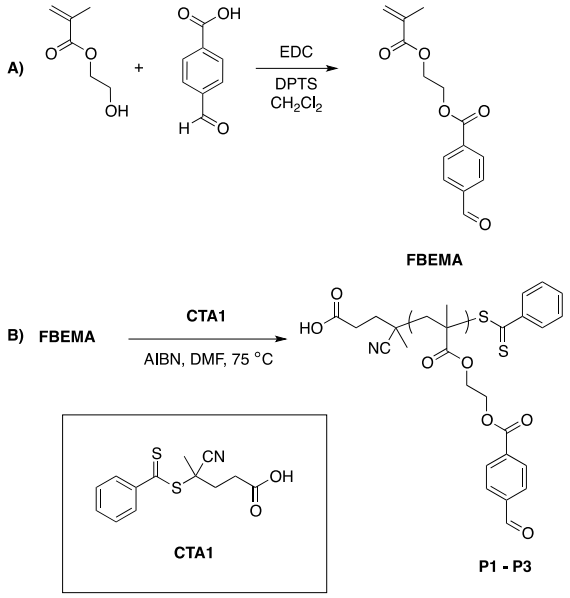

Scheme 4.1. Preparation of poly(FBEMA): (A) synthesis of FBEMA; (B) RAFT polymerization of poly(FBEMA).

4.5.1. RAFT Polymerization of FBEMA

The preparation of poly(FBEMA) was first reported in 1994.[43] However, to our knowledge there are no reports of a controlled radical polymerization of FBEMA. Therefore, a detailed kinetic

analysis was performed to assess the "livingness" of its polymerization. RAFT polymerization of FBEMA with the chain transfer agent (CTA) 4-cyano-4-(phenylcarbonothioylthio)pentanoic acid (**CTA1**) yielded polymers of controllable MW and low Đ (Scheme 4.1B). Polymerizations were initiated via the thermolysis of 2,2'-azobis(isobutyronitrile) (AIBN) at 75 °C. The polymerizations were conducted in DMF to minimize the occurrence of early termination reactions as well as to facilitate the fast propagation of FBEMA.[44] A stoichiometric ratio of 5:1 [CTA]/[AIBN] was chosen to maintain chain end fidelity of the resulting polymer and to avoid retardation in polymerization rate that can result from high CTA concentration. Our kinetic analysis of the polymerization is shown in Figure 4.1. The linear relationship in the plot of the number-average MW (M_n) vs. conversion is indicative of a living/controlled polymerization.[45] In addition, M_n increased linearly with time (up to ~80% conversion), and Đ decreased correspondingly over the course of the reaction.

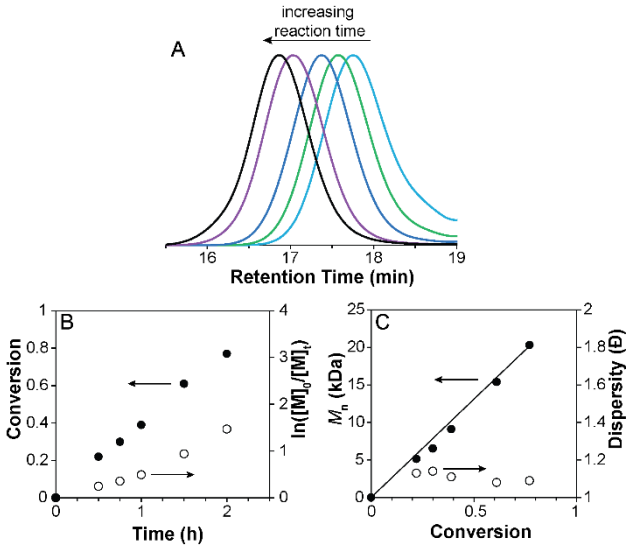

Figure 4.1. Kinetics of RAFT polymerization of FBEMA: (A) GPC traces showing decreasing retention time over the course of the reaction; (B) time dependence of monomer conversion as measured by ^{1}H NMR spectroscopy (filled circles) and ln($[M]_0/[M]_t$) (open circles); (C) relationship between M_n (GPC) (filled circles) and Đ (open circles) on monomer conversion (solid line shows theoretical M_n based on conversion as observed by ^{1}H NMR spectroscopy). (Polymerization conditions: [FBEMA]/[CTA]/[AIBN] = 100:1:0.2, 33% w/v FBEMA in DMF, 75 °C).

Polymers of M_n 8,500 (**P1**), 17,300 (**P2**), and 40,500 (**P3**) Da were prepared by varying the stoichiometry of the polymerization (FBEMA/CTA ratio) and isolated via precipitation into a 1:1 mixture of ether/hexanes (Table 4.1). GPC traces of **P1**-**P3** were monomodal and gave low polydispersities (1.07-1.16), indicating well-controlled polymerization of FBEMA (Figure 4S15). ^{1}H NMR spectroscopy of the pure polymers confirmed the preservation of the aldehyde functionality, evident as a singlet at 10.02 ppm (Figure 4S3). NMR analysis also showed retention of the dithioester on the ω-end of the polymer chains. The intact dithioester allowed for the polymer to be utilized as a macro-chain transfer agent. **P2** was chain-extended with methyl methacrylate (MMA) under conditions similar to those of the FBEMA homopolymerization to afford the block copolymer poly(FBEMA-*b*-MMA) (**P4**) (Figures 4S4, 4S16).

Table 4.1. Polymers prepared via RAFT polymerization of FBEMA.

polymer	monomer(s)	CTA	[M]/[CTA]/[AIBN]	M_n (GPC, Da)	$M_{n,theo}$ (^{1}H NMR, Da)[a]	Đ
P1	FBEMA	**CTA1**	90:1:0.2	8,500	9,900	1.07
P2	FBEMA	**CTA1**	300:1:0.2	17,300	19,800	1.12
P3	FBEMA	**CTA1**	500:1:0.2	40,500	40,900	1.16
P4	MMA	**P2**	2000:1:0.2	27,200	29,600	1.11
P5	FBEMA/MEO_2MA	**CTA1**	5:95:1:0.2	10,400	12,300	1.06

[a]Calculated using the equation (% conv*[M]/[CTA]*MW_M+MW_{CTA}) with conversion determined by ^{1}H NMR spectroscopy. All polymerizations were conducted for 1-1.5 h in DMF at 75 °C.

4.5.2. Pendant Aldehyde Reactivity

The modular nature of oxime and hydrazone "click" reactions allows for the facile conjugation of substrates bearing these functionalities to a variety of scaffolds, including polymers,[46,47] micelles,[48] peptides,[49] and hydrogels.[50] These reactions occur rapidly at room temperature and do not require a metal catalyst. To investigate the reactivity of the pendant aldehyde functional groups, polymer

P2 was mixed with an excess (5 equiv relative to aldehyde) of *O*-benzylhydroxylamine or *tert*-butyl carbazate in $CDCl_3$ at rt. After 24 h, ^1H NMR spectroscopy showed complete conversion to aldoxime/hydrazone, confirming the reactivity of the aldehydes of poly(FBEMA) (Figures 4S5-4S6).

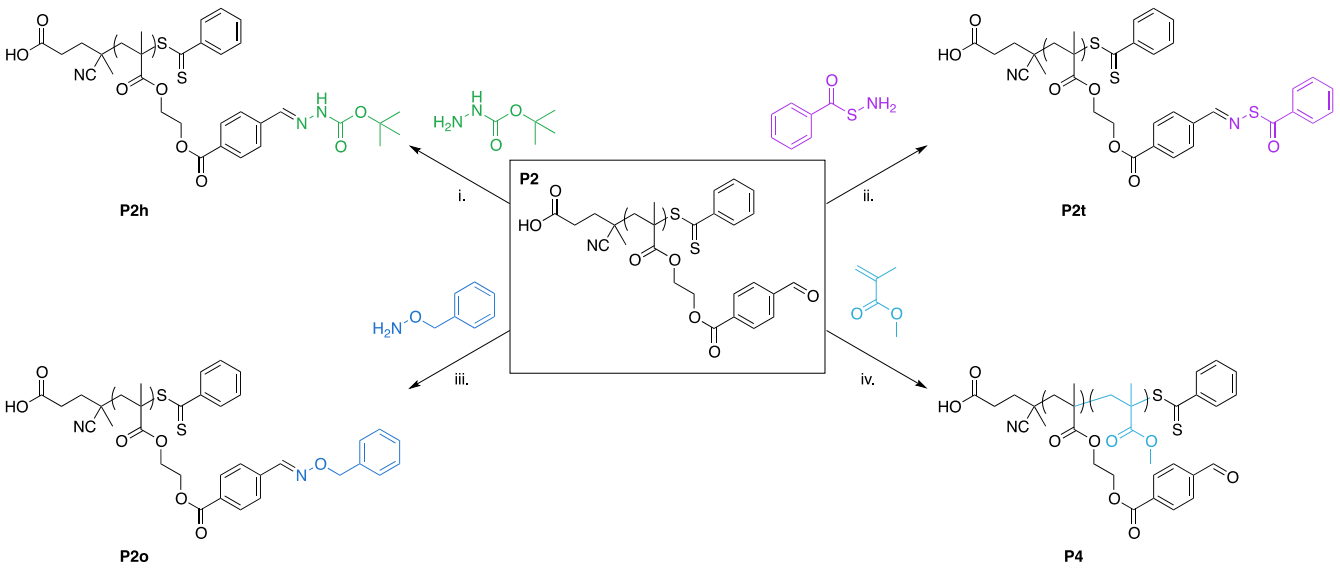

Scheme 4.2. Post-polymerization modification of poly(FBEMA). Shown are: hydrazone formed via reaction with *tert*-butylcarbazate (P2h); thiooxime formation reaction, conducted between poly(FBEMA) and *S*-benzoylthiohydroxylamine (SBTHA) (P2t); oxime formation from conjugation with *O*-benzylhydroxylamine (P2o); chain extension of poly(FBEMA) macroCTA with MMA (P4). Experimental conditions: (i) $CDCl_3$, rt; (ii) CH_2Cl_2, TFA (cat), rt; (iii) $CDCl_3$, rt; (iv) AIBN, DMF, 75 °C.

4.5.3. Thiooxime Polymer Functionalization

The viability of thiooxime formation as a post-polymerization modification reaction was evaluated. We recently reported on the preparation of H_2S donors based on the SATO motif.[19] These SATO compounds were synthesized by reacting *S*-aroylthiohydroxylamine (SATHA) and its derivatives with aromatic aldehydes or ketones. H_2S release was observed in the presence of thiols such as cysteine and glutathione, liberating the original aldehyde/ketone in the process. As

this reaction has never been attempted on a polymeric substrate, a systematic investigation was conducted to study the effects of a number of parameters on the reaction conversion.

Polymers **P1**-**P3** were mixed with varying amounts (1-10 equiv) of *S*-benzoylthiohydroxylamine in deuterated solvents at rt. Trifluoroacetic acid (TFA) was employed as the catalyst for all reactions. In addition, the effects of solvent and polymer M_n on the conversion to thiooxime were also investigated. After 24 h, a conversion was determined via ^{1}H NMR spectroscopy by comparing the relative integrations of the aldehyde proton resonance at 10.02 ppm to that of the thiooxime at 8.67 ppm (Figure 4.2). Three new peaks between 7.29 and 7.88 ppm were assigned to the aromatic protons of the SATHA-derived ring. A summary of our evaluation is provided in Table 4.2.

In general, full conversion was achieved for polymers **P1**-**P3** with the addition of at least 10 equiv of SBTHA. Five equiv of SBTHA was sufficient to achieve full conversion to thiooxime for **P1**; however, greater polymer molecular weight reduced the conversion of the pendant aldehydes of **P2** and **P3** to 89% and 79%, respectively. Solvent also influenced reaction conversion, with THF-d_8 and DMSO-d_6 yielding higher conversion relative to $CDCl_3$.

Table 4.2. Evaluation of the thiooxime formation reaction on poly(FBEMA).

polymer	polymer M_n (Da)[a]	equiv THA	solvent	% conv to thiooxime[b]
P1	8,500	1	$CDCl_3$	65
P1	8,500	5	$CDCl_3$	>99
P1	8,500	10	$CDCl_3$	>99
P2	17,300	1	$CDCl_3$	65
P2	17,300	5	$CDCl_3$	89
P2	17,300	10	$CDCl_3$	>99
P3	40,500	1	$CDCl_3$	57
P3	40,500	5	$CDCl_3$	79
P3	40,500	10	$CDCl_3$	>99
P2	17,300	1	$CDCl_3$	65
P2	17,300	1	THF-d_8	77
P2	17,300	1	DMSO-d_6	73

[a]Determined by GPC in THF, dn/dc = 0.140. [b]Calculated via ^{1}H NMR spectroscopy by comparing the relative integrations of the aldehyde and thiooxime peaks at 10.02 and 8.67 ppm, respectively.

The thiooxime formation reaction was repeated with **P2** at a larger scale, and the resulting modified polymer was isolated via precipitation from hexanes (**P2t**). ^{1}H NMR (Figure 4.2) and IR (Figure 4S14) analyses of the purified polymer revealed nearly quantitative consumption of the pendant aldehydes, and the GPC trace of the isolated thiooxime-functionalized polymer revealed a corresponding increase in the M_n from 17,300 Da to 27,200 Da (Figure 4S17) which is in good agreement with the theoretical M_n of 26,700 Da calculated assuming complete conversion of the pendant aldehyde groups.

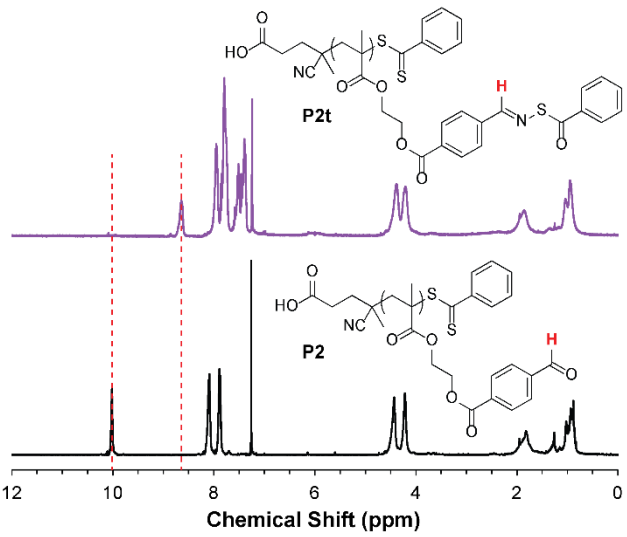

Figure 4.2. ^{1}H NMR spectra of P2 before (black trace) and after (purple trace) conjugation with SBTHA. Dashed red lines highlight the shift of the proton labeled in red from 10.02 ppm in polymer P2 to 8.67 ppm in polymer P2t.

4.5.4. Evaluation of H_2S Release Capability

SATOs release H_2S in response to cysteine and other thiol-containing compounds but do not react with other physiological nucleophiles such as amines and alcohols.[19] The rate of release can be tuned by controlling the electronics of the SATHA-derived ring, with electron donating groups retarding the release rate and electron withdrawing groups enhancing it. Given the vast therapeutic potential of H_2S,[20-22] we envisioned the conjugation of SATHAs to aldehyde-functionalized polymeric scaffolds as a potential route produce H_2S delivery vehicles with tunable release kinetics.

To establish the H_2S-releasing capability of the thiooxime-functionalized polymer, 2-(2-methoxyethoxy)ethyl methacrylate (MEO_2MA), was introduced into the polymerization to enhance the water solubility of the resulting copolymer (Scheme 4.3). FBEMA and MEO_2MA were loaded at a molar ratio of 5:95 in the feed and polymerized via RAFT to produce poly(FBEMA-*co*-MEO_2MA) (**P5**). An M_n of 10,400 Da was determined via GPC analysis of the

resulting copolymer. ^{1}H NMR spectroscopy showed incorporation of both monomers, with a composition of 10% FBEMA. As before, our NMR analysis also confirmed the retention of the dithioester moiety on the ω-chain end, a functional group that is reactive toward nucleophiles such as thiols and amines.[51] To prevent an undesired side-reaction between the terminal thiocarbonyl-thio moieties and the thiol-containing triggers we employed to generate H_2S, the dithioester end group was displaced with AIBN.[52] The copolymers were then condensed with three different SATHAs in the presence of TFA to prepare thiooxime-functionalized copolymers (**P6**-**P8**) (Scheme 4.3, Figure 4S18).

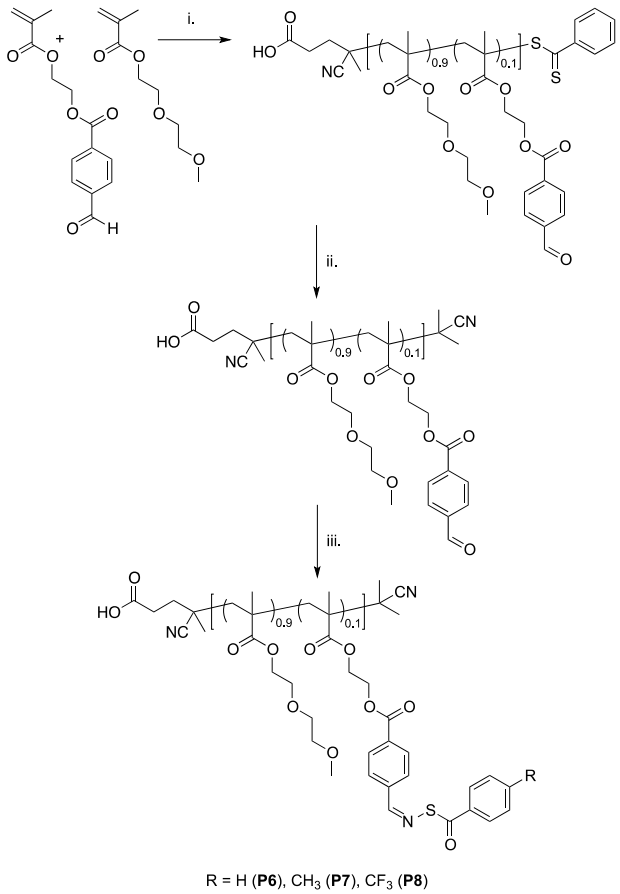

Scheme 4.3. Preparation of poly(FBEMA-*co*-MEO$_2$MA) copolymers via RAFT, followed by end group removal with AIBN and conjugation to different SATHAs. Experimental conditions: (i) CTA1, AIBN, DMF, 75 °C; (ii) AIBN, 1,4-dioxane, 80 ˚C; (iii) SATHA, CH_2Cl_2, TFA (cat), rt.

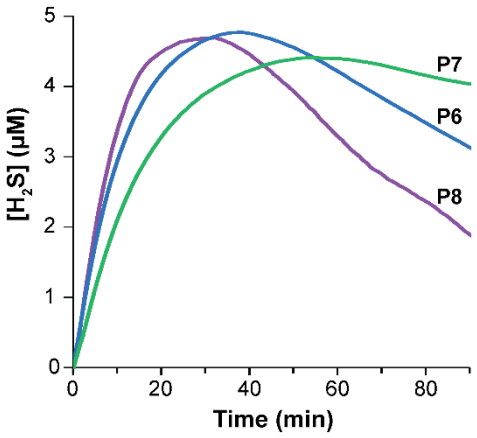

Figure 4.3. Cysteine-triggered H_2S release from P6-P8 measured using an H_2S-selective microelectrode.

An H_2S-selective microelectrode was utilized to detect the evolution of H_2S from polymers **P6-P8**. A solution of copolymer in a small amount of THF was injected into a buffered aqueous solution (pH = 7.4) containing 1 mM cysteine, resulting in the formation of H_2S. The electronics of the substituent at the *para* position of the SATHA-derived ring had a pronounced effect on the H_2S release profile of the corresponding functionalized copolymer. The relative rates of H_2S release from **P6-P8** were compared by measuring their peaking times—defined as the time at which the concentration of H_2S in solution reached a maximum value. Peaking times of 25 min, 53 min, and 36 min were determined **P6**, **P7**, and **P8**, respectively (Figure 4.3). This sensitivity to electronic effects is consistent with our findings for small molecule SATOs. Moreover, these data demonstrate facile fine-tuning of the H_2S release rate via a post polymerization methodology without altering polymer composition or MW.

4.5.5. Degradation of the Thiooxime Linkage

Based on data from small molecule SATOs,[19] we expected that the thiooxime linkage could be degraded via either of two mechanisms: the thiol-triggered decomposition discussed above, or hydrolysis under acidic conditions (Scheme 4.4). The hydrolysis of oximes and hydrazones

proceeds slowly at pH = 7, but the rate of hydrolysis increases rapidly with decreasing pH.[53] We investigated whether the same trend would hold in polymers bearing pendant SATOs.

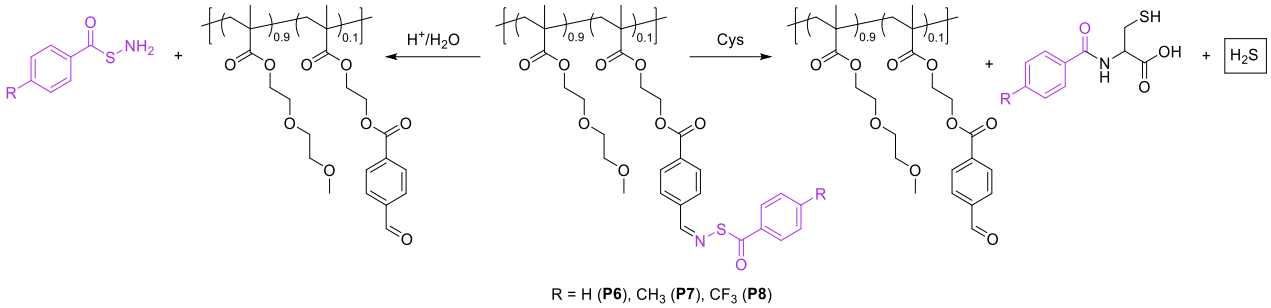

Scheme 4.4. Two possible routes of degradation of the thiooxime linkage.

The hydrolytic stability of **P6** was evaluated at physiological pH using UV-vis absorption spectroscopy, monitoring the decrease in the thiooxime peak absorption at 320 nm over several days (Figure 4S20). The thiooxime bond hydrolyzed slowly at pH = 7.4 (4% hydrolysis over 300 h), which is slower than the hydrolysis rate for a similar small molecule SATO.[19] To induce hydrolysis, **P6** was incubated in acidic media for 48 h. ^{1}H NMR spectroscopy of the reaction mixture confirmed quantitative regeneration of the pendant aldehyde functionality, evident as a clean shift of the resonance at 8.67 to 10.02. (Figure 4S21).

Thiol-driven degradation was also investigated to determine the state of the polymer side chains after complete SATO degradation and H_2S release. In our previous report, reaction of small molecule thiooximes with cysteine led to H_2S evolution.[19] However, given the presence of excess cysteine in the reaction mixture, the parent aldehydes were recovered as the corresponding thiazolidines. Therefore, to study thiooxime degradation by thiols, **P6** was instead reacted with glutathione (GSH) in a 1:1 mixture of H_2O and THF. After stirring for 24 h, the polymer was isolated by extraction with CH_2Cl_2 followed by precipitation into hexanes. ^{1}H NMR spectroscopy showed complete reversion of the pendant SATOs to aldehydes, confirming that the thiooxime linkage can be cleanly degraded by thiol functionality (Figure 4S13). In addition, H_2S evolution

was observed from **P6** in the presence of GSH using an H_2S-selective microelectrode (Figure 4S19).

4.6. Conclusions

In summary, we have demonstrated the RAFT homopolymerization of FBEMA to be a new and effective route toward the preparation of aldehyde-functionalized polymers of controllable M_n and low Đ. The pendant aldehyde functionality reacts rapidly and quantitatively with hydroxylamines and hydrazides to form aldoximes and hydrazones, respectively. Additionally, we present the first study evaluating the applicability of thiooxime formation as a post-polymerization modification reaction. For the three polymers prepared with differing molecular weights, 10 equiv of SBTHA was sufficient to achieve full conversion of the pendant aldehydes to thiooximes. Finally, random copolymers of FBEMA and MEO_2MA were prepared and functionalized via reaction with 3 different SATHAs. These copolymers released H_2S in response to cysteine and glutathione with tunable kinetics consistent with similar small molecule SATOs. To our knowledge, this is the first example of a deliberately triggered H_2S-releasing polymer potentially applicable to biological systems. We expect that H_2S-releasing polymers may play an important role in realizing the therapeutic potential of H_2S.

4.8. References

(1) Boaen, N. K.; Hillmyer, M. A. *Chem. Soc. Rev.* **2005**, *34*, 267.

(2) Gauthier, M. A.; Gibson, M. I.; Klok, H.-A. *Angew. Chem., Int. Ed.* **2009**, *48*, 48.

(3) Guenay, K. A.; Theato, P.; Klok, H.-A. *J. Polym. Sci., Part A: Polym. Chem.* **2013**, *51*, 1.

(4) Lutz, J.-F.; Sumerlin, B. S. In *Click Chemistry for Biotechnology and Materials Science*; John Wiley & Sons, Ltd: 2009, p 69.

(5) Kolb, H. C.; Finn, M. G.; Sharpless, K. B. *Angew. Chem., Int. Ed.* **2001**, *40*, 2004.

(6) Iha, R. K.; Wooley, K. L.; Nystrom, A. M.; Burke, D. J.; Kade, M. J.; Hawker, C. J. *Chem. Rev.* **2009**, *109*, 5620.

(7) Xi, W.; Scott, T. F.; Kloxin, C. J.; Bowman, C. N. *Adv. Funct. Mater.* **2014**, n/a.

(8) Maynard, H. D.; Broyer, R. M.; Kolodziej, C. M. In *Click Chemistry for Biotechnology and Materials Science*; John Wiley & Sons, Ltd: 2009, p 53.

(9) van der Ende, A. E.; Harrell, J.; Sathiyakumar, V.; Meschievitz, M.; Katz, J.; Adcock, K.; Harth, E. *Macromolecules* **2010**, *43*, 5665.

(10) Sumerlin, B. S.; Vogt, A. P. *Macromolecules* **2009**, *43*, 1.

(11) Durmaz, H.; Dag, A.; Altintas, O.; Erdogan, T.; Hizal, G.; Tunca, U. *Macromolecules* **2007**, *40*, 191.

(12) Gao, H.; Matyjaszewski, K. *Journal of the American Chemical Society* **2007**, *129*, 6633.

(13) Boyer, C.; Liu, J.; Bulmus, V.; Davis, T. P. *Aust. J. Chem.* **2009**, *62*, 830.

(14) O'Reilly, R. K.; Joralemon, M. J.; Wooley, K. L.; Hawker, C. J. *Chem. Mater.* **2005**, *17*, 5976.

(15) Bapat, A. P.; Roy, D.; Ray, J. G.; Savin, D. A.; Sumerlin, B. S. *Journal of the American Chemical Society* **2011**, *133*, 19832.

(16) Li, S.; Han, J.; Gao, C. *Polymer Chemistry* **2013**, *4*, 1774.

(17) Wu, P.; Malkoch, M.; Hunt, J. N.; Vestberg, R.; Kaltgrad, E.; Finn, M. G.; Fokin, V. V.; Sharpless, K. B.; Hawker, C. J. *Chem. Commun.* **2005**, 5775.

(18) Raasch, M. S. *J. Org. Chem.* **1972**, *37*, 3820.

(19) Foster, J. C.; Powell, C. R.; Radzinski, S. C.; Matson, J. B. *Org. Lett.* **2014**, *16*, 1558.

(20) Olson, K. R. *Am. J. Physiol.* **2011**, *301*, R297.

(21) Wang, R. *Physiol. Rev.* **2012**, *92*, 791.

(22) Whiteman, M.; Winyard, P. G. *Expert. Rev. Clin. Pharmacol.* **2010**, *4*, 13.

(23) Kimura, Y. D., R.; Schubert, D.; Kimura, H. *Antioxid. Redox Signaling* **2006**, *8*, 661.

(24) Polhemus, D. J.; Lefer, D. J. *Circ. Res.* **2014**, *114*, 730.

(25) Qiu, X.; Villalta, J.; Lin, G.; Lue, T. F. *Journal of andrology* **2012**, *33*, 529.

(26) Paul, B. D.; Snyder, S. H. *Nat Rev Mol Cell Biol* **2012**, *13*, 499.

(27) Kodela, R.; Chattopadhyay, M.; Kashfi, K. *ACS Med. Chem. Lett.* **2012**, *3*, 257.

(28) Wallace, J. L. *Trends Pharmacol. Sci.* **2007**, *28*, 501.

(29) Zhao, Y.; Wang, H.; Xian, M. *J. Am. Chem. Soc.* **2011**, *133*, 15.

(30) Ma, X.; Wang, X.; Song, C. *Journal of the American Chemical Society* **2009**, *131*, 5777.

(31) Mitsukami, Y.; Donovan, M. S.; Lowe, A. B.; McCormick, C. L. *Macromolecules* **2001**, *34*, 2248.

(32) Chiefari, J.; Chong, Y. K.; Ercole, F.; Krstina, J.; Jeffery, J.; Le, T. P. T.; Mayadunne, R. T. A.; Meijs, G. F.; Moad, C. L.; Moad, G.; Rizzardo, E.; Thang, S. H. *Macromolecules* **1998**, *31*, 5559.

(33) Lowe, A. B.; McCormick, C. L. *Prog. Polym. Sci.* **2007**, *32*, 283.

(34) Moad, G.; Rizzardo, E.; Thang, S. H. *Aust. J. Chem.* **2012**, *65*, 985.

(35) Li, R. C.; Hwang, J.; Maynard, H. D. *Chem. Commun.* **2007**, 3631.

(36) Rossi, N. A. A.; Zou, Y.; Scott, M. D.; Kizhakkedathu, J. N. *Macromolecules* **2008**, *41*, 5272.

(37) Stukel, J. M.; Li, R. C.; Maynard, H. D.; Caplan, M. R. *Biomacromolecules* **2010**, *11*, 160.

(38) Sun, G.; Cheng, C.; Wooley, K. L. *Macromolecules* **2007**, *40*, 793.

(39) Sun, G.; Fang, H.; Cheng, C.; Lu, P.; Zhang, K.; Walker, A. V.; Taylor, J.-S. A.; Wooley, K. L. *ACS Nano* **2009**, *3*, 673.

(40) Murray, B. S.; Jackson, A. W.; Mahon, C. S.; Fulton, D. A. *Chem. Commun.* **2010**, *46*, 8651.

(41) Whitaker, D. E.; Mahon, C. S.; Fulton, D. A. *Angew. Chem., Int. Ed.* **2013**, *52*, 956.

(42) Heinenberg, M.; Menges, B.; Mittler, S.; Ritter, H. *Macromolecules* **2002**, *35*, 3448.

(43) Monthéard, J.-P.; Chatzopoulos, F.; Amine, H. E.; Cachard, A.; Trouillet, A. *Angew. Makromol. Chem.* **1994**, *220*, 75.

(44) Keddie, D. J. *Chem. Soc. Rev.* **2014**.

(45) Greszta, D.; Mardare, D.; Matyjaszewski, K. *Macromolecules* **1994**, *27*, 638.

(46) Chen, B.; van der Poll, D. G.; Jerger, K.; Floyd, W. C.; Frechet, J. M.; Szoka, F. C. *Bioconjugate chemistry* **2011**, *22*, 617.

(47) Hill, M. R.; Mukherjee, S.; Costanzo, P. J.; Sumerlin, B. S. *Polym. Chem.* **2012**, *3*, 1758.

(48) Alani, A. W. G.; Bae, Y.; Rao, D. A.; Kwon, G. S. *Biomaterials* **2010**, *31*, 1765.

(49) Matson, J. B.; Stupp, S. I. *Chem. Commun.* **2011**, *47*, 7962.

(50) Lin, F.; Yu, J.; Tang, W.; Zheng, J.; Defante, A.; Guo, K.; Wesdemiotis, C.; Becker, M. L. *Biomacromolecules* **2013**.

(51) Willcock, H.; O'Reilly, R. K. *Polym. Chem.* **2010**, *1*, 149.

(52) Perrier, S.; Takolpuckdee, P.; Mars, C. A. *Macromolecules* **2005**, *38*, 2033.

(53) Kalia, J.; Raines, R. T. *Angew. Chem., Int. Ed.* **2008**, *47*, 7523.

4.9. Appendix

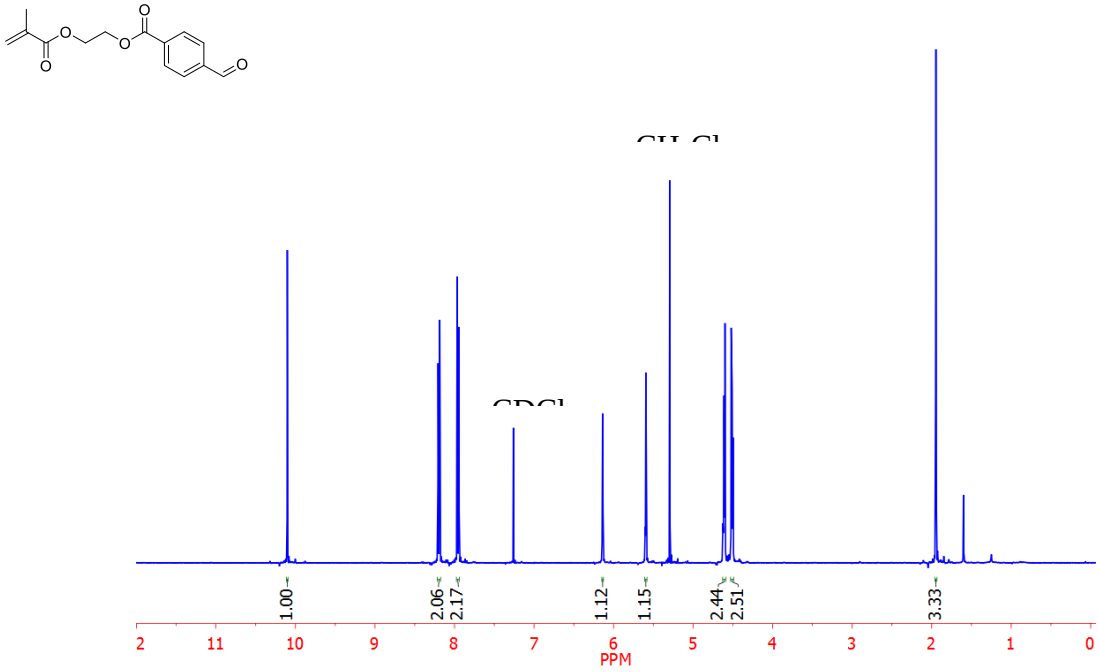

Figure 4S1. ^{1}H NMR of FBEMA in $CDCl_3$.

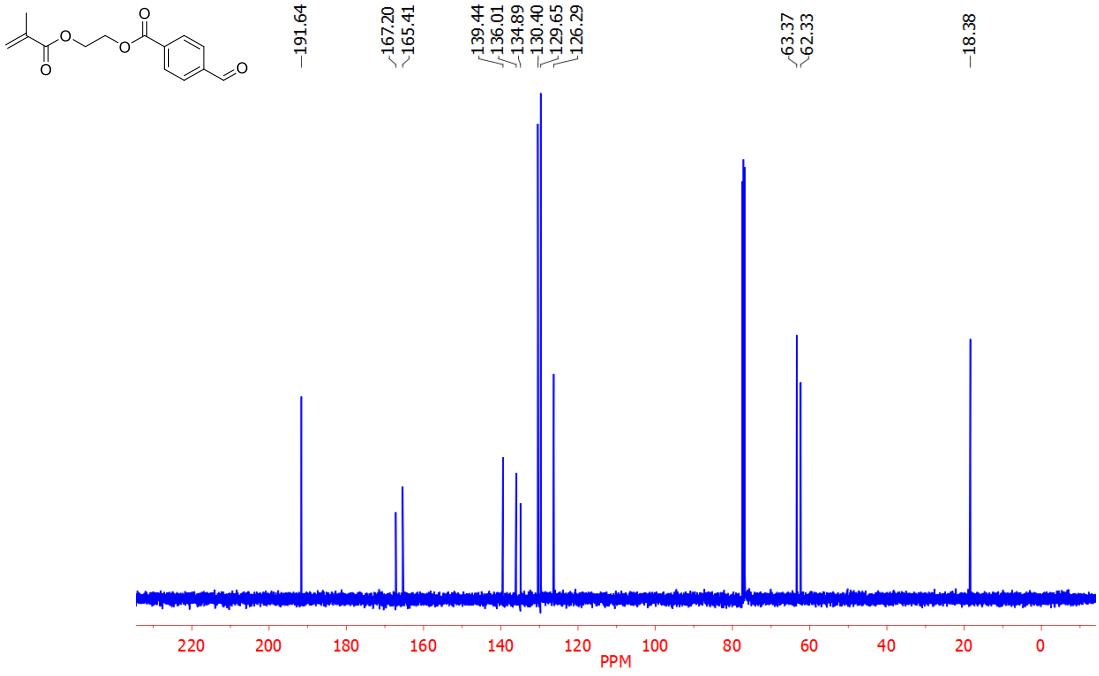

Figure 4S2. ^{13}C NMR of FBEMA in $CDCl_3$.

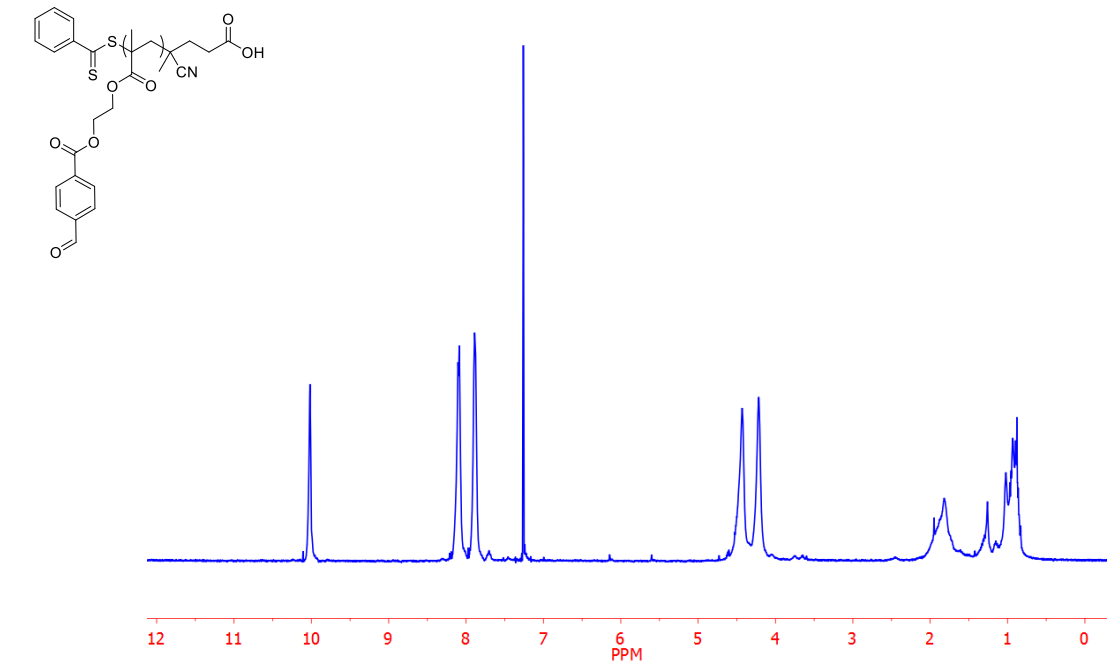

Figure 4S3. ^{1}H NMR of poly(FBEMA) in $CDCl_3$ (P2).

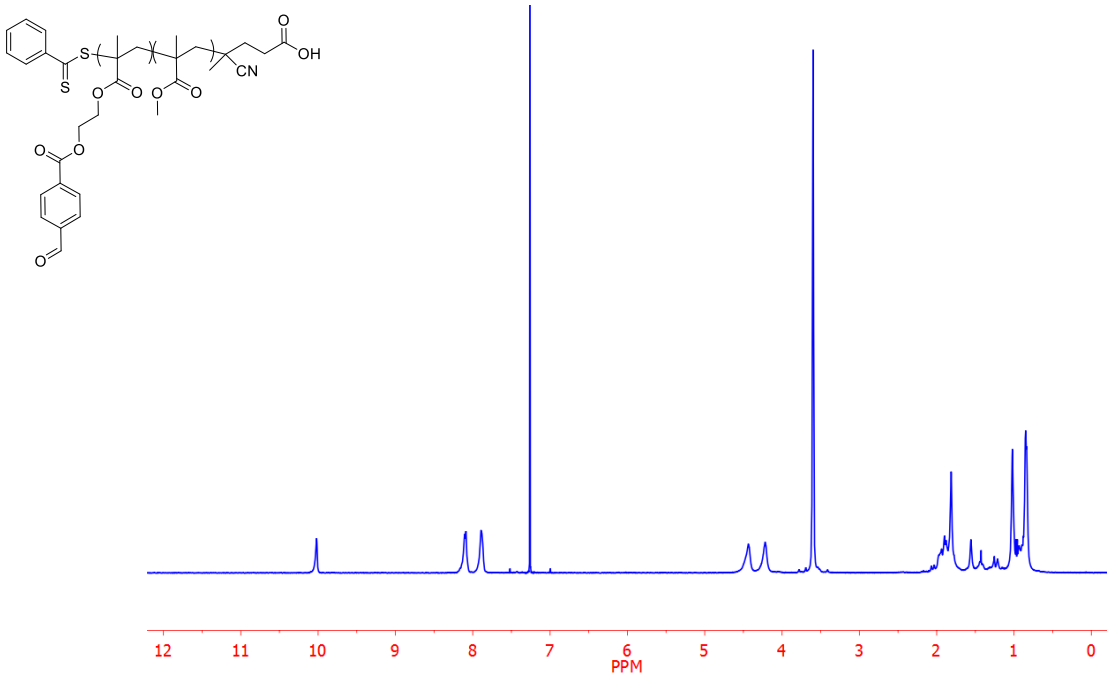

Figure 4S4. ^{1}H NMR of poly(FBEMA-b-MMA) in $CDCl_3$ (P4).

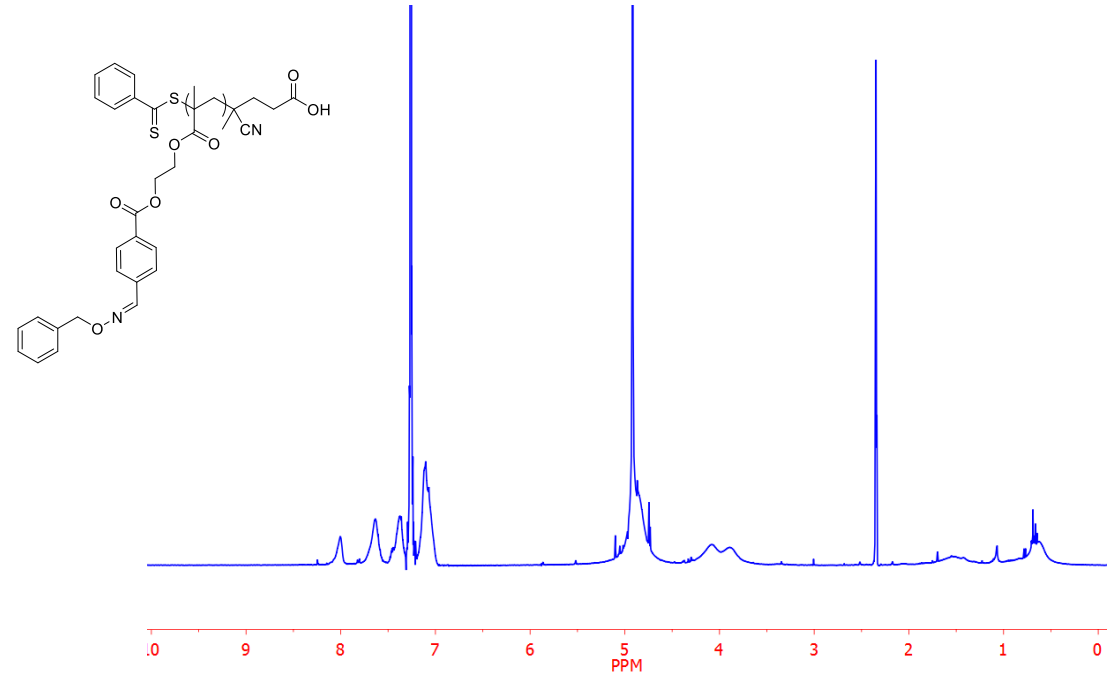

Figure 4S5. ^{1}H NMR of *O*-hydroxylamine-modified poly(FBEMA) in $CDCl_3$ (P2o).

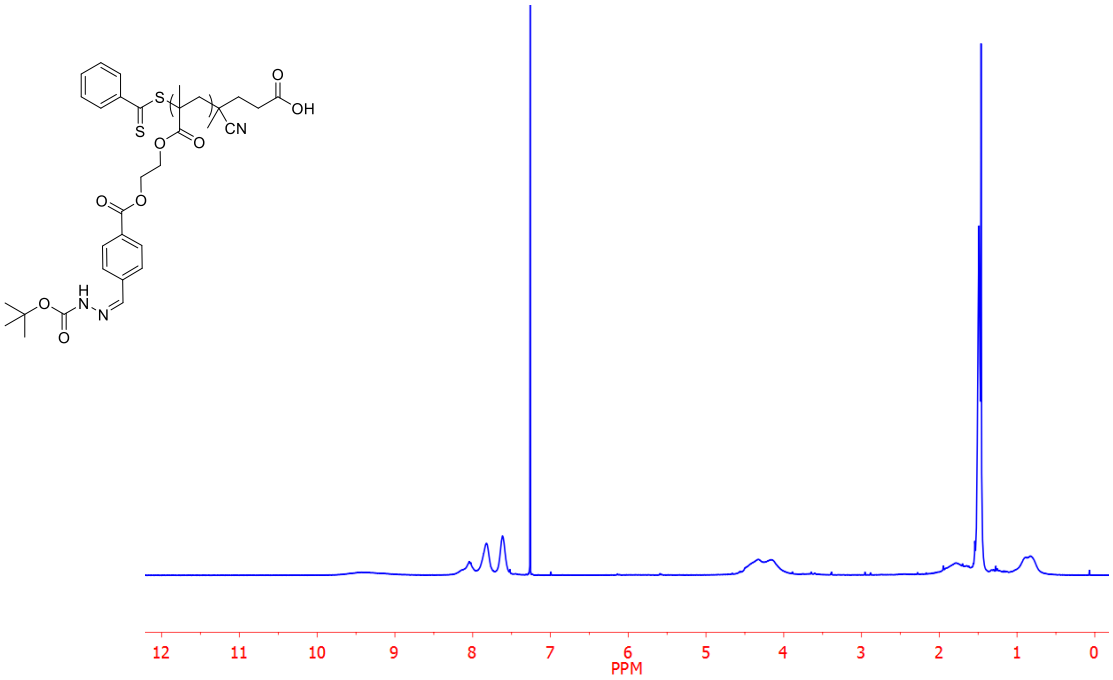

Figure 4S6. ^{1}H NMR of hydrazone-modified poly(FBEMA) in $CDCl_3$ (P2h).

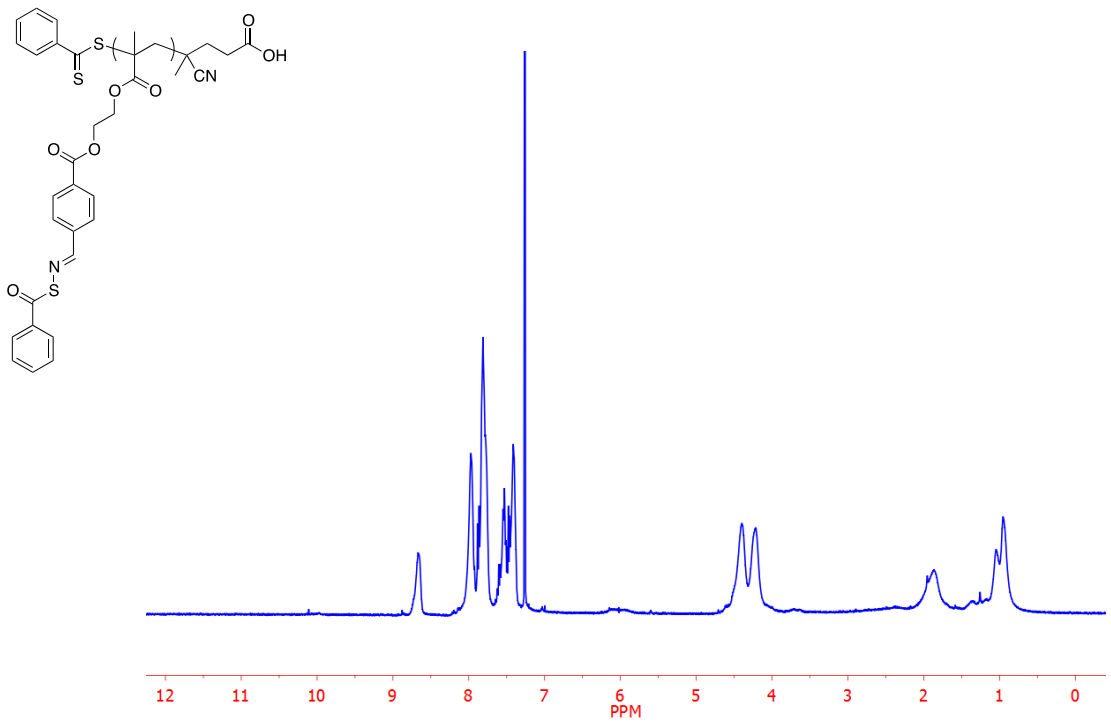

Figure 4S7. ^{1}H NMR of thiooxime-modified poly(FBEMA) in $CDCl_3$ (P2t).

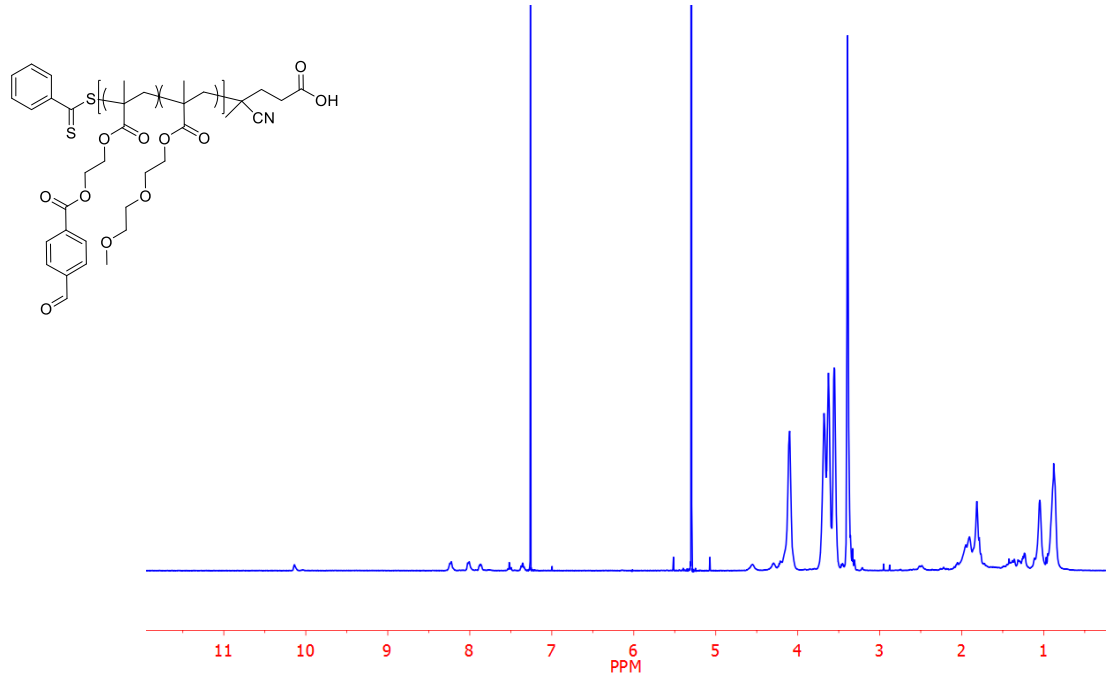

Figure 4S8. ^{1}H NMR of poly(FBEMA-*co*-MEO_2MA) in $CDCl_3$ (P5).

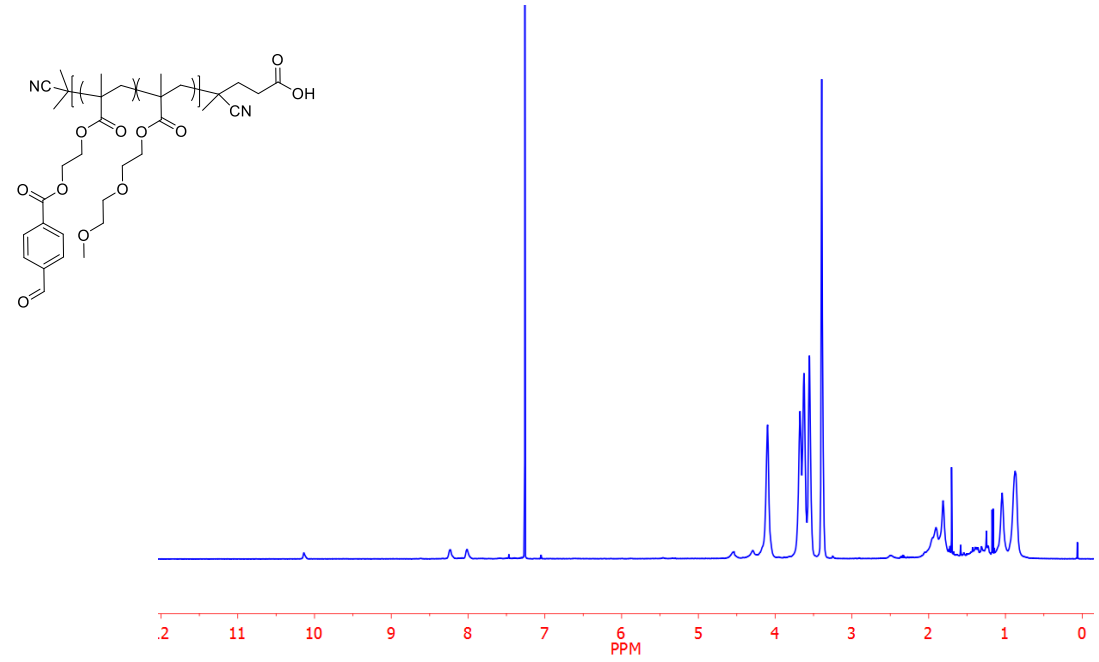

Figure 4S9. ^{1}H NMR of poly(FBEMA-*co*-MEO$_2$MA) following end group removal with AIBN in CDCl$_3$.

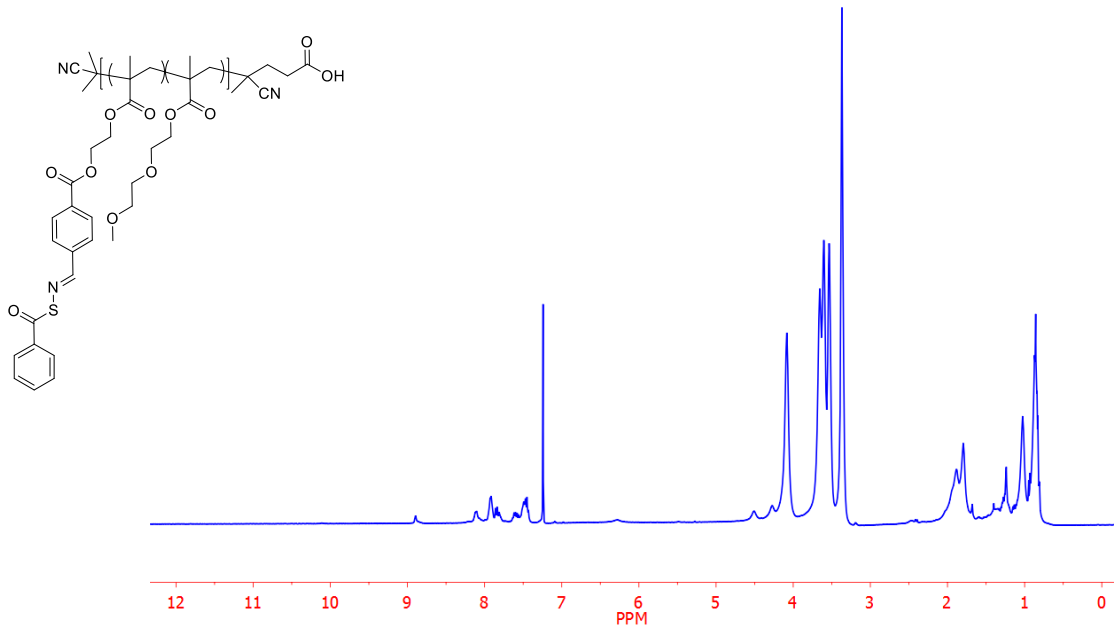

Figure 4S10. ^{1}H NMR of poly(FBEMA-*co*-MEO$_2$MA) following end group removal with AIBN and conjugation to SATHA in CDCl$_3$ (P6).

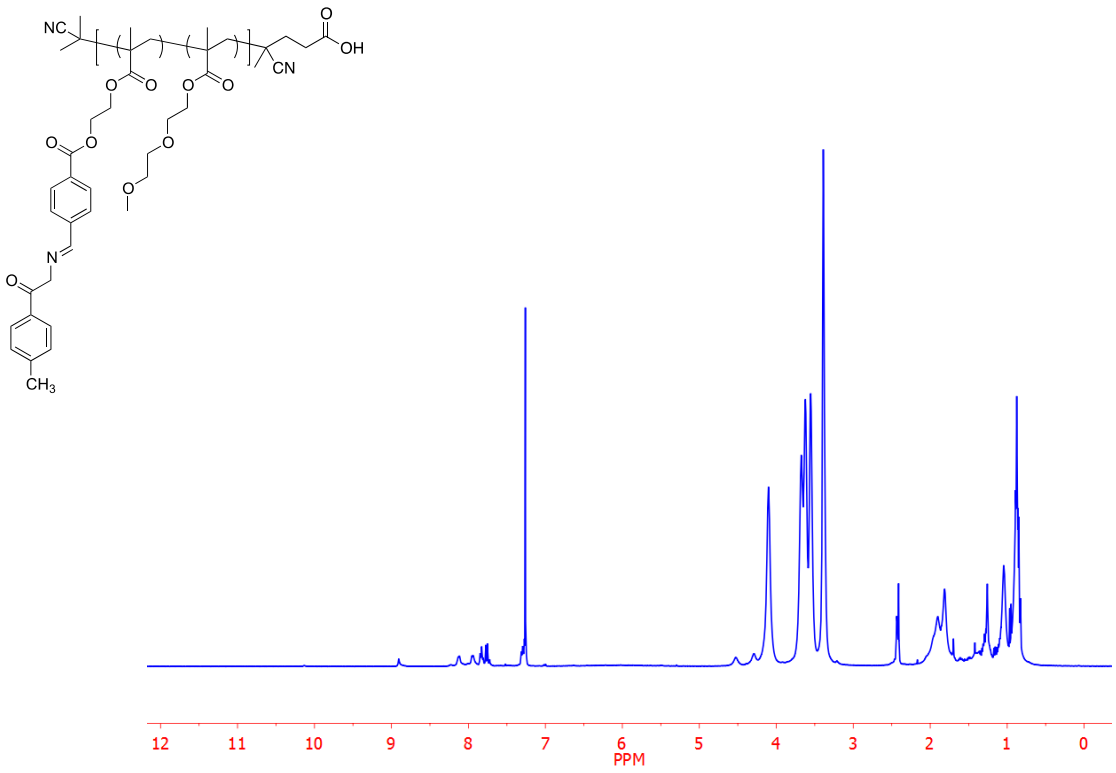

Figure 4S11. ^{1}H NMR of poly(FBEMA-*co*-MEO$_2$MA) following end group removal with AIBN and conjugation to SATHA in CDCl$_3$ (P7).

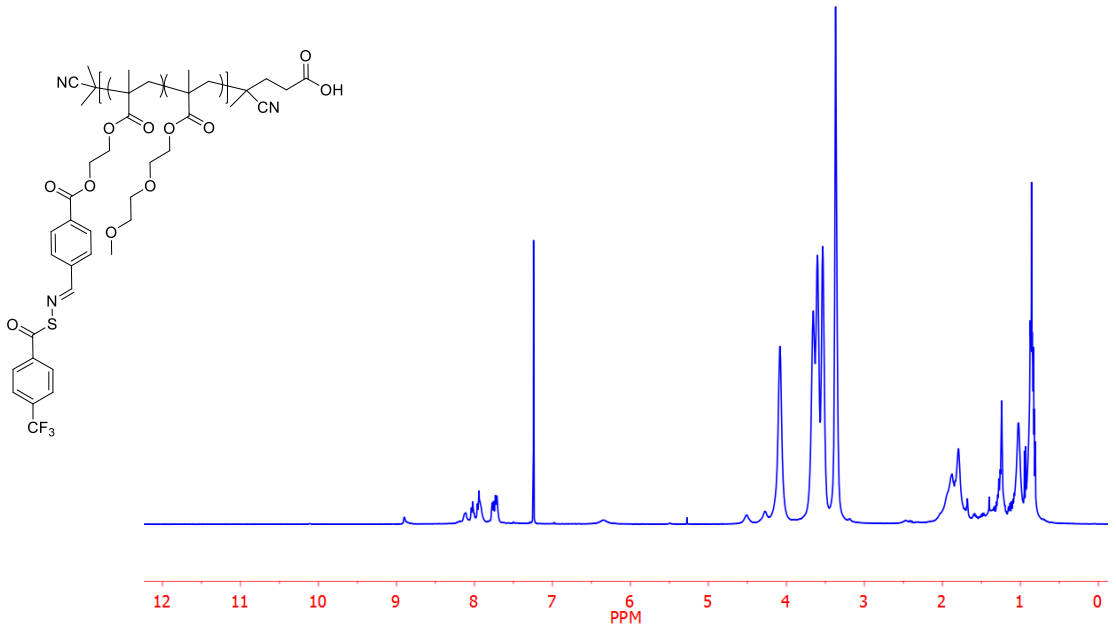

Figure 4S12. ^{1}H NMR of poly(FBEMA-co-MEO$_2$MA) following end group removal with AIBN and conjugation to SATHA in CDCl$_3$ (P8).

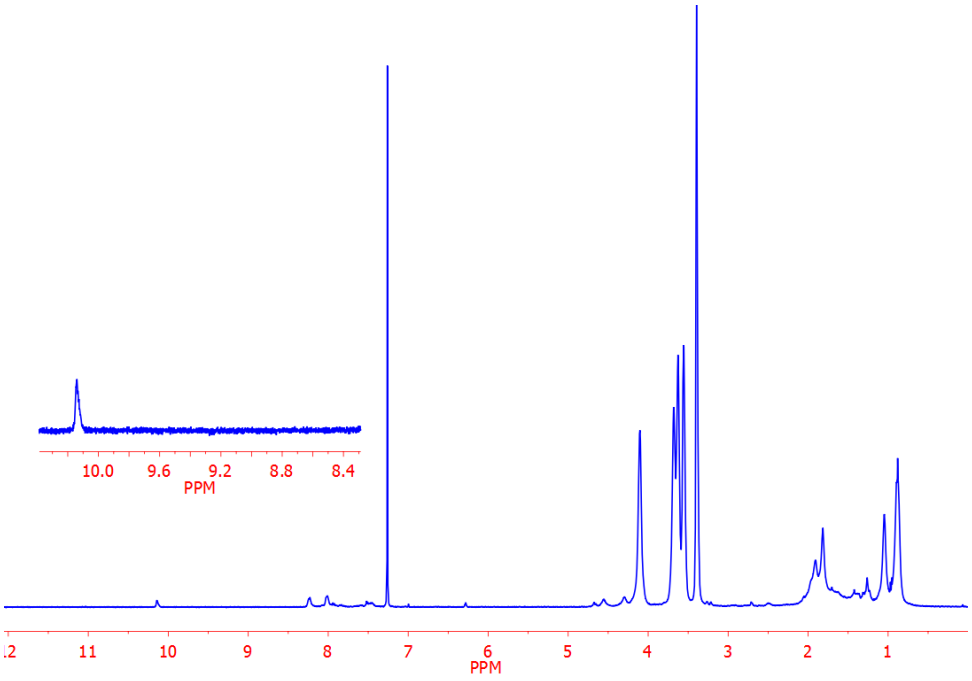

Figure 4S13. ^{1}H NMR of P6 following reaction with glutathione. Quantitative conversion of thiooxime to aldehyde is observed based on the disappearance of the thiooxime peak at 8.67 ppm and appearance of the aldehyde peak at 10.02 ppm.

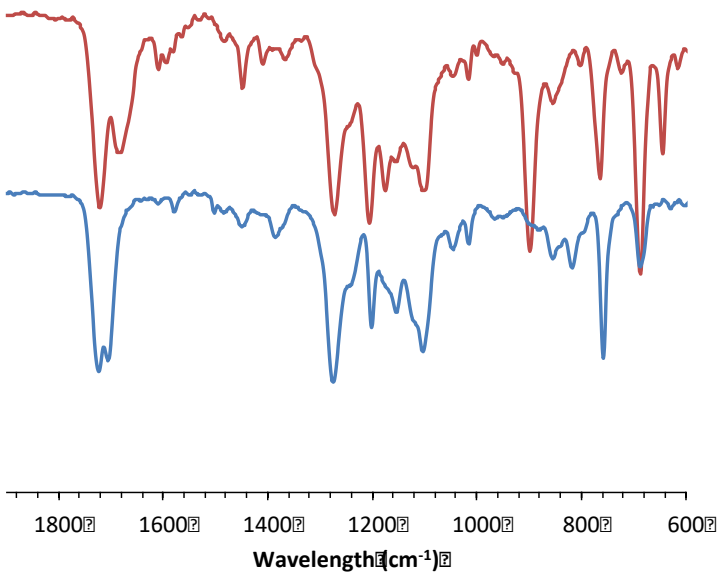

Figure 4S14. IR spectra of P2 (blue trace) and the same polymer following post polymerization reaction with SATHA (P2t) (red trace). The appearance of a peak at 1608 cm^{-1} corresponds to the stretching frequency of the thiooxime C=N bond.

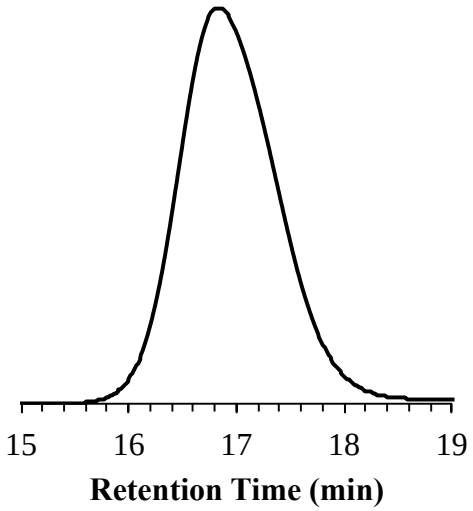

Figure 4S15. GPC trace of P2 in THF (M_n = 17,300 g/mol, Đ = 1.12, dn/dc = 0.140, [FBEMA]:[CTA]:[AIBN] = 300:1:0.2).

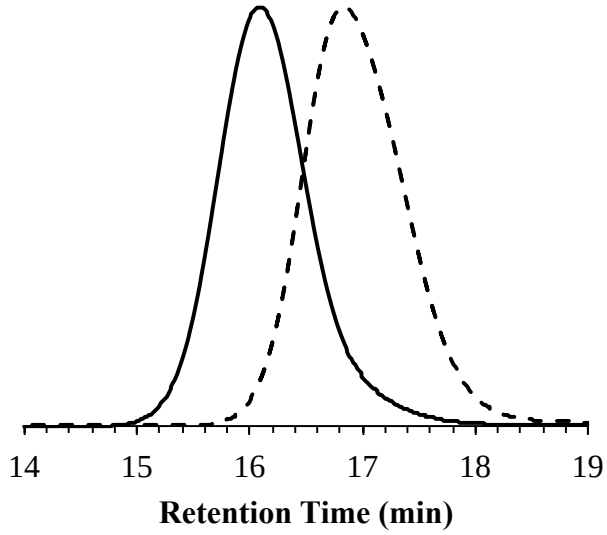

Figure 4S16. GPC trace of P2 (dashed line) chain extended with MMA (P4) (solid line) in THF (M_n = 27,200 g/mol, Đ = 1.11, dn/dc = 0.119, [FBEMA]:[CTA]:[AIBN] = 2000:1:0.2).

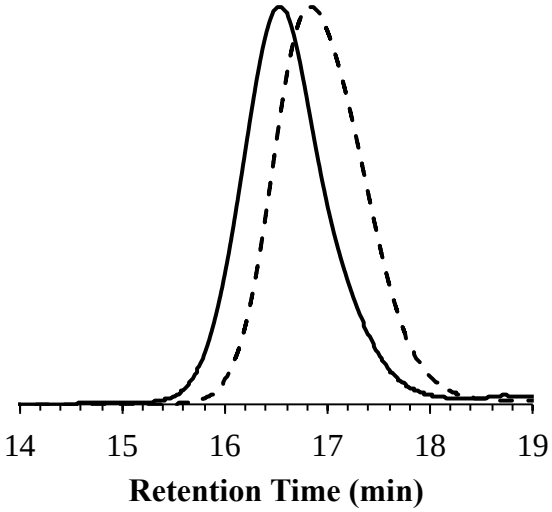

Figure 4S17. GPC trace of P2t (dashed line) following conjugation with SATHA (solid line) in THF (M_n = 25,900 g/mol, Đ = 1.12, dn/dc = 0.188).

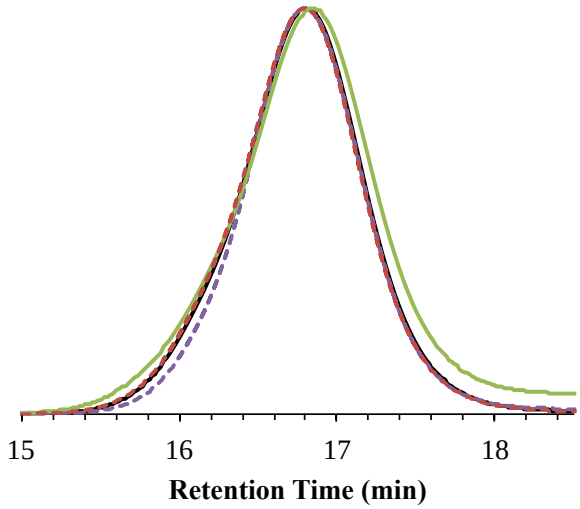

Figure 4S18. GPC traces of P5 following chain end removal with AIBN (red dashed trace, M_n = 11,900, Đ = 1.19, dn/dc = 0.079). The resulting polymer was reacted with three different SATHAs with various substituents at the para position of the SATHA ring (*p*-H, P6, green trace: M_n = 13,800 g/mol, Đ = 1.14, dn/dc = 0.085; *p*-CH_3, P7, purple dashed trace: M_n = 12,600 g/mol, Đ = 1.11, dn/dc = 0.081; *p*-CF_3, P8, black trace: M_n = 11,800 g/mol, Đ = 1.15, dn/dc = 0.078).

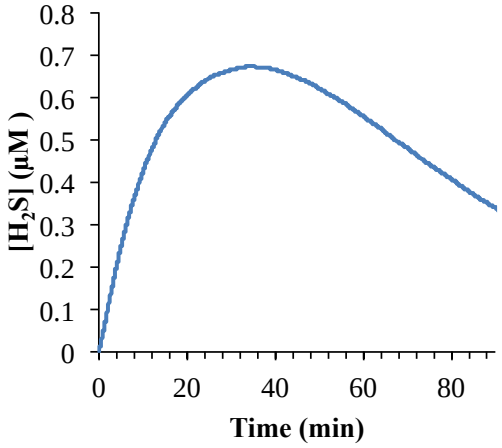

Figure 4S19. H_2S release profile of P6 (10 µM) in the presence of 1 mM glutathione in PBS buffer (pH = 7.4).

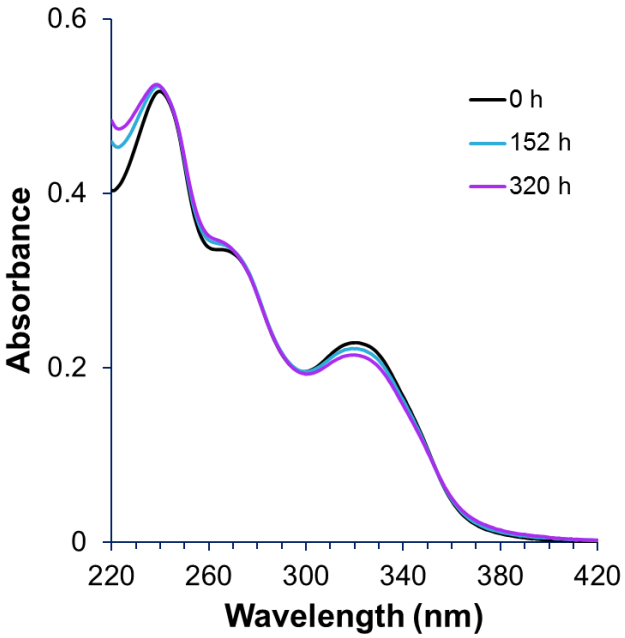

Figure 4S20. Hydrolysis of P2t in 30% ACN in 2 mM phosphate buffer (pH 7.4) at 25 µM starting *S*-aroylthiooxime concentration. Only select time points are shown for clarity. The peak absorbance at 320 nm is assigned to the *S*-aroylthiooxime based on previous work.[1] At 320 h only 4% of the *S*-aroylthiooxime has been hydrolyzed.

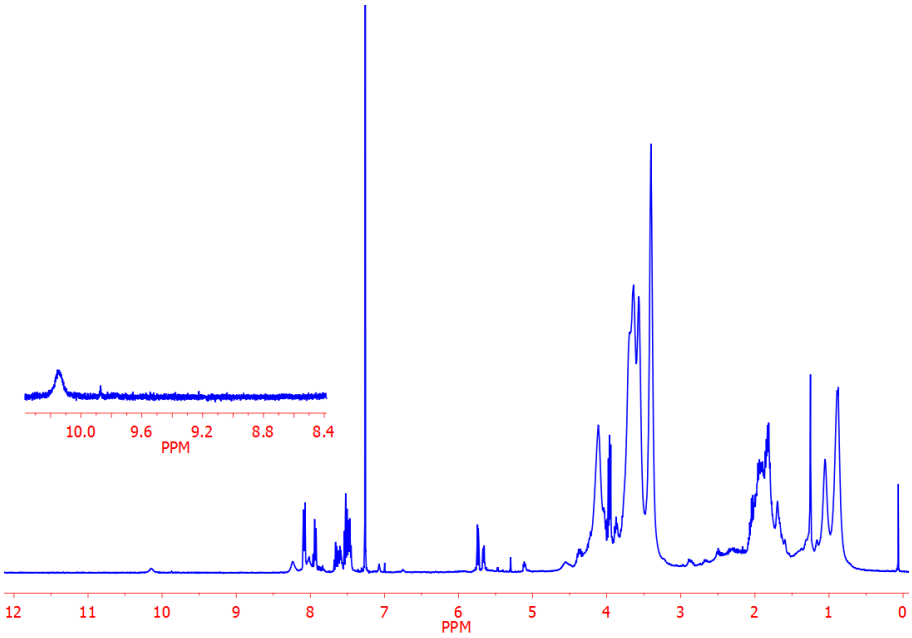

Figure 4S21. ^{1}H NMR spectrum of P6 following hydrolysis of the thiooxime bond for 48 h in THF + 10% HCl solution (2.5 M). Quantitative conversion of thiooxime to aldehyde is observed based on the disappearance of the thiooxime peak at 8.67 ppm and appearance of the aldehyde peak at 10.02 ppm.

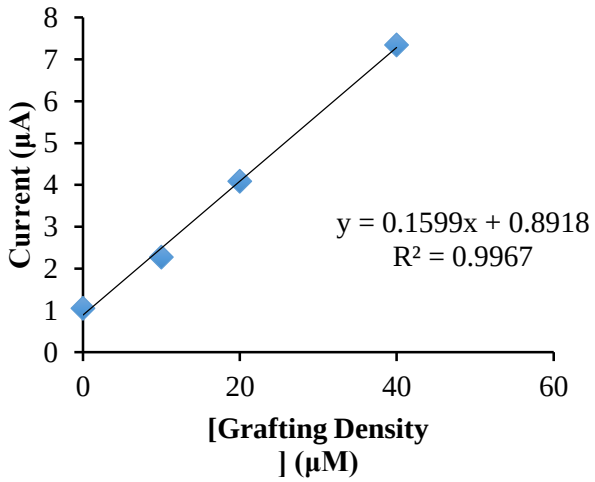

Figure 4S22. Calibration of H_2S-selective microelectrode.

References:

(1) Foster, J. C.; Powell, C. R.; Radzinski, S. C.; Matson, J. B. *Org. Lett.* **2014**, *16*, 1558.

Chapter 5. H_2S-Releasing Polymer Micelles for Studying Selective Cell Toxicity

5.1. Authors

Jeffrey C. Foster,[1] Scott C. Radzinski,[1] Xianlin Zou,[2] Carla V. Finkielstein,[2] John B. Matson[1]

[1]Department of Chemistry and Macromolecules Innovation Institute, Virginia Tech, Blacksburg, Virginia 24061, United States

[2]Department of Biological Sciences, Virginia Tech, Blacksburg, Virginia 24061, United States

5.2. Abstract

We report the preparation of *S*-aroylthiooxime (SATO) functionalized amphiphilic block copolymer micelles that release hydrogen sulfide (H_2S), a gaseous signaling molecule of relevance to various physiological and pathological conditions. The micelles release H_2S in response to cysteine with a half-life of 3.3 h, which is substantially slower than a related small molecule SATO. Exogenous administration of H_2S impacts growth and proliferation of cancer cells; however, the limited control over H_2S generation from inorganic sulfide sources results in conflicting reports. Therefore, we compare the cellular cytotoxicity of SATO-functionalized micelles, which release H_2S in a sustained manner, to Na_2S, which releases H_2S in a single dose. Our results show that H_2S-releasing micelles significantly reduce the survival of HCT116 colon cancer cells relative to Na_2S, GYY4137, and a small molecule SATO, indicating that release kinetics may play an

important role in determining toxicity of H_2S toward cancer cells. Furthermore, H_2S-releasing micelles are well tolerated by immortalized fibroblasts (NIH/3T3 cells), suggesting a selective toxicity of H_2S toward cancer cells.

5.3. Introduction

Hydrogen sulfide (H_2S) belongs to a classification of biologically relevant signaling gases known as gasotransmitters.[1] Gasotransmitters, which also include nitric oxide (NO) and carbon monoxide (CO), have attracted much interest in recent years due to their extensive roles in cellular signaling.[2] For example, H_2S regulates vasodilation, promotes angiogenesis, and generally exhibits beneficial effects as an anti-inflammatory agent.[3-8] To support these biological studies, new chemical tools have been developed over the past ~5 years. These include H_2S sensors, which report on H_2S concentrations in vivo and in vitro,[9-12] compounds triggered by endogenous H_2S to release drugs,[13] and compounds that release H_2S (H_2S donors),[14-22] usually through decomposition reactions initiated by a specific trigger.

The gaseous nature of H_2S and its fast reactivity in biological systems make controlled delivery a necessity and a difficult challenge. To date, most studies of H_2S biology have been conducted with sulfide salts (Na_2S and NaSH). These inorganic sulfide sources generate H_2S instantaneously upon dissolution, resulting in a rapid surge in H_2S concentration followed by a rapid decline. While experimentally convenient, sulfide salts can convolute the results of biological studies due to their rapid release, as the activity of H_2S profoundly depends on its local concentration. For example, evidence suggests that H_2S could be an effective therapeutic candidate due it is ability to selectively reduce survival in cancer cells.[23-24] This is likely the result of the high set point of oxidative stress that cancer cells maintain, making them more susceptible than healthy cells to the cytotoxic pro-oxidant effects exhibited by H_2S in highly oxidative environments.[25] Additionally,

H_2S passes through biological membranes without active transport mechanisms,[3] which may enable deep penetration into the tumor interstitium—a major problem with traditional small molecule chemotherapeutics.[26] Conversely, endogenous levels of H_2S provide a route for some cancer cells to evade standard treatment strategies by promoting angiogenesis, augmenting mitochondrial bioenergetics, activating anti-apoptotic pathways, and controlling cell cycle progression.[27-28] This apparent discrepancy over the response of cancer cells to H_2S may arise from different release rates among different H_2S donors.[23] Therefore, this and other challenges in H_2S biology may be resolved by developing advanced delivery vehicles that produce well-defined quantities of H_2S over controllable timescales.

In the past few years, reports have appeared of a multitude of H_2S-releasing small molecules that more aptly mimic the sustained endogenous production of the gas in vivo.[14-22] However, many small molecule H_2S donors suffer from limitations such as ill-defined release mechanisms, poor water solubility, and inherent (or latent) toxicity. Such small molecule H_2S donors also typically have no capacity for targeting any specific organ and, therefore, only provide systemic delivery of H_2S. More recently, a handful of polymers that release H_2S have addressed some shortcomings of small molecule H_2S donors.[29-33] However, these also have limitations—linear polymers are typically too small to avoid rapid renal clearance in the bloodstream and have limited capacity for targeting a specific site in the body. Polymer micelles made from amphiphilic block copolymers address these challenges because they are typically in the ideal size range (20-100 nm) for long bloodstream circulation and can target specific sites in the body (e.g., a solid tumor) through either passive or active mechanisms.[34-35] Polymer micelles that combine controlled H_2S release with the capacity for in vivo targeting and long bloodstream circulation are therefore needed to advance the field of H_2S biology and to develop novel therapeutics. We present in this report initial efforts to

develop polymer micelles as advanced H_2S delivery vehicles, which we use here for studying toxicity toward a cancer cell line.

5.4. Materials and Methods

Materials

All reagents were obtained from commercial vendors and used as received unless otherwise stated. 2,2′-Azobis(2-methylpropionitrile) (AIBN) was recrystallized from methanol prior to use. *S*-Aroylthiohydroxylamine (SATHA) and SATO1 ($(C_6H_5)C=OSNCH(C_6H_4)COOH$) were prepared according to a previously reported procedure.[17] The monomer 2-(4-formylbenzoyloxy)ethyl methacrylate (FBEMA) was also synthesized as previously reported.[29] Dry solvents were purified by passage through a solvent purification system (MBraun).

Methods

NMR spectra were measured on an Agilent 400 MHz spectrometer. ^1H and ^{13}C NMR chemical shifts are reported in ppm relative to internal solvent resonances. Yields refer to chromatographically and spectroscopically pure compounds unless otherwise stated. Size exclusion chromatography (SEC) was carried out in THF at 1 mL/min at 30 °C on two Agilent PLgel 10 μm MIXED-B columns connected in series with a Wyatt Dawn Heleos 2 light scattering detector and a Wyatt Optilab Rex refractive index detector. No calibration standards were used, and dn/dc values were obtained by assuming 100% mass elution from the columns. TEM samples were drop cast from 1 mg/mL solutions of micelles in H_2O onto carbon-coated copper 300 mesh TEM grids (Electron Microscopy Sciences). Samples were then stained with a 2% solution of uranyl acetate in water. Images were taken on a Philips EM420 TEM with a slow scan CCD camera. UV-Vis absorbance spectra were recorded on a Cary 5000 UV-Vis (Agilent) from 800 to

550 nm or on a Spectramax M2 plate reader (Molecular Devices). Dynamic light scattering (DLS) was conducted using a Malvern Zetasizer Nano operating at 25 °C. A solution of micelles was prepared at 1 mg/mL and filtered with a 0.2 μm filter prior to scanning. The calculations of the particle size distributions and distribution averages were conducted using CONTIN particle size distribution analysis routines with intensity averages. Measurements were made in triplicate and errors reflect standard deviations.

Synthesis of 4-cyano-4-(dodecylsulfanylthiocarbonyl)sulfanyl pentanoic acid (CTA)

Dodecanethiol (10 mL, 41.7 mmol) was dissolved in hexanes (150 mL) in a round bottom flask. To the flask was added a solution of potassium *tert*-butoxide (4.68 g, 41.7 mmol) in THF (50 mL). The reaction mixture was stirred at rt for 20 min. CS_2 was added (2.7 mL, 44.7 mmol), and the reaction was stirred for an additional 1 h. I_2 was then added in portions until the reaction mixture maintained a persistent dark brown color. The reaction mixture was stirred overnight at rt. The reaction mixture was transferred to a separatory funnel and washed consecutively with 10% $Na_2S_2O_3$, H_2O, and brine. The organic layer was then dried over Na_2SO_4 and rotovapped.

The resulting viscous yellow oil (22.8 g, 41.1 mmol) was redissolved in EtOAc (100 mL) in a round bottom flask. To the flask was added 4,4′-azobis(4-cyanovaleric acid) (11.6 g, 41.4 mmol). The reaction mixture was heated at reflux overnight. Silica gel was poured into the reaction flask, and the silica slurry was rotovapped to dryness. The silica was then dry-loaded onto a silica gel column, eluting with 9:1 hexanes/EtOAc. The product-containing fractions (Rf ~ 0.3 in the mobile phase) were combined and rotovapped to give the product as a yellow solid (9.50 g, 57% yield). ^{1}H NMR ($CDCl_3$): δ 3.33 (t, *J* = 4 Hz, 2H), 2.68 (t, *J* = 4 Hz, 2H), 2.54 (m, 1H), 2.39 (m, 1H), 1.88 (s, 3H), 1.69 (q, *J* = 8 Hz, 2H), 1.45-1.19 (m, 18H), 0.88 (t, *J* = 4 Hz, 3H). ^{13}C NMR ($CDCl_3$): δ

216.88, 177.63, 118.99, 46.30, 37.21, 33.58, 32.03, 29.74, 29.67, 29.66, 29.54, 29.46, 29.19, 29.05, 27.78, 24.96, 22.81, 14.25. HR-MS: $[M + H]^+$ calculated 404.1746; found 404.1749.

Synthesis of macroCTA

A round bottom flask was charged with CTA (0.81 g, 2.01 mmol), polyethylene glycol monomethyl ether (M_n = 5,000 g/mol, 2.0 g, 0.400 mmol), 4-dimethylamino pyridine (0.12 g, 0.982 mmol), and anhydrous CH_2Cl_2 (40 mL). *N*,*N*'-Dicyclohexylcarbodiimide (DCC) (0.41 g, 1.99 mmol) was dissolved in 5 mL of anhydrous CH_2Cl_2 in a vial. The DCC solution was added dropwise to the flask containing the other reagents, and the reaction mixture was stirred at rt overnight. The precipitated solids were removed by filtration. The desired product was isolated via precipitation from diethyl ether and was purified by repeated precipitations (2-4) from CH_2Cl_2 into diethyl ether to afford the product as a yellow solid (1.50 g, 69% yield). ^{1}H NMR ($CDCl_3$): δ 4.24 (t, *J* = 4 Hz, 2H), 3.80 (t, *J* = 4 Hz, 2H), 3.71-3.51 (m, 494H), 3.45 (t, *J* = 4 Hz, 2H), 3.36 (s, 3H), 3.31 (t, *J* = 8 Hz, 2H), 2.64 (t, *J* = 8 Hz, 2H), 2.51 (m, 1H), 2.37 (m, 1H), 1.86 (s, 3H), 1.68 (t, *J* = 8 Hz, 2H), 1.42-1.18 (m, 18H), 0.87 (t, *J* = 4 Hz, 3H).

Synthesis of PEG-b-poly(FBEMA)

A typical polymerization procedure is as follows: To an oven-dried Schlenk tube equipped with a magnetic stir bar was added macroCTA (127 mg, 25.0 μmol), FBEMA (1.00 g, 3.81 mmol), and 5 mL of anhydrous DMF. A solution of 2,2′-azobis(2- methylpropionitrile) (AIBN) was prepared by dissolving 4.2 mg (2.54 μmol) in 1 mL of anhydrous DMF in a vial. 100 μL of this solution was added to the Schlenk tube. The tube was deoxygenated by subjecting the contents to three freeze−pump−thaw cycles. The Schlenk tube was then backfilled with N_2 and submerged in an oil bath maintained at 75 °C. Samples were removed periodically by N_2-purged syringe to monitor

molecular weight evolution by GPC and conversion by ^{1}H NMR spectroscopy. The polymerization was quenched by submerging the tube into liquid N_2 and exposing the reaction solution to air. The resulting PEG-*b*-poly(FBEMA) was isolated via precipitation from a diethyl ether. If necessary, further precipitations from CH_2Cl_2 into diethyl ether were preformed to remove residual monomer.

Removal of Dithioester End Group

A round-bottom flask was charged with PEG-*b*-poly(FBEMA) (0.50 g, 14.0 μmol), AIBN (47.0 mg, 284 μmol), and 1,4-dioxane (3 mL). The flask was outfitted with a condenser, and the reaction mixture was heated in an oil bath maintained at 80 °C for 1.5 h. The reaction mixture was allowed to cool to rt, and the polymer was recovered via precipitation from diethyl ether.

Addition of SATHA to PEG-*b*-poly(FBEMA)

A general procedure for the SATO formation reaction is as follows. Following end group removal, PEG-*b*-poly(FBEMA) (100 mg, 3.21 μmol) was dissolved in CH_2Cl_2 (3 mL) in a 1 dram vial. To the vial was added SATHA (147 mg, 962 μmol) in one portion. Approximately 10 μL of trifluoroacetic acid (TFA) was added as a catalyst. The reaction mixture was left to stand at rt for 16 h over molecular sieves. ^{1}H NMR spectroscopy was conducted after this time to determine the conversion of aldehyde to SATO. The modified polymer was recovered via precipitation from diethyl ether.

Determination of Critical Micelle Concentrations (CMCs)

A micelle stock solution was prepared at 0.1 mg/mL in H_2O. This solution was diluted with water to afford concentrations of 0.05, 0.04, 0.03, 0.02, 0.01, 0.005, 0.001, 0.0001, 0.00001, and 0.000001 mg/mL. 2 μL of a 1 mg/mL Nile red solution in acetone was added to each dilution to make a final volume of 2 mL. The samples were transferred to a 96 well plate and were placed in

a vacuum oven set to 30 °C for at least 2 h to ensure complete evaporation of acetone. Fluorescence emission spectra were recorded for each sample (λ_{ex} = 530 nm), and the emission intensity at 630 nm was plotted against log(concentration). The CMC value was taken to be the intersection between the linear fits of the high and low concentration regimes.

H_2S Release Kinetics via Methylene Blue Method

Reactions for kinetics studies were run in triplicate, with each reaction vial containing 20 µL of phosphate buffer (1 M in H_2O, pH = 7), micelle solution (volume dependent on polymer concentration and SATO loading), 100 µL $Zn(OAc)_2$ solution (40 mM in H_2O), 20 µL cysteine solution (100 mM in H_2O), and DI H_2O to make 2 mL total volume. Final concentrations were 250 µM in SATO functional groups, 2 mM $Zn(OAc)_2$, and 1 mM Cys. A blank solution was also run for each experiment that did not contain micelles. At predetermined timepoints, 100 µL was removed from each vial. Each 100 µL aliquot was diluted with 100 µL $FeCl_3$ solution (30 mM in 1.2 M HCl) followed by 100 µL *N*,*N*-dimethyl-*p*-phenylenediamine (20 mM in 7.2 M HCl). Aliquots were stored for a minimum of 24 h after the final aliquot had been taken. The absorbance of each sample was measured at 750 nm using a plate reader. Kinetic analysis was done by subtracting the absorbance of the blank solution from the average absorbance at each timepoint. First-order half-lives of H_2S release were determined by plotting time vs. ln(1/(1 - %released), with $t_{1/2}$=ln(2)/slope. The conversion of the reaction was obtained by normalizing the absorbance values to the maximum absorbance that was measured for each experiment (or the value at which the plot of absorbance vs time reached a plateau).

Calibration Procedure for the Methylene Blue Assay

A 15 mM Na_2S stock solution was prepared by dissolving 24 mg of Na_2S in 20 mL of DI H_2O. This solution was then diluted 10X with H_2O to give a 1.5 mM Na_2S solution. Na_2S solutions at concentrations ranging from 5-100 μM were prepared in triplicate by mixing the appropriate volume of 1.5 mM Na_2S stock solution with 20 μL of 1M phosphate buffer and then diluting with DI H_2O to a total volume of 1 mL. Samples were prepared by removing 100 μL of each Na_2S solution and diluting with 100 μL $FeCl_3$ solution (30 mM in 1.2 M HCl) followed by 100 μL *N*,*N*-dimethyl-*p*-phenylenediamine (20 mM in 7.2 M HCl). Aliquots were stored for a minimum of 24 h after the final aliquot had been taken. The absorbance of each sample was measured at 750 nm using a plate reader. A calibration curve was prepared by plotting absorbance for each data point as a function of [Na_2S].

H_2S Release Profile via Methylene Blue Method

Reactions for measurement of the H_2S release profile were conducted in triplicate, with each reaction vial containing 20 μL of phosphate buffer (1 M in H_2O, pH = 7), micelle solution (volume dependent on polymer concentration and SATO loading), 20 μL cysteine solution (100 mM in H_2O), and DI H_2O to make 2 mL total volume. Final concentrations were 250 μM in SATO functional groups and 1 mM Cys. A blank solution was also run for each experiment that did not contain micelles. Additional controls without Cys were also conducted with and without micelles. At predetermined timepoints, 100 μL was removed from each vial. Each 100 μL aliquot was diluted with 100 μL $FeCl_3$ solution (30 mM in 1.2 M HCl) followed by 100 μL *N*,*N*-dimethyl-*p*-phenylenediamine (20 mM in 7.2 M HCl). Aliquots were stored for a minimum of 24 h after the

final aliquot had been taken. The absorbance of each sample was measured at 750 nm using a plate reader. The concentration of H_2S at each time point was then plotted using the calibration curve.

Cell culture and clonogenic survival assay

Colorectal carcinoma HCT116 cells (ATCC CCL-247) and embryonic fibroblast NIH/3T3 cells (ATCC CRL-1658) were obtained from ATCC. HCT116 cells were propagated in HyClone McCoy's 5a medium (GE Healthcare), supplemented with 10% fetal bovine serum (Corning), 50 IU/mL penicillin, and 50 μg/mL streptomycin (MP Biomedicals). Fibroblasts were maintained in ATCC-formulated Dulbecco's modified Eagle's Medium supplemented containing 10% calf serum (ATCC 31334) and penicillin/streptomycin antibiotics as above. For all experiments, cells were maintained at 37ºC/5% CO_2 until reaching 50-80% confluence.

For clonogenic assays, exponentially growing HCT116 or NIH/3T3 cells were harvested, and various dilutions of cells (500 to 2000 cells/well) were seeded into 6-well plates and allowed to attach overnight in the incubator before adding different formulations. Each cell type was titrated with various dose-concentration of SATO groups in active micelles ranging from 50 to 250 μM in the presence of 1 mM Cys for ~6 h. Corresponding controls include cells treated with 50–250 μM Na_2S, active micelles at 250 μM SATO in the absence of Cys, inactive micelles lacking the SATO group (250 μM aldehyde precursor) in the presence or absence of 1 mM Cys, or 1 mM Cys alone. Plates were transferred to 37ºC/5% CO_2 until cells in control wells had formed sufficiently large clones (~10 days), after which they were fixed with a mixture of 6% glutaraldehyde/0.5% crystal violet for 30 min at room temperature. After removing the fixative, plates with colonies were allowed to dry at room temperature before manual counting. The surviving fraction of cells after treatment was calculated, taking into account the plating efficiency of control cells. All

experiments were performed in triplicate, and the means and standard deviations were plotted using Excel and tested for statistical significance using a paired *t-test*.

5.5. Results and Discussion

We recently reported on the *S*-aroylthiooxime (SATO) functional group, which represents one type of versatile H_2S donor.[17] SATOs were efficiently prepared in one step via reaction of an *S*-aroylthiohydroxylamine (SATHA) with an aromatic aldehyde. H_2S release from SATOs was selectively triggered by a thiol, and release kinetics were fine-tuned by manipulating the substituents on the aromatic ring of the parent *S*-aroylthiohydroxylamine, with half-lives of release ranging from 8–82 min under the conditions tested. The SATO-forming reaction was also recently used for post-polymerization modification to prepare H_2S-releasing polymers.[29] Based on the versatility and robustness of SATOs, we sought to prepare a new type of supramolecular H_2S donor that exhibited sustained release, would possess enhanced pharmacokinetics in vivo, and could be further functionalized for specific tissue targeting to solid tumors.

To prepare a SATO-containing polymer amphiphile, a PEGylated chain transfer agent (CTA) for reversible addition–fragmentation chain transfer (RAFT) polymerization was synthesized. This macroCTA was employed in RAFT polymerization of 2-(4-formylbenzoyloxy)ethyl methacrylate (FBEMA) in the presence of 2,2′-azobis(2-methylpropionitrile) (AIBN) to produce a block copolymer of the form PEG-*b*-poly(FBEMA) (Figure 5.1A). The block polymer was of narrow dispersity (Đ = 1.05) with a monomodal molecular weight distribution (Figure 5.1B and Figure 5S8). A high degree of chain end functionalization with the desired PEG block was confirmed by comparing polymer number average molecular weights (M_ns) measured by SEC (17.9 kDa), calculated from monomer conversions (17.7 kDa), and determined by ^{1}H NMR end group analysis (16.9 kDa).

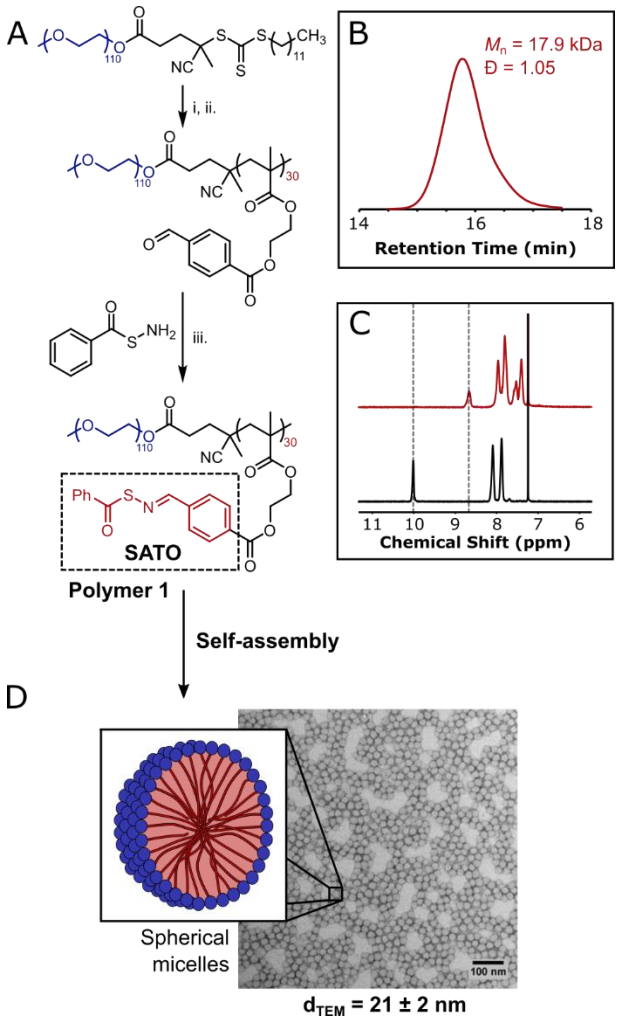

Figure 5.1. Synthesis of SATO-containing polymer 1. A) Synthetic route. Experimental conditions: i) FBEMA, AIBN, DMF, 70 °C; ii) AIBN, dioxane, reflux; iii) CH_2Cl_2, molecular sieves, TFA (cat), rt. B) SEC trace of polymer 1. C) ^{1}H NMR spectrum before (bottom trace) and after (top trace) SATO formation. Dashed lines at 10.0 and 8.6 ppm highlight the aldehyde and SATO resonances, respectively. D) Conventional TEM images of self-assembled micelles of polymer 1.

The thiocarbonyl-thio moiety can react with nucleophiles such as thiols to yield a variety of sulfur-containing byproducts, including H_2S.[36] Therefore, the trithiocarbonate end groups at the ω-chain ends were displaced by using an excess of AIBN in refluxing dioxane (Figures 5.1A and 5S12), as reported previously.[29] The polymer was then treated with 2 equiv of *S*-benzoylthiohydroxylamine in the presence of catalytic trifluoroacetic acid (TFA) to afford block copolymer **1**. ^{1}H NMR spectroscopy confirmed complete SATO formation. Importantly, SATO formation did not increase the modality of the SEC trace (Figure 5S8); the expected increase in

molecular weight was observed in accordance with the added mass of the newly-formed SATOs (Table 5S1).

To prepare H_2S-releasing micelles, the block copolymers were dissolved in THF, diluted with an equal volume of H_2O, and dialyzed against H_2O for 48 h. TEM revealed uniform spherical particles of average diameter of 21 ± 2 nm (Figure 5.1D and 5S12). This diameter represents the dimension of the hydrophobic micelle core, as the hydrophilic PEG coronae are not typically observed via TEM. The observed core diameter matches the expected value for spherical micelles of ~19 nm calculated assuming fully extended SATO block chains. DLS further confirmed a single population of aggregates of diameter 38 ± 4 nm (Figure 5S9). The slightly smaller size obtained from TEM is unsurprising as TEM is conducted on dried samples that do not possess extended hydration spheres.[37] The micelles were stable in DI H_2O and in PBS buffer (pH = 7) over a period of 24 h (Figure 5S10). Their critical aggregation concentration measured via the Nile red assay was 10 μg/mL (Figure 5S13).

The kinetics of H_2S release were measured with the methylene blue assay.[38] By monitoring the absorbance over time, the relative rate of methylene blue formation can be measured and correlated to the rate of H_2S release.[17, 39] H_2S release could also be triggered by other biologically relevant thiols such as glutathione (GSH);[17] however, GSH reduces methylene blue to the non-colored leucomethylene blue, making quantification of half-lives by the methylene blue assay difficult.[40] H_2S release kinetic experiments were carried out in the presence of $Zn(OAc)_2$ to capture the H_2S as it was released by the micelles. From these data, the pseudo-first-order half-life of H_2S release from the micelles triggered by Cys was calculated to be 3.3 ± 0.4 h (Figure 5.2). As expected, this half-life is significantly longer than that measured for a related small molecule SATO ($t_{1/2}$ = 22 min). We attribute this difference in rate to the slow diffusion of the Cys trigger into the

hydrophobic cores of the polymer micelles. The concentration profile of H_2S released from the micelles was also determined by conducting the methylene blue assay in the absence of the trapping agent $Zn(OAc)_2$. The concentration of H_2S at each time point was then calculated using a calibration curve. In this experiment, H_2S concentration reached a peaking value of ~9.5 μM after 1 h before slowly falling off (Figure 5S17). This low concentration of H_2S relative to H_2S donor is unsurprising given the slow release rate of the micelles and the transient nature of H_2S.

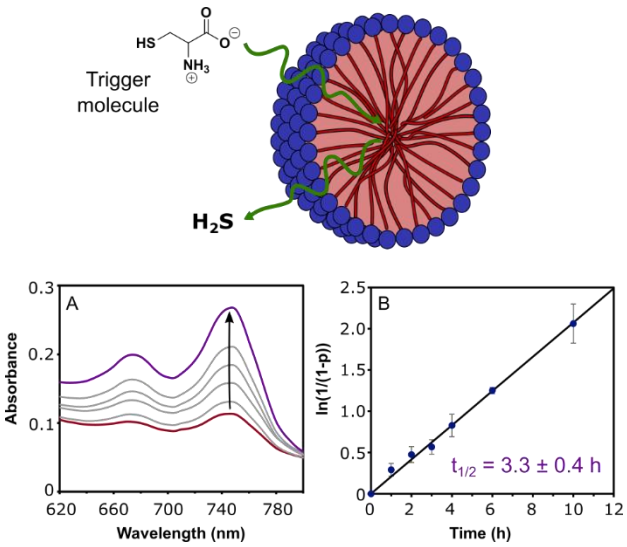

Figure 5.2. Kinetic analyses of H_2S release from micelles prepared from polymer 1. A) Raw output from methylene blue assay highlighting the increase in absorption at 750 nm. B) Pseudo-first-order kinetic plot of H_2S release reaction. Reactions were conducted at [SATO] = 250 μM in the presence of 1 mM Cys and 2 mM $Zn(OAc)_2$ in phosphate buffer (pH = 7).

We investigated the impact of the slow, sustained release of H_2S from SATO-functionalized micelles versus its burst release from Na_2S in cell viability by using a clonogenic assay. As a proof-of-concept, we selected two well-established and contrasting cellular models: HCT116 colon carcinoma cells, the model of choice for many cancer biology studies, and immortalized NIH/3T3 fibroblasts, a spontaneously-generated cell line that retains major normal characteristics and is considered the "normal" standard for comparisons with transformed cells. These cell lines, besides being relatively easy to manipulate, have been shown to be, in the case of HCT116, invasive and

motile in vitro,[41-42] highly tumorigenic in xenograft experiments,[43] and metastatic in orthotopic models;[44] whereas NIH/3T3 fibroblasts retain major normal cells characteristics including contact inhibition, monolayer growth, and are incapable of inducing tumorigenesis when injected in animals.[45]

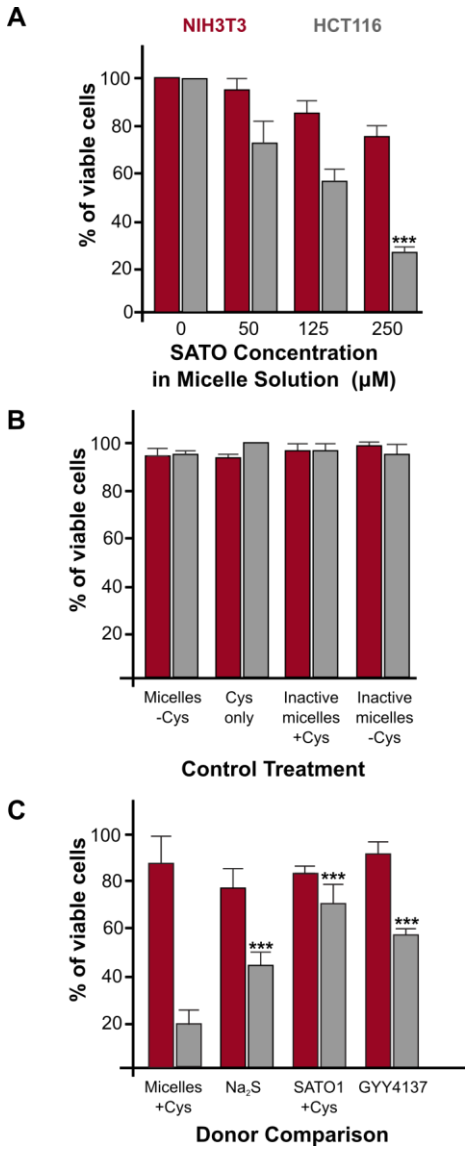

Figure 5.3. Clonogenic survival assay. A) Titration of cells with active micelles prepared from polymer 1 in the presence of 1 mM Cys. Statistical significance was determined by paired t-test; * indicates $p < 0.001$ compared to cell media alone. B) Control experiments demonstrating that toxicity toward cancer cells derives from H_2S release from the active micelles, which only occurs in the presence of Cys. Polymer concentration was held constant at 8.3 μM (corresponding to 250 μM SATO/aldehyde groups), and Cys was applied at 1 mM in all cases. C) Comparison of the effect of**

active micelles to other common H_2S donors on cell viability. Donor concentration was 250 μM for all experiments (in terms of [SATO] for the micelles) and Cys was applied at 1 mM where noted. Statistical significance was determined by paired t-test; * indicates $p < 0.001$ compared to active micelles. In all experiments, clonogenic assays of NIH/3T3 and HCT116 cells (red and grey bars, respectively) were performed in 6-well plates after treatment for 24 h. Data are presented as the mean ± s.d. from 2–3 independent experiments performed in triplicate.**

Experiments were performed by treating cells with micelles of polymer **1** in the presence or absence of Cys, Cys alone, and various other controls for 24 h, followed by quantification of the number of viable cells in each treatment group. A significant, concentration-dependent decrease in cell viability was observed for HCT116 cells treated with active micelles in the presence of added Cys (Figure 5.3A). H_2S released from micelles of polymer **1** led to a less pronounced, but still evident, decrease in viability for NIH/3T3 cells. Other related studies show an increase in NIH/3T3 cell viability with added H_2S.[39, 46] The reason for the discrepancy between our studies here and previous reports is unclear, but it may be due to the rate of H_2S release or minor differences in how the experiments were conducted. No significant decrease in viability was observed for either cell line for micelles in the absence of Cys (which would not produce H_2S) or Cys alone (Figure 5.3B). Additionally, inactive micelles prepared from a precursor to polymer **1** that lacked SATO functionalization (and cannot produce H_2S) had a similarly negligible effect on the viability of HTC116 or NIH/3T3 cells, both with and without added Cys. Finally, cells were treated with byproducts of the H_2S-releasing reaction, shown in Scheme 5S1, to determine their effect on cell viability. A solution of spent micelles was prepared by treating the micelles with 1 mM Cys in PBS buffer for 24 h. This spent micelle solution was assumed to contain both *N*-benzoylcysteine and cystine based on previous experiments with small molecule SATOs.[17] The spent micelle solution exhibited no significant cytotoxicity towards either cell line (Figure 5S15A). The cells were also treated with NH_4Cl, a source of NH_4^+, which we hypothesize is formed as a byproduct of H_2S release. The applied NH_4Cl did not reduce cell viability in the concentration

range tested (Figure 5S15B). Taken together, these control experiments suggest that the observed decrease in viability in HTC116 cells treated with active micelles originates from H_2S. Importantly, the difference in the survival of the two cell types indicates some selectivity for these micelles in killing cancer cells.

In addition, the reduction in cell viability observed with H_2S-releasing micelles of polymer **1** was compared to other common H_2S donors (Figure 5.3C), including Na_2S, **SATO1** (a small molecule SATO ($(C_6H_5)C=OSNCH(C_6H_4)COOH$)), and **GYY4137** (an H_2S donor with a release half-life on the order of days–weeks). In all cases, the H_2S-releasing micelles significantly decreased cell viability in HCT116 cells compared to alternative H_2S donors. No significant changes in viability were observed for NIH/3T3 cells across the different donor types. We attribute the enhanced toxicity of the micelles toward HCT116 cells compared to that of alternative donors to release rate. More mechanistic studies will be needed to optimize dosage and release rates, and to identify any selective intermediary molecules involved.

5.6. Conclusions

In summary, we have prepared H_2S-releasing micelles based on SATO-functionalized polymer amphiphiles. The micelles significantly reduced the survival of HCT116 cells compared to other common H_2S donors, including Na_2S, a small molecule SATO, and GYY4137. Promisingly, the micelles were well tolerated by healthy NIH/3T3 cells. These H_2S-releasing micelles provide a valuable tool for studying H_2S in biological systems, both in vitro and as potential targeted H_2S delivery vehicles in vivo.

5.7. References

1. Wang, R., Two's company, three's a crowd: can H_2S be the third endogenous gaseous transmitter? *FASEB J.* **2002,** *16* (13), 1792-1798.

2. Mustafa, A. K.; Gadalla, M. M.; Snyder, S. H., Signaling by Gasotransmitters. *Sci. Signal.* **2009,** *2* (68), re2.

3. Wang, R., Physiological Implications of Hydrogen Sulfide: A Whiff Exploration That Blossomed. *Physiol. Rev.* **2012,** *92* (2), 791-896.

4. Szabo, C., Hydrogen sulphide and its therapeutic potential. *Nat. Rev. Drug Discov.* **2007,** *6* (11), 917-935.

5. Papapetropoulos, A.; Pyriochou, A.; Altaany, Z.; Yang, G.; Marazioti, A.; Zhou, Z.; Jeschke, M. G.; Branski, L. K.; Herndon, D. N.; Wang, R.; Szabo, C., Hydrogen sulfide is an endogenous stimulator of angiogenesis. *Proc. Natl. Acad. Sci. U. S. A.* **2009,** *106* (51), 21972-21977, S21972/1-S21972/5.

6. Calvert, J. W.; Coetzee, W. A.; Lefer, D. J., Novel Insights Into Hydrogen Sulfide-Mediated Cytoprotection. *Antioxid. Redox Signal.* **2010,** *12* (10), 1203-1217.

7. Kashfi, K.; Olson, K. R., Biology and therapeutic potential of hydrogen sulfide and hydrogen sulfide-releasing chimeras. *Biochem. Pharmacol.* **2013,** *85* (5), 689-703.

8. Shibuya, N.; Koike, S.; Tanaka, M.; Ishigami-Yuasa, M.; Kimura, Y.; Ogasawara, Y.; Fukui, K.; Nagahara, N.; Kimura, H., A novel pathway for the production of hydrogen sulfide from D-cysteine in mammalian cells. *Nat Commun* **2013,** *4*, 1366.

9. Bailey, T. S.; Pluth, M. D., Chemiluminescent Detection of Enzymatically Produced Hydrogen Sulfide: Substrate Hydrogen Bonding Influences Selectivity for H_2S over Biological Thiols. *J. Am. Chem. Soc.* **2013,** *135* (44), 16697-16704.

10. Montoya, L. A.; Pluth, M. D., Selective turn-on fluorescent probes for imaging hydrogen sulfide in living cells. *Chem. Commun.* **2012,** *48* (39), 4767-4769.

11. Peng, B.; Zhang, C.; Marutani, E.; Pacheco, A.; Chen, W.; Ichinose, F.; Xian, M., Trapping Hydrogen Sulfide (H_2S) with Diselenides: The Application in the Design of Fluorescent Probes. *Org. Lett.* **2015,** *17* (6), 1541-1544.

12. Lin, V. S.; Chen, W.; Xian, M.; Chang, C. J., Chemical probes for molecular imaging and detection of hydrogen sulfide and reactive sulfur species in biological systems. *Chem. Soc. Rev.* **2015,** *44* (14), 4596-4618.

13. Zhang, H.; Kong, X.; Tang, Y.; Lin, W., Hydrogen Sulfide Triggered Charge-Reversal Micelles for Cancer-Targeted Drug Delivery and Imaging. *ACS applied materials & interfaces* **2016,** *8* (25), 16227-39.

14. Zhao, Y.; Wang, H.; Xian, M., Cysteine-activated hydrogen sulfide (H_2S) donors. *J. Am. Chem. Soc.* **2011,** *133*, 15-17.

15. Wallace, J. L., Hydrogen sulfide-releasing anti-inflammatory drugs. *Trends Pharmacol. Sci.* **2007,** *28* (10), 501-505.

16. Kodela, R.; Chattopadhyay, M.; Kashfi, K., NOSH-Aspirin: A Novel Nitric Oxide–Hydrogen Sulfide-Releasing Hybrid: A New Class of Anti-inflammatory Pharmaceuticals. *ACS Med. Chem. Lett.* **2012,** *3* (3), 257-262.

17. Foster, J. C.; Powell, C. R.; Radzinski, S. C.; Matson, J. B., S-Aroylthiooximes: A Facile Route to Hydrogen Sulfide Releasing Compounds with Structure-Dependent Release Kinetics. *Org. Lett.* **2014,** *16* (6), 1558-1561.

18. Devarie-Baez, N. O.; Bagdon, P. E.; Peng, B.; Zhao, Y.; Park, C.-M.; Xian, M., Light-Induced Hydrogen Sulfide Release from "Caged" gem-Dithiols. *Org. Lett.* **2013,** *15* (11), 2786-2789.

19. Zhao, Y.; Biggs, T. D.; Xian, M., Hydrogen sulfide (H_2S) releasing agents: chemistry and biological applications. *Chem. Commun.* **2014,** *50* (80), 11788-11805.

20. Chattopadhyay, M.; Kodela, R.; Nath, N.; Dastagirzada, Y. M.; Velazquez-Martinez, C. A.; Boring, D.; Kashfi, K., Hydrogen sulfide-releasing NSAIDs inhibit the growth of human cancer cells: A general property and evidence of a tissue type-independent effect. *Biochem. Pharmacol.* **2012,** *83* (6), 715-722.

21. Li, L.; Whiteman, M.; Guan, Y. Y.; Neo, K. L.; Cheng, Y.; Lee, S. W.; Zhao, Y.; Baskar, R.; Tan, C.-H.; Moore, P. K., Characterization of a Novel, Water-Soluble Hydrogen Sulfide-Releasing Molecule (GYY4137). *Circulation* **2008,** *117* (18), 2351-2360.

22. Szczesny, B.; Módis, K.; Yanagi, K.; Coletta, C.; Le Trionnaire, S.; Perry, A.; Wood, M. E.; Whiteman, M.; Szabo, C., AP39, a novel mitochondria-targeted hydrogen sulfide donor, stimulates cellular bioenergetics, exerts cytoprotective effects and protects against the loss of mitochondrial DNA integrity in oxidatively stressed endothelial cells in vitro. *Nitric Oxide* **2014,** *41*, 120-130.

23. Wu, D.; Si, W.; Wang, M.; Lv, S.; Ji, A.; Li, Y., Hydrogen sulfide in cancer: Friend or foe? *Nitric Oxide* **2015,** *50*, 38-45.

24. Lee, Z. W.; Teo, X. Y.; Tay, E. Y. W.; Tan, C. H.; Hagen, T.; Moore, P. K.; Deng, L. W., Utilizing hydrogen sulfide as a novel anti-cancer agent by targeting cancer glycolysis and pH imbalance. *Br. J. Pharmacol.* **2014,** *171* (18), 4322-4336.

25. Filomeni, G.; Aquilano, K.; Rotilio, G.; Ciriolo, M. R., Reactive Oxygen Species-dependent c-Jun NH2-terminal Kinase/c-Jun Signaling Cascade Mediates Neuroblastoma Cell Death Induced by Diallyl Disulfide. *Cancer Research* **2003,** *63* (18), 5940-5949.

26. Cairns, R.; Papandreou, I.; Denko, N., Overcoming Physiologic Barriers to Cancer Treatment by Molecularly Targeting the Tumor Microenvironment. *Clin. Cancer. Res.* **2006,** *4* (2), 61-70.

27. Szabo, C.; Coletta, C.; Chao, C.; Módis, K.; Szczesny, B.; Papapetropoulos, A.; Hellmich, M. R., Tumor-derived hydrogen sulfide, produced by cystathionine-β-synthase, stimulates bioenergetics, cell proliferation, and angiogenesis in colon cancer. *PNAS* **2013,** *110* (30), 12474-12479.

28. *Chemistry, Biochemistry and Pharmacology of Hydrogen Sulfide*. Springer International Publishing: Switzerland, 2015; Vol. 230.

29. Foster, J. C.; Matson, J. B., Functionalization of Methacrylate Polymers with Thiooximes: A Robust Postpolymerization Modification Reaction and a Method for the Preparation of H_2S-Releasing Polymers. *Macromolecules* **2014,** *47* (15), 5089-5095.

30. Hasegawa, U.; van der Vlies, A. J., Design and Synthesis of Polymeric Hydrogen Sulfide Donors. *Bioconjugate Chem.* **2014,** *25* (7), 1290-1300.

31. Carter, J. M.; Qian, Y.; Foster, J. C.; Matson, J. B., Peptide-based hydrogen sulphide-releasing gels. *Chem. Commun. (Cambridge, U. K.)* **2015,** *51* (66), 13131-13134.

32. Long, T. R.; Wongrakpanich, A.; Do, A.-V.; Salem, A. K.; Bowden, N. B., Long-term release of a thiobenzamide from a backbone functionalized poly(lactic acid). *Polym. Chem.* **2015,** *6* (40), 7188-7195.

33. Qian, Y.; Matson, J. B., Gasotransmitter delivery via self-assembling peptides: Treating diseases with natural signaling gases. *Adv. Drug Deliv. Rev.*

34. Nguyen, M. M.; Carlini, A. S.; Chien, M.-P.; Sonnenberg, S.; Luo, C.; Braden, R. L.; Osborn, K. G.; Li, Y.; Gianneschi, N. C.; Christman, K. L., Enzyme-Responsive Nanoparticles for Targeted Accumulation and Prolonged Retention in Heart Tissue after Myocardial Infarction. *Adv. Mater.* **2015,** *27* (37), 5547-5552.

35. Ambade, A. V.; Savariar, E. N.; Thayumanavan, S., Dendrimeric Micelles for Controlled Drug Release and Targeted Delivery. *Mol. Pharm.* **2005,** *2* (4), 264-272.

36. Willcock, H.; O'Reilly, R. K., End group removal and modification of RAFT polymers. *Polym. Chem.* **2010,** *1* (2), 149-157.

37. Matson, J. B.; Grubbs, R. H., Synthesis of Fluorine-18 Functionalized Nanoparticles for use as in vivo Molecular Imaging Agents. *J. Am. Chem. Soc.* **2008,** *130* (21), 6731-6733.

38. Siegel, L. M., A direct microdetermination for sulfide. *Anal. Biochem.* **1965,** *11* (1), 126-132.

39. Feng, S.; Zhao, Y.; Xian, M.; Wang, Q., Biological thiols-triggered hydrogen sulfide releasing microfibers for tissue engineering applications. *Acta Biomaterialia* **2015,** *27,* 205-213.

40. Kelner, M. J.; Alexander, N. M., Methylene blue directly oxidizes glutathione without the intermediate formation of hydrogen peroxide. *J. Bio. Chem.* **1985,** *260* (28), 15168-15171.

41. Sawhney, R. S.; Zhou, G.-H. K.; Humphrey, L. E.; Ghosh, P.; Kreisberg, J. I.; Brattain, M. G., Differences in Sensitivity of Biological Functions Mediated by Epidermal Growth Factor Receptor Activation with Respect to Endogenous and Exogenous Ligands. *J. Bio. Chem.* **2002,** *277* (1), 75-86.

42. Awwad, R. A.; Sergina, N.; Yang, H.; Ziober, B.; Willson, J. K. V.; Zborowska, E.; Humphrey, L. E.; Fan, R.; Ko, T. C.; Brattain, M. G.; Howell, G. M., The Role of Transforming Growth Factor α in Determining Growth Factor Independence. *Cancer Res.* **2003,** *63* (15), 4731-4738.

43. Wang, J.; Sun, L.; Myeroff, L.; Wang, X.; Gentry, L. E.; Yang, J.; Liang, J.; Zborowska, E.; Markowitz, S.; Willson, J. K. V.; Brattain, M. G., Demonstration That Mutation of the Type II Transforming Growth Factor β Receptor Inactivates Its Tumor Suppressor Activity in Replication Error-positive Colon Carcinoma Cells. *J. Bio. Chem.* **1995,** *270* (37), 22044-22049.

44. Rajput, A.; Dominguez San Martin, I.; Rose, R.; Beko, A.; LeVea, C.; Sharratt, E.; Mazurchuk, R.; Hoffman, R. M.; Brattain, M. G.; Wang, J., Characterization of HCT116 Human Colon Cancer Cells in an Orthotopic Model. *J. Surg. Res.* **2008,** *147* (2), 276-281.

45. Todaro, G. J.; Green, H., Quantitative studies of the growth of mouse embryo cells in culture and their development into established lines. *J. Cell. Biol.* **1963,** *17* (2), 299-313.

46. Wu, J.; Li, Y.; He, C.; Kang, J.; Ye, J.; Xiao, Z.; Zhu, J.; Chen, A.; Feng, S.; Li, X.; Xiao, J.; Xian, M.; Wang, Q., Novel H_2S Releasing Nanofibrous Coating for In Vivo Dermal Wound Regeneration. *ACS Appl. Mat. Interfaces* **2016,** *8* (41), 27474-27481.

5.8. Appendix

Table 5S1. Summary of polymer characterization.

				After RAFT Polymerization					After SATO Formation			
Polymer	**n**	**m**[a]	**l_{core}**[b] **(nm)**	**%conv RAFT**[c]	**$M_{n,GPC}$ (kDa)**[d]	**$M_{n,NMR}$ (kDa)**[e]	**$M_{n,theo}$ (kDa)**[f]	**Đ**[d]	**$M_{n,GPC}$ (kDa)**[d]	**$M_{n,NMR}$ (kDa)**[f]	**$M_{n,theo}$ (kDa)**[e]	**Đ**[d]
1	112	30	9.2	31	13.8	13.2	13.5	1.18	17.9	16.9	17.7	1.05

[a]Calculated by ^{1}H NMR spectroscopy by comparing the relative integrations of peaks from the PEG and SATO blocks. [b]Length of core-forming block assuming fully extended chains. Calculated using degree of polymerization of the hydrophobic block (m). [c]Determined from ^{1}H NMR spectroscopy of the crude polymerization reaction mixture. [d]Absolute molecular weight measured by light scattering. [e]Determined from ^{1}H NMR spectra using end-group analysis. [f]Calculated using M_n = [M]/[macroCTA] * %conv + $M_{n,PEG}$.

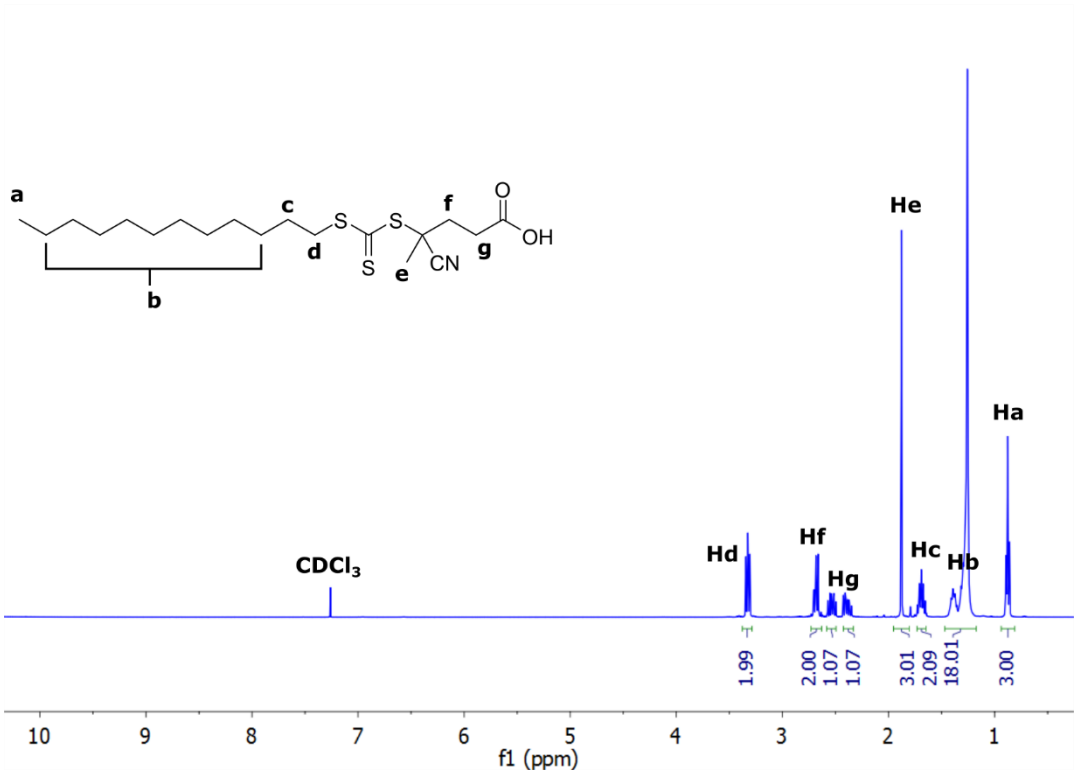

Figure 5S1. ^{1}H NMR spectrum of CTA.

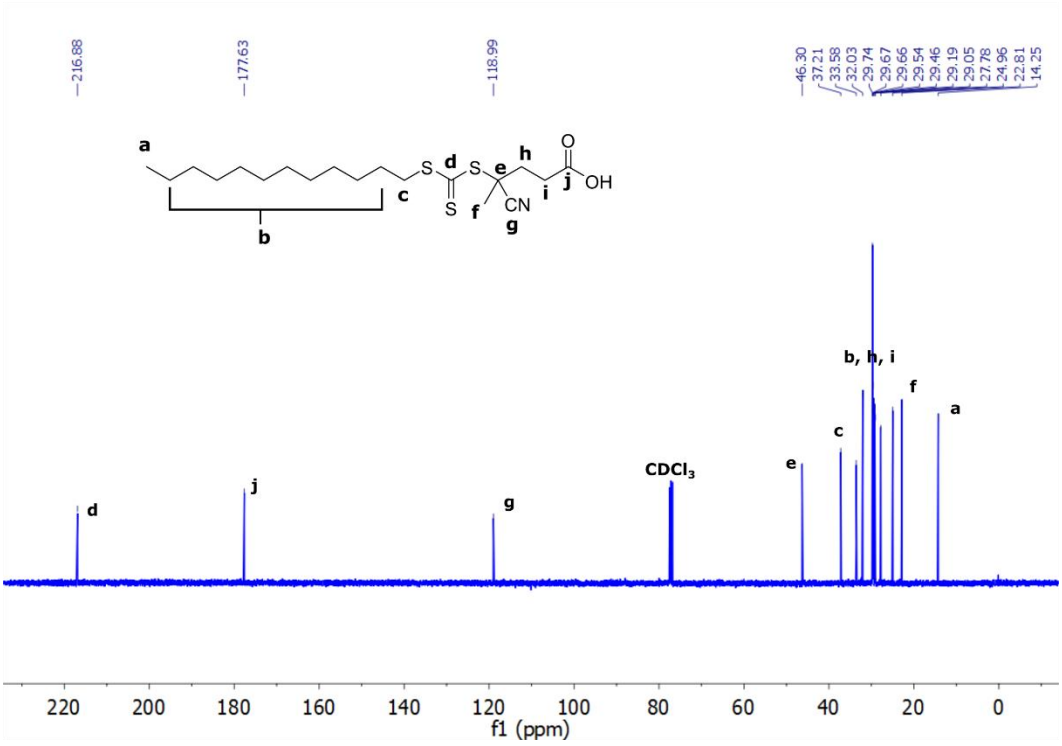

Figure 5S2. ^{13}C NMR spectrum of CTA.

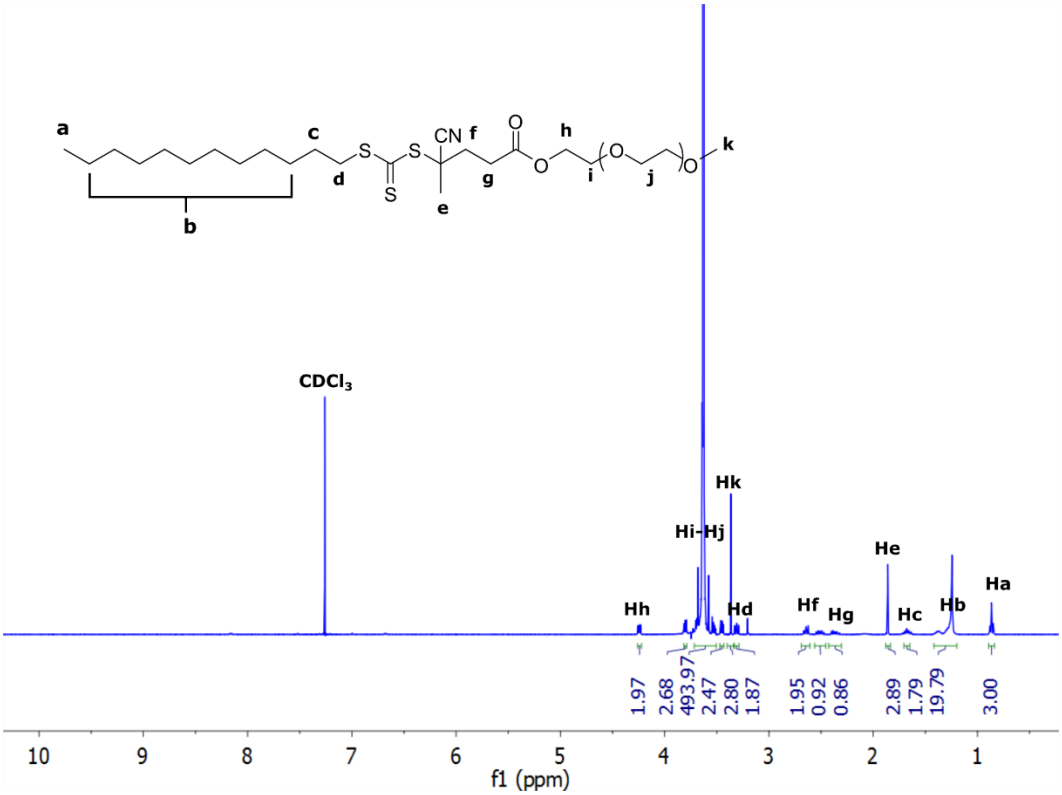

Figure 5S3. ^{1}H NMR spectrum of PEG macroCTA.

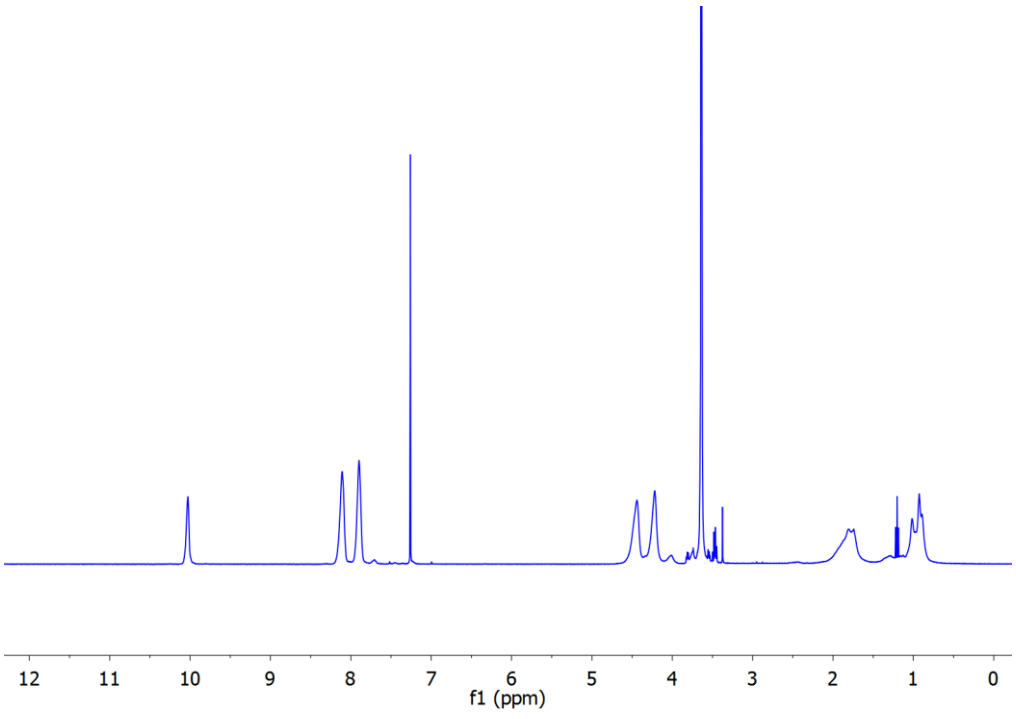

Figure 5S4. ^{1}H NMR spectrum of PEG-*b*-poly(FBEMA) block copolymer following RAFT polymerization.

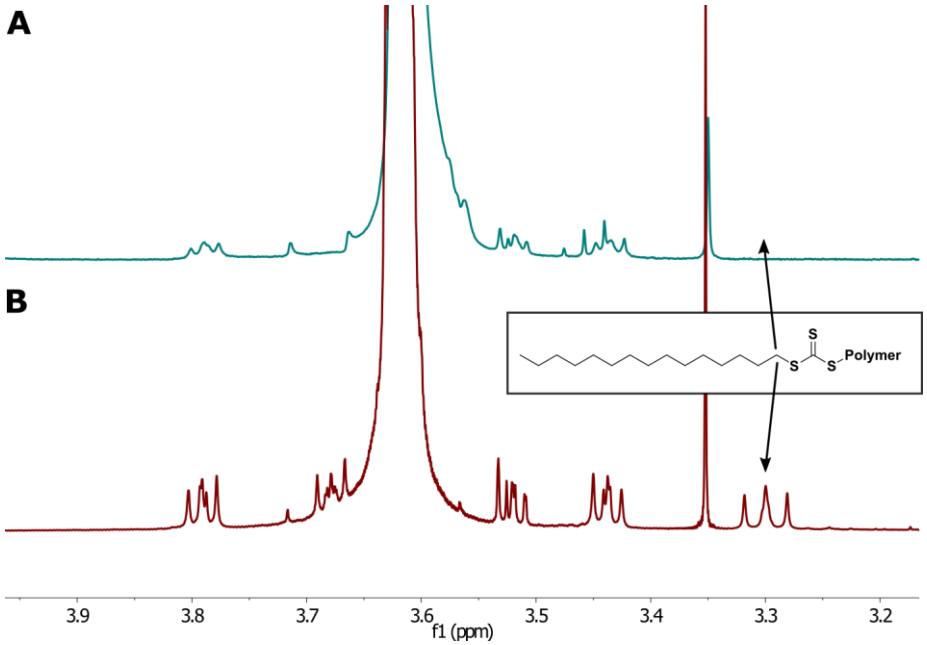

Figure 5S5. Example of removal of trithiocarbonate end group from polymer 1 (A) evidenced by the disappearance of the methylene resonance at ~3.3 ppm adjacent to the trithiocarbonate, which is present in the macroCTA (B).

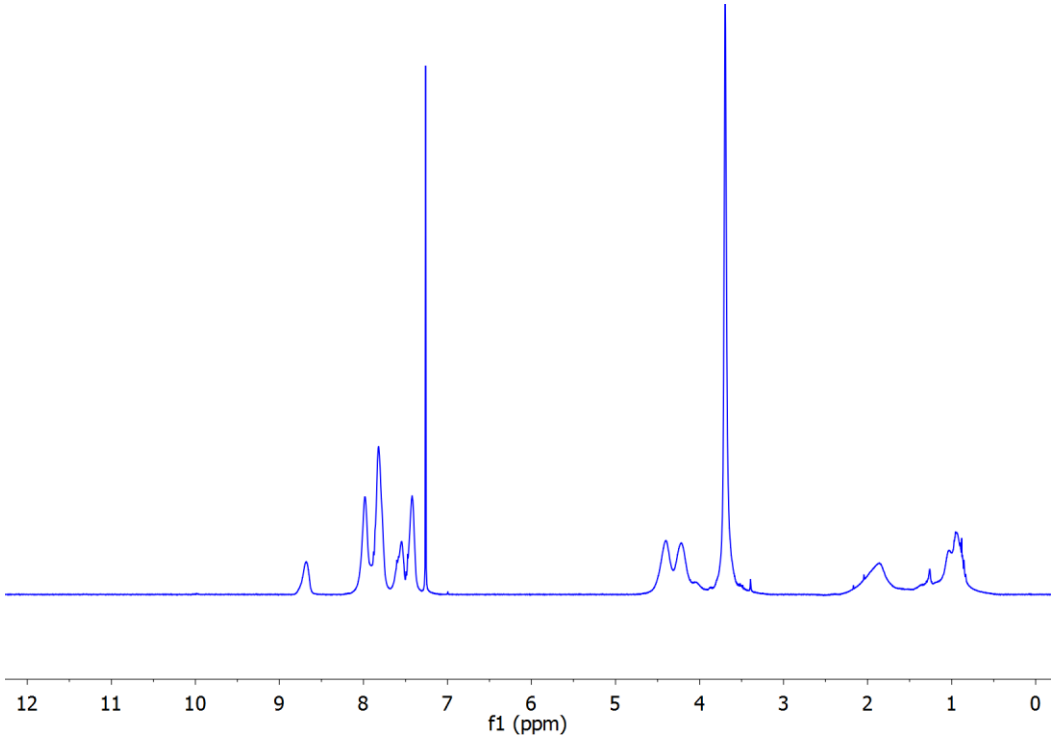

Figure 5S6. ^{1}H NMR spectrum of PEG-*b*-poly(SATO) after dithioester end group removal and subsequent SATHA conjugation.

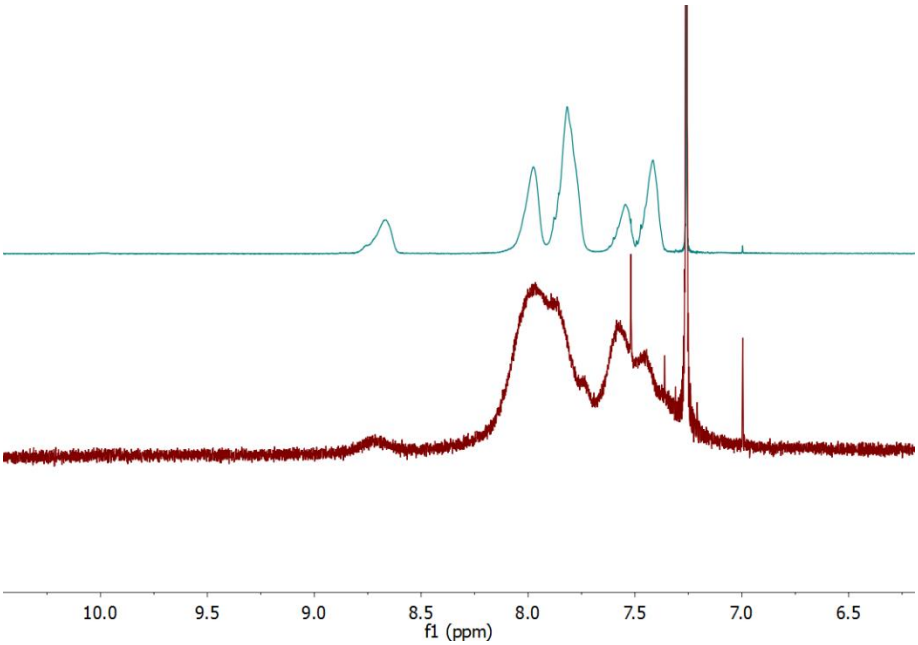

Figure 5S7. Comparison of ^{1}H NMR spectra of polymer 1 immediately following SATO formation (top) and after micelle formation and incubation in DI H_2O for 72 h (bottom). The latter spectrum was collected after the micelle solution was lyophilized. These spectra highlight the lack of aldehyde signals near ~10 ppm, indicating that SATO hydrolysis did not occur.

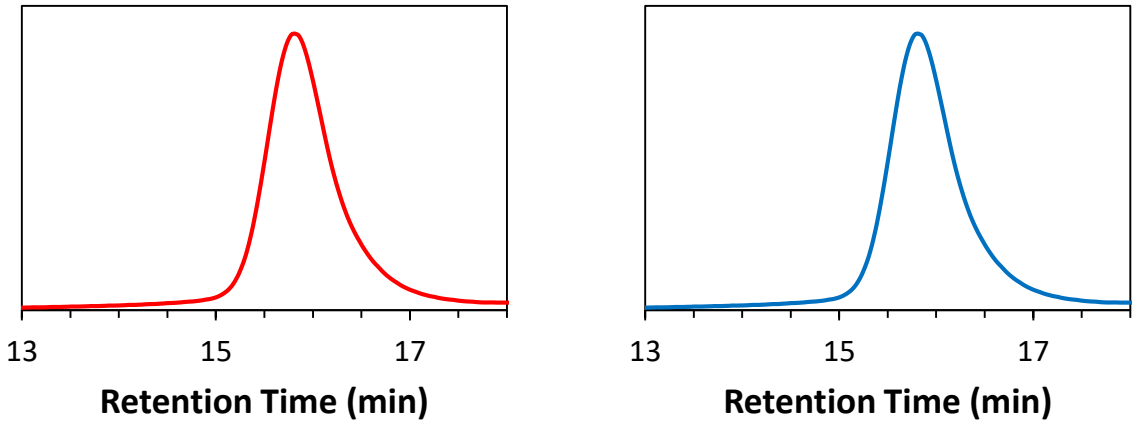

Figure 5S8. SEC traces of polymer 1 following RAFT polymerization (left) and after AIBN end group displacement and SATHA conjugation (right).

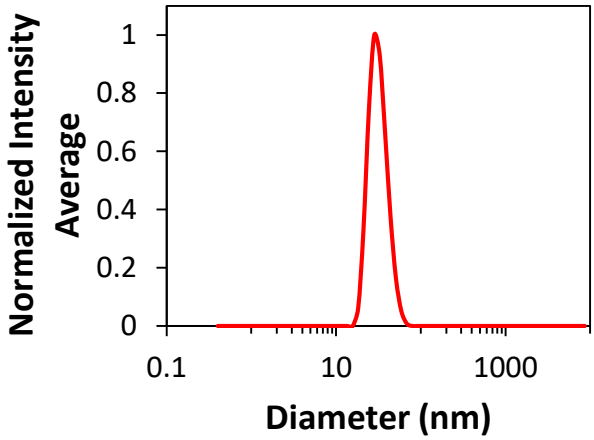

Figure 5S9. DLS trace for micelles assembled from polymer 1 conducted in H_2O at 0.1 mg/mL polymer. The micelles possess an average diameter of 38 ± 4 nm as measured by DLS.

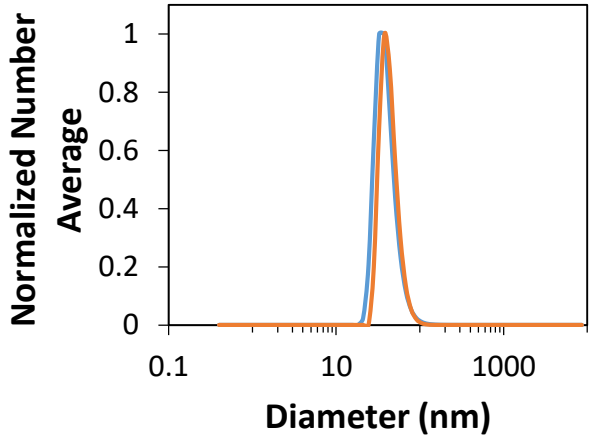

Figure 5S10. DLS trace for micelles assembled from polymer 1 conducted in 1X PBS buffer (pH = 7) at 0.1 mg/mL polymer immediately after dilution (blue trace) and following incubation for 48 h (orange trace) in the buffer solution. The micelles possess average diameters of 37 ± 11 nm and 44 ± 11 nm for the freshly prepared and incubated samples, respectively.

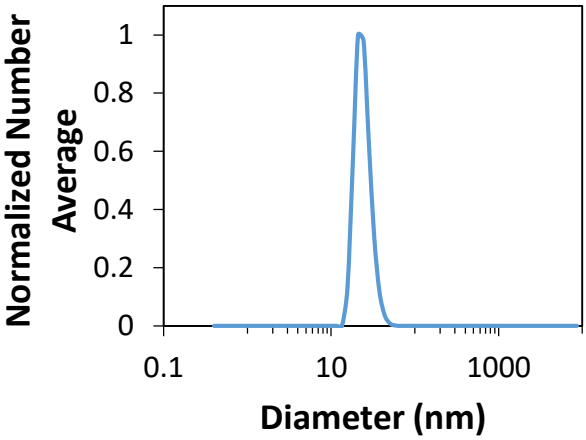

Figure 5S11. DLS trace for micelles assembled from a precursor to polymer 1 in H_2O. The micelles possess an average diameter of 25 ± 5 nm as measured by DLS.

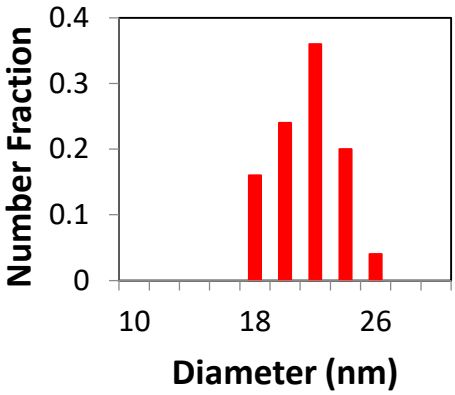

Figure 5S12. Size distribution histogram generated from TEM images for micelles made from polymer 1.

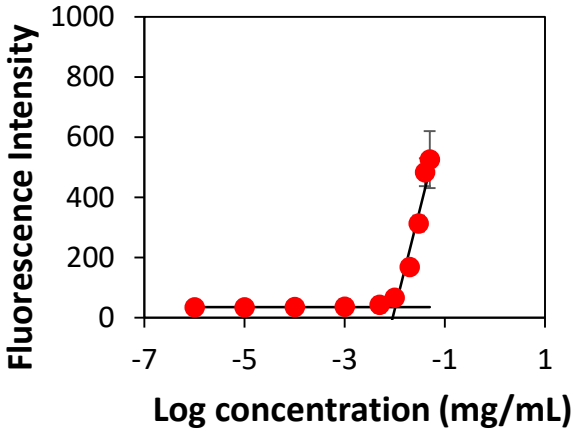

Figure 5S13. Determination of critical micelle concentration for polymer 1 using the Nile red assay.

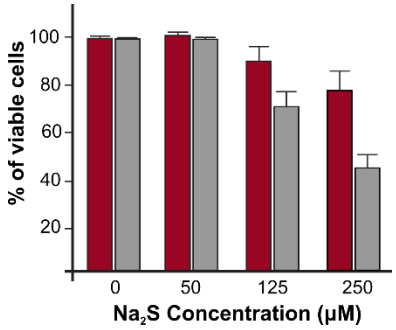

Figure 5S14. Clonogenic survival assay following exposure of cells to various concentrations of Na_2S. Clonogenic assay of NIH/3T3 and HCT116 cells (red and grey bars, respectively) were performed in 6-well plates after incubation with Na_2S (0 - 250 μM). Data are presented as the mean ± s.d. from 2–3 independent experiments performed in triplicate.

Evaluation of Byproduct Toxicity

Cell viability colorimetric assay. Cells, either NIH/3T3 or HCT116, were seeded at about 10,000 cells/well into a 96-well plate (Corning Cellgro) and maintained in culturing media. Viability was evaluated using the tetrazolium salt MTT following manufacturer's instructions (Abnova). To evaluate NH_4^+ toxicity, cells were incubated with NH_4Cl (0.1, 1, 10 μM) for 24 h at 37°C/5% CO_2 before the MTT reagent was added and absorbance measured at 570 nm. To evaluate the effect in viability of decomposing products from micelles, cells were incubated with a suspension of micelles (250 μM) containing 1 mM cysteine previously maintained at room temperature for 24 h. Cells were then transferred to a 37°C/5% CO_2 incubator, and viability was tested at 24 h after treatment. A positive control was performed in the presence of saponin (0.5%). In all cases, blanks were subtracted and values normalized to those containing saponin in the former or NH_4Cl for the later experiment. Values represent the mean ± SD of triplicated samples.

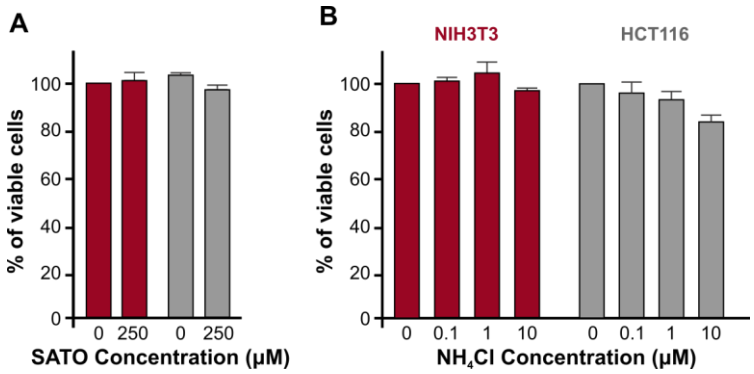

Figure 5S15. Effect of byproducts of SATO micelles on cell survival. A) Treatment of cells with micelles prepared from polymer 1 after incubating with Cys for 24 h. B) Titration of cells with active NH_4Cl. No significance is observed between treatments.

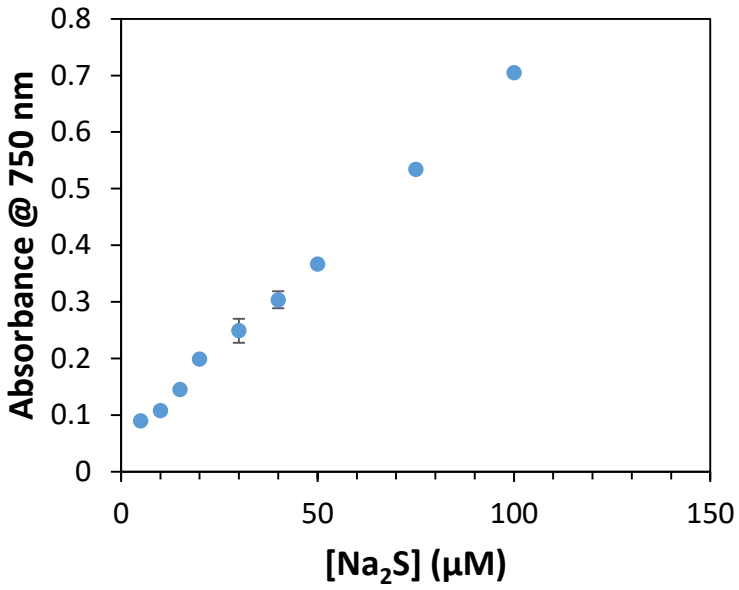

Figure 5S16. MB calibration curve conducted using Na_2S. A = 0.0065 * [Na_2S], r^2 = 0.998.

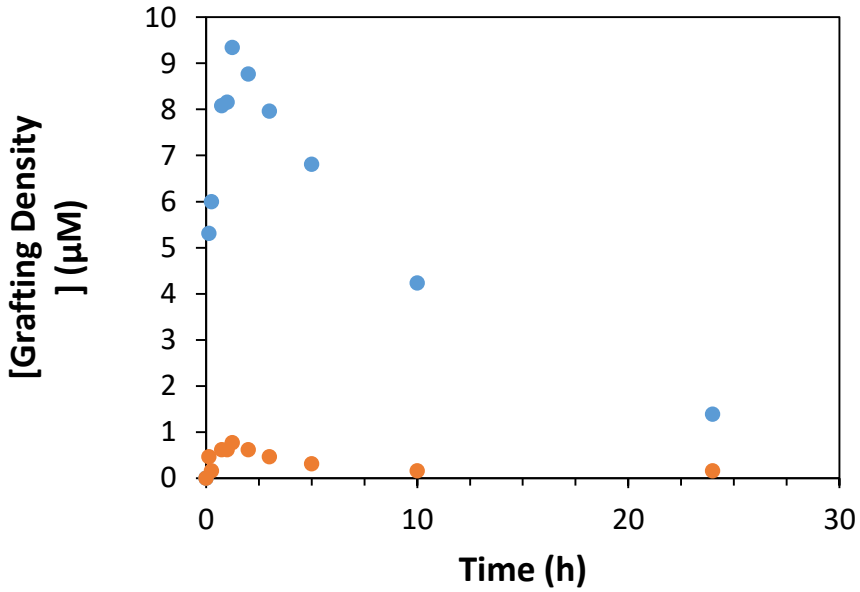

Figure 5S17. H_2S release profile of micelles prepared from polymer 1 at 250 µM in the presence (blue circles) and absence (orange circles) of 1 mM Cys in phosphate buffer (pH = 7).

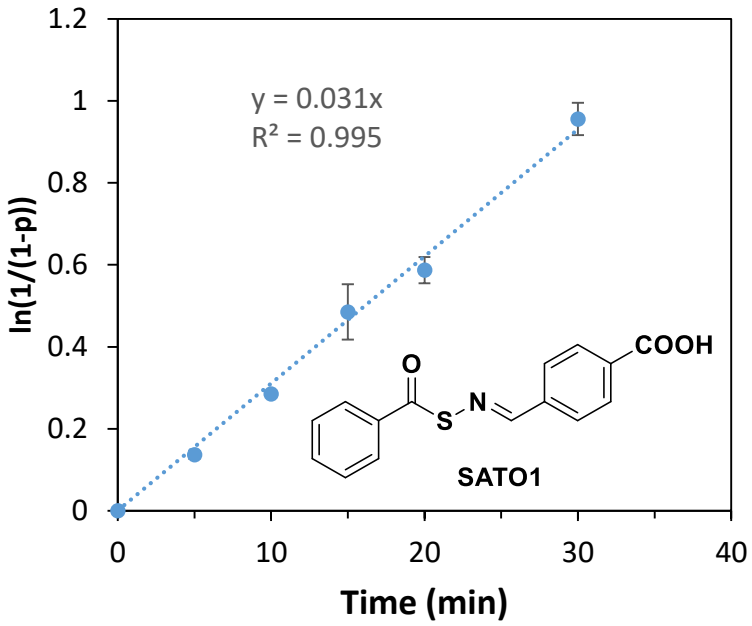

Figure 5S18. Kinetics of H_2S release from SATO1 as measured by the methylene blue assay. Assay conducted at [SATO1] = 250 µM in the presence of 1 mM Cys in phosphate buffer (pH = 7).

Scheme 5S1. H_2S release from SATOs.

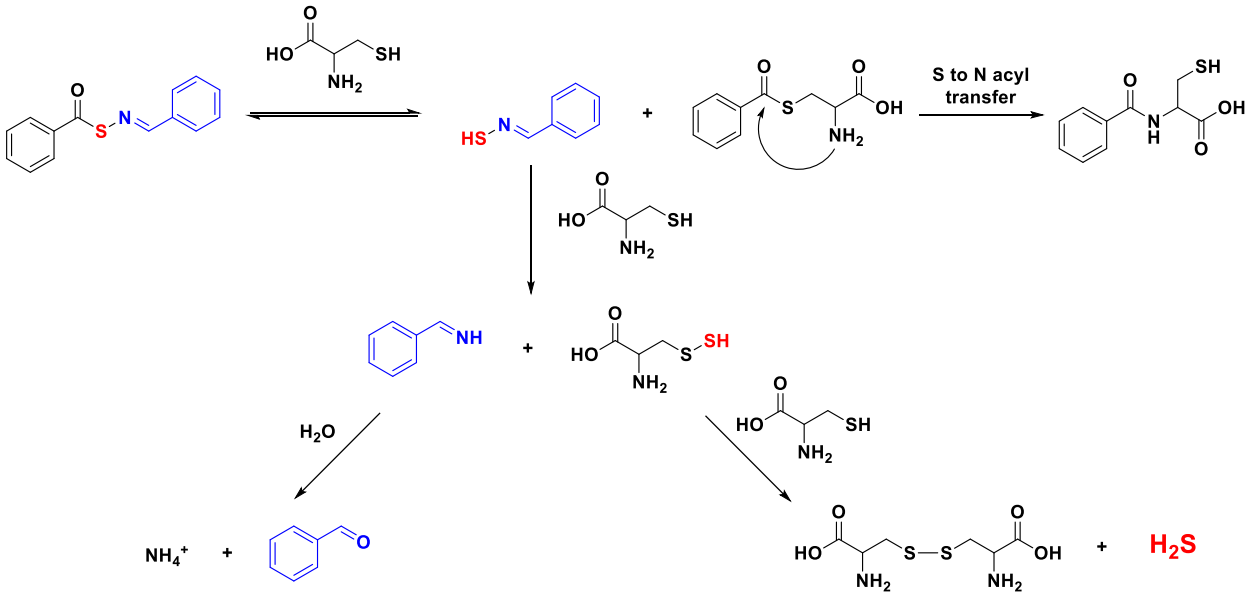

References

(1) Foster, J. C.; Powell, C. R.; Radzinski, S. C.; Matson, J. B. *Org. Lett.* 2014, *16*, 1558.

(2) Foster, J. C.; Matson, J. B. *Macromolecules* 2014, *47*, 5089.

Chapter 6. Graft Polymer Synthesis by RAFT Transfer-to

6.1. Authors

Jeffrey C. Foster,[†] Scott C. Radzinski,[†] John B. Matson[†]

[†]Department of Chemistry and Macromolecules Innovation Institute, Virginia Tech, Blacksburg, Virginia 24061, USA

6.2. Abstract

The synthesis of graft polymers via controlled polymerization techniques has enabled the facile modification of the surface properties of a variety of substrates. Three grafting methods are typically highlighted in the literature: grafting-to, grafting-from, and grafting-through. However, a fourth method exists when grafting is conducted using reversible addition-fragmentation chain transfer (RAFT) polymerization, which we refer to as transfer-to. Transfer-to differs from the other grafting strategies in the types of structural defects and impurities that arise during polymerization. This review addresses important considerations when conducting RAFT transfer-to, including RAFT chain transfer agent selection, monomer structure, and reaction conditions. In addition, we highlight key mechanistic differences between grafting-from and transfer-to and their effects on the structure and sample composition of the resulting graft polymers.

6.3. Keywords

Bottlebrush polymer, Z-group approach, Z-RAFT, surface-initiated polymerization, grafting-from

6.4. Introduction

Polymer chemists have found that attaching polymers onto surfaces, nanoparticles, proteins, and even other polymers can enable a number of applications. By grafting polymers onto various substrates, the interface that separates the substrate from its external environment can be manipulated. Interfacial properties such as adhesion, wettability, chemical reactivity, and biocompatibility can be tuned through rational design of the grafted polymer layer. For example, polymers grafts are widely utilized to protect macroscopic substrates from UV damage and corrosion, alter their hydrophobicity, prevent interaction with cells and/or biomacromolecules, and imbue substrates with antibacterial properties.[1,2] Grafting of polymers onto nanoparticles is used widely to prevent nanoparticle aggregation, add bioactive components, and provide photonic properties.[3] Proteins are regularly grafted with polymer chains to increase their circulation half-life, modify their activity, and improve their stability to long-term storage.[4] Finally, grafting of polymers onto other polymers allows chemists to create complex polymer topologies, including star polymers and graft polymers (which may also be called comb, or bottlebrush polymers depending on grafting density).[5] It is clear that polymer grafting can have a dramatic effect on properties, regardless of the size of the underlying substrate. Throughout this review, the term substrate will be used to refer broadly to the surface to which the polymer chains are attached during a graft polymerization. This could be, for example, a silicon wafer, a nanoparticle surface, or a soluble multifunctional initiator, biomacromolecule, or polymer bearing multiple initiating functionalities.

Despite the wide variety of applications for polymer grafting, only two or three different strategies are typically identified for attaching a polymer to a substrate. Grafting is typically achieved by either attaching pre-formed polymers to a substrate through the formation of a covalent bond

(grafting-to) or by growing a polymer chain from an initiator or chain transfer agent (CTA) attached to a substrate (grafting-from).[6] If the substrate is another polymer, grafting can be carried out by stringing together pre-formed polymers via polymerization of an end group (grafting-through).[7,8] Each strategy has advantages and disadvantages. For example, when polymers are grown from a surface using the grafting-from technique, a high grafting density can be achieved, but some side reactions such as polymer-polymer coupling may occur. In contrast, grafting-through can provide "perfect" grafting densities with few structural defects under optimized conditions.[9]

We have recently begun studying a fourth grafting strategy that is mechanistically distinct from the other three. Termed "transfer-to" by Sumerlin in a 2011 review paper in the context of protein grafting, this synthetic strategy relies on a chain transfer reaction to attach actively growing polymer chains onto a substrate.[10] Transfer-to can be thought of as a hybrid between the grafting-from and grafting-to approaches, but it has its own limitations and advantages compared with the other grafting methods. It has been used to graft polymers onto surfaces, nanoparticles, proteins and other polymers, primarily using reversible addition–fragmentation chain transfer (RAFT) polymerization. In many reports in which transfer-to has been used, the grafting strategy is incorrectly identified as grafting-from; in others it is correctly recognized but referred to by another name (often the Z-group or Z-star approach). While most reports concerning transfer-to pertain to its use in grafting polymerization via RAFT, this strategy is not limited to RAFT polymerization. Therefore, we recommend use of the term transfer-to rather than Z-group approach in order to more broadly identify this synthetic strategy. This review will focus on the use of transfer-to polymerization to prepare graft polymers in view of our current understanding of its advantages

and shortcomings. In addition, previous work in the field of transfer-to graft polymerization from protein, nanoparticle, and macroscopic substrates will be identified and reviewed.

6.5. Reversible-deactivation Radical Polymerization

The development of reversible-deactivation radical polymerization (RDRP) techniques reinvigorated the field of radical polymerization by facilitating the preparation of precisely-defined polymers of targeted size and narrow molecular weight distribution.[11] Nitroxide-mediated polymerization was the first RDRP to be developed,[12,13] followed by atom-transfer radical polymerization (ATRP)[14] and RAFT polymerization.[15] Prior to the advent of RDRPs, the synthesis of complex polymer topologies was non-trivial, often requiring intricate apparatuses and stringent reaction conditions. However, using RDRP, complex topologies are routinely prepared using a broad selection of functional monomers and reaction conditions. These topologies include multiblock copolymers,[16-18] hyperbranched polymers,[19,20] star polymers (having one or more type of arms),[21] and graft copolymers.[22,23]

6.5.1. RAFT Polymerization

RAFT polymerization is perhaps the most versatile RDRP technique. Using RAFT, polymerization of a wide variety of vinyl monomers can be achieved by careful selection of the CTA and reaction conditions. In addition, RAFT polymerization is tolerant to most functional groups including electrophilic functionalities such as aldehydes[24] and challenging nucleophiles like acyl hydrazides.[25] RAFT CTAs contain a thiocarbonyl-thio moiety, an R-group (leaving group) that forms a stable radical upon cleavage,[26] and a Z-group (stabilizing group) that modulates reactivity towards monomer-derived radicals.[27] Polymerization proceeds via degenerative chain transfer between a radical (initiator- or monomer-derived) and the CTA, effectively swapping the

thiocarbonyl-thio functionality between polymer chains. The control afforded by RAFT polymerization arises from a rapid equilibrium of chains such that all chains are given an equal opportunity to grow. As shown in Figure 6.1, the structures of RAFT CTAs are variable, with numerous dithioester, trithiocarbonate, dithiocarbamate, and xanthate compounds reported. The capability of a certain CTA to effectively mediate the polymerization of a specific monomer is largely determined by its chemical structure (i.e., the R and Z groups used). For example, dithiobenzoate or trithiocarbonate CTAs are generally well suited for polymerizing more-activated monomers (MAMs) such as methyl methacrylate (MMA), methyl acrylate (MA), and styrene, while dithiocarbamates and xanthates are appropriate when polymerizing less-activated monomers (LAMs) such as vinyl acetate and n-vinyl pyrrolidone. The reader is referred to several excellent reviews on the mechanism and scope of RAFT polymerization for further discussion.[28-36]

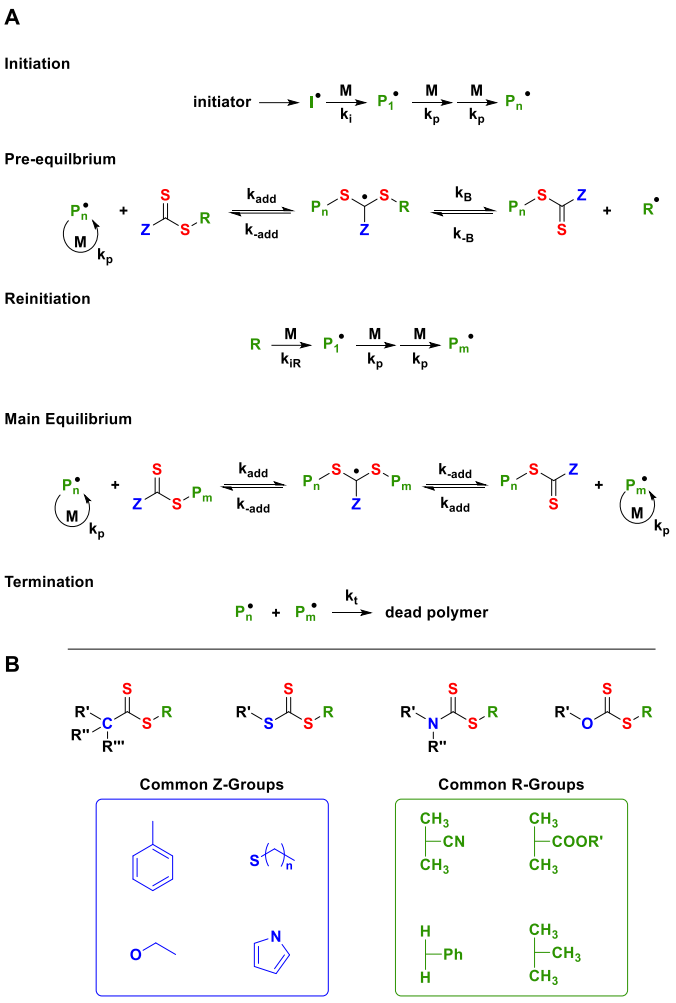

Figure 6.1. A) Mechanism of RAFT polymerization. Polymerization of vinyl monomers is mediated by degenerative chain transfer of radicals between dormant and active states. B) Typical structures of RAFT CTAs highlighting different thiocarbonyl-thio functionalities (dithioesters, trithiocarbonates, dithiocarbamates, and xanthates) and common Z- and R- groups. Reproduced from Ref. 28 with permission from The Royal Society of Chemistry.

6.5.2. Graft Polymerizaton Using RAFT

Polymer grafts can be grown from substrates using RAFT polymerization through either the grafting-from or transfer-to technique. The principal difference between RAFT grafting-from and transfer-to is the location of the polymer radical and thiocarbonyl-thio compound during propagation. The direction of attachment of the CTA to the substrate regulates these mechanistic

details, which determine types of imperfections and byproducts that can arise during polymerization. If the CTA is attached to the substrate via the R-group, then grafting-from is the operative mechanism (Figure 6.2). Conversely, if the CTA is anchored to the substrate through the Z-group, then transfer-to polymerization results.

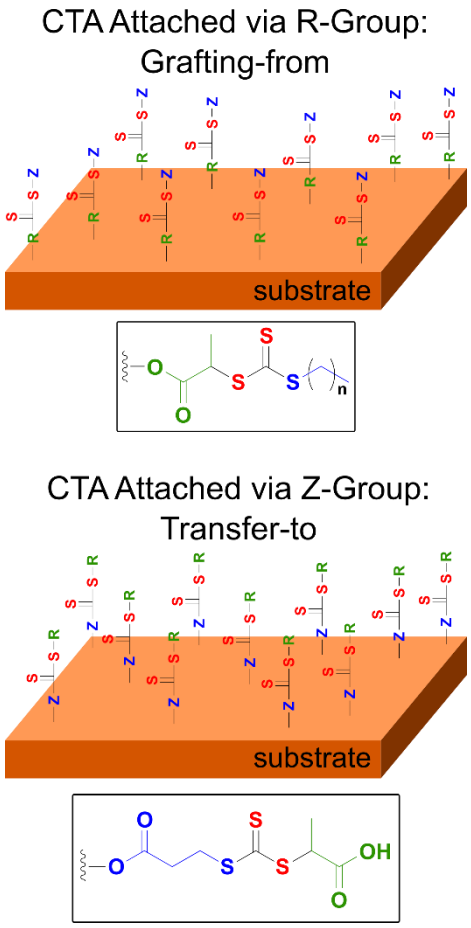

Figure 6.2. Attachment of the CTA to the substrate determines the mechanism of polymerization. If the substrate is attached through the R group, grafting-from operates. Conversely, transfer-to is the mechanism if the CTA is attached through the Z group.

6.6. Grafting-From

Grafting-from is perhaps the most studied grafting methodology, largely because many CTA R-groups contain carboxylic acids or other reactive functionalities that facilitate derivatization. Indeed, many grafting reactions are likely conducted using the grafting-from strategy

coincidentally instead of through rational design. When preparing graft polymers by grafting-from, the CTA is attached to the grafting surface or polymer backbone through its R-group (Figure 6.2). During polymerization, the CTA fragments, resulting in an R-group-derived radical that remains tethered to the grafting surface and a thiocarbonyl-thio component that dissociates (Figure 6.3A). The surface bound radical can react with monomer to form polymer, with a CTA resulting in degenerative chain transfer, or with another surface bound radical. The latter case is a termination reaction that takes one of three forms: 1) disproportion to form two polymer chains that are bound to the substrate but no longer living; 2) coupling to form an intramolecular "loop"; or 3) coupling that results in the creation of an intermolecular cross-link. Intermolecular coupling reactions are most relevant for nano-scale grafting applications such as star/bottlebrush copolymers synthesis or grafting from nanoparticles, and these side reactions contaminate the polymer sample with coupled byproducts much larger than the desired size.

In RAFT grafting-from there exists one more type of impurity that can form: unattached linear polymers. The dissociated thiocarbonyl-thio component acts like a "free" CTA in solution and can return to the substrate via chain-transfer with a surface-bound polymer radical. CTA in solution is also capable of reacting with radicals that are not bound to the grafting substrate, which come from initiator fragments or initiator-derived chains. This process results in the formation of linear polymer chains that are free in solution. These initiator-derived chains will always form to some extent, regardless of reaction conditions. Similar to traditional RAFT, initiator-derived chains in grafting-from undergo living polymerization to form linear polymer, but these solution-initiated polymers can never attach to the substrate during grafting-from. Because concentrations of linear polymers can be low under optimized conditions, this consideration is often overlooked, especially in the context of macroscopic surfaces where the linear polymer in solution can be easily washed

away. However, these undesired side products become more important when making star or graft polymers by grafting-from, where linear polymer impurities are more challenging to remove from the star or graft polymer sample.

As with traditional RAFT polymerization, factors that limit the occurrence of termination—low radical concentration, high CTA concentration, high k_p, high pressure, and low monomer conversion—can help to eliminate impurities that arise as the result of inter- or intramolecular radical reactions. However, linear polymer species will always form to some degree, as will imperfections in the polymer graft resulting from termination.

6.6.1. Grafting Density During Grafting-from

The density of polymers on the substrate is another important consideration when choosing a grafting strategy. The degree of chain extension of a polymeric graft is related to grafting density on the grafting substrate. At low grafting densities, the pendant polymer chains collapse, taking on a globular structure referred to as mushroom-like. In contrast, high grafting densities result in chain elongation, tight chain packing, and notable chain end effects as these are more likely to be found on the periphery of the polymer brush. Indeed, the properties of the resultant material often depend on the grafting density of the attached polymer chains. For example, the thickness of polymer films on macroscopic surfaces is directly related to the grafting density above a critical value, with higher grafting densities resulting in thicker films.[37] High grafting densities also inhibit the interaction/adhesion of biomacromolecules with surfaces.[38] Grafting density is also critically important for bottlebrush polymers, as their morphology (and properties) depend largely on the steric interactions between numerous pendant polymer chains. Deffieux and coworkers have demonstrated a dependence of the bottlebrush polymer persistence length on the grafting density using neutron scattering, with high grafting densities resulting in much larger persistence lengths

for bottlebrush polymers with polystyrene grafts.[39] This phenomenon was also observed via dynamic mechanical analysis.[40]

The grafting density achieved during RAFT grafting-from depends on three factors: (1) the density of initiator/CTA moieties on the substrate; (2) the degree of termination that occurs during polymerization; and (3) the reinitiation efficiency of the polymerization (i.e., the ability of the R group to come off of the CTA and initiate polymerization). The first factor is determined by chemistry that is unrelated to the polymerization reaction and will not be discussed here. The second factor is termination reactions, which result in the loss of an active radical. If grafting density is taken to mean the density of polymer chains that are above a certain threshold MW (i.e., not oligomers), then termination reactions effectively reduce the grafting density of the polymer brush if they occur in the early stages of polymerization. The third factor, reinitiation efficiency, is another time dependent phenomenon that affects the grafting density of the polymer brush. At low conversions, some of the substrate-bound CTAs have not yet reacted with initiator fragments. Thus, grafting density is low early in the polymerization but rises quickly in an ideal RAFT polymerization. The re-initiation efficiency of a RAFT polymerization depends on several factors, most notably the selection of monomer and CTA. This will be discussed in further detail below.

Grafting density is difficult to calculate directly, but information about the grafting density can be inferred by inspecting the quantity of dead polymers that form during polymerization. Each dead polymer represents a chain that is no longer attached to a bottlebrush polymer and therefore reduces the overall grafting density of the sample. In addition, the bottlebrush polymer grafting density can also be inferred by comparing the observed MWs of the bottlebrush polymers to expected values. In the absence of significant termination, lower than expected bottlebrush polymer MWs most probably originate from the fact that they possess grafting densities less than

1. Grafting density can also be approximated by cleaving the polymer sidechains from the bottlebrush backbone and then dividing the observed bottlebrush polymer MW by the MW of the sidechains.

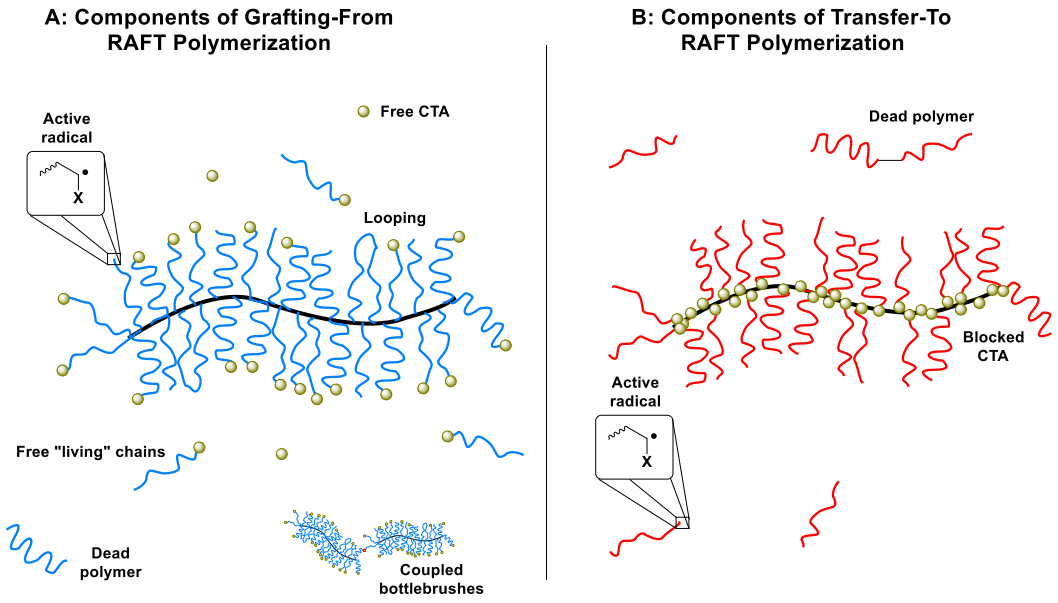

Figure 6.3. Comparison of the grafting-from and transfer-to methods of grafting.

6.7. Transfer-to

In contrast to grafting-from, when conducting RAFT transfer-to the CTA is attached to the substrate via the Z-group.[41] Z-groups with reactive functionalities are uncommon, contributing to far fewer studies using this grafting technique. Despite this fact, a number of groups have applied RAFT transfer-to to grow polymer brushes from a variety of substrates including macroscopic silicon surfaces,[42,43] silica particles,[44,45] solid support resins,[46,47] single-walled carbon nanotubes,[48] and proteins.[49-51] Star polymers have been prepared from various initiating cores such as β-cyclodextrins[52] or hyperbranched polymers and dendrimers.[53-55] Polymers functionalized with pendant CTAs have mediated RAFT transfer-to polymerization to form bottlebrush polymers.[56-60]

Like traditional RAFT, transfer-to is initiated via thermal decomposition of the radical source. As in all RAFT reactions, this initiator-derived radical can add to monomer or CTA. A pre-equilibrium phase exists wherein initiator-derived radicals or short initiator-derived oligomers add to CTAs, followed by fragmentation of the CTA R-groups. This continues until all CTA R-groups have been consumed and the reaction enters the main equilibrium.

During the main equilibrium of RAFT transfer-to, the substrate-bound thiocarbonyl-thio compounds fragment and active polymer radicals detach from the substrate (Figure 6.3B). The detached polymeric radicals are free to propagate away from the substrate. They can then return to the substrate via a chain-transfer reaction. Here, the graft polymers are in equilibrium with "free" linear propagating chains, allowing the polymer brush as a whole to grow in a controlled manner.[61] It is important to note that for RAFT transfer-to, active radicals are never present on substrate-bound polymer grafts and that propagation and termination always occur away from the substrate.

The difference in the location of polymer growth between grafting-from (from the surface) and transfer-to (free in solution) is important because it determines the types of impurities that form. Because the active radical is never tethered to the substrate in transfer-to, imperfections caused by intramolecular radical reactions (looping) do not arise. Moreover, intermolecular coupling is also absent. Termination through disproportionation also does not lead to impurities on the grafting surface. In short, transfer-to effectively eliminates side reactions that lead to defects on substrates in grafting-from polymerization.

Although termination reactions do not lead to loops, crosslinks, or short chains on a substrate when using RAFT transfer-to, termination reactions still occur, as in all RDRP reactions. Similar to traditional RAFT polymerization, linear polymer chains can undergo termination reactions. Dead

polymer arises during transfer-to as the result of termination reactions between active radicals on these linear chains. These are, in fact, the only types of impurities that are present in transfer-to polymerization. The quantity of these linear impurities that arise as a result of termination reactions can be kept low by employing conditions that limit termination, which we discuss further below. Dead polymer formation is unavoidable, however, and it becomes more prolific as the molecular weights of the polymer grafts increase due to steric interactions between these chains and the grafting surface. Therefore, under non-ideal conditions, large amounts of dead linear polymer can form in transfer-to graft polymerization.

6.7.1. Grafting Density During Transfer-to

Another important distinction between grafting-from and transfer-to polymerization is grafting density. For RAFT transfer-to, the grafting density of the graft polymer depends on the same primary factors as grafting-from—initial CTA density on the substrate, loss of chains to termination, and reinitiation efficiency. In addition to these considerations, grafting density in transfer-to is also affected by the steric shielding phenomenon. Grafting density during RAFT transfer-to will be discussed with respect to a number of considerations in the subsequent sections.

6.8. Considerations When Conducting RAFT Transfer-to

Similar to traditional RAFT polymerization, the conditions of the transfer-to polymerization reaction affect the polymer brushes that form. Factors affecting RAFT transfer-to have been studied by the groups of Vana,[62] Davis,[41] and Matson.[63] The length of the polymer grafts, their molecular weight distribution, the types and quantities of impurities (imperfections and/or byproducts) formed, and the grafting density of the graft polymer can all be manipulated by

changing the CTA or monomer used, the reaction temperature, the substrate, or a number of other variables. These considerations will be discussed individually as they apply to RAFT transfer-to.

6.8.1. CTA Structure and Concentration

As with traditional RAFT polymerization, choosing an appropriate CTA is critical to achieving controlled polymerization. Poor CTA/monomer pairing can result in uncontrolled polymerization if addition to the thiocarbonyl-thio compound occurs significantly more slowly than propagation.[26,27] Therefore, rational selection of the appropriate CTA for the desired monomer is paramount. Much work has gone into studying the polymerization of common monomer classes (i.e., acrylates, methacrylates, styrenics, etc.) using a variety of CTAs, and several optimal combinations have been identified.[64] For example, methyl methacrylate (MMA) polymerization is well controlled by dithioester CTAs due to their high chain transfer coefficients.[28] In contrast, xanthate CTAs do not control MMA polymerization because the polymer radicals add more rapidly to monomer than they do to the xanthate CTAs, but xanthates are ideal CTAs for vinyl acetate and related LAMs. For traditional RAFT polymerization, poor control due to bad monomer/CTA pairing manifests as a broadening of the molecular weight distribution and, in most cases, deviation from expected molecular weights.[65]

For RAFT transfer-to, the choice of CTA has a variety of outcomes. Most importantly, the CTA in its "free" form (i.e., in traditional RAFT for linear polymer synthesis) must control polymerization of the monomer. If this is the case, then the substrate bound CTA is also expected to control polymerization. In other words, the guidelines for CTA R and Z group selection established for traditional RAFT polymerization translate well to transfer-to (Figure 6.4). For example, trithiocarbonate CTAs have been employed to mediate the polymerization of styrene to grow brush polymers from a variety of substrates.[52,55,57] Similarly, a xanthate CTA was found to

control the polymerization of N-vinylcarbazole to form a star polymer,[53] and dithiocarbamate CTAs coupled to a poly(norbornene) backbone were used to prepare bottlebrush polymers with poly(vinyl acetate) grafts.[66] However, CTAs that work only moderately well for traditional RAFT may not perform well in RAFT transfer-to. Fairly small deviations from ideal behavior are exasperated when conducting transfer-to, as low molecular weight byproducts or unconsumed CTAs are rarely detected in a traditional RAFT polymerization.

It is important to note that if the CTA does not control the polymerization of a given monomer during RAFT transfer-to polymerization, the desired polymer brush topology *will not form*. Initiation and propagation both occur away from the substrate when conducting transfer-to. In the case of a poor monomer/CTA pair in which the chain transfer efficiency is low, the vast majority of the polymer chains will not add to the substrate-bound CTAs, so few chains will be grafted to the substrate. Well controlled RAFT polymerization must therefore be verified by first conducting a solution polymerization using the chosen monomer/CTA pair.

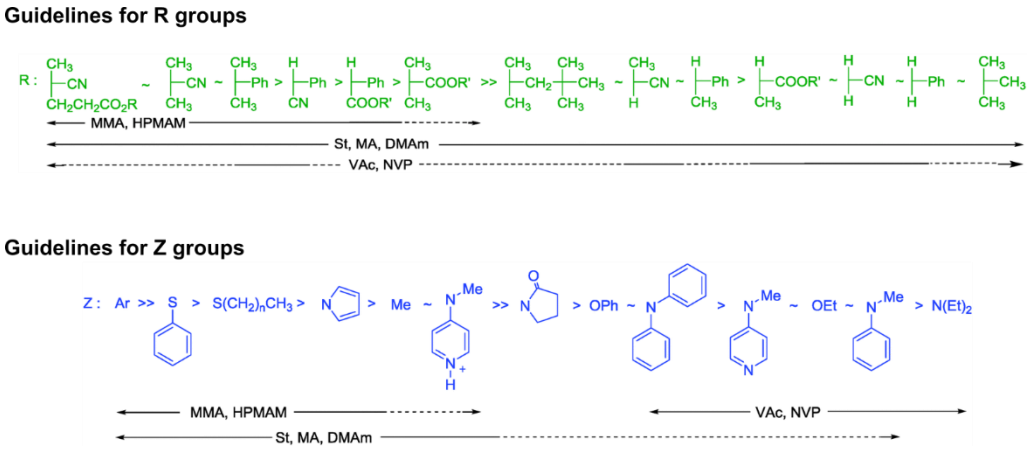

Figure 6.4. Guidelines for the selection of RAFT agent R and Z groups. Dashed lines indicate partial control over polymerization is achieved. For RAFT transfer-to, partial control is likely not sufficient to prepare well-defined graft polymers. Reproduced from Ref. 28 with permission from The Royal Society of Chemistry.

6.8.1.1. Effect on Termination

Termination reactions also become prevalent in RAFT transfer-to when a CTA does not adequately control the polymerization of a given monomer. Termination becomes more probable at high radical concentrations as is the case for polymerizations in which chain transfer between the active radical and the CTA occurs at a low rate relative to propagation. An example of this type of behavior would be the polymerization of styrene using a xanthate CTA.[67] Termination is particularly problematic for RAFT transfer-to due to the fact that termination reactions always occur away from the substrate. Termination between detached linear chains reduces the grafting density of the polymer brush and contaminates the sample with impurities that can sometimes be difficult to remove.

6.8.1.2. Effect on Polymerization Kinetics

Beyond controlled polymerization, the choice of CTA also affects the kinetics of the polymerization, with retardation and/or inhibition possible based on CTA and monomer structure. Retardation/inhibition typically originates from one of two sources: 1) unfavorable re-initiation by the leaving R-group (also referred to as poor re-initiation efficiency); or 2) slow fragmentation due to the stability of the adduct radical.[68] In traditional RAFT polymerization, this phenomenon is most typically observed in the polymerization of LAMs. Retardation/inhibition is also possible for RAFT transfer-to. For example, Vana and coworkers reported significant inhibition effects in the polymerization of vinyl acetate using a tetra-functional xanthate CTA with either a benzyl or a phenylethyl R-group.[69] Incubation times of ~10 h were observed for both R-groups, and this effect was attributed to the differences in radical stability of the R group relative to vinyl acetate.

Long incubation times in RAFT polymerization are related to poor re-initiation efficiencies. Re-initiation efficiency during RAFT transfer-to is a significant contributor to the structure of the resulting polymer brush. A common misconception of RDRPs is that all polymer chains begin growing immediately once the polymerization reaction is started. However, when conducting RAFT polymerization this is often not the case. Conditions for the polymerization need to be chosen such that the CTA is rapidly consumed during the initial stages. This will only be the case if the chosen CTA has a high chain transfer coefficient (C_{tr}) in the monomer being polymerized. C_{tr}, defined in equation 6.1, depends on the rate constant of chain transfer, k_{tr}, as well as the rate constant of propagation, k_p.

$$C_{tr} = \frac{k_{tr}}{k_p} \tag{6.1}$$

For RAFT polymerization, k_{tr} is given by the following expression:[70]

$$k_{tr} = k_{add} * \frac{k_{\beta}}{k_{-add} + k_{\beta}} \tag{6.2}$$

The rate constant k_{tr} is determined by the structure of the CTA; therefore, C_{tr} is determined by the CTA/monomer pair. If C_{tr} is low for a given monomer/CTA pair, then the CTA will not be consumed until the later stages of the reaction. It is therefore important to consider the consequences of slow pre-equilibration that could result from monomer/CTA pairs with low C_{tr}. C_{tr} is especially important for RAFT transfer-to due to its impact on grafting density. Boschmann et. al. showed the importance of re-initiation efficiency using ^{1}H NMR spectroscopy by studying the consumption of CTAs over the course of RAFT transfer-to polymerization in star polymer synthesis.[71] For the polymerization of styrene by a hexafunctional trithiocarbonate CTA with a benzyl R-group, complete re-initiation was not achieved until ~60% monomer conversion (Figure

6.5). The poor re-initiation efficiency of this system manifested as a reduction in grafting density (less than the expected 6 arms per star polymer) and star polymer MWs lower than expected values. By changing to an ethylbenzyl R-group, re-initiation was complete at only ~10% monomer conversion, resulting in star polymers with grafting densities near their theoretical maxima. Many reports on star or bottlebrush synthesis by RAFT transfer-to have attributed observed deviations in star/bottlebrush MW from theoretical values to termination or steric effects without considering the impact of CTA structure on C_{tr} and its associated consequences. This work clearly shows that even though certain monomer/CTA pairs may work fairly well for traditional RAFT, C_{tr} is an important variable to consider when conducting RAFT transfer-to polymerization.

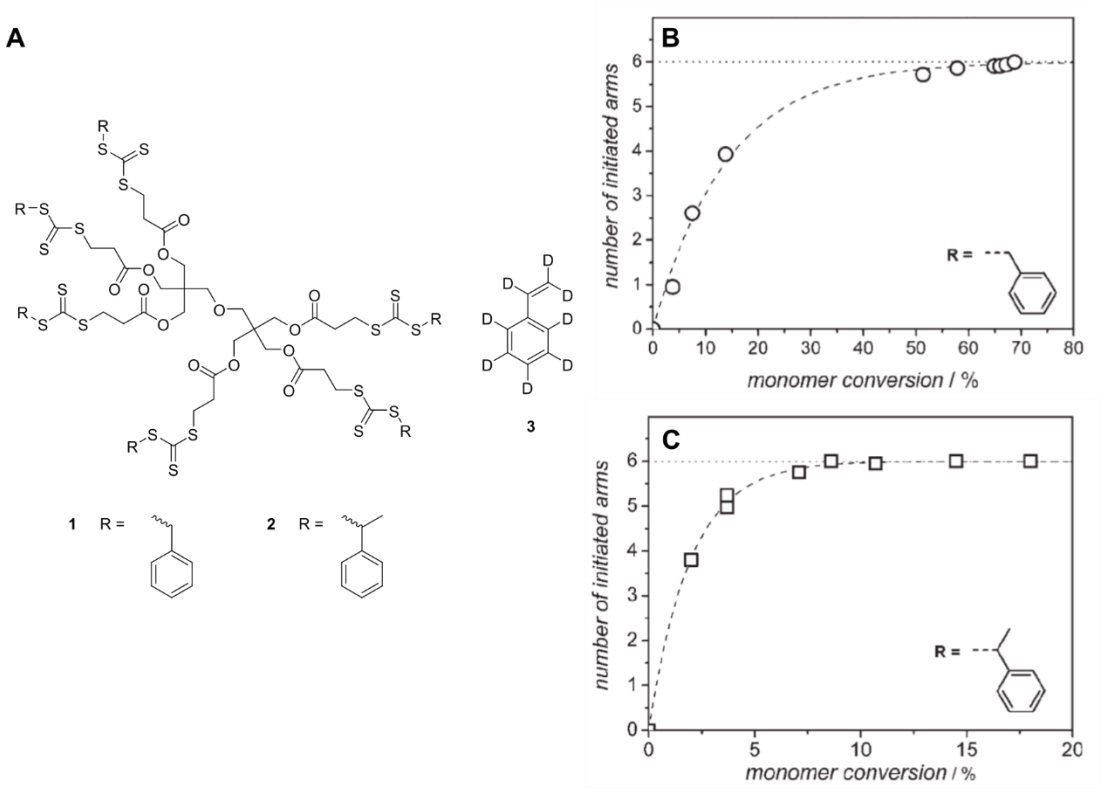

Figure 6.5. Effect of re-initiation efficiency on RAFT transfer-to. (A) Chemical structure of 6-arm star RAFT initiator in the polymerization of styrene-d_8 with two different R groups. (B) Number of successfully initiated arms versus monomer conversion for R = benzyl. (C) Number of successfully initiated arms versus monomer conversion for R = phenylethyl. Reproduced from Ref. 71 with permission from Wiley Periodicals.

Finally, CTA concentration is important to consider when conducting RAFT transfer-to. In general, better control is achieved at high CTA concentration due to more rapid addition of active radicals to CTAs. High CTA concentrations lead to narrow molecular weight distributions and MWs that are close to theoretical values when conducting RAFT transfer-to.[52] In addition, high CTA concentrations minimize the amount of dead linear polymer impurities that form during transfer-to grafting reactions.[61,63]

6.8.2. The k_p/k_t Ratio

The ratio of the rate constant of propagation to the rate constant of termination, k_p/k_t, is an important factor to consider while performing RAFT transfer-to. Increasing this ratio leads to a reduced incidence of termination, meaning fewer dead polymers in solution and substrates with higher grafting densities. Several factors are important to consider that influence the k_p/k_t of the system, including monomer structure, solvent, temperature, and pressure.

6.8.2.1. Monomer Structure

The structure of the monomer utilized in a radical chain polymerization is the primary determinant of the k_p/k_t ratio. In general, acrylates and acrylamides possess high rate constants of propagation relative to termination, while styrene has a significantly lower k_p/k_t value.[72] Radzinski et. al. studied the effects of using different monomers during bottlebrush synthesis by RAFT transfer-to. Mediated by a polymeric dithiocarbamate CTA, the kinetics of RAFT polymerization of three different monomers—styrene, methyl acrylate (MA), and acryloyl morpholine (ACMO)—were investigated under identical conditions. Monomer choice had a large effect on the quantity of linear polymer impurities that formed during RAFT transfer-to polymerization, with high k_p/k_t monomers yielding the least amount of linear polymer even at high conversions (Table 6.1).[63]

Table 6.1. Effect of monomer on RAFT transfer-to polymerization.

Monomer	Mn (kDa)	Đ	%Dead	% Conv
Sty	97.0	1.08	21	29
MA	400	1.05	14	89
ACMO	740	1.04	11	82

All polymerizations were carried out at [Monomer] = 17 v/v% using the same polymeric CTA.

6.8.2.2. Solvent

The solvent choice for the polymerization has a direct effect on the k_p/k_t ratio in two ways: 1) propagation rate generally increases with solvent polarity, and 2) the equilibrium between the polymeric radicals and adduct radicals in the RAFT main equilibrium is biased towards the polymeric radical when more polar solvents are used due to decreased C_{tr}.[73] Both outcomes are expected to increase the MW of the polymer grafts and the quantity of dead linear polymer when conducting RAFT transfer-to.

Fröhlich used Monte Carlo simulations to investigate the use of good solvents vs theta solvents during RAFT transfer-to. It was determined that shielding effects (discussed in more detail below) were chain length dependent under good solvent conditions but became less pronounced when using a theta condition. Decreased shielding, i.e., the blocking of reactive CTA moieties by nearby polymer side-chains, was hypothesized to increase the contact probability of the active radical and the CTA, thereby increasing the rate of addition to CTA. These simulations were complemented

by transfer-to experiments that yielded star polymers with smaller dispersity values in cyclohexane (a poor solvent) than those in toluene (a good solvent).[74]

6.8.2.3. Temperature

Temperature affects a variety of rates in RAFT polymerization. For thermally initiated polymerizations, increased temperatures cause faster initiator decomposition rates, leading to increased radical concentrations.[75] Propagation and termination rates also increase with increasing temperature. In addition, some evidence suggests that fragmentation of the intermediate RAFT radical may be enhanced relative to addition to CTA at high temperatures.[76] Finally, thermal decomposition of the RAFT agent is also possible at high temperatures, leading to some loss of living character throughout the course of the polymerization.[77] Overall, high temperatures generally result in a broadening of the molecular weight distribution and a deviation from expected MW. However, high temperature also reduces the duration of the polymerization. Therefore, a balance must be struck to achieve controlled polymerization in a reasonable time scale.

Further complexity is added by the shielding effect during RAFT transfer-to. Stenzel and coworkers evaluated the effect of polymerization temperature on star polymer synthesis using RAFT transfer-to.[52] At high CTA concentrations, a marked temperature dependence was observed, with higher temperatures leading to star polymers with MWs in good agreement between theoretical and experimental values. Dispersities of the star polymers did not vary substantially in this CTA concentration regime. In contrast, at low CTA concentrations, star polymer MW was not temperature-dependent, but dispersity values of the star polymers increased with increasing temperature. In addition to radical and chain exchange kinetics, the accessibility of the polymeric radical to the substrate-bound CTAs may also be influenced by temperature. It is therefore important to evaluate the effects of temperature on each system individually.

6.8.2.4. Pressure

Increasing the pressure in a RAFT polymerization will increase the rate of propagation while decreasing the rate of termination. These changes in rates are attributed to an increase in the rates of chemically controlled reactions whereas the rates of diffusion controlled reactions decrease.[78] Pressures up to 2,500 bar have proven to be advantageous in traditional RAFT polymerization, enhancing both the rate and control of the polymerization. High pressures have also proven to be beneficial for transfer-to polymerization. Vana and coworkers evaluated the effect of pressure on star polymer synthesis via RAFT transfer-to polymerization. By employing high pressure (2,600 bar), the amount of dead polymer was reduced by a factor of 2.5 compared to polymerizations run at atmospheric pressure.[79] This reduction in the amount of dead chains was attributed to an increase in the k_p/k_t ratio.

6.8.3. Shielding Effect/Core Size

The shielding effect is a phenomenon unique to the grafting-to and transfer-to methodologies. For RAFT transfer-to, this concept describes the interactions between large polymeric radicals and the CTAs on the grafting substrate. Steric interactions between these large objects have been observed in multiple systems.[52,56,57,80,81] Most often, high dead polymer quantities and low grafting densities result from a substantial shielding effect.

The shielding effect becomes more prominent when the polymer grafts are large, as is often the case when the RAFT transfer-to polymerization reaches high conversions. This has been observed both experimentally and in silico.[82] For example, Radzinski et al varied the initial [M]/[CTA] ratio utilized in RAFT transfer-to synthesis of a bottlebrush polymer with styrene as the monomer to evaluate the effect of side-chain MW. They observed a relationship between the amount of dead

linear polymer that formed during the polymerizations and the initial [M]/[CTA] ratio utilized (Figure 6.6).[63] Because the length of the growing polymeric radicals is related to the [M]/[CTA] ratio, high [M]/[CTA] ratios promote dead polymer formation due to increased side-chain MW leading to greater steric shielding and therefore a greater incidence of termination.

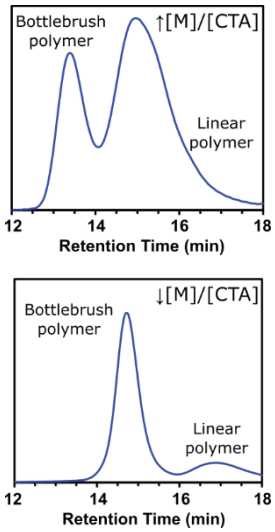

Figure 6.6. Effect of initial [M]/[CTA] ratio (top: 1000:1; bottom: 50:1) on bottlebrush polymer sample composition prepared via RAFT transfer-to using a polymeric dithiocarbamate CTA and styrene as the monomer. Reproduced from Ref. 63 with permission from The Royal Society of Chemistry.

Fröhlich et. al. have demonstrated in silico an exponential relationship between the length of the growing polymer graft, n, and the steric shielding factor, K, as shown in equation 6.3.[82]

$$K = A * n^{-0.45} \tag{6.3}$$

Here, A is a scaling constant and K is defined as:

$$K = \frac{k}{k_0} \tag{6.4}$$

where k is the rate constant of a bimolecular polymer-polymer reaction and k_0 is the rate constant of a similar reaction that is not located at a polymer chain. K is small for high steric shielding and approaches unity in the absence of steric interactions.

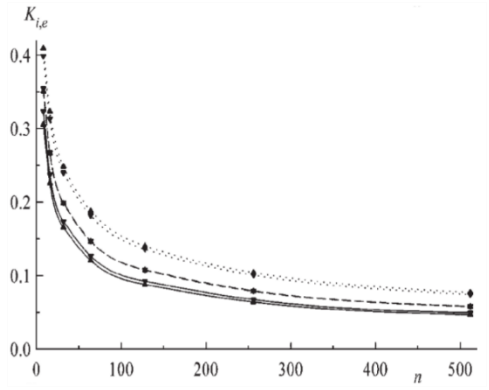

Figure 6.7. Shielding factors as functions of chain length n for polymers with different chain stiffnesses (K falls off faster for stiffer chains). Reproduced from Ref. 82 with permission from WILEY-VCH Verlag GmbH & Co.

The steric shielding factor decreases rapidly as chain length increases before asymptotically approaching zero. As the simulations in Figure 6.7 show, K approaches 0.1 with n ~100, indicating that the rate of addition of a growing polymer radical to a substrate-bound CTA is 10x slower than it would be in the absence of steric interactions. The principal outcome of this effect is an increased probability of termination with increasing polymer molecular weight. It should be noted that the shielding effect can be slightly reduced by increasing the distance between the CTA and the substrate. By expanding the tetrafunctional initiators in their computational model via the addition of non-relaxable segments between the core and the reactive CTA moieties, the researchers observed that the exponent relating the shielding factor and chain length was reduced to -0.43.[82]

6.8.4. Star-Star Coupling

The RAFT transfer-to mechanism involves the fragmentation of the RAFT adduct radical to yield an unattached polymer radical. Because the polymer racial is not attached to the substrate during

propagation, star-star coupling reactions are not expected to occur. However, under certain conditions star-star coupling has been observed.[80] Using a hexafunctional trithiocarbonate CTA, Vana and coworkers synthesized methyl acrylate (MA), butyl acrylate (BA), and dodecyl acrylate (DA) star polymers using the RAFT transfer-to method. At low conversions, high molecular weight star polymers were produced with low dispersity values. However, as conversion increased, SEC analysis revealed high molecular weight byproducts (Figure 6.8A). The origin of these high MW impurities was attributed to star-star coupling that occurs through an intermolecular chain transfer reaction between the propagating radical and arms of the star (chain transfer to polymer) (Figure 6.8B). This chain transfer event results in the creation of a radical on the arms of the star polymer that can add to a CTA attached to a different star polymer. Star-star coupling during RAFT transfer-to was modeled by kinetic (PREDICI) simulations, and this phenomenon was determined to be monomer dependent. Star-star coupling using RAFT transfer-to polymerization has only been observed with acrylates at high conversions, and this side reaction is generally easily prevented by avoiding conditions that promote chain transfer reactions to polymer.

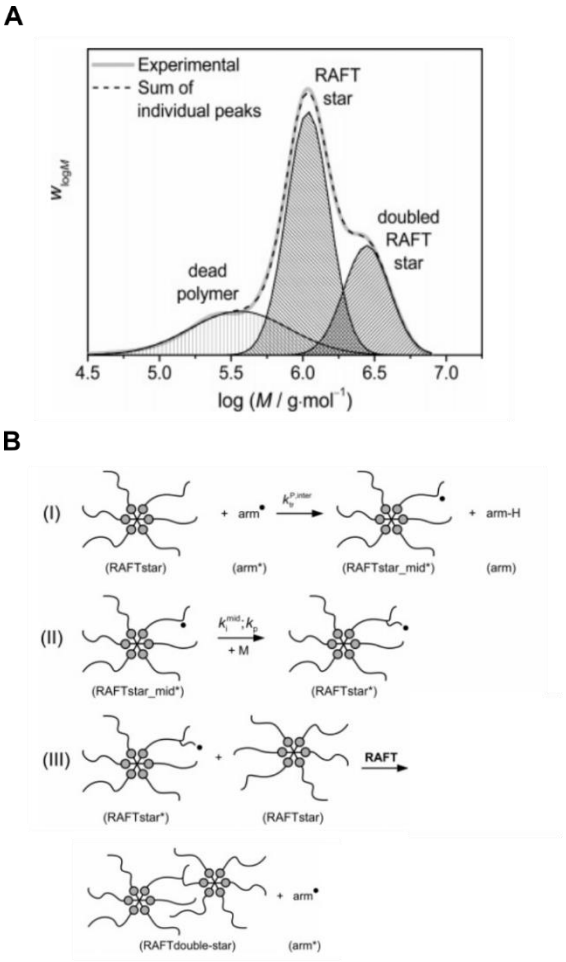

Figure 6.8. (A) Peak fitting of the SEC curve obtained from RAFT transfer-to polymerization of BA from a hexafunctional star polymer initiator. (B) The proposed mechanism for star-star coupling in RAFT transfer-to polymerization, which involves chain transfer to polymer. Adapted with permission from Boschmann, D.; Vana, P. *Macromolecules* 2007, *40*, 2683. Copyright 2007 American Chemical Society.

6.9. Conclusions

The transfer-to method in brush polymer synthesis is underutilized compared with other synthetic strategies for preparing brush polymers. In this review, we aimed to highlight both the advantages and shortcomings of this method compared with the more commonly used grafting-from method. We also showed how the transfer-to method can be optimized to provide brush polymers with few imperfections and impurities. Several factors contributing to the structure and sample composition of graft polymers prepared by RAFT transfer-to were discussed, including CTA selection,

monomer structure, and reaction conditions such as solvent, temperature, and pressure. To prepare high purity graft polymers using this method, conditions should be chosen that minimize termination and reduce steric shielding. In most cases this can be achieved by choosing RAFT agents have high C_{tr} in the monomer being polymerized, employing low initial [M]/[CTA] ratios, using non-polar solvents, and stopping the polymerization at low conversion.

RAFT transfer-to is ideally suited for the functionalization of nano-scale substrates due to the fact that the transfer-to mechanism prevents formation of coupled byproducts except in rare cases. As such, we expect transfer-to to be particularly useful for nanoparticle and protein grafting and star or bottlebrush polymer synthesis. Due to the relative lack of CTAs that are amenable to conducting RAFT transfer-to, the development of a library of CTAs with functional Z-groups could expand the scope of this method.

6.10. References

(1) Kato, K.; Uchida, E.; Kang, E.-T.; Uyama, Y.; Ikada, Y. *Prog. Polym. Sci.* **2003**, *28*, 209.

(2) Siedenbiedel, F.; Tiller, J. C. *Polymers* **2012**, *4*, 46.

(3) Kango, S.; Kalia, S.; Celli, A.; Njuguna, J.; Habibi, Y.; Kumar, R. *Prog. Polym. Sci.* **2013**, *38*, 1232.

(4) Heredia, K. L.; Maynard, H. D. *Org. Biomol. Chem* **2007**, *5*, 45.

(5) Verduzco, R.; Li, X.; Pesek, S. L.; Stein, G. E. *Chem. Soc. Rev.* **2015**, *44*, 2405.

(6) Sheiko, S. S.; Sumerlin, B. S.; Matyjaszewski, K. *Prog. Polym. Sci.* **2008**, *33*, 759.

(7) Xia, Y.; Kornfield, J. A.; Grubbs, R. H. *Macromolecules* **2009**, *42*, 3761.

(8) Radzinski, S. C.; Foster, J. C.; Matson, J. B. *Macromol. Rapid Commun.* **2016**, *37*, 616.

(9) Radzinski, S. C.; Foster, J. C.; Chapleski, R. C.; Troya, D.; Matson, J. B. *J. Am. Chem. Soc.* **2016**, *138*, 6998.

(10) Sumerlin, B. S. *ACS Macro Lett.* **2012**, *1*, 141.

(11) Matyjaszewski, K.; Spanswick, J. *Mater. Today* **2005**, *8*, 26.

(12) Hawker, C. J.; Bosman, A. W.; Harth, E. *Chem. Rev.* **2001**, *101*, 3661.

(13) Moad, G.; Rizzardo, E.; Solomon, D. H. *Macromolecules* **1982**, *15*, 909.

(14) Matyjaszewski, K.; Xia, J. *Chem. Rev.* **2001**, *101*, 2921.

(15) Chiefari, J.; Chong, Y. K.; Ercole, F.; Krstina, J.; Jeffery, J.; Le, T. P. T.; Mayadunne, R. T. A.; Meijs, G. F.; Moad, C. L.; Moad, G.; Rizzardo, E.; Thang, S. H. *Macromolecules* **1998**, *31*, 5559.

(16) Gody, G.; Maschmeyer, T.; Zetterlund, P. B.; Perrier, S. *Nat. Commun.* **2013**, *4*, 2505.

(17) Chong, Y. K.; Le, T. P. T.; Moad, G.; Rizzardo, E.; Thang, S. H. *Macromolecules* **1999**, *32*, 2071.

(18) Mühlebach, A.; Gaynor, S. G.; Matyjaszewski, K. *Macromolecules* **1998**, *31*, 6046.

(19) Hawker, C. J.; Frechet, J. M. J.; Grubbs, R. B.; Dao, J. *J. Am. Chem. Soc.* **1995**, *117*, 10763.

(20) Gaynor, S. G.; Edelman, S.; Matyjaszewski, K. *Macromolecules* **1996**, *29*, 1079.

(21) Gao, H.; Ohno, S.; Matyjaszewski, K. *J. Am. Chem. Soc.* **2006**, *128*, 15111.

(22) Bolton, J.; Rzayev, J. *ACS Macro Lett.* **2012**, *1*, 15.

(23) Cheng, C.; Khoshdel, E.; Wooley, K. L. *Nano Lett.* **2006**, *6*, 1741.

(24) Foster, J. C.; Matson, J. B. *Macromolecules* **2014**, *47*, 5089.

(25) Hoff, E. A.; Abel, B. A.; Tretbar, C. A.; McCormick, C. L.; Patton, D. L. *Polym. Chem.* **2017**.

(26) Chong, Y. K.; Krstina, J.; Le, T. P. T.; Moad, G.; Postma, A.; Rizzardo, E.; Thang, S. H. *Macromolecules* **2003**, *36*, 2256.

(27) Chiefari, J.; Mayadunne, R. T. A.; Moad, C. L.; Moad, G.; Rizzardo, E.; Postma, A.; Thang, S. H. *Macromolecules* **2003**, *36*, 2273.

(28) Keddie, D. J. *Chem. Soc. Rev.* **2014**, *43*, 496.

(29) Chiefari, J.; Chong, Y. K.; Ercole, F.; Krstina, J.; Jeffery, J.; Le, T. P. T.; Mayadunne, R. T. A.; Meijs, G. F.; Moad, C. L.; Moad, G.; Rizzardo, E.; Thang, S. H. *Macromolecules* **1998**, *31*, 5559.

(30) Moad, G.; Rizzardo, E.; Thang, S. H. *Aust. J. Chem.* **2006**, *59*, 669.

(31) Moad, G.; Rizzardo, E.; Thang, S. H. *Aust. J. Chem.* **2009**, *62*, 1402.

(32) Moad, G.; Rizzardo, E.; Thang, S. H. *Aust. J. Chem.* **2012**, *65*, 985.

(33) Perrier, S.; Takolpuckdee, P. *J. Poly. Sci. Part A: Polym. Chem.* **2005**, *43*, 5347.

(34) Barner-Kowollik, C.; Davis, T. P.; Heuts, J. P. A.; Stenzel, M. H.; Vana, P.; Whittaker, M. *J. Poly. Sci. Part A: Polym. Chem.* **2003**, *41*, 365.

(35) Boyer, C.; Stenzel, M. H.; Davis, T. P. *J. Poly. Sci. Part A: Polym. Chem.* **2011**, *49*, 551.

(36) Barner-Kowollik, C.; Perrier, S. *J. Poly. Sci. Part A: Polym. Chem.* **2008**, *46*, 5715.

(37) Wu, T.; Efimenko, K.; Genzer, J. *J. Am. Chem. Soc.* **2002**, *124*, 9394.

(38) Norde, W.; Gage, D. *Langmuir* **2004**, *20*, 4162.

(39) Lecommandoux, S.; Chécot, F.; Borsali, R.; Schappacher, M.; Deffieux, A.; Brûlet, A.; Cotton, J. P. *Macromolecules* **2002**, *35*, 8878.

(40) Berry, G. C.; Kahle, S.; Ohno, S.; Matyjaszewski, K.; Pakula, T. *Polymer* **2008**, *49*, 3533.

(41) Barner-Kowollik, C.; Davis, T. P.; Stenzel, M. H. *Aust. J. Chem.* **2006**, *59*, 719.

(42) Peng, Q.; Lai, D. M. Y.; Kang, E. T.; Neoh, K. G. *Macromolecules* **2006**, *39*, 5577.

(43) Stenzel, M. H.; Zhang, L.; Huck, W. T. S. *Macromolecular Rapid Communications* **2006**, *27*, 1121.

(44) Zhao; Perrier, S. *Macromolecules* **2006**, *39*, 8603.

(45) Zhao, Y.; Perrier, S. *Macromolecular Symposia* **2007**, *248*, 94.

(46) Takolpuckdee, P.; Mars, C. A.; Perrier, S. *Org. Lett.* **2005**, *7*, 3449.

(47) Perrier, S.; Takolpuckdee, P.; Mars, C. A. *Macromolecules* **2005**, *38*, 6770.

(48) Wang, G.-J.; Huang, S.-Z.; Wang, Y.; Liu, L.; Qiu, J.; Li, Y. *Polymer* **2007**, *48*, 728.

(49) Liu, J.; Bulmus, V.; Herlambang, D. L.; Barner-Kowollik, C.; Stenzel, M. H.; Davis, T. P. *Angew. Chemie. Int. Ed.* **2007**, *46*, 3099.

(50) Boyer, C.; Bulmus, V.; Liu, J.; Davis, T. P.; Stenzel, M. H.; Barner-Kowollik, C. *J. Am. Chem. Soc.* **2007**, *129*, 7145.

(51) Boyer, C.; Bulmus, V.; Davis, T. P.; Ladmiral, V.; Liu, J.; Perrier, S. *Chem. Rev.* **2009**, *109*, 5402.

(52) Stenzel, M. H.; Davis, T. P. *J. Poly. Sci. Part A: Polym. Chem.* **2002**, *40*, 4498.

(53) Mori, H.; Ookuma, H.; Endo, T. *Macromol. Symp.* **2007**, *249-250*, 406.

(54) Jesberger, M.; Barner, L.; Stenzel, M. H.; Malmström, E.; Davis, T. P.; Barner-Kowollik, C. *J. Poly. Sci. Part A: Polym. Chem.* **2003**, *41*, 3847.

(55) Shi, X.; Zhao, Y.; Gao, H.; Zhang, L.; Zhu, F.; Wu, Q. *Macromolecular Rapid Communications* **2012**, *33*, 374.

(56) Radzinski, S. C.; Foster, J. C.; Matson, J. B. *Polym. Chem.* **2015**, *6*, 5643.

(57) Hernández-Guerrero, M.; Davis, T. P.; Barner-Kowollik, C.; Stenzel, M. H. *Eur. Polym. J.* **2005**, *41*, 2264.

(58) Stenzel, M. H.; Davis, T. P.; Fane, A. G. *J. Mater. Chem.* **2003**, *13*, 2090.

(59) Fleet, R.; McLeary, J. B.; Grumel, V.; Weber, W. G.; Matahwa, H.; Sanderson, R. D. *Eur. Polym. J.* **2008**, *44*, 2899.

(60) Bernard, J.; Favier, A.; Davis, T. P.; Barner-Kowollik, C.; Stenzel, M. H. *Polymer* **2006**, *47*, 1073.

(61) Mayadunne, R. T. A.; Jeffery, J.; Moad, G.; Rizzardo, E. *Macromolecules* **2003**, *36*, 1505.

(62) Boschmann, D.; Mänz, M.; Fröhlich, M. G.; Zifferer, G.; Vana, P. In *Controlled/Living Radical Polymerization: Progress in RAFT, DT, NMP & OMRP*; American Chemical Society: 2009; Vol. 1024, p 217.

(63) Radzinski, S. C.; Foster, J. C.; Lewis, S. E.; French, E. V.; Matson, J. B. *Polym. Chem.* **2017**, *10.1039/C6PY01982J*.

(64) Moad, G.; Rizzardo, E.; Thang, S. H. *Polymer* **2008**, *49*, 1079.

(65) Rizzardo, E.; Chiefari, J.; Mayadunne, R. T. A.; Moad, G.; Thang, S. H. In *Controlled/Living Radical Polymerization*; American Chemical Society: 2000; Vol. 768, p 278.

(66) Foster, J. C.; Radzinski, S. C.; Lewis, S. E.; Slutzker, M. B.; Matson, J. B. *Polymer* **2015**, *79*, 205.

(67) Destarac, M.; Brochon, C.; Catala, J.-M.; Wilczewska, A.; Zard, S. Z. *Macromol. Chem. Phys.* **2002**, *203*, 2281.

(68) Perrier, S.; Barner-Kowollik, C.; Quinn, J. F.; Vana, P.; Davis, T. P. *Macromolecules* **2002**, *35*, 8300.

(69) Boschmann, D.; Vana, P. *Polymer Bulletin* **2005**, *53*, 231.

(70) Moad, G.; Mayadunne Roshan, T. A.; Rizzardo, E.; Skidmore, M.; Thang San, H. In *Advances in Controlled/Living Radical Polymerization*; American Chemical Society: 2003; Vol. 854, p 520.

(71) Boschmann, D.; Mänz, M.; Pöppler, A.-C.; Sörensen, N.; Vana, P. *J. Poly. Sci. Part A: Polym. Chem.* **2008**, *46*, 7280.

(72) Odian, G. *Principles of Polymerization*; 4th ed.; John Wiley & Sons, Inc.: New Jersey, 2004.

(73) Benaglia, M.; Rizzardo, E.; Alberti, A.; Guerra, M. *Macromolecules* **2005**, *38*, 3129.

(74) Fröhlich, M. G.; Nardai, M. M.; Förster, N.; Vana, P.; Zifferer, G. *Polymer* **2010**, *51*, 5122.

(75) Walling, C. *J. Poly. Sci.* **1954**, *14*, 214.

(76) Arita, T.; Buback, M.; Vana, P. *Macromolecules* **2005**, *38*, 7935.

(77) Xu, J.; He, J.; Fan, D.; Tang, W.; Yang, Y. *Macromolecules* **2006**, *39*, 3753.

(78) Arita, T.; Buback, M.; Janssen, O.; Vana, P. *Macromolecular Rapid Communications* **2004**, *25*, 1376.

(79) Boschmann, D.; Edam, R.; Schoenmakers, P. J.; Vana, P. *Polymer* **2008**, *49*, 5199.

(80) Boschmann, D.; Vana, P. *Macromolecules* **2007**, *40*, 2683.

(81) Darcos, V.; Dureault, A.; Taton, D.; Gnanou, Y.; Marchand, P.; Caminade, A.-M.; Majoral, J.-P.; Destarac, M.; Leising, F. *Chem. Commun.* **2004**, 2110.

(82) Fröhlich, M. G.; Vana, P.; Zifferer, G. *Macromol. Theory Simul* **2007**, *16*, 610.

Chapter 7. Synthesis of Bottlebrush Polymers via Transfer-To and Grafting-Through Approaches Using a RAFT Chain Transfer Agent with a ROMP-Active Z-Group

"Radzinski, S. C.; Foster, J. C.; Matson, J. B., *Polymer Chemistry*, **2015**, 6, 5643-5652. Published by the Royal Society Chemistry."

7.1. Authors

Scott C. Radzinski,[†] Jeffrey C. Foster,[†] John B. Matson.*

*Department of Chemistry and Macromolecules and Interfaces Institute, Virginia Tech, Blacksburg, Virginia 24061, United States.

[†]These authors contributed equally to this work.

7.2. Abstract

A novel dithiocarbamate chain transfer agent (**CTA1**) with a directly polymerizable Z-group was synthesized for use in reversible addition-fragmentation chain transfer polymerization (RAFT). This CTA effectively mediated RAFT polymerization of styrenic and acrylic monomers with dispersities (Đ) < 1.08. Utilizing the polymerizable Z-group on the ω-chain end that is inherited from the RAFT process, bottlebrush polymers were synthesized via ring-opening metathesis polymerization (ROMP) in a grafting-through process. The effect of a number of parameters on the grafting process was studied, and optimized conditions yielded bottlebrush polymers of controllable molecular weights, narrow molecular weight distributions, and high conversions (> 90%). Bottlebrush polymers made by a transfer-to strategy were also synthesized from **CTA1**. In this case, ROMP was first carried out to produce poly(**CTA1**) (**PCTA1**), then RAFT was

performed from the **PCTA1** backbone. This technique allows for the preparation of high molecular weight bottlebrush polymers without radical coupling between bottlebrush polymers. Lastly, regardless of the synthetic method, all bottlebrush polymers produced using **CTA1** are composed of polymeric side chains that are attached to the bottlebrush backbone through a labile dithiocarbamate linkage that can be cleaved in the presence of nucleophiles such as amines. The unique combination of these capabilities allows for the study of bottlebrush polymer formation by both transfer-to and grafting-through strategies using a single agent.

7.3. Introduction

Over the past two decades, bottlebrush polymers have become an increasingly relevant polymer topology as a result of their well-defined structures, shape persistence, nanoscopic dimensions, and unique mechanical and rheological properties.[1] Bottlebrush polymers are comprised of polymeric side-chains grafted to a polymer backbone, and given sufficient grafting density, steric repulsion between polymeric neighbors causes the backbone to adopt a chain-extended conformation.[2,3] Consequently, cylindrical,[4,5] spherical,[6,7] or worm-like,[8] morphologies can be realized in single macromolecules by tuning polymer composition, grafting density, or side-chain molecular weight. Additionally, important polymeric properties, such as amphiphilicity or stimuli-responsiveness, can be extrapolated to bottlebrush systems by tuning the chemical composition of the polymeric side-chains.[9-11] In terms of mechanical properties, bottlebrush polymers differ from linear polymers primarily due to their inability to interact via chain entanglements—a phenomenon from which many of the physical properties of linear polymers arise. Therefore, bottlebrush polymers have garnered interest for use in applications such as rheology modifiers and super-soft elastomers.[12] Lastly, their size and shape-persistence makes bottlebrush polymers well suited for the *in vivo* delivery of therapeutic agents.[13]

Bottlebrush polymers can be prepared via one of four approaches: (1) the grafting-from strategy, whereby polymer side chains are grown from a polymeric backbone decorated with initiating functionalities; (2) the grafting-to methodology involving the attachment of pre-formed polymers to reactive sites on a polymer backbone; (3) the grafting-through or macromonomer (MM) approach, in which polymers fitted with a polymerizable moiety are utilized as MMs in an subsequent polymerization; and, (4) the transfer-to strategy (sometimes called the RAFT Z-group approach). Transfer-to is a unique hybrid of the grafting-from and grafting-to strategies in which polymeric radicals detach from the bottlebrush backbone, propagate freely in solution, and return to the backbone through a chain-transfer reaction with a pendant CTA.[14] While the grafting-from, grafting-to, and transfer-to strategies yield macromolecules with a bottlebrush topology, the grafting process is hindered by steric interactions between adjacent polymer chains, resulting in low grafting densities.[15] However, despite this shortcoming, grafting-from (and to a greater extent transfer-to) can be employed to synthesize bottlebrush polymers with relatively higher molecular weights (on the order of $\geq 10^6$ Da) than are possible with grafting-through. In contrast, grafting-through results in "perfectly grafted" (i.e. the highest possible grafting density) bottlebrush polymers, as each repeat unit bears a polymeric side chain. In view of the high grafting density and synthetic versatility of the grafting-through technique, recent efforts have focused on its application.[11,16-31]

To prepare well-defined bottlebrush polymers via the grafting-through strategy, reversible-deactivation radical polymerization techniques such as atom transfer radical polymerization (ATRP) and reversible addition-fragmentation chain transfer polymerization (RAFT) are often employed.[1] Generally, semi-telechelic MMs of predefined MW and low dispersity (Đ) are

synthesized via one of these techniques. In a second step, the resulting MMs are functionalized with a polymerizable moiety in a post polymerization reaction, and the MMs are subsequently polymerized using an additional polymerization method in the third and final step.[20,23] Alternatively, in a two-step method, MM synthesis can be conducted in the presence of an initiator or chain-transfer agent (CTA) containing an orthogonal functionality.[17,21,22] For example, norbornene and derivatives thereof have been coupled to dithioester and trithiocarbonate CTAs.[19] In this case, RAFT was utilized to prepare the MM grafts, and ring-opening metathesis polymerization (ROMP) was employed in a subsequent grafting-through step. ROMP is particularly well suited for this purpose because of the high functional group tolerance and rapid propagation rate of several ruthenium-based olefin metathesis catalysts (Figure 7.1).[16] Bottlebrush polymers have been prepared via a combination of these two polymerization techniques in separate steps as described above, or more simply via a one-pot strategy wherein a ROMP catalyst is added to a terminated RAFT reaction mixture.[18]

Figure 7.1. ROMP catalysts used in this work.

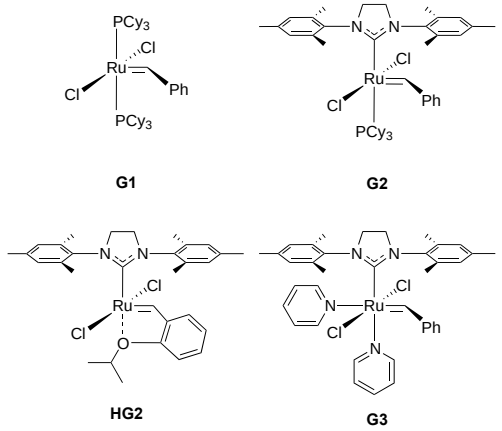

RAFT polymerization is mediated by a thiocarbonylthio-containing agent with an activating Z-group and a leaving group (R-group) that is comparable in radical stability to that of the monomer-derived radical. A number of R- and Z-groups have been utilized to gain control over the RAFT

polymerization of a wide range of vinyl monomers.[32] However, to our knowledge, there exists no report in the literature on the incorporation of a directly polymerizable Z-group such as *exo*-norbornene imide into a RAFT agent (Scheme 7.1). We envisioned that such a CTA (**CTA1**) could be employed in both RAFT transfer-to and ROMP grafting-through methodologies.

Scheme 7.1. Proposed CTA structure with directly polymerizable Z-group.

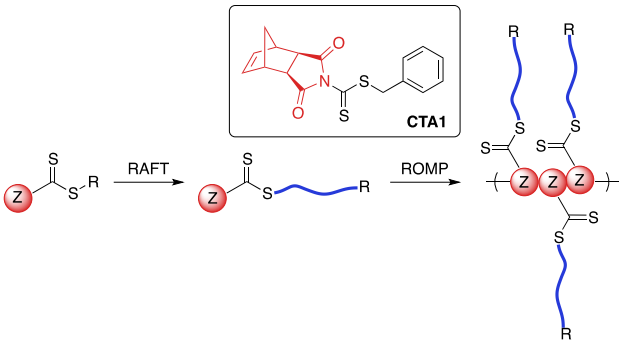

While directly polymerizable R-groups have been incorporated into RAFT CTAs,[18,19] a directly polymerizable Z-group would experience the benefits inherent in the Z-group, or transfer-to, approach.[33-36] Such benefits are a result of the RAFT mechanism when applied in a graft polymerization. During a RAFT transfer-to polymerization, growing polymer chains detach from the bottlebrush polymer backbone during propagation and then add back to the backbone through reaction with a pendant thiocarbonylthio group. Because the growing "arms" are free in solution, coupling between growing adjacent "arms" attached to the bottlebrush backbone does not occur. In addition, radical coupling between growing bottlebrush polymers cannot occur, as the propagating radical resides on the detached polymeric side chains. As a result, the transfer-to approach affords bottlebrush polymers with lower dispersities and higher possible conversions relative to conventional RAFT grafting-from using the R group approach.[36,37] An additional advantage of the incorporation of a directly polymerizable Z-group is the location of the thiocarbonylthio group in the bottlebrush polymer. In the case of bottlebrush polymers prepared

from **CTA1**, the thiocarbonylthio group would link the polymeric arms to the backbone polymer, in contrast to systems using directly polymerizable R-groups, which leave the thiocarbonylthio group on the bottlebrush surface. Given the wealth of literature concerning the post-polymerization removal of RAFT end groups,[38] we envisioned the possibility of thiocarbonylthio degradation-driven side chain dissociation. Herein, we investigate the efficacy of **CTA1** as a mediator of RAFT polymerization and the availability of the norbornene functionality for ROMP. Additionally, we evaluate the preparation of bottlebrush polymers via both transfer-to and grafting-through strategies. Finally, we explore side-chain cleavage by aminolysis to investigate side chain molecular weights and molecular weight distributions.

7.4. Materials and Methods

Materials. All reagents were obtained from commercial vendors and used as received unless otherwise stated. Styrene and *n*-butyl acrylate were passed through small columns of basic alumina prior to use. ROMP catalysts $(PCy_3)_2(Cl)_2Ru{=}CHPh$ (**G1**), $(H_2IMes)(Cl)_2(PCy_3)Ru{=}CHPh$ (**G2**) and $(H_2IMes)(Cl)_2(PCy_3)Ru{=}CH(2\text{-}OiPrPh)$ (**HG2**) were obtained as a generous gift from Materia. ROMP catalyst $(H_2IMes)(pyr)_2(Cl)_2Ru{=}CHPh$ (**G3**) was prepared from **G2** according to literature procedures.[39,40]

Methods. NMR spectra were measured on Agilent 400 MHz or Bruker 500 MHz spectrometers. ^1H and ^{13}C NMR chemical shifts are reported in ppm relative to internal solvent resonances. Yields refer to chromatographically and spectroscopically pure compounds unless otherwise stated. Size exclusion chromatography (SEC) was carried out in THF at 1 mL/min, 30°C on two Agilent PLgel 10 μm MIXED-B columns connected in series with a Wyatt Dawn Helios 2 light scattering detector and a Wyatt Optilab Rex refractive index detector. No calibration standards were used, and dn/dc values were obtained by assuming 100% mass elution from the columns. Atomic force

microscopy (AFM) was conducted using a Veeco BioScope II AFM in tapping mode in air at room temperature using Nano World Pointprobe-silicon SPM Sensor tips (spring constant = 7.4 N/m, resonance frequency = 160 kHz). Dynamic light scattering (DLS) was conducted using a Malvern Zetasizer Nano operating at 25 °C. Polymer solutions were prepared at 1 mg/mL and were filtered with a 0.25 μm filter prior to scanning. The calculations of the particle size distributions and distribution averages were conducted using CONTIN particle size distribution analysis routines. All measurements were made in triplicate and errors reflect standard deviations.

Synthesis of CTA1. KOH (0.60 g, 10.7 mmol) was ground to a fine powder with a mortar and pestle and placed in a 100 mL round bottom flask. To the flask was added *exo*-norbornene imide (1.33 g, 8.15 mmol) followed by 30 mL of DMF. This mixture was stirred for 5 min, followed by dropwise addition of CS_2 (2.46 mL, 40.8 mmol). The solution developed a deep red color. After an additional 3 h of stirring, benzyl bromide (4.84 mL, 40.8 mmol) was added dropwise, and the reaction mixture was stirred at rt for 12 h. The following day, the reaction mixture was diluted with diethyl ether (~50 mL) and washed with H_2O (3 x 150 mL) and brine. The organic layer was dried over Na_2SO_4, and the solvent was removed under reduced pressure. The crude product was purified on a silica gel column, eluting with 1:1 CH_2Cl_2/hexanes, to give 1.30 g of **CTA1** as a yellow solid (48% yield). ^{1}H NMR ($CDCl_3$): δ 1.57 (m, 2H), 2.82 (s, 2H), 3.39 (s, 2H), 4.50 (s, 2H), 6.33 (s, 2H), 7.35 (m, 5H). ^{13}C NMR ($CDCl_3$): δ 199.31, 173.75 138.29, 132.93, 129.34, 128.95, 128.26, 48.27, 46.47, 43.62, 43.22. HRMS (m/z): calculated 330.0617, found 330.0627.

Synthesis of Polystyrene MMs. A typical polymerization procedure of styrene is as follows: To an oven-dried Schlenk tube equipped with a magnetic stir bar was added **CTA1** (29.0 mg, 87.0 μmol), 2,2'-azobis(2-methylpropionitrile)(AIBN) (1.43 mg, 8.73 μmol), styrene (1 mL, 8.7 mmol), and 1 mL of THF. The reaction mixture was deoxygenated by three freeze-pump-thaw cycles. The

Schlenk tube was then backfilled with N_2 and submerged in an oil bath maintained at 75 °C. Samples were removed periodically by N_2-purged syringe to monitor molecular weight evolution by SEC and conversion by ^{1}H NMR spectroscopy. The polymerization was quenched by submerging the tube into liquid N_2 and exposing the reaction mixture to air. The resulting polystyrene was purified via precipitation from MeOH (3x).

Synthesis of Poly(n-butyl Acrylate) (nBA) MMs. A typical polymerization procedure of nBA is as follows: To an oven-dried Schlenk tube equipped with a magnetic stir bar was added **CTA1** (46.0 mg, 140 μmol), 2,2'-azobis(2-methylpropionitrile)(AIBN) (2.29 mg, 14.0 μmol), nBA (2 mL, 14 mmol), and 2 mL of THF. The reaction mixture was deoxygenated by three freeze-pump-thaw cycles. The Schlenk tube was then backfilled with N_2 and submerged in an oil bath maintained at 60 °C. Samples were removed periodically by N_2-purged syringe to monitor molecular weight evolution by SEC and conversion by ^{1}H NMR spectroscopy. The polymerization was quenched by submerging the tube into liquid N_2 and exposing the reaction solution to air. The resulting poly(nBA) was purified via precipitation from hexanes (3x).

Synthesis of Poly(CTA1) (PCTA1). A typical polymerization procedure of **CTA1** is as follows: **CTA1** (109 mg, 329 μmol) was dissolved in 1.5 mL of anhydrous CH_2Cl_2 in a 1-dram vial. A solution of **G3** in anhydrous CH_2Cl_2 was prepared at 9.6 mg/mL in a second vial. 0.5 mL of this **G3** soln was added rapidly to the vial containing **CTA1**. The polymerization was quenched after 20 min by adding of 1-3 drops of ethyl vinyl ether. The polymer was isolated via precipitation from hexanes and dried under vacuum to yield 93 mg of pure polymer as an off-white powder (85% yield).

Synthesis of Poly(CTA1-*g*-styrene) by RAFT transfer-to. To an oven-dried Schlenk tube equipped with a magnetic stir bar was added poly(**CTA1**) (22.0 mg, 873 μmol, M_n = 25 100 g/mol), 2,2'-azobis(2-methylpropionitrile)(AIBN) (0.014 mg, 0.087 μmol), styrene (5 mL, 43 mmol), and 5 mL of THF. The reaction mixture was deoxygenated by three freeze-pump-thaw cycles. The Schlenk tube was then backfilled with N_2 and submerged in an oil bath maintained at 75 °C. Samples were removed periodically by N_2-purged syringe to monitor molecular weight evolution by SEC and conversion by ^{1}H NMR spectroscopy. The polymerization was quenched by submerging the tube into liquid N_2 and exposing the reaction solution to air. The resulting poly(**CTA1**-*g*-styrene) was purified via precipitation from MeOH.

Synthesis of Poly(CTA1-*g*-styrene) by RAFT grafting-through. A typical grafting-through polymerization procedure is as follows: To a vial containing **MM** in anhydrous CH_2Cl_2 was added rapidly a soln of **G3** in anhydrous CH_2Cl_2 to make a final polymer concentration of 100 mg/mL. The polymerization was stirred at rt. After 1 h, the polymerization was quenched by adding 1-3 drops of ethyl vinyl ether. The resulting bottlebrush polymer was isolated via precipitation from a MeOH/H_2O mixture and dried under vacuum.

Aminolysis of bottlebrush polymers. Bottlebrush polymer was dissolved in 0.3 mL of THF in a 1-dram vial equipped with a stir bar. To the vial was added 0.3 mL of a 40 w/v % soln of methylamine in H_2O. The reaction mixture was stirred at rt in air for 72 h to ensure complete thiol oxidation. A few drops of THF were added to dissolve the precipitated solids, and the resulting aminolyzed side chains were isolated via precipitation from MeOH and were dried under vacuum overnight.

7.5. Results and Discussion

7.5.1. CTA1 Synthesis

CTA1 was synthesized in one-pot starting from *exo*-norbornene imide (see Supporting Information for further details) as shown in Scheme 7.2. The reaction proceeds via the potassium hydroxide-assisted attack of the imide nitrogen on carbon disulfide, forming a dithiocarbamate salt. In the second step, the dithiocarbamate intermediate reacts with benzyl bromide in a substitution reaction to yield the desired product.

Scheme 7.2. One-pot synthesis of CTA1.

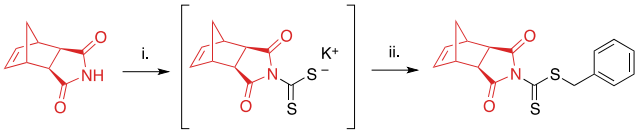

[a]Experimental conditions: (i) CS_2, KOH, DMF; (ii) benzyl bromide.

Column purification was required to remove unreacted starting materials, and isolated yields ranged from 35-48%. While this range is lower than reported values for the synthesis of other dithiocarbamates,[41,42] many such CTAs are derived from electron-rich secondary amines in contrast to the relatively electron-deficient imide employed in our study. This electron-deficiency results in the limited nucleophilicity of the imide nitrogen,[43] hindering its addition to electrophiles such as CS_2. Longer reaction times or increased temperatures were not found to increase yields.

7.5.2. RAFT Polymerization

The success of a RAFT polymerization is tied to many factors, chief among which is the matching of monomer reactivity to that of the CTA.[44-48] More activated monomers (MAMs) (i.e., methacrylates, acrylates, styrenes) require electron deficient C=S bonds, such as those present in dithioester and trithiocarbonate RAFT agents, while less activated monomers (LAMs) (i.e., vinyl

esters and amides) can only be polymerized in the presence of more electron rich thiocarbonyl-containing compounds such as xanthates. In fact, reaction of LAMs with dithiobenzoate or certain trithiocarbonate CTAs can result in complete inhibition of polymerization.[49] The use of *N*-pyrrolyl and *N*-phthalimidyl moieties as Z-groups in dithiocarbamate RAFT CTAs was first reported by Cheifari and coworkers.[50] These CTAs are suitable for controlling the polymerization of many MAMs.[47,51-53] Therefore, we envisioned that **CTA1** could be employed to mediate the polymerization of this class of vinyl monomers.

To evaluate our hypothesis, RAFT polymerizations of styrene and *n*-butyl acrylate (nBA) were carried out in the presence of **CTA1** (Scheme 7.3). The polymerizations were conducted in THF (1:1 v/v% THF/monomer) at 75 °C for styrene or 60 °C for nBA in the presence of 2,2'-azobis(isobutyronitrile) (AIBN). To maintain a high level of chain end fidelity, a [CTA]/[AIBN] ratio of 10:1 was chosen.[54] Kinetic analysis was performed by removing aliquots of the polymerization solution at various time points via N_2-purged syringe. The polymerizations were quenched by exposing the reaction mixture to air and submerging the reaction vessel into liquid N_2. Molecular weight (MW) and dispersity (Đ) were determined by size-exclusion chromatography (SEC), and conversions were measured by ^{1}H NMR spectroscopy. **CTA1**-mediated RAFT polymerization of styrene and nBA yielded polymers of controllable molecular weights with narrow molecular weight distributions (Đ < 1.08). As previously reported for similar dithiocarbamate CTAs,[55] polymerization of methyl methacrylate was uncontrolled. On the opposite end of the monomer reactivity spectrum, polymerization of vinyl acetate was completely inhibited in the presence of **CTA1**.

Scheme 7.3. CTA1-mediated RAFT polymerization of styrene or nBA.

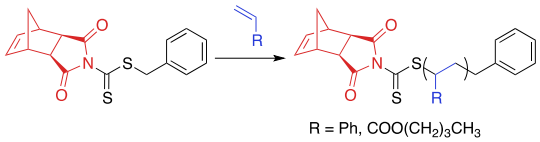

[a]Experimental conditions: AIBN, THF, 75 °C for styrene or 60 °C for nBA.

Kinetic analysis of **CTA1**-mediated polymerization of styrene and nBA is shown in Figure 7.2. Molecular weight distributions determined by SEC were monomodal with low Đ, indicative of a well-controlled polymerization and a high chain transfer efficiency of **CTA1** under the conditions investigated. Conversion increased linearly with time for nBA, and Đ decreased over the course of the reaction for both nBA and styrene. In the case of styrene, a non-linear relationship was observed in the semi-logarithmic plot (Figure 7.2C) and a maximum conversion of only 48% was obtained after 24 h, indicative of the occurrence of termination reactions during the polymerization. The polymerization was repeated under more dilute conditions (2:1 v/v% THF/styrene), resulting in a reduction of termination reactions and a higher terminal conversion (81% after 24 h). For both monomers, the linear relationship between MW and conversion corroborated the controlled nature of the polymerization (Figure 7.2D).

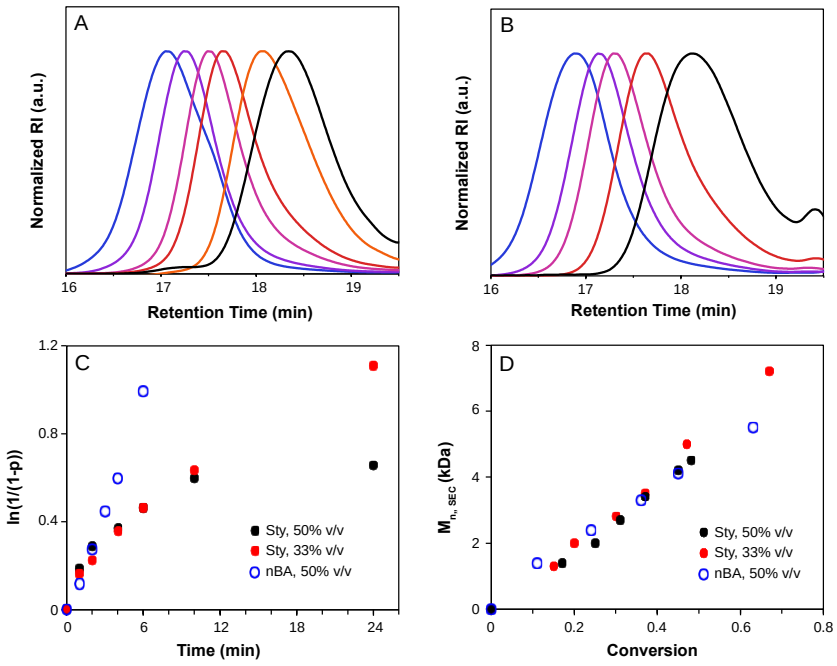

Figure 7.2. Kinetic analysis of CTA1-mediated RAFT polymerization. A and B) SEC traces show evolution of MW during the polymerizations of styrene (A) and nBA (B). C) ln(1/(1-p)) vs. time for the polymerization of styrene ([styrene]/[CTA]/[I] = 100:1:0.1, 50% v/v in THF, 75 °C, black circles; [styrene]/[CTA]/[I] = 100:1:0.1, 33% v/v in THF, 75 °C, red circles) and nBA ([nBA]/[CTA]/[I] = 100:1:0.1, 50% v/v in THF, 60 °C, blue open circles). D) M_n as a function of conversion for the polymerization of styrene and nBA.

Chain extension of a polymer prepared using **CTA1** was attempted to further validate its capability to mediate controlled RAFT polymerization. For the first block, poly(nBA) of MW = 6900 Da (Đ = 1.06) was synthesized using **CTA1**. This polymerization yielded a macroCTA with a dithiocarbamate at the ω-chain end. The poly(nBA) macroCTA was utilized in a second step to control the polymerization of styrene ([M]/[CTA]/[AIBN] = 1000:1:0.1), ultimately resulting in the formation of a block copolymer. After 4 h, the polymer had grown to 27.0 kDa as measured by SEC (Đ = 1.05) (Figure 7S9). This measured MW agreed with the expected value of 26.6 kDa based on conversion as measured by ^{1}H NMR spectroscopy.

To prepare macromonomers for ROMP grafting-through, a series of polymers of differential MW were synthesized, and the isolated polymers were characterized by SEC and ^{1}H NMR spectroscopy (Figures 7S8 and 7S10). A summary of our analysis is provided in Table 7.1. The subscripts in the polymer name assignments refer to the degree of polymerization of the polystyrene component of the macromonomers. Polymers with relatively narrow molecular weight distributions were obtained. In addition, MWs measured by SEC were in good agreement with those calculated from conversion using ^{1}H NMR spectroscopy.

Table 7.1. Polystyrene MMs prepared by RAFT polymerization.

Polymer[a]	$M_{n\ (SEC)}$ (Da)	$M_{n\ (theo)}$[b] (Da)	Đ
MM_{29}	3,300	3,100	1.05
MM_{52}	5,700	6,000	1.02
MM_{113}	12,100	13,300	1.04

[a]Average degree of polymerization shown as a subscript calculated from SEC data using the formula DP = $(M_n\text{-}MW_{CTA})/MW_{styrene}$. [b]Determined by ^{1}H NMR spectroscopy using the formula $M_{n\ (theo)} = MW_{styrene} * ([styrene]/[CTA]) * \%\ conv$

An important outcome of **CTA1**-mediated RAFT polymerization is the preservation of the reactive norbornene olefin moiety on the ω-end of the resulting polymer chain, allowing for subsequent bottlebrush formation via ROMP grafting-through. The orthogonality of the norbornene olefin with reversible deactivation radical polymerization has been previously shown.[56] The poor reactivity of the internal norbornene olefin in RAFT relative to the terminal, vinyl groups of acrylic monomers is attributed to their differences in electronics. ^{1}H NMR spectroscopic analysis of the pure MMs confirmed the preservation of the norbornene olefin, evident as a singlet at 6.2 ppm (Figure 7S8).

7.5.3. RAFT Transfer-To

There exist four methodologies for preparing bottlebrush polymers, and careful consideration is warranted to select the best strategy for a given system. For example, adoption of a grafting-through approach is appropriate when high grafting density is needed. However, bottlebrush formation via grafting-through is hindered by high MW macromonomers, limiting the use of this strategy to applications in which bottlebrushes with relatively short side chains are acceptable.[57] In contrast, the transfer-to technique allows for the synthesis of bottlebrush polymers with high MW side chains, but can potentially suffer from broad side chain dispersities and lower than "perfect" grafting densities due to termination reactions during the polymerization.[58]

Scheme 7.4. Preparation of bottlebrush polymers from CTA1 by transfer-to or grafting-through.

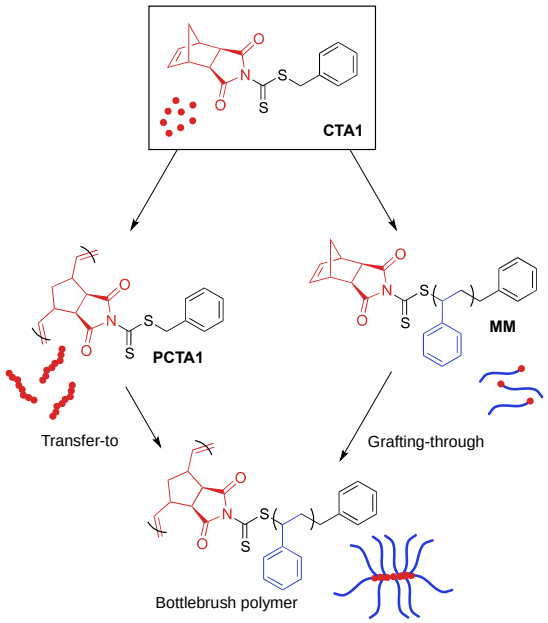

CTA1 can be utilized for both transfer-to and grafting-through strategies, creating a unique opportunity to evaluate the differences between these two techniques while using identical chemistry. To evaluate the ability of **CTA1** to control the growth of high MW side chains from a polymeric backbone by RAFT transfer-to, **CTA1** was first polymerized by ROMP (Scheme 7.4)

using Grubbs' 3rd generation catalyst ($(H_2IMes)(Cl)_2(pyr)_2Ru=CHPh$) (**G3**) (50:1 [**CTA1**]/[**G3**]) to yield a poly(**CTA1**) (**PCTA1**) consisting of a poly(norbornene) backbone with a dithiocarbamate group on each repeat unit (Figures 7.3 and 7S7). Following our characterization of the resulting polymeric CTA, **PCTA1** was then subjected to RAFT polymerization conditions ([styrene]/[macroCTA]/[AIBN] = 50,000:1:0.1, THF, 75 °C), and the progress of the reaction was monitored by SEC. Molecular weight distributions of the growing bottlebrush polymer were monomodal, and the corresponding polymers exhibited successively shorter retention times, indicative of increasing MW (Figure 7.3). After 91 h, the polymer had grown from 25.1 kDa (for **PCTA1**) to 1250 kDa, with Đ remaining low (< 1.02) throughout the course of the polymerization. A second peak in the SEC traces at ~15 min corresponds to dead polymer arising from termination reactions between detached polymeric radicals. This phenomenon is discussed in further detail below.

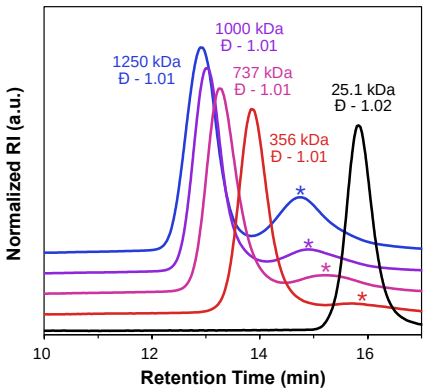

Figure 7.3. RAFT transfer-to mediated by PCTA1 (black trace), sampled at 19 h (red trace), 42 h (magenta trace), 67 h (purple trace), and 91 h (blue trace). Starred peaks correspond to "dead" polymer. Baselines are shifted for clarity.

7.5.4. ROMP Grafting-Through

The presence of a strained, cyclic olefin at the ω-chain end of polymers prepared via RAFT using **CTA1** allows for the direct synthesis of bottlebrush polymers by ROMP. In order to prepare

bottlebrush polymers by ROMP, polystyrene MMs were precipitated three times from THF into methanol to ensure the complete removal of styrene, which can participate in olefin metathesis in the presence of Ru catalysts.[59] The existence of residual styrene during ROMP has been shown to result in chain transfer and a broadening of the molecular weight distribution.[60] Therefore, MM purity was confirmed by monitoring the disappearance of styrene olefin peaks at 5.5 and 5.0 ppm by ^{1}H NMR spectroscopy between precipitations.

A series of Ru-based metathesis catalysts were evaluated for their efficacy towards the grafting-through polymerization of **CTA1**-derived polystyrene (**MM_{29}**)(Scheme 7.4). Toward this end, ROMP of **MM_{29}** was conducted in the presence of various ROMP catalysts at a [MM]/[catalyst] ratio of 50 : 1 (Figure 7S11). Grafting-through polymerizations initiated by Grubbs' 1st ((PCy_3)$_2$(Cl)$_2$Ru=CHPh) (**G1**) and 2nd generation ((H_2IMes)(Cl)$_2$(PCy_3)Ru=CHPh) (**G2**) catalysts showed poor conversion to the corresponding bottlebrush polymer after 1 h in CH_2Cl_2 (Table 7.2, entries 1 and 2, respectively). The Hoveyda-Grubbs' 2nd generation catalyst ((H_2IMes)(Cl)$_2$(PCy_3)Ru=CH(2-OiPrPh)) (**HG2**) effected higher conversion to bottlebrush polymer (78%); however, the resulting polymer had a broad molecular weight distribution (Đ = 1.50) (Table 7.2, entry 3). Grafting-through by the modified Grubbs' 2nd generation catalyst (**G3**) showed 91% conversion to bottlebrush polymer with Đ = 1.03 and a monomodal molecular weight distribution (Table 7.2, entry 5). Based on this analysis, **G3** was utilized for further experiments.

Table 7.2. Investigation of the effect of catalyst, MW, and MM concentration on conversion to bottlebrush.

entry	MM	MM $M_{n,SEC}$ (kDa)[a]	cat.	[MM]/[I]	[MM] (mg/mL)	%conv to BB[b]	BB $M_{n,theo}$ (kDa)[c]	BB $M_{n,SEC}$ (kDa)[a]	BB Đ[a]
1	**MM_{29}**	3.3	**G1**	50:1	100	8	13.2	21.1	1.11
2	**MM_{29}**	3.3	**G2**	50:1	100	16	26.4	353	1.48
3	**MM_{29}**	3.3	**HG2**	50:1	100	78	129	334	1.50
4	**MM_{29}**	3.3	**G3**	25:1	100	91	75.0	85.6	1.04
5	**MM_{29}**	3.3	**G3**	50:1	100	91	150	152	1.03
6	**MM_{29}**	3.3	**G3**	75:1	100	89	220	240	1.14
7	**MM_{29}**	3.3	**G3**	100:1	100	87	330	340	1.25
8	**MM_{29}**	3.3	**G3**	50:1	25	70	116	100	1.10
9	**MM_{29}**	3.3	**G3**	50:1	50	80	132	125	1.09
10	**MM_{52}**	5.6	**G3**	50:1	100	65	182	190	1.09
11	**MM_{113}**	12.1	**G3**	50:1	100	40	242	180	1.16

[a]Measured by SEC using absolute MW determination by light scattering. [b]Determined from SEC by comparing the integrations of BB and MM peaks. [c]Calculated using the formula % conv*([M]/[I])*$M_{n,MM}$. Polymerizations conducted for 1 h in CH_2Cl_2.

Macromonomer MW was found to influence ROMP grafting-through polymerization (Table 7.2, entries 5, 10-11, Figure 7S12). Comparing the grafting-through polymerization of three MMs of differing MW (3.3 KDa, 5.6 KDa, and 12 KDa) revealed an inverse correlation between MW and conversion. This observed dependence of conversion on MW is attributed to steric factors.[57] The MW of the isolated bottlebrush polymer made from **MM_{29}** was 152 kDa, which is in good agreement with the expected molecular weight of 150 kDa. Despite lower conversions, polymerizations of **MM_{52}** and **MM_{113}** showed reasonable agreement between theoretical and observed M_n values and maintained fairly low dispersities.

To further confirm the livingness of grafting-through polymerization of **CTA1**-derived MMs, the [**MM$_{29}$**]/[**G3**] ratio was varied from 25:1 to 100:1 (Table 7.2, entries 4-7). The resulting bottlebrush polymers were monomodal and their SEC traces exhibited the expected inverse relationship between MW and retention time (Figure 7.4A). M_n values determined by SEC are in good agreement with theoretical MWs. A plot of M_n vs [M]/[I] showed the anticipated linear trend (Figure 7.4B).[61] Additionally, dispersity values were low, ranging from 1.04-1.25 throughout the series.

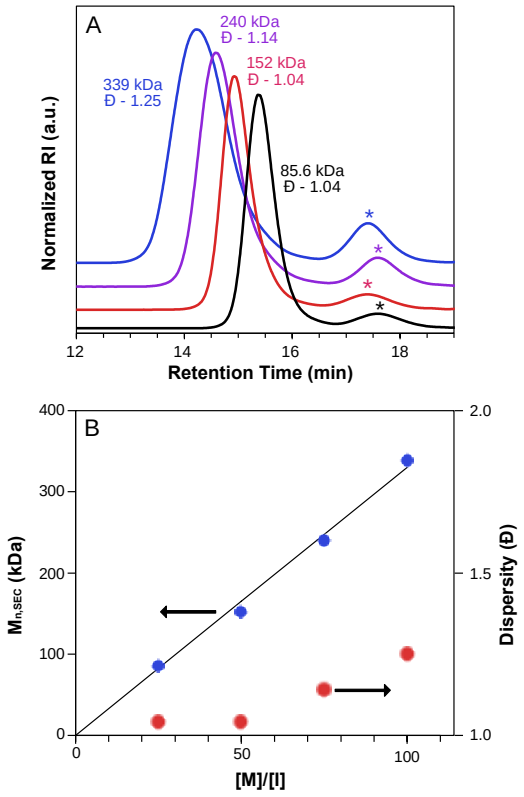

Figure 7.4. Assessment of the livingness of ROMP grafting-through of MM$_{29}$. A) SEC traces illustrating the increase in MW with increasing [MM]/[G3] ratio (black = [25]:[1], red = [50]:[1], purple = [75]:[1], blue = [100]:[1]). Starred peaks are assigned to residual MMs. Baselines are shifted for clarity. B) Plot of MW vs [M]/[I] ratio. The black line represents the theoretical MW for each [MM]/[G3].

Macromonomer concentration was shown to have a small but significant influence on the conversion to bottlebrush polymer (Table 7.2, entries 5, 8-9, Figure 7S13). Measured conversions

varied from 70% to 80% to 91% for the evaluated concentration range (25 mg/mL to 100 mg/mL), with increasing concentration resulting in higher conversion to BB.

It is important to note that MM conversion could not be increased beyond 91%, even under optimized conditions. Given the wealth of literature regarding the dependence of RAFT chain-end fidelity on a number of factors including [M]/[I] and [CTA]/[I] ratios,[49] it can be hypothesized that the observed conversion limit of 91% originates from the existence of "non-living" chains, or those that do not possesses a thiocarbonylthio group on the ω-chain end, in the MM samples. It has been shown that ca. 8% of polymer chains prepared by RAFT polymerization under similar conditions are of this "non-living" type.[54,62] Polymers of this "non-living" variety do not possess a norbornene on the chain end and thus will not polymerize during ROMP grafting-through.

7.5.5. Aminolysis of Bottlebrush Polymers.

The dithiocarbamate linkage is susceptible to reaction with nucleophiles such as amines.[38] Reaction of this functional group proceeds via an addition-elimination mechanism, resulting in detachment of polymeric side chains and their replacement by the nucleophile. The displaced side chains bear thiol groups at their ω-chain ends, which oxidize in air to form disulfide linkages between polymer chains.[38,63] Therefore, nucleophilic displacement initially yields a mixture of free side chains, side chain dimers, and the poly(norbornene) bottlebrush backbone. Over time, the remaining thiol-terminated polymers become quantitatively oxidized. Disulfide reduction is possible, but this process generally requires elevated temperatures and long reaction times.[64]

Scheme 7.5. Displacement of polymeric side chains by methylamine.

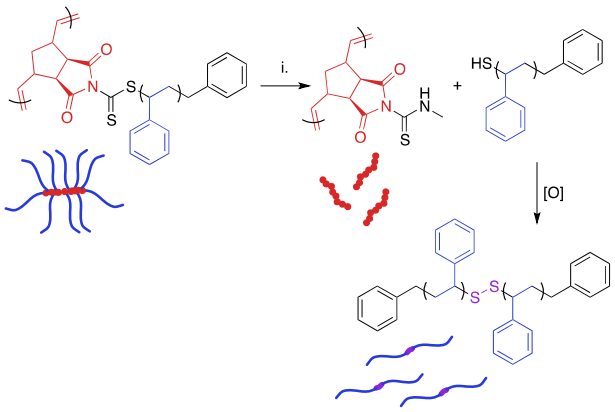

Experimental conditions: (i) CH_3NH_2, H_2O/THF.

Table 7.3. RAFT transfer-to mediated by PCTA1 and subsequent aminolysis.

polymerization time (h)	$M_{n,\,SEC}$ (kDa)[a]	$Đ$[a]	$M_{n,\,sidechains\,theo}$ (kDa)[b]	$M_{n,\,sidechains\,SEC}$ (kDa)[a]	$Đ$ Aminolysis[a]
0	25.1	1.02	---	---	---
19	356	1.01	4.7	19.5	1.15
42	737	1.01	9.9	35.5	1.21
67	1000	1.01	13.2	47.4	1.23
91	1250	1.01	16.5	56.9	1.28

[a]Measured by SEC using absolute MW by light scattering. [b]Determined using the formula: $M_{n,sidechains} = M_{n,\,BB}/DP_{MCTA1}$.

The presence of the dithiocarbamate moiety adjacent to the bottlebrush backbone allowed for the cleavage of the polystyrene side chains (Scheme 7.5). A series of bottlebrush polymers prepared by RAFT transfer-to were dissolved in THF and exposed to a 40% w/v solution of methylamine in H_2O for 72 h. The resulting mixture of backbone and dimerized side chain polymers was separated from residual reactants via precipitation. SEC analysis of the aminolyzed bottlebrush polymers showed a clean shift of the molecular weight distribution to a longer retention time, indicating that the side chains had been quantitatively cleaved (Figure 7S14). Interestingly, the

measured MWs of the dissociated side chains were higher than the expected values calculated by dividing the experimental BB MW by the DP of **PCTA1** (Table 3). We attribute this deviation to three independent phenomena. First, oxidation of ω-chain end thiols liberated during aminolysis resulted in disulfide bond formation, as has been previously reported.[63] This reaction doubles the observed molecular weight of the side chains. Second, increased steric crowding of the dithiocarbamate CTAs near the bottlebrush backbone by the attached polystyrene sidechains likely led to radical termination reactions between detached polymeric radicals during the transfer-to process, as has also been observed.[65,66] This side reaction not only yielded a significant amount of dead polymer, evident as a low MW peak in the SEC trace (Figure 7.3), but also likely resulted in lower than perfect grafting density and a higher than expected average side chain MW. Lastly, "dead" polymer arising during the RAFT polymerization is also incorporated into this sample. Although the concentration of "dead" polymer is surely eclipsed by the more abundant aminolyzed sidechains, these "dead" polymer chains could explain the observed broadening of the molecular weight distributions of the aminolyzed polymers relative to those of the bottlebrush polymers prior to aminolysis. While ultrahigh MW polymers can be obtained via RAFT transfer-to, the limitations of this methodology (i.e., limited control over grafting density) are made clear by this aminolysis experiment.

To further evaluate bottlebrush polymers prepared by the grafting-through approach, we subjected these polymers to aminolysis as well. ROMP of **MM$_{29}$** at a [MM]/[I] ratio of 50:1 was carried out to give a BB with degradable side chain linkages. A MW of 164 kDa was determined for the BB, with Đ = 1.07 (Figure 7.6). Aminolysis of the BB proceeded rapidly and quantitatively at rt in the presence of an excess of methylamine in THF/H_2O. SEC analysis of the precipitated reaction mixture revealed a narrow molecular weight distribution and a MW approximately double that of

the starting MM (5400 Da, Đ = 1.01), as expected for polystyrene side chain disulfide dimers. Quantitative aminolysis was confirmed by the complete disappearance of the bottlebrush peak in the SEC trace. Additionally, DLS analysis of the cleaved bottlebrushes exhibited a shift in the size of the macromolecules from 11.8 ± 3.1 nm for the BB to 2.6 ± 0.4 nm for the dissociated side chain dimers (original **MM$_{29}$** = 2.0 ± 0.5 nm) (Figure S15).

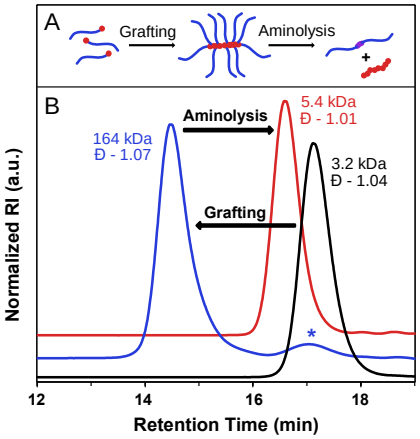

Figure 7.6. A) Graphical representation of grafting-through and aminolysis. B) BB synthesis by ROMP grafting-through (blue trace) from MM$_{29}$ (black trace) and subsequent aminolysis with methylamine (red trace). The starred peak corresponds to residual MM. Baselines are shifted for clarity.

7.6. Conclusions

A novel RAFT CTA with a directly polymerizable Z-group was prepared in a one-pot synthesis from an *exo*-norbornene imide. **CTA1**-mediated RAFT polymerizations of styrene and nBA were conducted successfully, yielding polymers of controllable MW and low dispersity bearing a polymerizable norbornene moiety on the ω-chain end. We demonstrated that **CTA1** could be utilized effectively for transfer-to and grafting-through methodologies, with the former resulting in high MW bottlebrush polymers (1250 kDa). Polystyrene MMs prepared using **CTA1** were polymerized by ROMP via a grafting-through strategy. In general, ROMP polymerization of **CTA1**-derived MMs proceeded efficiently when catalyzed by Grubbs' 3rd generation catalyst, with

conversions on the order of 70-90%. Macromonomer MW, concentration, and the [MM]/[catalyst] ratio of the polymerization were found to influence the conversion to BB. In general, an inverse relationship between MW of the MM and the conversion to BB was observed, with the smallest MM (3300 Da) resulting in the highest conversion. Increasing the MM concentration from 25 to 100 mg/mL also enhanced conversion, while increasing the [MM]/[**G3**] ratio from 25:1 to 100:1 resulted in decreased conversion and a broadening of the molecular weight distribution. Side chain scission via aminolysis was quantitative and revealed significant differences between the bottlebrush polymers prepared by the two different approaches. **CTA1** is unique in that it allows for the preparation of bottlebrush polymers utilizing functionality built into the chain-transfer agent. We expect **CTA1** will prove to be useful for the facile preparation of bottlebrush polymers possessing inherent side chain lability via the transfer-to or grafting-through approach.

7.7. References

(1) Sheiko, S. S.; Sumerlin, B. S.; Matyjaszewski, K. *Prog. Polym. Sci.* **2008**, *33*, 759.

(2) Grigoriadis, C.; Nese, A.; Matyjaszewski, K.; Pakula, T.; Butt, H.-J.; Floudas, G. *Macromol. Chem. Phys.* **2012**, *213*, 1311.

(3) Pietrasik, J.; Sumerlin, B. S.; Lee, H.-i.; Gil, R. R.; Matyjaszewski, K. *Polymer* **2007**, *48*, 496.

(4) Yuan, J.; Lu, Y.; Schacher, F.; Lunkenbein, T.; Weiss, S.; Schmalz, H.; Muller, A. H. E. *Chem. Mater.* **2009**, *21*, 4146.

(5) Bolton, J.; Rzayev, J. *ACS Macro Lett.* **2012**, *1*, 15.

(6) Pesek, S. L.; Li, X.; Hammouda, B.; Hong, K.; Verduzco, R. *Macromolecules* **2013**, *46*, 6998.

(7) Dalsin, S. J.; Hillmyer, M. A.; Bates, F. S. *ACS Macro Lett.* **2014**, *3*, 423.

(8) Wintermantel, M.; Gerle, M.; Fischer, K.; Schmidt, M.; Wataoka, I.; Urakawa, H.; Kajiwara, K.; Tsukahara, Y. *Macromolecules* **1996**, *29*, 978.

(9) Lee, H.-i.; Pietrasik, J.; Sheiko, S. S.; Matyjaszewski, K. *Prog. Polym. Sci.* **2010**, *35*, 24.

(10) Nese, A.; Li, Y.; Averick, S.; Kwak, Y.; Konkolewicz, D.; Sheiko, S. S.; Matyjaszewski, K. *ACS Macro Lett.* **2011**, *1*, 227.

(11) Li, Y.; Themistou, E.; Zou, J.; Das, B. P.; Tsianou, M.; Cheng, C. *ACS Macro Lett.* **2011**, *1*, 52.

(12) Matyjaszewski, K.; Tsarevsky, N. V. *Nat Chem* **2009**, *1*, 276.

(13) Johnson, J. A.; Lu, Y. Y.; Burts, A. O.; Lim, Y.-H.; Finn, M. G.; Koberstein, J. T.; Turro, N. J.; Tirrell, D. A.; Grubbs, R. H. *J. Am. Chem. Soc.* **2010**, *133*, 559.

(14) Sumerlin, B. S. *ACS Macro Lett.* **2011**, *1*, 141.

(15) Minko, S. In *Polymer Surfaces and Interfaces*; Stamm, M., Ed.; Springer Berlin Heidelberg: 2008, p 215.

(16) Bielawski, C. W.; Grubbs, R. H. *Angew. Chem.* **2000**, *112*, 3025.

(17) Hawker, C. J.; Mecerreyes, D.; Elce, E.; Dao, J.; Hedrick, J. L.; Barakat, I.; Dubois, P.; Jérôme, R.; Volksen, W. *Macromol. Chem. Phys.* **1997**, *198*, 155.

(18) Li, A.; Ma, J.; Sun, G.; Li, Z.; Cho, S.; Clark, C.; Wooley, K. L. *J. Polym. Sci., Part A: Polym. Chem.* **2012**, *50*, 1681.

(19) Li, Z.; Ma, J.; Cheng, C.; Zhang, K.; Wooley, K. L. *Macromolecules* **2010**, *43*, 1182.

(20) Masuda, E.; Kishiro, S.; Kitayama, T.; Hatada, K. *Polym J* **1991**, *23*, 847.

(21) Moughton, A. O.; Sagawa, T.; Gramlich, W. M.; Seo, M.; Lodge, T. P.; Hillmyer, M. A. *Polym. Chem.* **2013**, *4*, 166.

(22) Neugebauer, D.; Zhang, Y.; Pakula, T.; Sheiko, S. S.; Matyjaszewski, K. *Macromolecules* **2003**, *36*, 6746.

(23) Xia, Y.; Kornfield, J. A.; Grubbs, R. H. *Macromolecules* **2009**, *42*, 3761.

(24) Kim, K. O.; Choi, T.-L. *Macromolecules* **2013**, *46*, 5905.

(25) Kim, K. O.; Shin, S.; Kim, J.; Choi, T.-L. *Macromolecules* **2014**, *47*, 1351.

(26) Zou, J.; Jafr, G.; Themistou, E.; Yap, Y.; Wintrob, Z. A. P.; Alexandridis, P.; Ceacareanu, A. C.; Cheng, C. *Chem. Commun.* **2011**, *47*, 4493.

(27) Jha, S.; Dutta, S.; Bowden, N. B. *Macromolecules* **2004**, *37*, 4365.

(28) Engler, A. C.; Chan, J. M. W.; Fukushima, K.; Coady, D. J.; Yang, Y. Y.; Hedrick, J. L. *ACS Macro Lett.* **2013**, *2*, 332.

(29) Li, C.; Gunari, N.; Fischer, K.; Janshoff, A.; Schmidt, M. *Angew. Chem., Int. Ed.* **2004**, *43*, 1101.

(30) Nese, A.; Lebedeva, N. V.; Sherwood, G.; Averick, S.; Li, Y.; Gao, H.; Peteanu, L.; Sheiko, S. S.; Matyjaszewski, K. *Macromolecules* **2011**, *44*, 5905.

(31) Stenzel, M. H.; Zhang, L.; Huck, W. T. S. *Macromol. Rapid Commun.* **2006**, *27*, 1121.

(32) Moad, G.; Rizzardo, E.; Thang, S. H. *Polymer* **2008**, *49*, 1079.

(33) Tsujii, Y.; Ejaz, M.; Sato, K.; Goto, A.; Fukuda, T. *Macromolecules* **2001**, *34*, 8872.

(34) Stenzel, M. H.; Davis, T. P.; Fane, A. G. *J. Mater. Chem.* **2003**, *13*, 2090.

(35) Barner, L.; Davis, T. P.; Stenzel, M. H.; Barner-Kowollik, C. *Macromol. Rapid Commun.* **2007**, *28*, 539.

(36) Hernández-Guerrero, M.; Davis, T. P.; Barner-Kowollik, C.; Stenzel, M. H. *Eur. Polym. J.* **2005**, *41*, 2264.

(37) Barner-Kowollik, C.; Davis, T. P.; Heuts, J. P. A.; Stenzel, M. H.; Vana, P.; Whittaker, M. *J. Polym. Sci., Part A: Polym. Chem.* **2003**, *41*, 365.

(38) Willcock, H.; O'Reilly, R. K. *Polym. Chem.* **2010**, *1*, 149.

(39) Love, J. A.; Morgan, J. P.; Trnka, T. M.; Grubbs, R. H. *Angew. Chem., Int. Ed.* **2002**, *41*, 4035.

(40) Liu, J.; Gao, A. X.; Johnson, J. A. *J. Vis. Exp.* **2013**, e50874.

(41) Skey, J.; O'Reilly, R. K. *Chem. Commun.* **2008**, 4183.

(42) Azizi, N.; Aryanasab, F.; Saidi, M. R. *Org. Lett.* **2006**, *8*, 5275.

(43) Breugst, M.; Tokuyasu, T.; Mayr, H. *J. Org. Chem.* **2010**, *75*, 5250.

(44) Moad, G.; Rizzardo, E.; Thang, S. H. *Aust. J. Chem.* **2012**, *65*, 985.

(45) Moad, G.; Mayadunne Roshan, T. A.; Rizzardo, E.; Skidmore, M.; Thang San, H. In *Advances in Controlled/Living Radical Polymerization*; American Chemical Society: 2003; Vol. 854, p 520.

(46) Chiefari, J.; Chong, Y. K.; Ercole, F.; Krstina, J.; Jeffery, J.; Le, T. P. T.; Mayadunne, R. T. A.; Meijs, G. F.; Moad, C. L.; Moad, G.; Rizzardo, E.; Thang, S. H. *Macromolecules* **1998**, *31*, 5559.

(47) Moad, G.; Rizzardo, E.; Thang, S. H. *Aust. J. Chem.* **2006**, *59*, 669.

(48) Donovan, M. S.; Lowe, A. B.; Sumerlin, B. S.; McCormick, C. L. *Macromolecules* **2002**, *35*, 4123.

(49) Keddie, D. J. *Chem. Soc. Rev.* **2014**.

(50) Chiefari, J.; Chong, Y. K.; Ercole, F.; Krstina, J.; Jeffery, J.; Le, T. P. T.; Mayadunne, R. T. A.; Meijs, G. F.; Moad, C. L.; Moad, G.; Rizzardo, E.; Thang, S. H. *Macromolecules* **1998**, *31*, 5559.

(51) Mayadunne, R. T. A.; Rizzardo, E.; Chiefari, J.; Chong, Y. K.; Moad, G.; Thang, S. H. *Macromolecules* **1999**, *32*, 6977.

(52) Moad, G.; Chong, Y. K.; Postma, A.; Rizzardo, E.; Thang, S. H. *Polymer* **2005**, *46*, 8458.

(53) Zhou, D.; Zhu, X.; Zhu, J.; Yin, H. *J. Polym. Sci., Part A: Polym. Chem.* **2005**, *43*, 4849.

(54) Vandenbergh, J.; Junkers, T. *Macromolecules* **2014**.

(55) Keddie, D. J.; Moad, G.; Rizzardo, E.; Thang, S. H. *Macromolecules* **2012**, *45*, 5321.

(56) Dong, Z.-m.; Liu, X.-h.; Tang, X.-l.; Li, Y.-s. *Macromolecules* **2009**, *42*, 4596.

(57) Hilf, S.; Kilbinger, A. F. M. *Macromol. Rapid Commun.* **2007**, *28*, 1225.

(58) Beers, K. L.; Gaynor, S. G.; Matyjaszewski, K.; Sheiko, S. S.; Möller, M. *Macromolecules* **1998**, *31*, 9413.

(59) Chatterjee, A. K.; Choi, T.-L.; Sanders, D. P.; Grubbs, R. H. *J. Am. Chem. Soc.* **2003**, *125*, 11360.

(60) Crowe, W. E.; Mitchell, J. P.; Gibson, V. C.; Schrock, R. R. *Macromolecules* **1990**, *23*, 3534.

(61) Wagaman, M. W.; Grubbs, R. H. *Macromolecules* **1997**, *30*, 3978.

(62) Gody, G.; Maschmeyer, T.; Zetterlund, P. B.; Perrier, S. *Nat. Commun.* **2013**, *4*, 2505.

(63) Wang, Z.; He, J.; Tao, Y.; Yang, L.; Jiang, H.; Yang, Y. *Macromolecules* **2003**, *36*, 7446.

(64) Tsarevsky, N. V.; Matyjaszewski, K. *Macromolecules* **2005**, *38*, 3087.

(65) Zhao; Perrier, S. *Macromolecules* **2006**, *39*, 8603.

(66) Stenzel, M. H.; Davis, T. P. *J. Polym. Sci., Part A: Polym. Chem.* **2002**, *40*, 4498.

7.8. Appendix

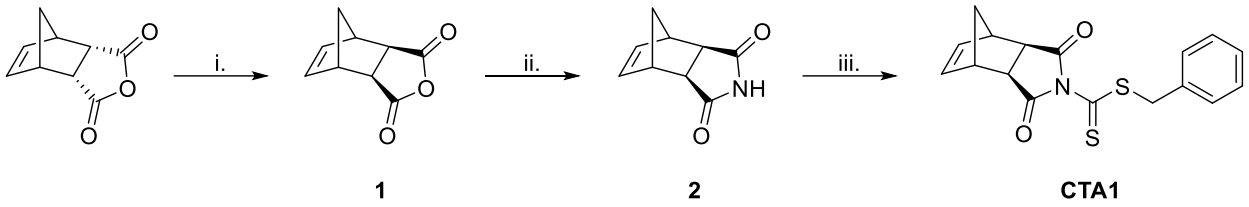

Scheme 7S1: Synthesis of CTA1. Experimental conditions: i. 1,2-dichlorobenzene at reflux; ii. urea, 135 °C; iii. KOH, CS_2, benzyl bromide, rt.

Synthesis of *cis*-5-norbornene-*exo*-2,3-dicarboxylic anhydride (1). A round-bottom flask was charged with *cis*-5-norbornene-*endo*-2,3-dicarboxylicanhydride (200 g). 200 mL 1,2-dicholorobenzene was added, a condenser was attached, and the reaction apparatus was immersed in an oil bath at 185 ºC for 2.5 h. Once cool, the flask was further cooled to 0 °C, and the precipitate was recovered by filtration and washed with hexanes. This crude product was recrystallized from benzene three times to yield 50.0 g pure *exo* product (25% yield). ^{1}H NMR ($CDCl_3$): δ 1.46 (d, 1H, *J* = 8 Hz), 1.66 (d, 1H, *J* = 8 Hz), 3.00 (s, 2H), 3.45 (s, 2H), 6.33 (s, 2H). ^{13}C NMR ($CDCl_3$): δ 171.69, 138.09, 48.90, 47.02, 44.26. HRMS: calculated 165.0552, found 165.0536 $[M+H]^+$.

Synthesis of *exo*-norbornene imide (2). A 100 mL round bottom flask was charged with **(1)** (4.02 g, 24.5 mmol) and urea (1.61 g, 26.8 mmol). The flask was fitted with a condenser. The reaction was conducted in the melt at 140 ˚C for 30 min. The reaction mixture was allowed to cool to rt. The crude product was purified by recrystallization from H_2O. The resulting white crystals were recovered via vacuum filtration and were dried under vacuum overnight to yield 2.84 g of pure product (71% yield). ^{1}H NMR ($CDCl_3$): δ 1.43 (d, 1H, J = 8 Hz), 1.51 (d, 1H, J = 8 Hz), 2.69 (s, 2H), 3.24 (s, 2H), 6.24 (s, 2H), 9.20 (bs, 1H). ^{13}C NMR ($CDCl_3$): δ 178.98, 137.80, 49.26, 45.16, 42.95. HRMS: calculated 162.0555, found 162.0546 $[M-H]^-$.

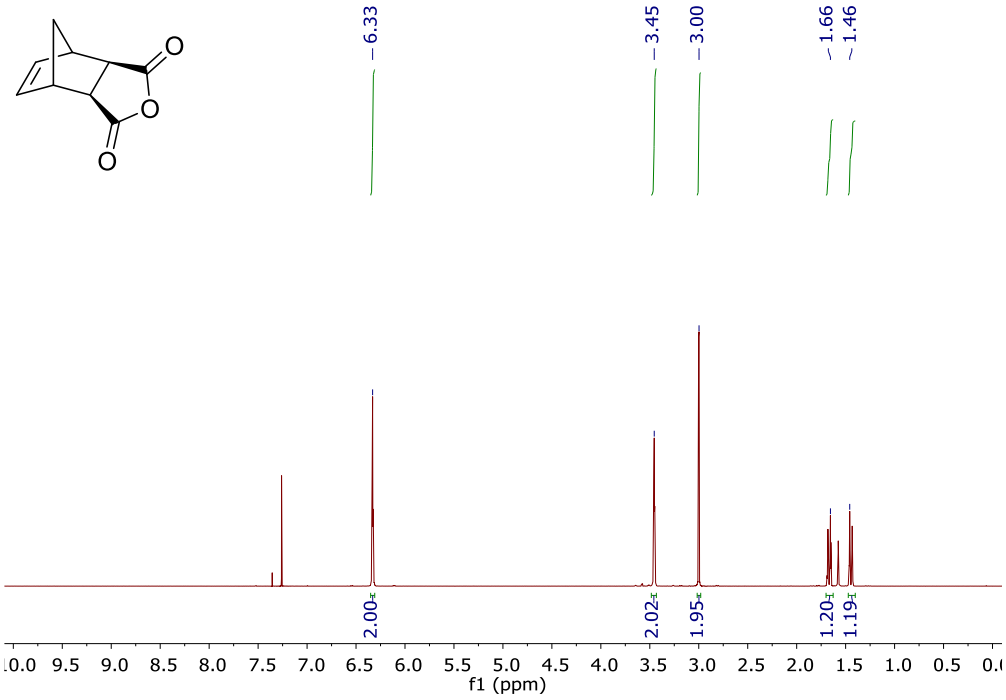

Figure 7S1: ^{1}H NMR of (1)

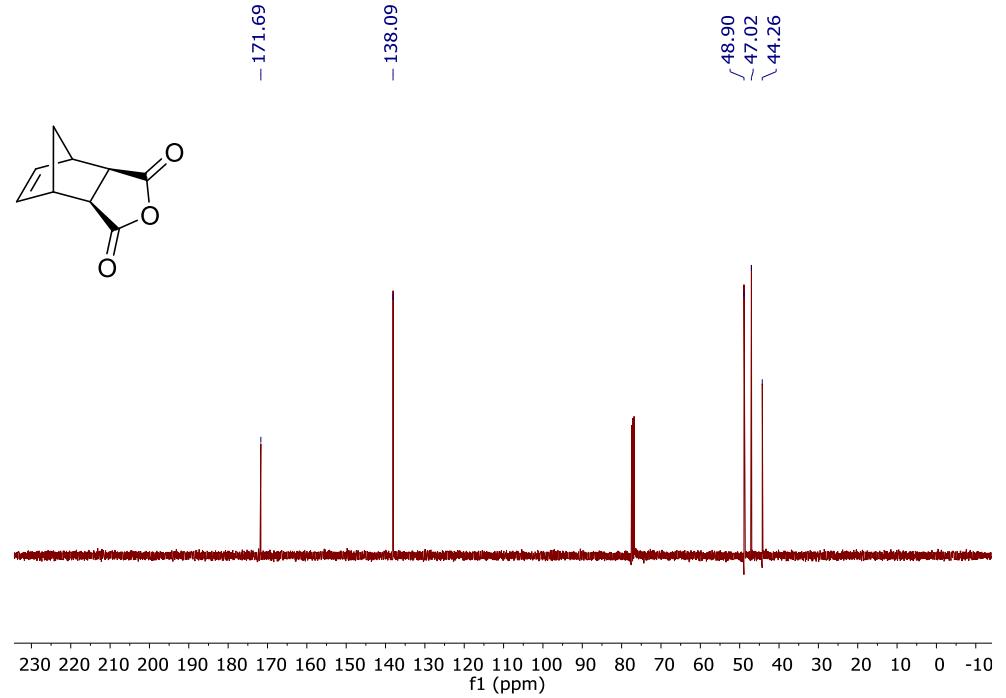

Figure 7S2: ^{13}C NMR of (1)

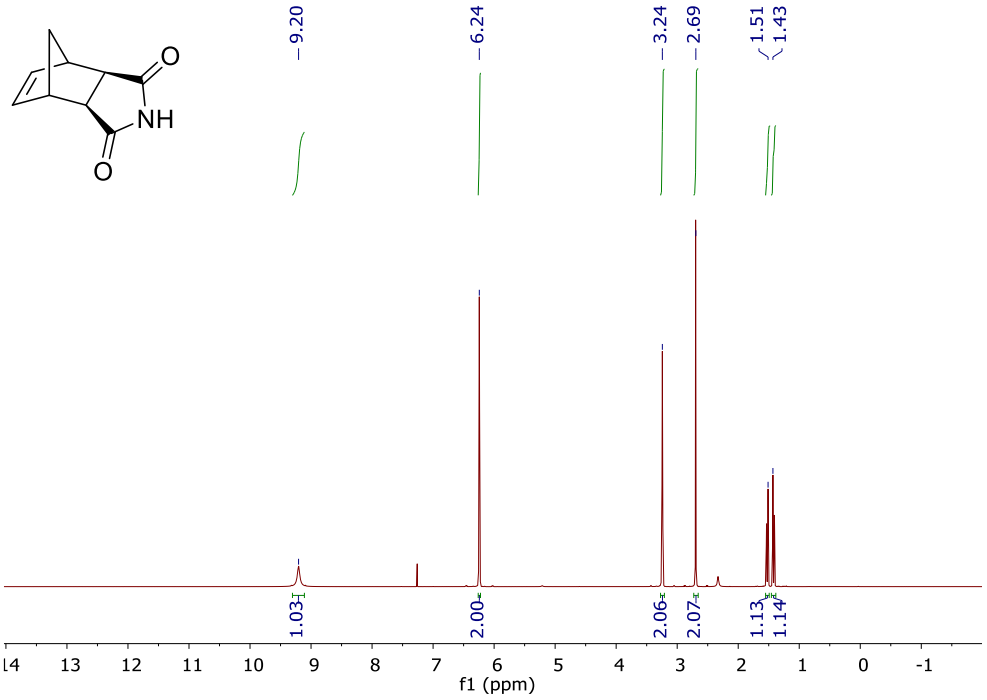

Figure 7S3: ^{1}H NMR of (2)

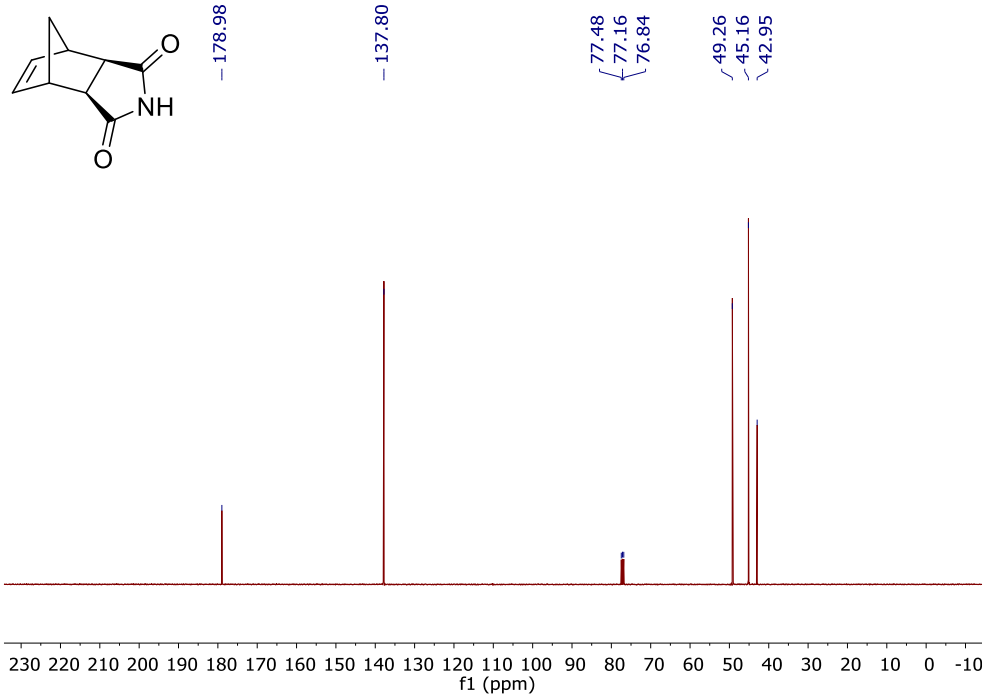

Figure 7S4: ^{13}C NMR of (2)

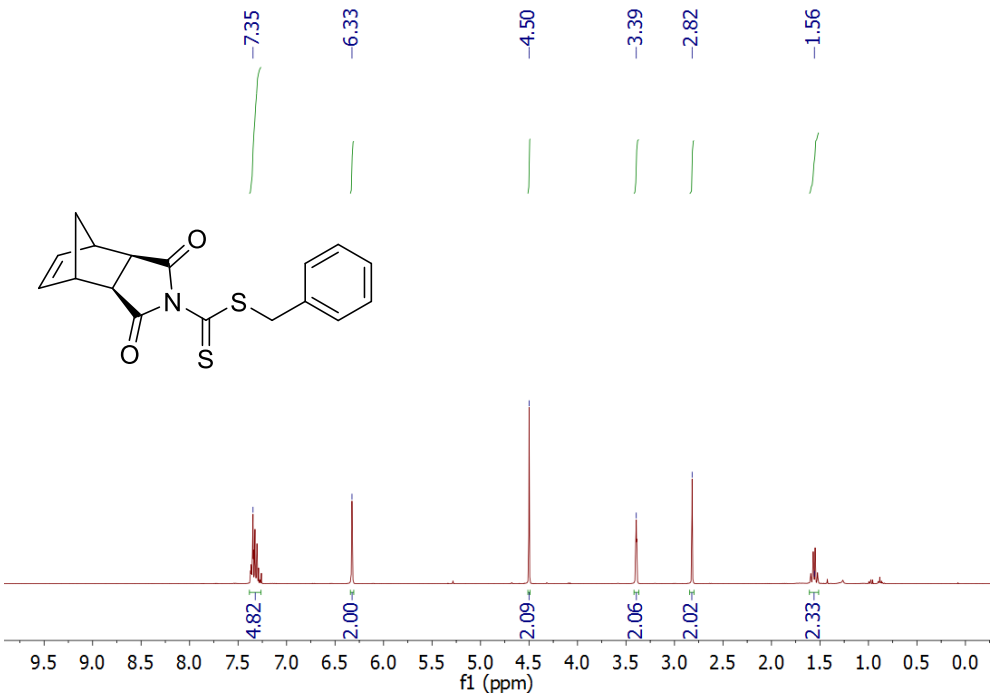

Figure 7S5: ^{1}H NMR of CTA1

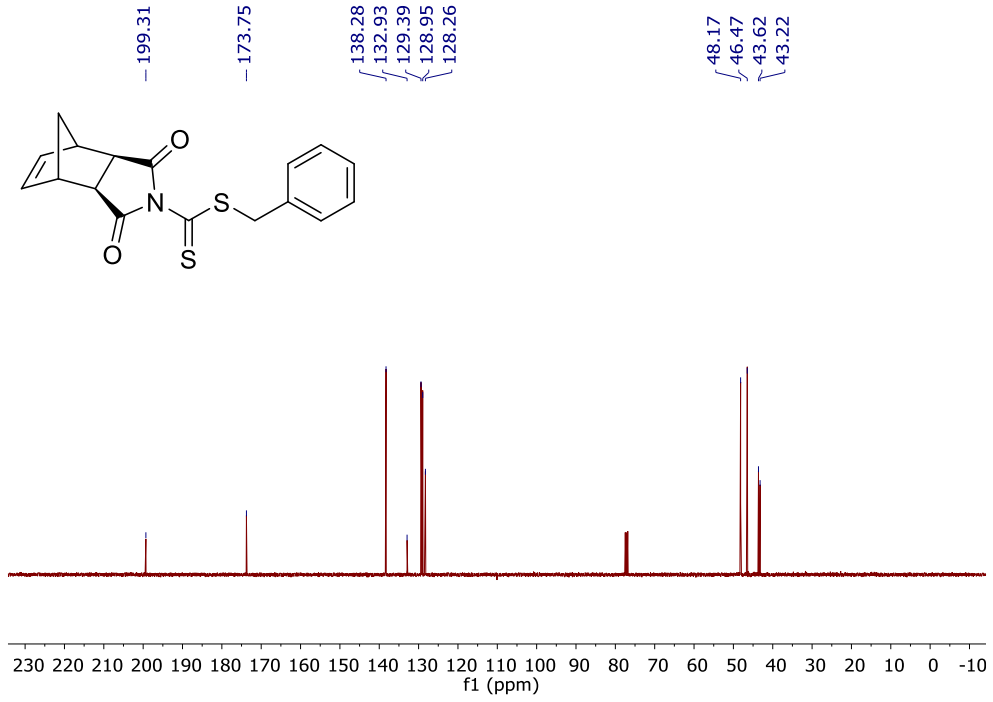

Figure 7S6: ^{13}C NMR of CTA1

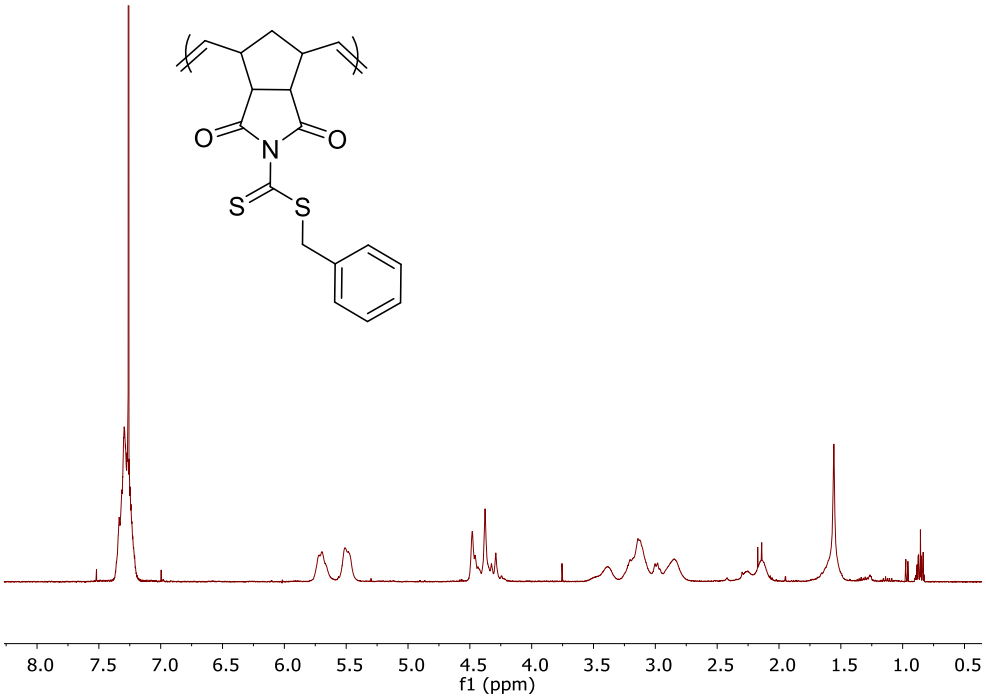

Figure 7S7: ^{1}H NMR of poly(CTA1)

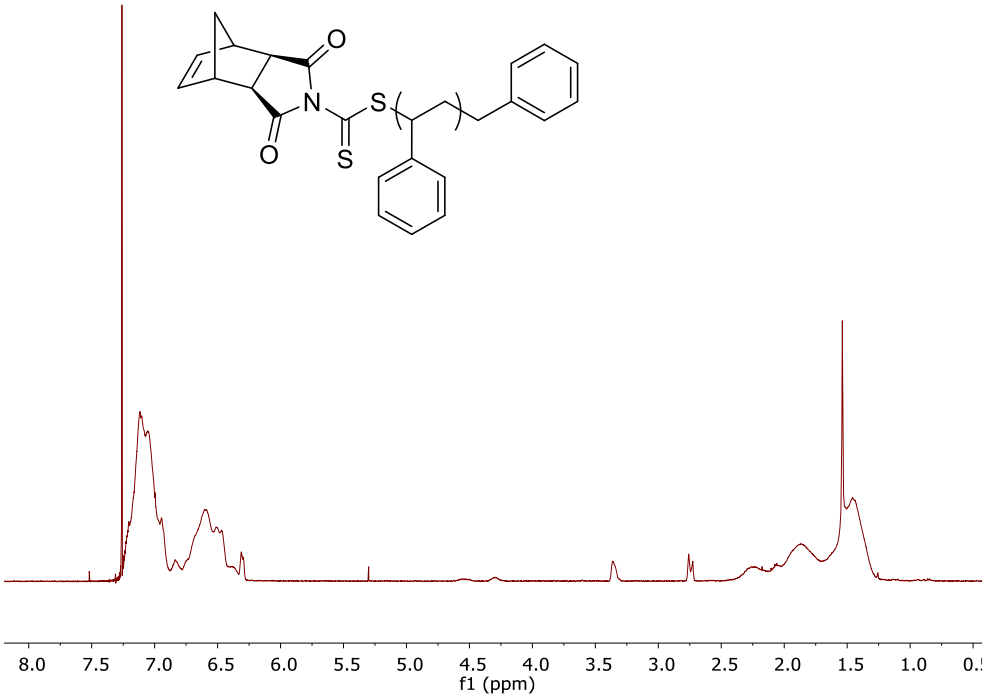

Figure 7S8: ^{1}H NMR of MM_{29}

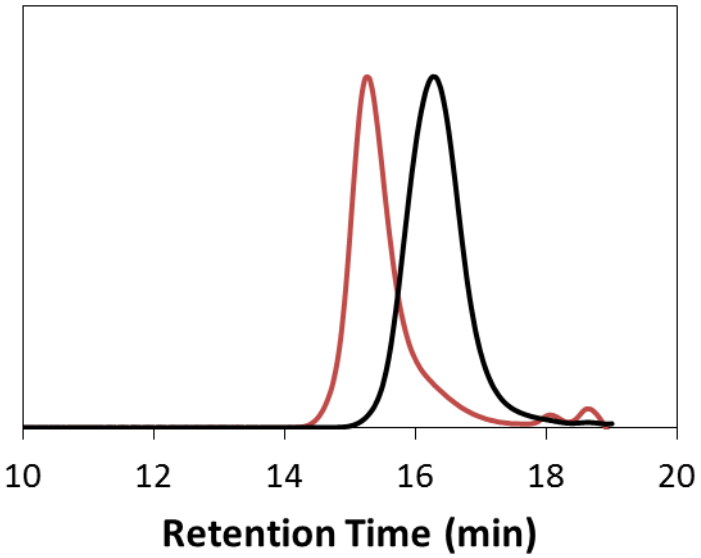

Figure 7S9: SEC traces of the RAFT chain extension with a PnBA Macro CTA (black line) with styrene to form a diblock copolymer (red line).

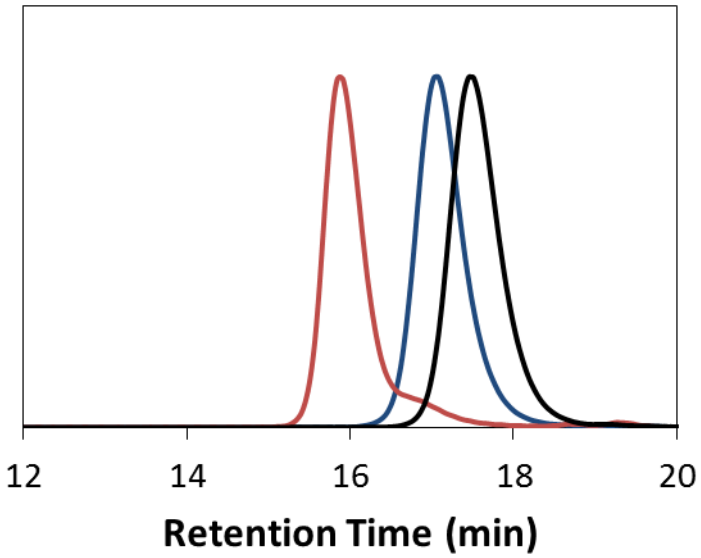

Figure 7S10: SEC traces of MM_{29} (black line), MM_{52} (blue line), and MM_{113} (red line).

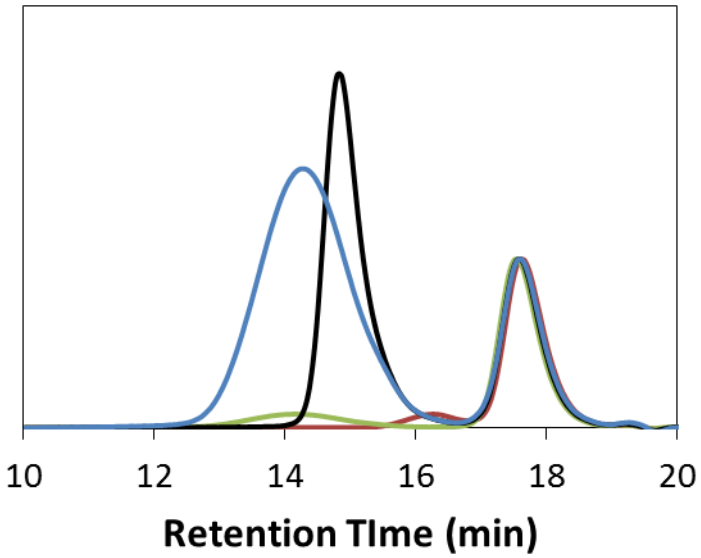

Figure 7S11: SEC traces of bottlebrush polymers prepared via grafting-through from MM_{29} using G1 (red line), G2 (green line), G3 (black line), and HG2 (blue line). Traces normalized to macromonomer peak height.

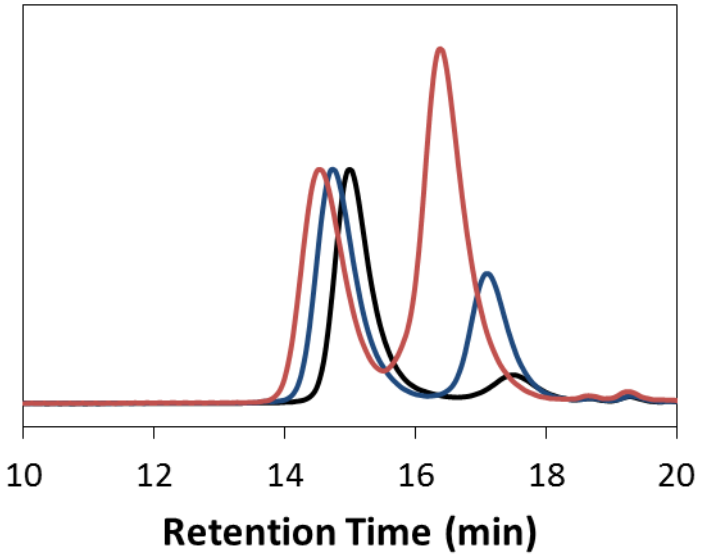

Figure 7S12: SEC traces of bottlebrush polymers prepared via grafting-through from MM_{29} (black line), MM_{52} (blue line), and MM_{113} (red line) using G3. Traces normalized to bottlebrush polymer peak height.

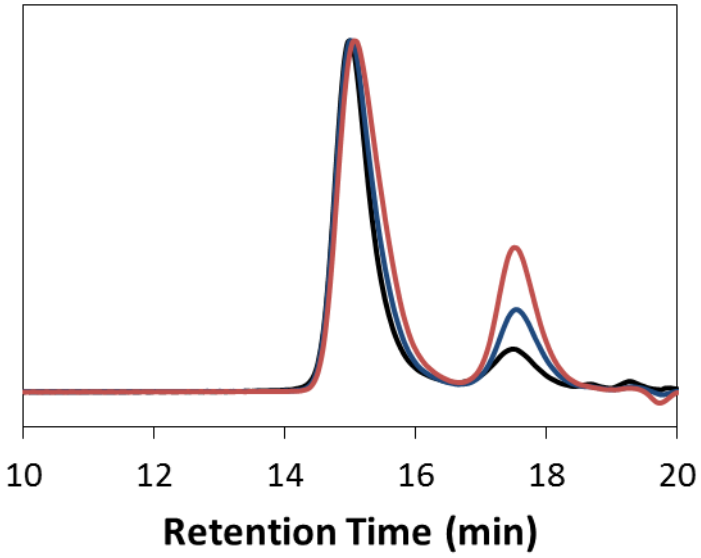

Figure 7S13: SEC traces of bottlebrush polymers prepared via grafting-through from MM_{29} at 100 mg/ml (black line), 50 mg/ml (blue line), and 25 mg/ml (red line). Traces normalized to bottlebrush polymer peak height.

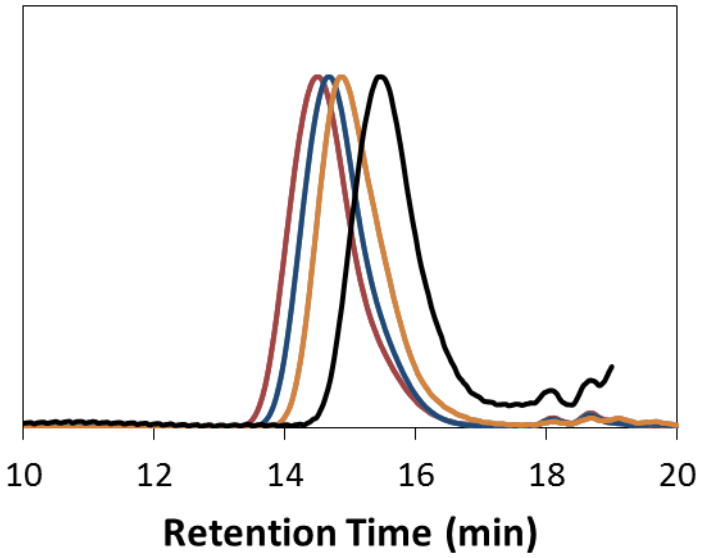

Figure 7S14: SEC traces of side chains aminolyzed from bottlebrush polymers prepared by transfer-to after 19 h (black line), 42 h (orange line), 67 h (blue line), and 91 h (red line).

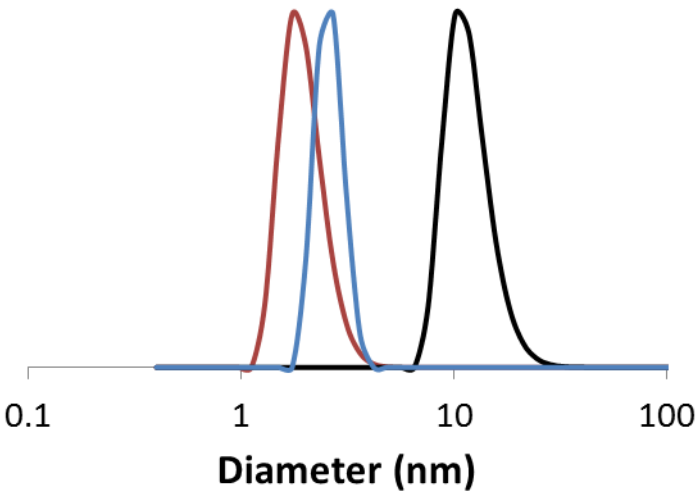

Figure 7S15: DLS traces of MM_{29} (red line), BB from MM_{29} (black line), and aminolysis product from the BB (blue line).

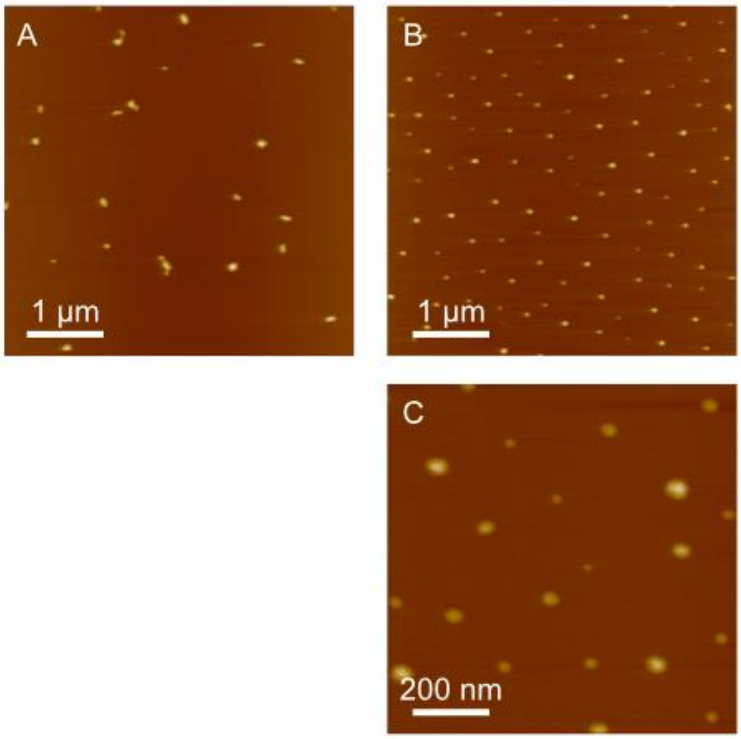

Figure 7S16: AFM height images of BB prepared from (A) transfer-to using poly(CTA1), (B) and (C) grafting-through using MM_{29} (Table 2 entry 5).

Chapter 8. Norbornene-Containing Dithiocarbamates for use in Reversible Addition–Fragmentation Chain Transfer (RAFT) Polymerization and Ring-Opening Metathesis Polymerization (ROMP)

8.1. Authors

Jeffrey C. Foster,[‡] Scott C. Radzinski,[‡] Sally E. Lewis, Matthew B. Slutzker, and John B. Matson[*]

*Department of Chemistry and Macromolecules and Interfaces Institute, Virginia Tech, Blacksburg, Virginia 24061, United States.

[‡]These authors contributed equally to this work.

8.2. Keywords

RAFT polymerization, graft polymer, poly(vinyl acetate)

8.3. Abstract

Two new dithiocarbamate chain transfer agents (CTAs) with norbornene-containing Z-groups were prepared for use in reversible addition–fragmentation chain transfer (RAFT) polymerization. CTA **1b**, which contains an electron deficient norbornene imide Z-group, was found to effectively mediate RAFT polymerization of 2° more activated monomers (MAMs) but did not facilitate RAFT of 3° MAMs or less activated monomers (LAMs). In contrast, CTA **2**, derived from a norbornene amine, was well suited for the polymerization of LAMs, but did not control RAFT of MAMs. Poly(vinyl acetate) (PVAc), prepared by RAFT polymerization mediated by CTA **2,** possessed the expected CTA-derived α- and ω-end groups. Ring-opening metathesis

polymerization (ROMP) of **2** was carried out, and full conversion to polymer was achieved within 20 min. Based on this result, ROMP grafting-through of a PVAc macromonomer derived from CTA **2** was carried out, resulting in the formation of a well-defined PVAc bottlebrush polymer with a narrow molecular weight distribution.

8.4. Introduction

Reversible deactivation radical polymerization (RDRP) techniques are versatile tools for the preparation of a variety of polymers with controlled molecular weights (MWs), narrow and symmetrical molecular weight distributions, and well-defined macromolecular architectures.[1-3] Examples of RDRPs include atom transfer radical polymerization (ATRP),[4,5] nitroxide-mediated radical polymerization (NMRP),[6] single electron transfer polymerization (SET-LRP),[7] and reversible addition–fragmentation chain transfer polymerization (RAFT).[8] In recent years, RAFT polymerization has been utilized extensively due its applicability to a wide range of monomers and reaction conditions. RAFT polymerization has been employed to functionalize biomolecules with stabilizing polymers,[9-12] mediate the formation of complex morphologies in suspension polymerizations,[13-16] prepare multiblock polymers containing up to 20 blocks,[17] and prepare advanced drug-releasing scaffolds,[18-21] among many other diverse applications.[22] RAFT polymerization has also been used to prepare macromonomers for use in bottlebrush synthesis,[23-25] a topic of interest to our group and others.

RAFT polymerization relies on reversible deactivation of the propagating or "active" radical species by a thiocarbonyl-thio-containing chain transfer agent (CTA).[26] Tremendous effort over the past two decades has been dedicated toward the design and synthesis of RAFT CTAs to improve their selectivity towards certain monomer types, to diversify the routes of their synthesis, to achieve specific built-in functionality that can be utilized in downstream processes, and to

realize new classes of CTAs capable of mediating the polymerization of monomers across the radical stability spectrum (e.g., universal or switchable CTAs).[27] The structure of the dithio compound [Z-C(S)-S-R] determines the types of monomers that can be polymerized by a given CTA. Specifically, the Z-group modulates the reactivity of the thiocarbonyl bond toward radicals, with more stable monomer radicals requiring more electron withdrawing Z-groups, in general.[28] The relative radical stability of the leaving R-group determines the partition coefficient for the monomer/CTA pair.[29] The partition coefficient is a term that describes the propensity of the CTA R-group to fragment with respect to the polymer radical. If the difference in relative radical stability between the R-group-derived radical and the polymer-derived radical is large, the polymerization can be either uncontrolled (if the polymer-derived radical is more stable) or inhibited (if the fragmented R-group radical is more stable). The rational selection of R and Z-groups allows chemists to design CTAs that mediate polymerization of a wide variety of monomer types.

Structural variation among RAFT CTAs allows for modulation of reactivity towards certain monomers as well as for tuning of non-RAFT specific parameters such as solubility, stability/lability (useful for aminolysis, as an example), and built-in functionality. Dithiobenzoate, trithiocarbonate, xanthate, and dithiocarbamate CTAs have been prepared from aryl Gringard, thiol, alcohol, and amine starting materials, respectively.[26,30,31] In the case of dithiocarbamate CTAs, the electron withdrawing ability of the nitrogen atom plays a critical role in the reactivity of the resulting CTA. More electron-deficient Z-groups such as those derived from amides, pyrrole, or imidazole effectively mediate the polymerization of the broad class of more-activated monomers (MAMs), while electron donating Z-groups allow for polymerization of less-activated monomers (LAMs).[32] We recently reported on the synthesis of a norbornene-imide-derived

dithiocarbamate CTA with a benzyl R-group (CTA **1a**, Figure 8.1).[33] This novel dithio compound was shown to effectively mediate the polymerization of styrene and *n*-butyl acrylate. In addition, the norbornene-containing Z-group was readily polymerized in the presence of a Ru-based metathesis catalyst, undergoing ring-opening metathesis polymerization (ROMP) to form a poly(CTA) with pendant chain transfer functionality on each repeat unit. This poly(CTA) was utilized subsequently in RAFT transfer-to polymerization to produce monodisperse bottlebrush polymers with molecular weights (MWs) in excess of 1 MDa. CTA **1a** was also utilized to prepare macromonomers for use in bottlebrush synthesis by the grafting-through approach.

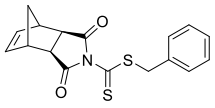

1a

Figure 8.1. CTA evaluated in our previous work.[33]

The norbornene-derived CTA previously reported by our group was incapable of mediating RAFT polymerization of the 3° MAM methyl methacrylate (MMA) or the LAM vinyl acetate (VAc). RAFT polymerization of 3° MAMs such as MMA requires a CTA with a deactivated, 3° R-group such as $–C(CH_3)_2CN$. Therefore, the poor control over the polymerization of MMA was attributed to the low partition coefficient of the benzyl R-group with respect to MMA. Polymerization of VAc in the presence of **1a** was completely inhibited, with no polymer product detected even after 48 h. Here, it was speculated that the electron withdrawing norbornene imide (**NI**) Z-group renders the C=S bond of the CTA derivative unreactive towards LAM radicals. To expand the scope of monomers that could be polymerized by norbornene-based CTAs, we sought to prepare new dithio compounds with different R- and Z-groups.

Based on our previous work, we hypothesized that replacing the benzyl R-group of **1a** with an R-group more suitable for the polymerization of MMA would yield a CTA suitable for mediating

RAFT polymerization of methacrylate and methacrylamide monomers while still utilizing the ROMP-active norbornene-containing Z-group. We also envisioned a norbornene-derived CTA with a less active Z-group and a less stable homolytic leaving group (i.e., R = $–CH_2CN$) might facilitate the RAFT polymerization of LAMs such as VAc. In this contribution, we describe the synthesis and characterization of new dithiocarbamate CTAs with norbornene-containing Z-groups. In addition, we evaluate the ability of these novel CTAs to mediate RAFT polymerization of 5 different monomers—MMA, styrene, acryloylmorpholine (ACMO), methyl acrylate (MA), and VAc—encompassing common monomer types from 3° MAMs, 2° MAMs, and LAMs.

8.5. Materials and Methods

Materials

All reagents were obtained from commercial vendors and used as received unless otherwise stated. MMA, styrene, ACMO, MA, and VAc were passed through small columns of basic alumina prior to use. 2,2′-Azobis(2-methylpropionitrile) (AIBN) and 1,1′-azobis(cyclohexanecarbonitrile) (ACHN) were recrystallized from methanol prior to use. ROMP catalyst $(H_2IMes)(Cl)_2(PCy_3)Ru{=}CHPh$ (**G2**) was obtained as a generous gift from Materia. ROMP catalyst $(H_2IMes)(pyr)_2(Cl)_2Ru{=}CHPh$ (**G3**) was prepared from **G2** according to literature procedures.[34,35] exo-Norbornene imide (**NI**) was prepared according to a previous report.[33]

Methods

NMR spectra were measured on Agilent 400 MHz or Bruker 500 MHz spectrometers. ^1H and ^{13}C NMR chemical shifts are reported in ppm relative to internal solvent resonances. Yields refer to chromatographically and spectroscopically pure compounds unless otherwise stated. Size exclusion chromatography (SEC) was carried out in THF on two Agilent PLgel 10 μm MIXED-B

columns connected in series with a Wyatt Dawn Helios 2 light scattering detector and a Wyatt Optilab Rex refractive index detector. No calibration standards were used, and dn/dc values were obtained by assuming 100% mass elution from the columns. High-resolution mass spectra were taken on an Agilent Technologies 6230 TOF LC/MS mass spectrometer. UV-Vis absorbance spectra were recorded on a Cary 5000 UV-Vis (Agilent) from 550 to 300 nm.

Synthesis of CTA 1b

KOH (0.360 g, 6.43 mmol) was ground to a fine powder with a mortar and pestle and placed in a 100 mL round bottom flask. To the flask was added **NI** (1.00 g, 6.13 mmol) followed by 15 mL of DMF. This mixture was stirred for 5 min, followed by dropwise addition of CS_2 (1.11 mL, 18.4 mmol). The solution developed a deep red color. After an additional 3 h of stirring, (1-bromoethyl)benzene (1.67 mL, 12.3 mmol) was added dropwise, and the reaction mixture was stirred at rt for 12 h. The reaction mixture was then diluted with CH_2Cl_2 (50 mL) and washed with H_2O (3 × 150 mL) and brine. The organic layer was dried over Na_2SO_4, and the solvent was removed by rotary evaporation. The crude product was purified on a silica gel column, eluting with 1:1 CH_2Cl_2/hexanes, to give 0.59 g of **1b** as a yellow solid (28% yield, 8:2 mixture of *S*- and *N*-alkylated products that could not be separated via column chromatography). ^{1}H NMR ($CDCl_3$): δ 7.5-7.2 (m, 5H), 6.32 (t, 2H), 4.96 (q, 1H), 3.38 (s, 2H), 2.79 (s, 2H), 1.81 (d, 3H), 1.57 (m, 2H). ^{13}C NMR ($CDCl_3$) δ 198.63, 173.76, 139.61, 138.32, 128.93, 128.24, 127.90, 52.30, 48.20, 46.49, 43.24, 20.46. HRMS (m/z): calculated 344.0773, found 344.0757.

Synthesis of Reduced Imide CTA 2

A 3-necked round bottom flask was charged with $LiAlH_4$ (2.09 g, 55.2 mmol). The flask was placed in an ice bath. To the flask was slowly added 30 mL of dry THF under N_2 atmosphere. **NI**

(3.00 g, 18.4 mmol) was dissolved in 70 mL of dry THF in a second flask. The imide solution was transferred to an addition funnel and was added dropwise to the $LiAlH_4$ slurry. After the addition was complete, the reaction mixture was allowed to warm to rt and then was heated at reflux for 12 h. To quench the reaction, the reaction mixture was placed in an ice bath, and 2 mL of H_2O was added slowly, followed by 2 mL NaOH solution (10% w/v in water) and then 6 mL H_2O. Upon warming to rt the solids became white. The quenched reaction mixture was diluted with diethyl ether (~200 mL) and filtered through celite. This solution was concentrated and washed with brine, dried over Na_2SO_4, and rotovapped. The resulting yellow oil norbornene amine (**NA**) was used in the next step without further purification.

NA was dissolved in 15 mL of EtOH in a round bottom flask. The flask was placed in an ice bath. To the flask was added CS_2 (1.23 mL, 20.3 mmol) followed by dropwise addition of 2.3 mL of 50 % wt/v aqueous KOH (1.1 equiv). The reaction mixture was allowed to warm to room temperature and was stirred for 12 h. The reaction mixture was then diluted with MeOH (~40 mL), dried over Na_2SO_4, and rotovapped. The residue was used in the next step without further purification.

The crude dithiocarbamate salt was dissolved in 40 mL of acetone in a round bottom flask. The flask was placed in an ice bath. To the flask was added bromoacetonitrile (1.40 mL, 20.1 mmol) dropwise. The reaction mixture was allowed to warm to room temperature and was stirred for 12 h. The reaction mixture was then rotovapped and the residue was dissolved in CH_2Cl_2. The CH_2Cl_2 solution was washed with H_2O and brine, dried over Na_2SO_4, and rotovapped. The crude product was purified on a silica gel column, eluting with 2:3 CH_2Cl_2/hexanes to give the pure product (**2**) as an off white powder (2.80 g, 61% yield). ^{1}H NMR ($CDCl_3$): δ 6.13 (q, 2H), 4.19 (s, 2H), 4.06 (m, 1H), 3.76 (m, 2H), 3.40 (m, 1H), 2.74 (d, 2H), 2.44 (m, 2H), 1.46 (d, 1H), 1.32 (d,

1H). ^{13}C NMR ($CDCl_3$): δ 187.20, 137.79, 137.20, 116.11, 60.41, 54.98, 47.69, 47.62, 45.36, 42.86, 42.20, 22.29. HRMS (m/z): calculated 251.0671, found 251.0671.

Representative RAFT Polymerization Procedure

A typical polymerization procedure is as follows: To an oven-dried Schlenk tube equipped with a magnetic stir bar was added CTA, azo initiator, monomer, and solvent (if applicable). The tube was deoxygenated by subjecting the contents to three freeze−pump−thaw cycles. The Schlenk tube was then backfilled with N_2 and submerged in an oil bath maintained at the appropriate temperature. Samples were removed periodically by N_2-purged syringe to monitor molecular weight evolution by SEC and conversion by ^1H NMR spectroscopy.

Synthesis of poly(2)

CTA **2** (50 mg) was dissolved in 1.5 mL of dry CH_2Cl_2 in a vial equipped with a stir bar. A 5.8 mg/mL solution of **G3** was prepared in a second vial by dissolving an amount of **G3** in dry CH_2Cl_2. 0.5 mL of this **G3** solution was added rapidly to the first vial. After 20 min, a few drops of ethyl vinyl ether were added to terminate the polymerization, and the reaction mixture was stirred for an additional 5 min. The polymer was isolated via precipitation from hexanes.

Synthesis of PVAc Bottlebrush

Macromonomer **NA-PVAc** (40 mg) was dissolved in 0.3 mL of dry CH_2Cl_2 in a vial equipped with a stir bar. A 2.3 mg/mL solution of **G3** was prepared in a second vial by dissolving an amount of **G3** in dry CH_2Cl_2. 0.1 mL of of this **G3** solution was added rapidly to the first vial. After 60 min, a few drops of ethyl vinyl ether were added to terminate the polymerization, and the reaction mixture was stirred for an additional 5 min. The polymer was isolated via precipitation from diethyl ether.

8.6. Results and Discussion

8.6.1. R-Group Modification

To prepare **NI**-derived CTAs with various R-groups, we initially adopted a strategy that involved the *in situ* generation of a norbornene-imide dithiocarbamate intermediate that could be transformed into the desired CTA via addition of the appropriate alkyl-halide, as shown in Scheme 8.1. Similar to our previous report in which we obtained **1a** in moderate yields (30-40%) using a facile 1-pot procedure,[33] we attempted to synthesize additional norbornene-containing dithiocarbamates (**1a**-**1f**) by first dissolving the nucleophilic exo-norbornene imide (**NI**) in DMF, adding finely ground potassium hydroxide followed by dropwise addition of carbon disulfide (CS_2). Finally, the appropriate alkyl halide was added after a period of 1-2 h to form the desired product, which we would attempt to isolate using standard aqueous workup and/or column chromatography. Benzyl bromide (Table 8.1, entry **a**), (1-bromoethyl)benzene (**b**), *N*-(chloromethyl)phthalimide (**c**), 2-bromo-2-methylpropionic acid (**d**), ethyl α-bromoisobutyrate (**e**), or 2-bromopropionic acid (**f**), was utilized to attempt to alkylate the intermediate in the final step. Of these, only **a** and **b** were found to yield the desired product in an appreciable quantity (see Table 8.1). Starting materials or *N*-alkylated byproducts were recovered from reactions with the other alkylating agents.

Scheme 8.1. Preparation of dithiocarbamate CTAs from NI.

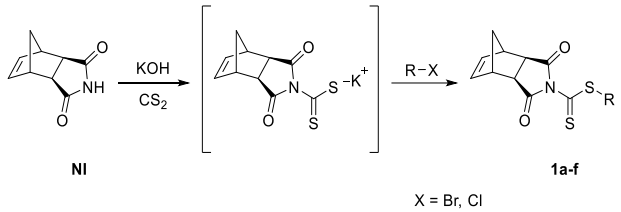

Table 8.1. Isolated yields from alkylation of NI-derived dithiocarbamate intermediate using various alkylating agents.

Entry	Alkylating Agent	Product	Isolated Yield
a	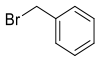	1a	40 %
b	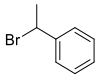	1b	28 %
c	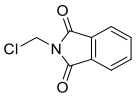	1c	< 1 %
d	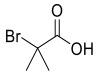	1d	--[a]
e	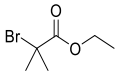	1e	--[a]
f	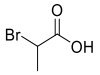	1f	--[a]

[a]Compounds not isolated from reaction mixtures.

To explain these results, a product analysis of the synthesis of **1a** was performed. ^{1}H NMR spectroscopy of a mixture of **NI**, KOH, and CS_2 that had been allowed to react in DMSO-d_6 revealed an important insight: the equilibrium between the deprotonated imide and the dithiocarbamate intermediate depicted in Scheme 8.1 is strongly biased in favor of the reactants (K_{eq} = 0.024 by relative integration). We attribute this observation to both the poor nucleophilicity of the **NI** nitrogen and the instability of the dithiocarbamate salt, which may decompose via a zwitterionic intermediate formed through protonation of the N atom in a similar manner to related compounds.[36] After 2 h benzyl bromide was added, and the composition of the reaction mixture was re-evaluated after 12 h by ^{1}H NMR spectroscopy. By comparing integrations of the various benzyl methylene resonances, and knowing the identity of each of these species by matching against pure spectra of molecules isolated from the crude reaction mixture, it was determined that the *N*-alkylated norbornene imide was in fact the major product, with the desired dithiocarbamate

(CTA **1a**) and a trithiocarbamate byproduct forming to a lesser extent (Scheme 8.2). Increasing the equivalents of CS_2 to attempt to drive the equilibrium toward the product had a negligible effect on the isolated yield.

Scheme 8.2. Product analysis of synthesis of CTA 1a.

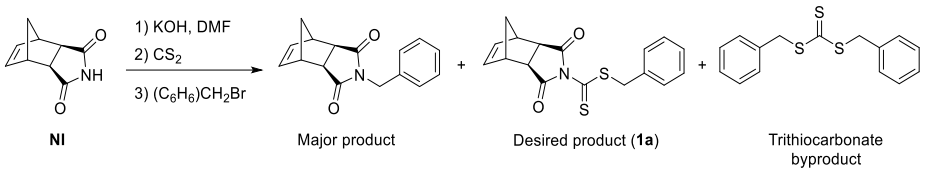

Given this analysis, it is not surprising that alkylating agents with carboxylic acid functionalities (**d** and **f**) could not be employed to synthesize dithiocarbamate CTAs with the **NI** Z-group. Alkylation using ethyl α-bromoisobutyrate (**e**, the ethyl ester of **c**) also proved fruitless, likely due to the fact that S_N2 at the α-carbon is sterically hindered and S_N1 using this particular alkyl bromide is unlikely due to the destabilization of the carbocation adjacent to the electron-withdrawing carbethoxy group. Neutralization of **d** with triethylamine prior to alkylation was also attempted without success. Based on these observations, we speculate that the structures of CTAs with the norbornene imide Z-group may be limited to those prepared using alkylating agents that are sterically unhindered and do not contain acidic functionalities that may catalyze CTA decomposition (e.g., **a** or **b**). These limitations are at odds with the structural requirements of a good R-group for 3° MAMs.

We previously reported on the successful RAFT polymerization of styrene and *n*-butyl acrylate (2° MAMs) mediated by CTA **1a**. We therefore expected that CTA **1b** would effectively mediate RAFT polymerization of styrene, MA, and ACMO (2° MAMs). The polymerizations were carried out in THF at 50 v/v% at 60 ˚C for MA and ACMO and at 75 ˚C for styrene in the presence of 2,2′-azobis(2-methylpropionitrile) (AIBN) to provide initiating radicals by thermal decomposition.

For each monomer type a [M] / [**1b**] / [AIBN] ratio of 100 : 1 : 0.1 was employed. Table 8.2 summarizes a series of polymers prepared by RAFT polymerization using CTA **1b**. In general, the polymers possessed low dispersities and MWs that were close to expected values. Kinetic analysis of these polymerizations revealed propagation rate profiles that were first order in monomer consumption (Figure 8.2A). As shown in Figure 8.2B, plots of number average molecular weight (M_n) (determined by size exclusion chromatography (SEC)) vs. conversion were linear, indicating well controlled polymerizations. SEC traces of aliquots taken at specific timepoints during kinetic analysis were generally narrow and monomodal (as in Figure 8.3). In general, polymerizations using CTA **1b** progressed more rapidly than those previously reported for CTA **1a**. We attribute this phenomenon to the relatively more stable homolytic leaving group of CTA **1b**, which likely accelerates consumption of the RAFT agent during the pre-equilibrium phase compared with CTA **1a**.[29] RAFT polymerization of MMA and VAc were also attempted. As was the case with CTA **1a**, polymerization of MMA mediated by CTA **1b** was uncontrolled, while RAFT of VAc using this CTA was completely inhibited for > 48 h.

Table 8.2. Polymers prepared by RAFT polymerization using CTA 1b.

Monomer	**% Conv[a]**	**M_n (Da)[b]**	**$M_{n,\ expected}$ (Da)[c]**	**Đ[b]**
MMA	14	62,000	1,800	1.40
ACMO	99	15,000	17,500	1.09
MA	70	6,100	7,500	1.03
Styrene	40	4,400	5,200	1.01
VAc	0	--[d]	--[d]	--[d]

[a]Determined using ^{1}H NMR spectroscopy. [b]Measured by SEC-MALLS in THF at 30 °C. [c]Calculated based on monomer conversion measured by ^{1}H NMR spectroscopy. [d]No polymer was detected by SEC. Data represent the ultimate timepoint taken from kinetic analyses.

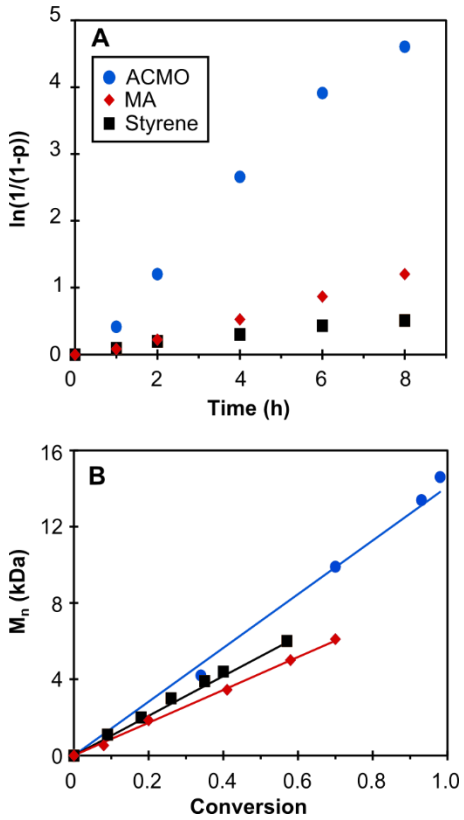

Figure 8.2. A) Kinetic analysis of RAFT polymerization of styrene (squares), MA (diamonds), and ACMO (spheres) using 1b. B) Plot of M_n vs. conversion for the same polymerizations. The solid lines represent the theoretical M_n values calculated from conversions as determined by ^{1}H NMR spectroscopy.

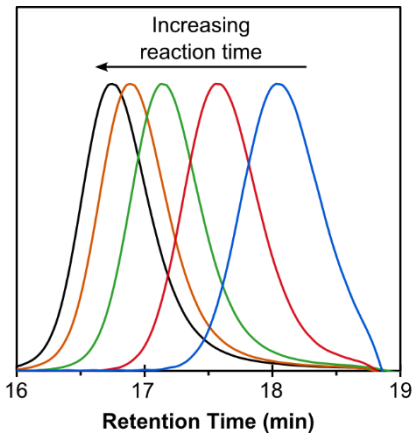

Figure 8.3. SEC traces of aliquots removed during the kinetic evaluation of the polymerization of styrene mediated by CTA 1b.

8.6.2. Z-Group Modification

To access the class of LAMs, we pursued an alternative strategy in which **NI** was reduced to the corresponding secondary amine (Scheme 8.3)—a significantly more reactive nucleophile. The increased electron density of the nitrogen atom of the resulting dithiocarbamates is not desirable for mediation of the polymerization of MAMs; however, this change in electronics was expected to enable RAFT of LAMs such as VAc. The reduction of **NI** was accomplished using $LiAlH_4$,[37] giving norbornene amine (**NA**) in nearly quantitative yield. Treatment of this compound with CS_2 and aqueous KOH gave the dithiocarbamate potassium salt, which could be isolated from excess reagents. Alkylation was conducted in acetone at 0 ˚C using bromoacetonitrile. Using this strategy, a second generation norbornene-containing CTA(CTA **2**) was prepared in 3 steps from **NI** in 61% overall yield.

Scheme 8.3. Preparation of dithiocarbamate CTA, 2, from NA.

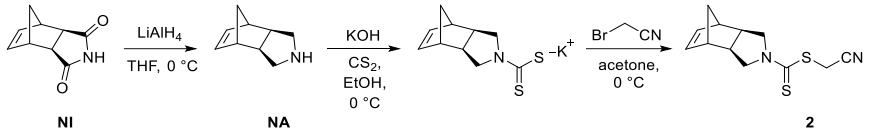

NI **NA** **2**

The dialkyl dithiocarbamate CTA **2** possesses an electron rich dialkyl amine Z-group. Typically, the electron-donating character of the N atom in dithiocarbamates renders the C=S bond less reactive toward radicals than CTAs that contain more electron-withdrawing Z-groups.[28] This has the effect of decreasing the chain transfer efficiency of the CTA, thereby increasing the active radical concentration. As a result, dialkyl dithiocarbamate CTAs tend to mediate the polymerization of LAMs effectively but lead to uncontrolled polymerization of MAMs. To assess the quality of the polymerization of various MAMs by RAFT using CTA **2**, reactions were conducted for 2 h using conditions similar to those employed when using CTA **1b**. Our evaluation is summarized in Table 8.3. SEC and ^{1}H NMR analysis of the crude reaction mixtures showed that

RAFT polymerizations of MMA, MA, styrene, and ACMO were poorly controlled, giving polymers of moderate to broad dispersity with MWs significantly higher than expected. In addition, the anticipated CTA-derived polymer end groups were absent from the ^{1}H NMR spectrum of a purified poly(styrene) sample polymerized in the presence of CTA **2** (see Figure 8S8), supporting the expected low propensity of CTA **2** to react with MAM radicals. This result is further corroborated by comparing the UV-Vis absorption spectrum of CTA **2** to that of **1b** (Figure 8S10). The decreased λ_{max} of CTA **1b** relative to CTA **2** is consistent with increased electron density on C=S.[38]

Table 8.3. Polymers prepared by RAFT polymerization using CTA 2.

Monomer	**% Conv[a]**	**M_n (Da)[b]**	**$M_{n,\ expected}$ (Da)[c]**	**Đ[b]**
MMA	25	168,000	2,500	1.63
ACMO	> 99	61,800	14,000	2.05
MA	75	17,300	6,500	1.58
Styrene	16	37,600	1,700	1.31
VAc	48	6,600	4,100	1.43

[a]Determined using ^{1}H NMR spectroscopy. [b]Measured by SEC-MALLS in THF at 30 °C. [c]Calculated based on monomer conversion measured by ^{1}H NMR spectroscopy.

RAFT polymerization of VAc mediated by CTA **2** was more successful than the other monomers tested. The dialkyl amine Z-group has been shown to mediate (to a degree) RAFT polymerization of LAMs such as VAc.[32] The reduced reactivity of the C=S bond of alkyl dithiocarbamates and xanthates in particular promotes sufficient fragmentation of the CTA-polymer adduct, allowing for polymerization of LAMs to progress without retardation. VAc polymerizations using CTA **2** were conducted neat at 80 °C using 1,1′-azobis(cyclohexanecarbonitrile) (ACHN) as the radical source. As expected, the formation of polymer was observed when CTA **2** was used in the

polymerization of VAc. However, the reaction exhibited a long incubation period of > 7 h, after which propagation proceeded rapidly. An isolated polymer prepared via RAFT of VAc mediated by CTA **2** was monomodal by SEC with an M_n that agreed with the expected value (Table 8.3). The relatively high Đ of this polymer likely resulted from two independent phenomena: (1) intermolecular termination by coupling (also supported by the higher than expected MW); and (2) the presence of a population of high MW species that typically form early in the polymerization of VAc.[39] ^{1}H NMR spectroscopy of the polymer sample showed the appropriate CTA-derived α- and ω-chain ends (Figure 8.4), and end group analysis gave a MW value that was in relatively good agreement with those determined by SEC and monomer conversion (5,200 Da). Taken together, these data suggest that CTA **2** effectively mediates the polymerization of VAc.

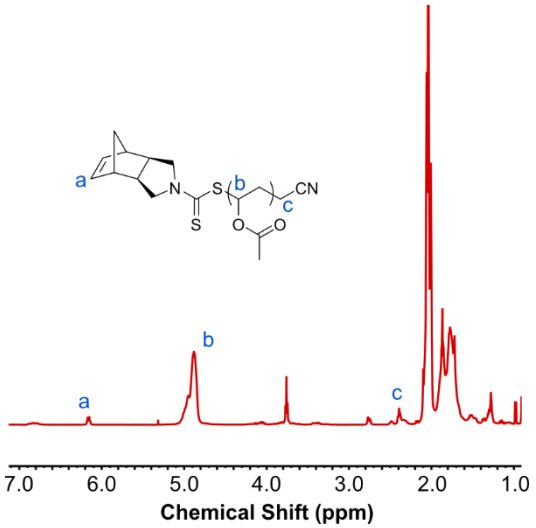

Figure 8.4. ^{1}H NMR spectrum of a PVAc MM prepared using CTA 2 highlighting the CTA-derived α- and ω-chain ends (protons a and c). Spectrum was taken in $CDCl_3$.

CTAs with norbornene Z-groups can be utilized in the synthesis of bottlebrush polymers by both the transfer-to and grafting-through approaches. Both strategies rely on ring-opening metathesis polymerization (ROMP) to generate the bottlebrush backbone. ROMP of CTA **2** was performed to prepare poly(**2**) as shown in Figures 8.5 and 8S9. Polymerizations by the modified 2nd generation

Grubbs' catalyst (**G3**) at a [M]/[**G3**] ratio of 50 : 1 achieved quantitative conversion in < 20 min. The SEC trace of the resulting polymer (Mn = 12,700 Da) was monomodal with low Đ (1.01). ^{1}H NMR spectroscopy of the crude reaction mixture confirmed quantitative consumption of the olefin functionality, evidenced by the disappearance of the resonance at 6.13 ppm. A pair of new peaks between 5.2 and 5.6 ppm were assigned to the backbone olefins of poly(**2**).

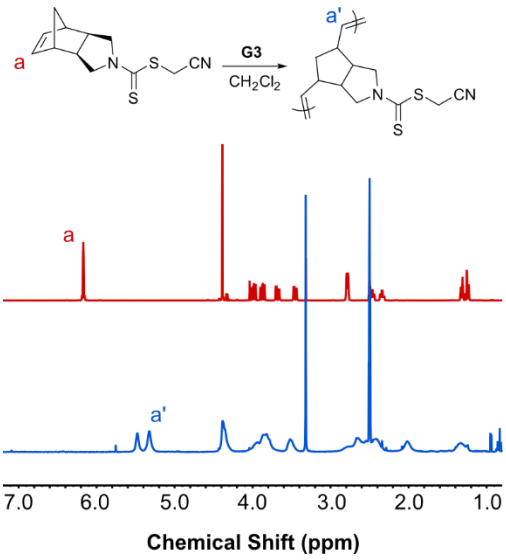

Figure 8.5. ^{1}H NMR spectra of 2 (top spectrum) and a crude spectrum of a polymer prepared via ROMP of 2 (bottom spectrum) highlighting the quantitative consumption of olefin protons. Spectra were taken in DMSO-d_6.

Scheme 8.4. Preparation of PVAc bottlebrush by ROMP grafting-through.

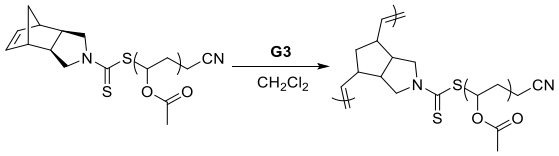

Based on this positive result, we considered whether ROMP grafting-through of PVAc prepared using **2** could be accomplished to form a bottlebrush polymer (as shown in Scheme 8.4). The

grafting-through technique involves the polymerization of a macromolecule functionalized with a polymerizable group on one chain end (macromonomer, MM). Bottlebrush polymers prepared using this method are considered to have perfect grafting density, as each repeat unit bears a pendant polymer side chain. Bottlebrush polymers possessing PVAc side chains have been synthesized previously via radical grafting-through using a vinyl-functionalized PVAc MM,[40] through a tandem ATRP/RAFT method by grafting-from,[41] and employing an all-RAFT method using the R-group (grafting-from) and Z-group (transfer-to) approaches.[42] These macromolecules are precursors to poly(vinyl alcohol) (PVOH)-based materials that have interesting industrial and biomedical applications.[43] In addition, branched PVOHs possess different physical properties than linear ones, such as decreased solution viscosity.[44]

As shown in Figure 8.4, the norbornene functionality of CTA **2** is retained on the ω-chain end after the polymerization of VAc. This ROMP-active moiety can be utilized to form a bottlebrush polymer via grafting-through. ROMP grafting-through was carried out at a [MM]/[**G3**] ratio of 25:1 using a PVAc MM prepared via RAFT polymerization mediated by CTA **2** (**NA-PVAc**)(M_n = 6,600 Da). The resulting bottlebrush polymer had a MW of 110 kDa with a narrow and symmetrical molecular weight distribution (Đ = 1.26). Full conversion of norbornene-functionalized MMs was confirmed by ^{1}H NMR spectroscopy. A second population of macromolecules centered on 17 min in the SEC trace in Figure 8.6 corresponds to residual PVAc MM that was not consumed during ROMP. These "dead chains" arise primarily from termination reactions during RAFT polymerization that leave the polymer chain without the desired ω-end group. The minimal fraction of residual polymer after ROMP grafting-through further supports the capability of CTA **2** to control RAFT polymerization of VAc, as the majority of the macromonomers possess the norbornene ω-end group.

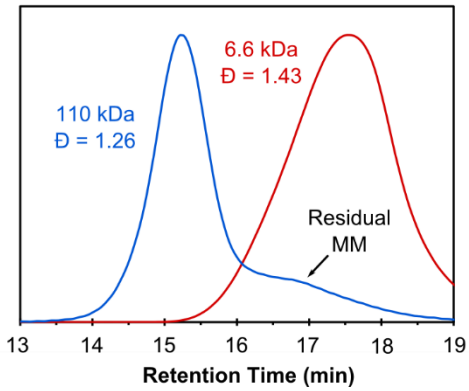

Figure 8.6. SEC traces of PVAc MM prepared using CTA 2 (NA-PVAc) (longer retention time) and a bottlebrush polymer prepared using this MM via ROMP grafting-through (shorter retention time).

8.7. Conclusions

In summary, we have prepared two new dithiocarbamate CTAs with Z-groups derived from **NI** and the corresponding reduced secondary amine. Based on the electronics of **NI**, it is apparent that only certain alkylating agents—sterically unhindered alkyl halides lacking acidic functionalities—can be employed to prepare CTAs derived from this Z-group. Nevertheless, CTA **1b** was prepared in moderate yields and was found to efficiently mediate RAFT polymerization of 2° MAMs—styrene, MA, and ACMO. Reduction of **NI** was conducted to reduce the electron withdrawing ability of the Z-group. Novel dithiocarbamate CTA **2** prepared from norbornene amine did not control the polymerization of 2° or 3° MAMs; however, it provided moderate control over the polymerization of VAc, yielding polymers with the appropriate CTA-derived end groups. ROMP of a PVAc MM prepared using CTA **2** was carried out to give a bottlebrush polymer with PVAc side chains using the grafting-through technique. To the best of our knowledge, this work represents the first preparation of a bottlebrush polymer with PVAc side chains by the grafting-through method. We expect that this contribution will assist in the rational design of CTAs capable of mediating RAFT polymerization to form polymers functionalized with ROMP-active norbornene moieties.

8.8. References

(1) Matyjaszewski, K. *Macromolecules* **2012**, *45*, 4015.

(2) Moad, G.; Rizzardo, E.; Thang, S. H. *Aust. J. Chem.* **2012**, *65*, 985.

(3) Perrier, S.; Takolpuckdee, P. *J. Polym. Sci., Part A: Polym. Chem.* **2005**, *43*, 5347.

(4) Wang, J.-S.; Matyjaszewski, K. *Macromolecules* **1995**, *28*, 7901.

(5) Wang, J.-S.; Matyjaszewski, K. *J. Am. Chem. Soc.* **1995**, *117*, 5614.

(6) Sciannamea, V.; Jerome, R.; Detrembleur, C. *Chem. Rev.* **2008**, *108*, 1104.

(7) Zhang, N.; Samanta, S. R.; Rosen, B. M.; Percec, V. *Chem. Rev.* **2014**, *114*, 5848.

(8) Chiefari, J.; Chong, Y. K.; Ercole, F.; Krstina, J.; Jeffery, J.; Le, T. P. T.; Mayadunne, R. T. A.; Meijs, G. F.; Moad, C. L.; Moad, G.; Rizzardo, E.; Thang, S. H. *Macromolecules* **1998**, *31*, 5559.

(9) Vázquez-Dorbatt, V.; Tolstyka, Z. P.; Maynard, H. D. *Macromolecules* **2009**, *42*, 7650.

(10) Bulmus, V. *Polym. Chem.* **2011**, *2*, 1463.

(11) De, P.; Li, M.; Gondi, S. R.; Sumerlin, B. S. *J. Am. Chem. Soc.* **2008**, *130*, 11288.

(12) Sumerlin, B. S. *ACS Macro Lett.* **2012**, *1*, 141.

(13) Ratcliffe, L. P. D.; Ryan, A. J.; Armes, S. P. *Macromolecules* **2013**, *46*, 769.

(14) Warren, N. J.; Armes, S. P. *J. Am. Chem. Soc.* **2014**, *136*, 10174.

(15) Figg, C. A.; Simula, A.; Gebre, K. A.; Tucker, B. S.; Haddleton, D. M.; Sumerlin, B. S. *Chem. Sci.* **2015**, *6*, 1230.

(16) Kang, Y.; Pitto-Barry, A.; Maitland, A.; O'Reilly, R. K. *Polym. Chem.* **2015**, *6*, 4984.

(17) Gody, G.; Maschmeyer, T.; Zetterlund, P. B.; Perrier, S. *Nat. Commun.* **2013**, *4*, 2505.

(18) Foster, J. C.; Matson, J. B. *Macromolecules* **2014**, *47*, 5089.

(19) Zhang, L.; Liu, W.; Lin, L.; Chen, D.; Stenzel, M. H. *Biomacromolecules* **2008**, *9*, 3321.

(20) York, A. W.; Kirkland, S. E.; McCormick, C. L. *Adv. Drug. Deliv. Rev.* **2008**, *60*, 1018.

(21) Cerritelli, S.; Velluto, D.; Hubbell, J. A. *Biomacromolecules* **2007**, *8*, 1966.

(22) Moad, G.; Rizzardo, E.; Thang, S. H. *Chemistry – An Asian Journal* **2013**, *8*, 1634.

(23) Teo, Y. C.; Xia, Y. *Macromolecules* **2015**, *48*, 5656.

(24) Li, Z.; Zhang, K.; Ma, J.; Cheng, C.; Wooley, K. L. *J. Poly. Sci. Part A, Polym. Chem.* **2009**, *47*, 5557.

(25) Li, X.; ShamsiJazeyi, H.; Pesek, S. L.; Agrawal, A.; Hammouda, B.; Verduzco, R. *Soft Matter* **2014**, *10*, 2008.

(26) Moad, G.; Rizzardo, E.; Thang, S. H. *Polymer* **2008**, *49*, 1079.

(27) Hill, M. R.; Carmean, R. N.; Sumerlin, B. S. *Macromolecules* **2015**, *48*, 5459.

(28) Chiefari, J.; Mayadunne, R. T. A.; Moad, C. L.; Moad, G.; Rizzardo, E.; Postma, A.; Thang, S. H. *Macromolecules* **2003**, *36*, 2273.

(29) Chong, Y. K.; Krstina, J.; Le, T. P. T.; Moad, G.; Postma, A.; Rizzardo, E.; Thang, S. H. *Macromolecules* **2003**, *36*, 2256.

(30) Keddie, D. J.; Moad, G.; Rizzardo, E.; Thang, S. H. *Macromolecules* **2012**, *45*, 5321.

(31) Skey, J.; O'Reilly, R. K. *Chem. Commun.* **2008**, 4183.

(32) Mayadunne, R. T. A.; Rizzardo, E.; Chiefari, J.; Chong, Y. K.; Moad, G.; Thang, S. H. *Macromolecules* **1999**, *32*, 6977.

(33) Radzinski, S. C.; Foster, J. C.; Matson, J. B. *Polym. Chem.* **2015**, *6*, 5643.

(34) Love, J. A.; Morgan, J. P.; Trnka, T. M.; Grubbs, R. H. *Angew. Chem., Int. Ed.* **2002**, *41*, 4035.

(35) Liu, J.; Gao, A. X.; Johnson, J. A. *J. Vis. Exp.* **2013**, e50874.

(36) Humeres, E.; Debacher, N. A.; Sierra, M. M. d. S.; Franco, J. D.; Schutz, A. *J. Org. Chem.* **1998**, *63*, 1598.

(37) Van Vliet, L. D.; Ellis, T.; Foley, P. J.; Liu, L.; Pfeffer, F. M.; Russell, R. A.; Warrener, R. N.; Hollfelder, F.; Waring, M. J. *J. Med. Chem.* **2007**, *50*, 2326.

(38) McKenzie, T. G.; Fu, Q.; Wong, E. H. H.; Dunstan, D. E.; Qiao, G. G. *Macromolecules* **2015**, *48*, 3864.

(39) Stenzel, M. H.; Cummins, L.; Roberts, G. E.; Davis, T. P.; Vana, P.; Barner-Kowollik, C. *Macromol. Chem. Phys.* **2003**, *204*, 1160.

(40) Ohnaga, T.; Sato, T. *Polymer* **1996**, *37*, 3729.

(41) Nese, A.; Kwak, Y.; Nicolaÿ, R.; Barrett, M.; Sheiko, S. S.; Matyjaszewski, K. *Macromolecules* **2010**, *43*, 4016.

(42) Bernard, J.; Favier, A.; Davis, T. P.; Barner-Kowollik, C.; Stenzel, M. H. *Polymer* **2006**, *47*, 1073.

(43) Baker, M. I.; Walsh, S. P.; Schwartz, Z.; Boyan, B. D. *J. Biomed. Mater. Res. Part B Appl. Biomater.* **2012**, *100B*, 1451.

(44) Baudry, R.; Sherrington, D. C. *Macromolecules* **2006**, *39*, 5230.

8.9. Appendix

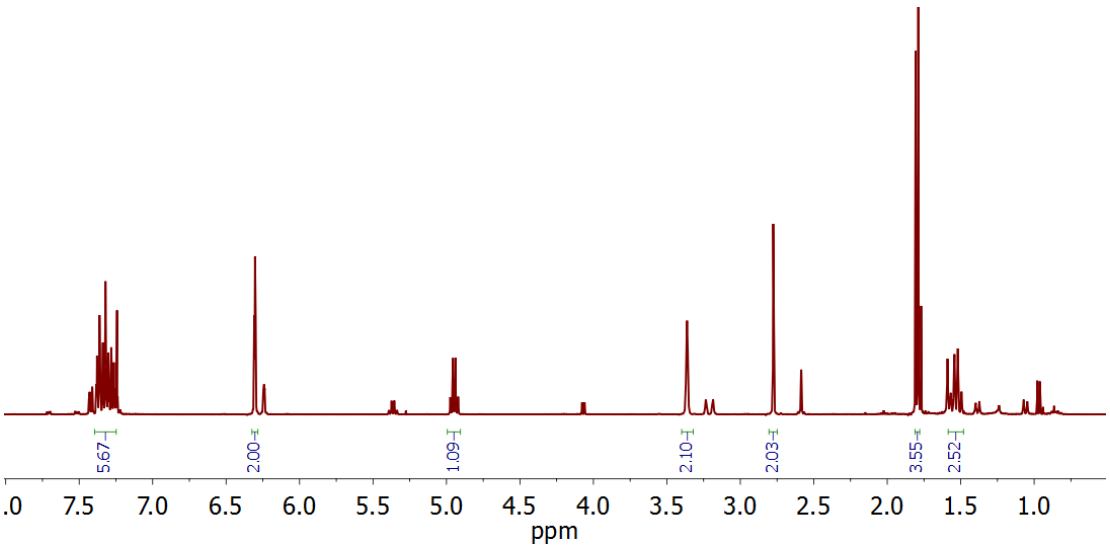

Figure 8S1. ^{1}H NMR spectrum of CTA 1b. The starred peaks correspond to *N*-alkylated byproduct.

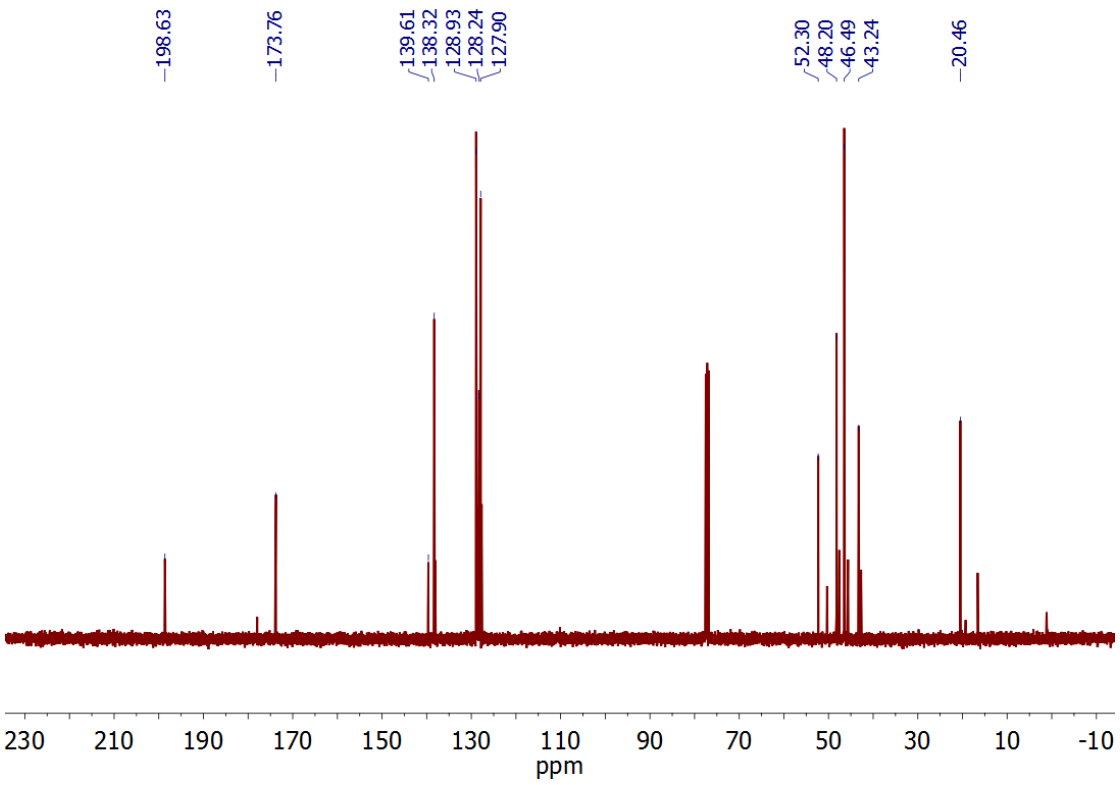

Figure 8S2. ^{13}C NMR spectrum of CTA 1b. Starred peaks correspond to *N*-alkylated byproduct.

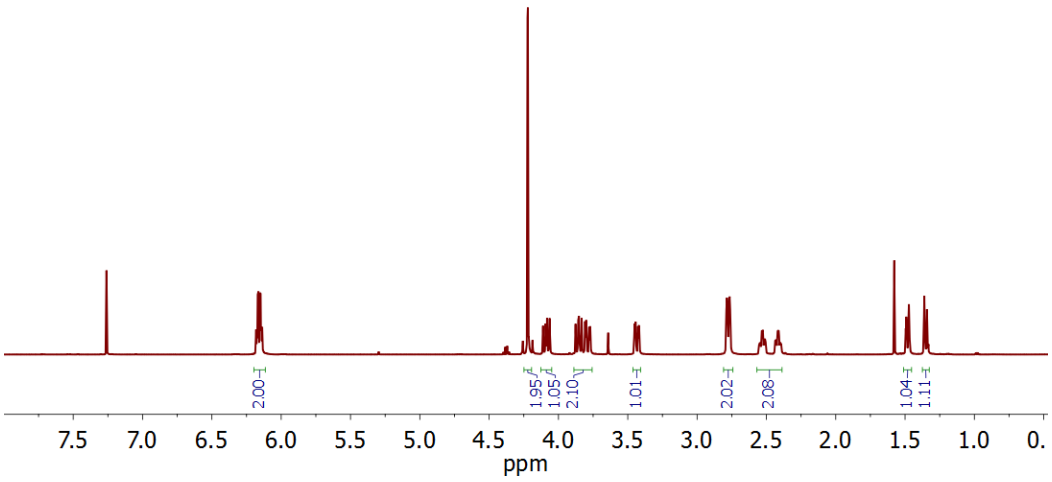

Figure 8S3. ^{1}H NMR spectrum of CTA 2.

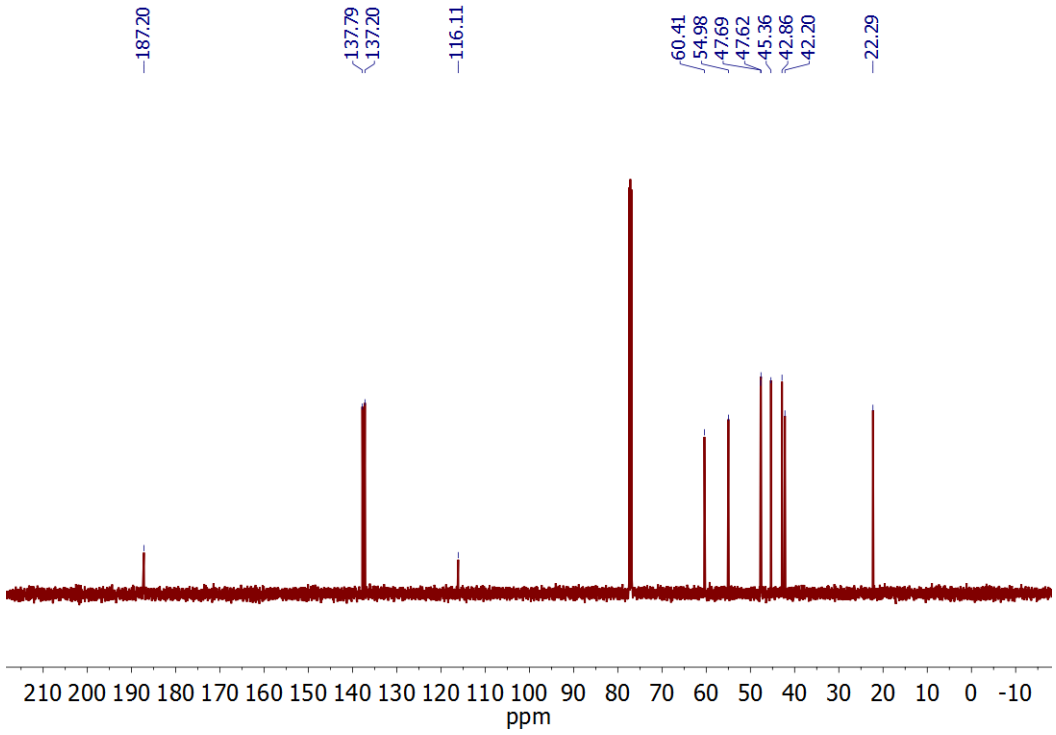

Figure 8S4. ^{13}C NMR spectrum of CTA 2.

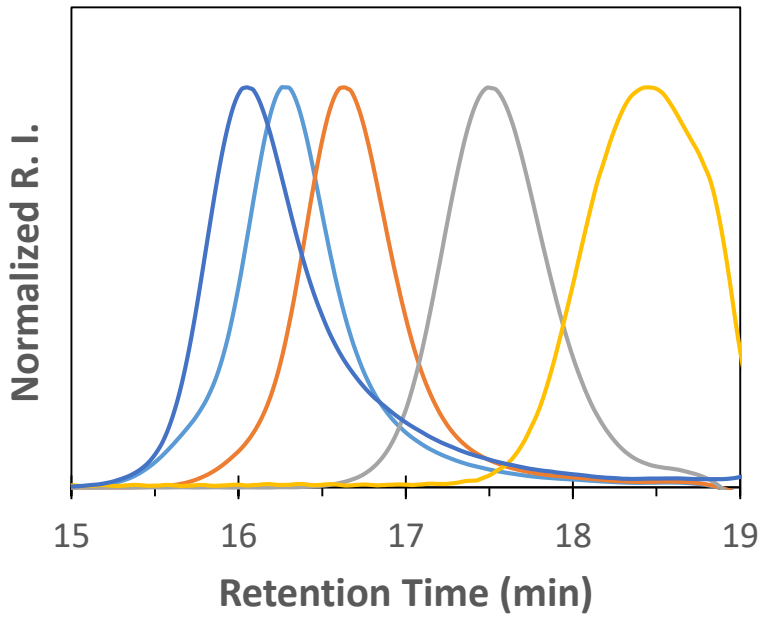

Figure 8S5. SEC traces of aliquots removed during the kinetic evaluation of the polymerization of MA mediated by CTA 1b.

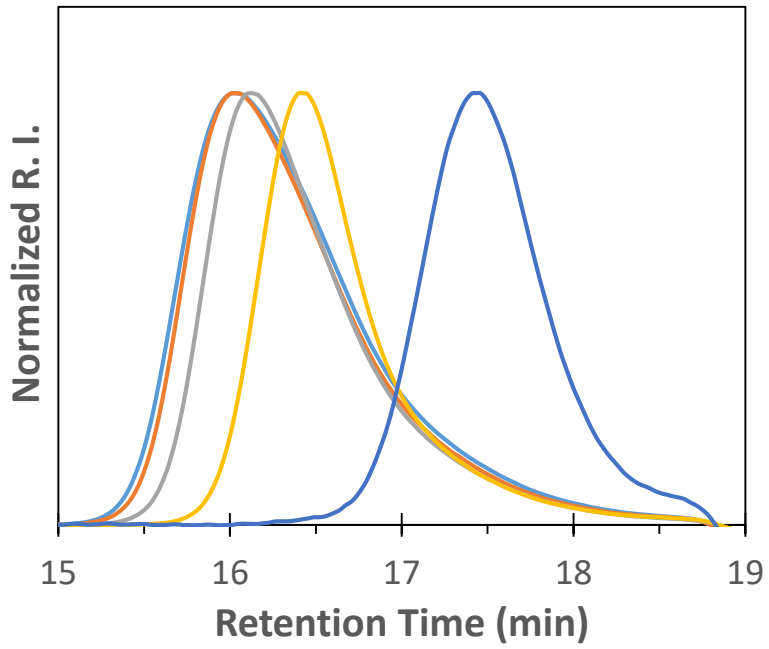

Figure 8S6. SEC traces of aliquots removed during the kinetic evaluation of the polymerization of ACMO mediated by CTA 1b.

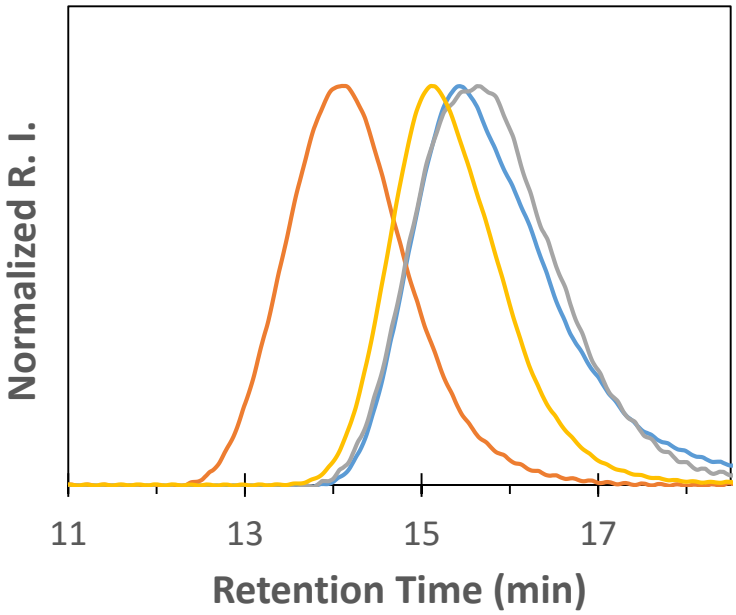

Figure 8S7. SEC traces of RAFT polymerizations of MMA (orange trace), ACMO (yellow trace), styrene (blue trace), and MA (grey trace) using CTA 2.

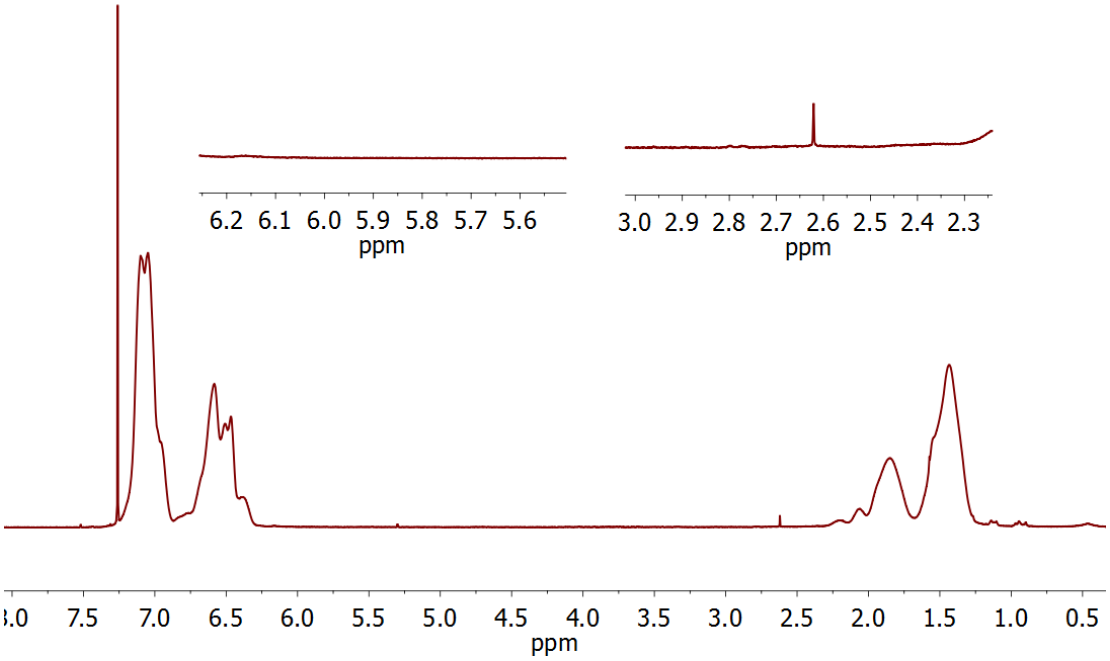

Figure 8S8. ^{1}H NMR spectrum of PS prepared using CTA 2 highlighting the absence of the expected CTA-derived end groups that should appear around 2.4 ppm and 6 ppm for the α and ω chain ends, respectively.

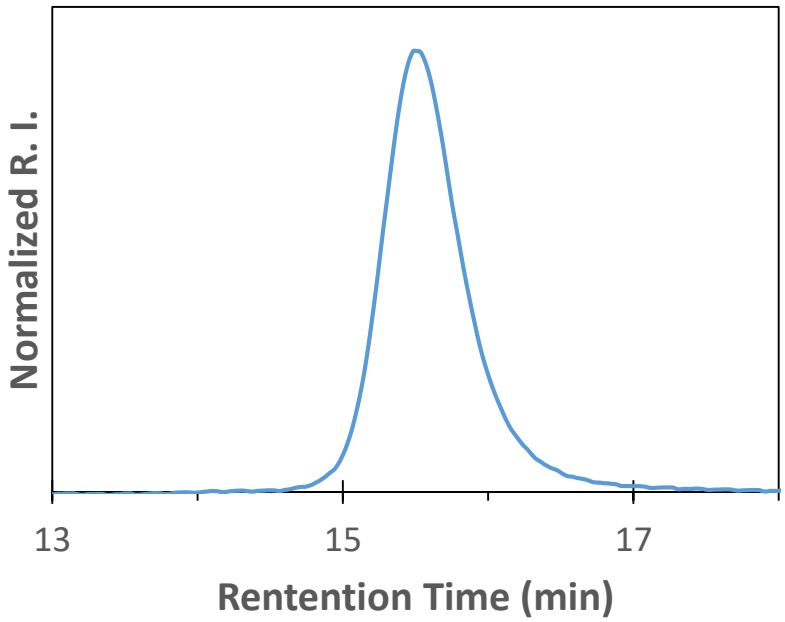

Figure 8S9. SEC trace of poly(2) prepared by ROMP of CTA 2.

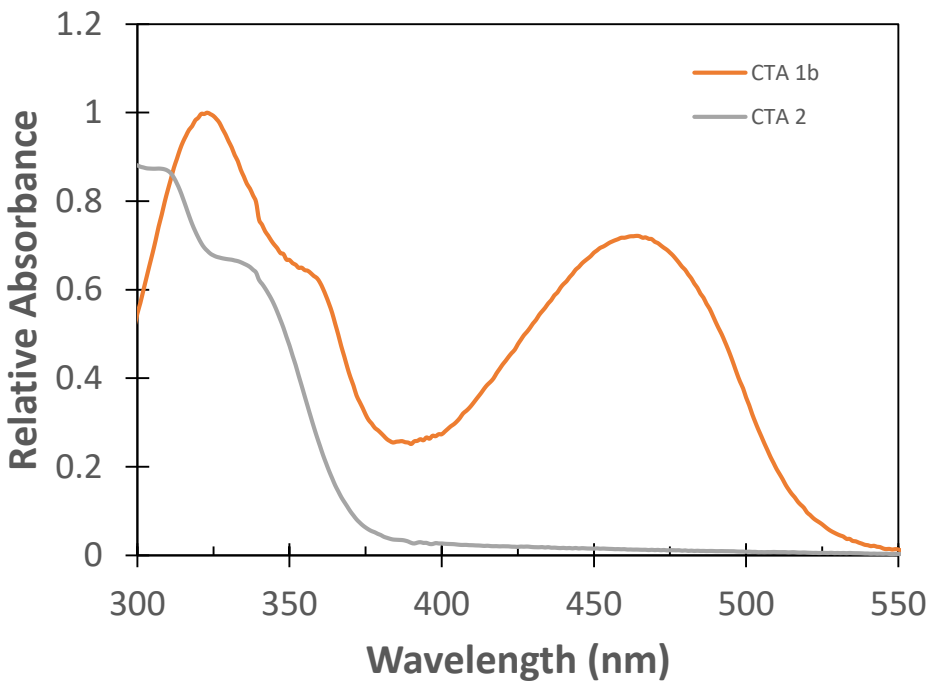

Figure 8S10. UV-Vis absorbance spectra of CTA 1b (orange trace) and CTA 2 (grey trace) taken at 2 mg/mL in THF.

Chapter 9. Factors Affecting Bottlebrush Polymer Synthesis by the Transfer-to Method Using Reversible Addition–Fragmentation Chain Transfer (RAFT) Polymerization

"Radzinski, S. C.; Foster, J. C.; Matson, J. B., *Polymer Chemistry*, **2017**, 8, 1636-1643. Published by the Royal Society of Chemistry."

9.1 Authors

Scott C. Radzinski,[†,Ð] Jeffrey C. Foster, [†,Ð] Sally E. Lewis,[†] Eric V. French,[†] John B. Matson[†]

[†]Department of Chemistry and Macromolecules Innovation Institute, Virginia Tech, Blacksburg, Virginia, 24601

[Ð]Authors contributed equally to this work.

9.2. Abstract

The transfer-to method is a unique way to prepare bottlebrush polymers by reversible addition-fragmentation chain transfer (RAFT) polymerization. This little-studied bottlebrush polymer synthesis strategy is distinct from the grafting-from, grafting-to, and grafting-through strategies and therefore may have specific advantages over these other synthetic approaches. Herein, we study the factors affecting the composition of bottlebrush polymer samples prepared by RAFT transfer-to, with particular emphasis on bottlebrush polymer molecular weight (MW) and dispersity (Đ) and the percentage of "dead" linear polymer as a function of initiator concentration, [M]/[CTA] ratio, backbone length, and monomer type. The lowest quantities of dead polymer were obtained under conditions that limited the MW of the bottlebrush polymer side-chains and that

discouraged termination reactions. Under optimized conditions, high MW bottlebrush polymers were prepared with low dispersities and few dead polymer impurities.

9.3. Introduction

The unique properties of bottlebrush polymers have made this rich polymer topology a potential contributor in applications ranging from super-soft materials[1,2] to photonic crystals,[3,4] to drug delivery.[5,6] These properties arise from the densely grafted nature of bottlebrush polymers, which results in steric repulsion between polymeric side-chains that force the macromolecules to adopt a shape-persistent, chain-extended conformation.[7-10] In recent years, the field of bottlebrush polymer synthesis has advanced dramatically, with controlled polymerization techniques such as reversible addition–fragmentation chain transfer (RAFT)[11] polymerization and ring-opening metathesis polymerization (ROMP)[12] enabling precise control over the size and dispersity of the bottlebrush polymer backbone as well as the pendant polymeric side-chains.[13-19] However, despite this progress, the synthesis of high molecular weight (MW) bottlebrush polymers with controllable dimensions remains challenging.[20]

Bottlebrush polymers are prepared by one of four methods: grafting-to, grafting-from, grafting-through, or transfer-to. The polymers produced by these methods differ in their structures (i.e., grafting densities, imperfections, etc.) and sample compositions depending on the advantages and limitations of each method. For example, grafting-from allows for direct control over the synthesis of the polymer backbone, but the side-chains do not all match their theoretical MW due to undesirable side reactions. These include looping (intramolecular coupling) and brush-brush (intermolecular coupling) reactions that originate from the tethering of the propagating species to the bottlebrush polymer backbone.[21] These termination pathways yield imperfections, high MW impurities, and sometimes crosslinking in the resulting polymer samples. Despite these limitations,

grafting-from is perhaps the most thoroughly studied bottlebrush polymer synthesis technique. The transfer-to approach, while similar to grafting-from, has the potential to completely eliminate these bottlebrush polymer coupling and looping side reactions.[22]

Both grafting-from and transfer-to can be mediated by a polymeric RAFT chain transfer agent (CTA).[22-25] RAFT CTAs contain an R group, which is homolytically cleaved from the CTA to initiate chain-growth polymerization, and a Z group, which is immobile and regulates the reactivity of the CTA. The difference in the two strategies lies in the direction of CTA attachment to the polymer backbone. In RAFT grafting-from, the R group is attached to the polymer backbone, so growing radicals remain tethered to the bottlebrush polymer throughout the polymerization. In RAFT transfer-to, the CTA is attached through the Z-group (transfer-to is sometimes called the Z-group or Z-Star approach).[26,27] In this case, polymer-derived radicals do not remain tethered to the bottlebrush polymer backbone; instead, they detach and propagate freely in solution, eventually returning to a bottlebrush polymer via a chain-transfer reaction (Figure 9.1).[14,19] During polymerization, the detached linear chains are in equilibrium with the bottlebrush polymer side-chains; therefore, absent substantial termination, the MWs of these two populations are expected to be approximately equal.[28] Termination reactions between linear polymers lead to the formation of "dead" linear polymer but do not create loops or coupled bottlebrushes.

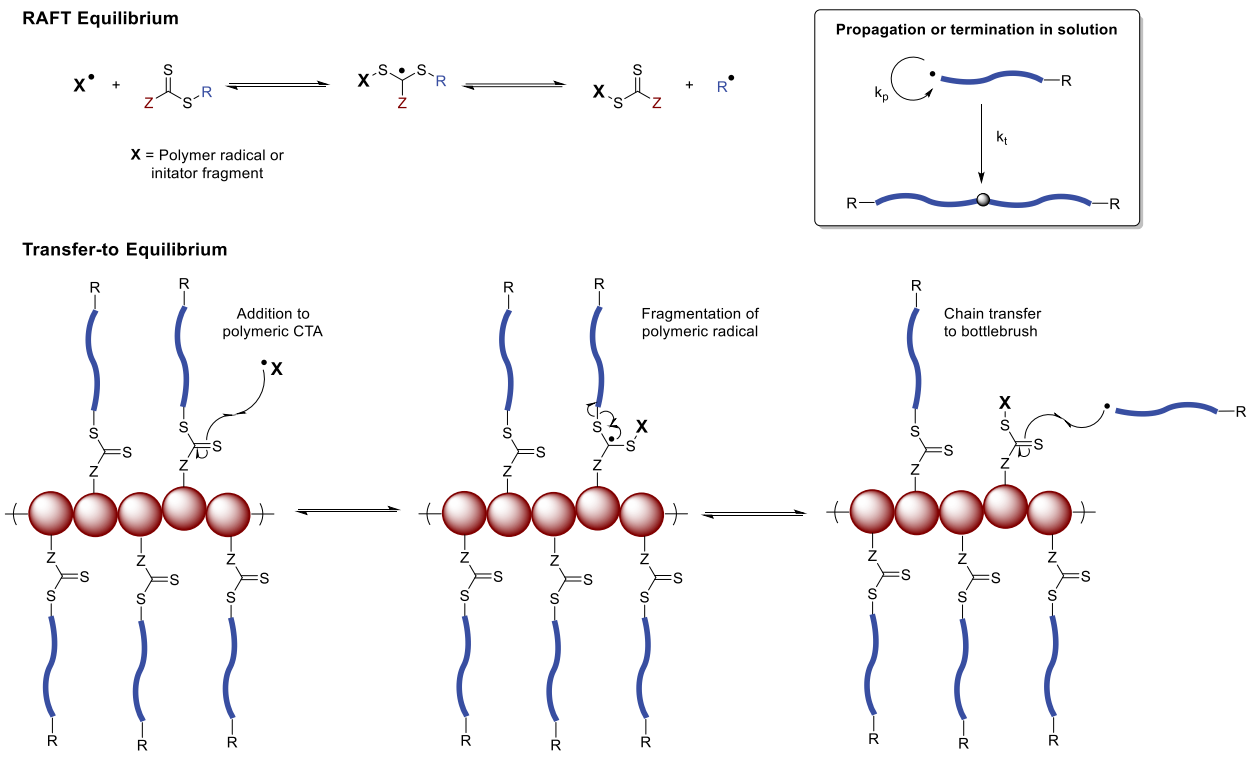

Figure 9.1. Illustration of idealized RAFT transfer-to equilibrium. The red spheres designate the bottlebrush polymer backbone repeat units, while the blue lines represent side-chains. The polymerization is mediated by polymeric RAFT CTAs, which fragment to yield polymeric radicals that grow freely in solution.

In our previous report on RAFT transfer-to polymerization, we observed the formation of a substantial fraction of dead polymer chains as the polymerizations progressed.[14] These dead polymers are sometimes difficult to separate from the bottlebrush polymers and could potentially affect the mechanical properties of the sample. In addition, loss of bottlebrush polymer side-chains to termination reactions results in a reduction in the grafting density of the bottlebrush polymer. Grafting density is difficult to measure directly due to the dynamic nature of RAFT transfer-to, but information about the grafting density can be inferred by inspecting the quantity of dead polymers that form during polymerization. Each dead polymer represents a chain that is no longer attached to a bottlebrush polymer and therefore reduces the overall grafting density of the sample. In addition, the bottlebrush polymer grafting density can also be inferred by comparing the

observed MWs of the bottlebrush polymers to expected values based on monomer conversion. In the absence of considerable termination, lower than expected bottlebrush polymer MWs most probably originate from the fact that they possess grafting densities less than 100%. Grafting density can also be approximated by isolating the bottlebrush polymer and cleaving the polymer side-chains from the bottlebrush polymer backbone and then dividing the observed bottlebrush polymer MW by the MW of the side-chains.

In this contribution, we sought to optimize the polymerization to achieve controlled bottlebrush polymer synthesis while decreasing the dead chain population without significantly extending its timescale. Toward this end, we investigate the effect of initiator concentration, initial [M]/[CTA] ratio, reaction time, bottlebrush polymer backbone DP, and monomer selection on the MW and dispersity (Đ) of the resulting bottlebrush polymers as well as the fraction of dead linear chains.

9.4. Experimental

Materials. All reagents were obtained from commercial vendors and used as received unless otherwise stated. Styrene, methyl acrylate (MA), and 4-acryloylmorpholine (ACMO) were passed through small columns of basic alumina prior to use. ROMP catalyst $(H_2IMes)(Cl)_2(PCy_3)Ru{=}CHPh$ (**G2**) was obtained as a generous gift from Materia. ROMP catalyst $(H_2IMes)(pyr)_2(Cl)_2Ru{=}CHPh$ (**G3**) was prepared from **G2** according to literature procedures.[29,30]

Methods. NMR spectra were measured on an Agilent 400 MHz spectrometer. ^{1}H and ^{13}C NMR chemical shifts are reported in ppm relative to internal solvent resonances. Size exclusion chromatography (SEC) was carried out in THF at 1 mL/min at 30°C on two Agilent PLgel 10 μm MIXED-B columns connected in series with a Wyatt Dawn Heleos 2 light scattering detector and

a Wyatt Optilab Rex refractive index detector. No calibration standards were used, and dn/dc values were obtained by assuming 100% mass elution from the columns. **CTA1** was synthesized from previous literature reports.[14,31]

Typical synthesis of Poly(CTA1) (PCTA1). A typical polymerization procedure of **CTA1** is as follows: A solution of **G3** in anhydrous CH_2Cl_2 was prepared in a vial at 40X the desired concentration (0.02 to 0.001 equivalents with respect to monomer). A 100 μL aliquot of this **G3** solution was added rapidly to a vigorously stirring solution of **CTA1** (200 mg) in 3.9 mL of anhydrous CH_2Cl_2 in a 1 dram vial to make a final volume of 4 mL and a final monomer concentration of 50 mg/mL. The polymerization was quenched after 20 min by adding of 1-3 drops of ethyl vinyl ether. The polymer was isolated via precipitation from hexanes and dried under vacuum to yield the pure polymer as an off-white powder.

Typical synthesis of Poly(CTA1-*g*-polymer) by RAFT transfer-to. To an oven-dried Schlenk tube equipped with a magnetic stir bar was added **PCTA1** (2.88 mg, 0.18 mmol, M_n = 17,000 g/mol), styrene (1 mL, 8.73 mmol), and 5 mL of DMF. A stock solution of 2,2'-azobis(2-methylpropionitrile) (AIBN) was prepared by dissolving 2.9 mg in 10 mL of DMF. 100 μL of this stock solution was then added to the Schlenk tube. The reaction mixture was deoxygenated by three freeze-pump-thaw cycles. The Schlenk tube was then backfilled with N_2 and submerged in an oil bath maintained at 75 °C. Samples were removed periodically by N_2-purged syringe to monitor MW evolution by SEC and conversion by ^{1}H NMR spectroscopy. The polymerization was quenched by submerging the tube into liquid N_2 and exposing the reaction solution to air.

Peak Fitting. The relative weight fractions of bottlebrush polymer and dead linear polymer were determined via peak fitting of SEC RI data according to literature procedures.[32,33] These data are provided in the Supporting Information (Figures 9S1-S13).

9.5. Results and Discussion

To study bottlebrush polymer synthesis by RAFT transfer-to polymerization, we first synthesized a dithiocarbamate CTA (**CTA1**) according to our previously reported procedure.[14] This CTA contains a norbornene-imide Z group and is suitable for mediating polymerization of acrylates, acrylamides, and styrene.[31] **CTA1** also contains a norbornene moiety that can be utilized in ROMP. Next, poly(CTA)s (PCTAs) were prepared via ROMP of **CTA1** initiated by Grubbs' 3rd generation catalyst, $(H_2IMes)(pyr)_2(Cl)_2Ru{=}CHPh$ (**G3**) as shown in Scheme 9.1. These polyCTAs were then utilized in various RAFT transfer-to polymerizations as discussed below.

Scheme 9.1. Idealized bottlebrush polymer synthesis by RAFT transfer-to polymerization.

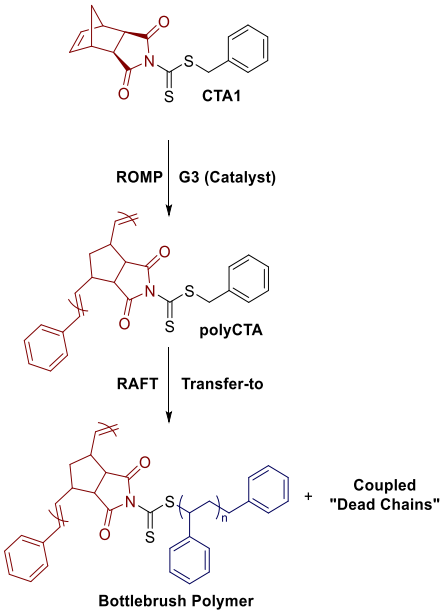

9.5.1. Effect of Radical Initiator Concentration

The amount of initiator utilized in a RAFT polymerization affects the polymerization kinetics and therefore the duration of the polymerization.[34] In addition, similar to conventional radical polymerization, the rate of termination is directly related to the concentration of actively propagating radicals.[35] Termination reactions during RAFT transfer-to result in dead linear polymer that cannot return to the bottlebrush polymer backbone. Therefore, limiting these termination events is critical to maintaining a low quantity of dead linear polymers. To test the effect of the [AIBN]/[CTA] ratio on RAFT transfer-to polymerizations, two experiments were performed with constant [M]/[CTA] ratio using a PCTA with a backbone degree of polymerization (DP) of 50, but with [AIBN]/[CTA] ratios of either 0.02 or 0.2 (Table 9.1, entries 1 and 2). The order of magnitude difference in AIBN concentration had an effect on the timescale of the polymerization and the amount of dead chains in solution. The polymerization with [AIBN]/[CTA] = 0.2 exhibited faster kinetics than the polymerization with less initiator (Figure 9S15). Size exclusion chromatographic (SEC) analysis of the 6 h time point of the polymerization with [AIBN]/[CTA] = 0.02 revealed a number average MW (M_n) of 114 kDa, while the the polymerization with [AIBN]/[CTA] = 0.2 reached a larger M_n of 293 kDa. We chose to evaluate the 6 h time points to relate data at low conversions with minimal influence from high viscosity or termination reactions. Based on the SEC traces in Figure 9.2, the bottlebrush polymer weight fraction was calculated for each time point by comparing the area under the curve of the bottlebrush polymer peak at lower retention time to that of the dead linear polymer peak at greater retention time using a peak-fitting algorithm.[32,33] The polymerization with a lower AIBN concentration possessed a dead chain fraction of 37%. In contrast, the polymerization with more AIBN had a significantly larger fraction of dead chains (57%). The dispersity (Đ) of the bottlebrush polymer

was unaffected by AIBN concentration as the bottlebrush polymer peak of both polymer samples was narrowly dispersed. Low bottlebrush polymer dispersity values are expected for RAFT transfer-to due to the absence of looping or bottlebrush polymer coupling reactions common in grafting-from.[26] Based on these results, a higher proportion of AIBN allows for faster polymerization and higher MWs at the cost of increased dead polymer. We chose to utilize the higher AIBN loading ([AIBN]/[CTA] = 0.2) in subsequent experiments to achieve reasonable polymerization timescales. We then aimed to reduce the fraction of dead chains by tuning other parameters of the reaction.

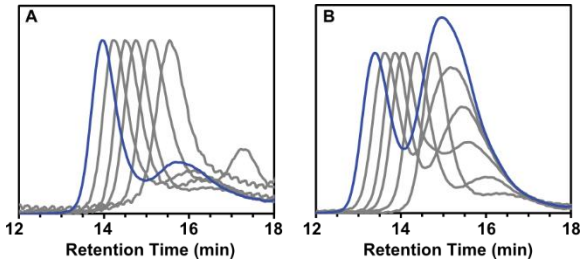

Figure 9.2. Effect of [AIBN]/[CTA] ratio on RAFT transfer-to polymerization (Table 9.1, entries 1 and 2), demonstrating that higher AIBN concentrations lead to a higher percentage of dead polymer. Shown above are SEC traces (refractive index detector) at various time points for (A) low AIBN loading (0.02 equiv with respect to CTA), (B) high AIBN loading (0.2 equiv with respect to CTA). The final time point for each run (blue lines) was taken after 24 h, while the gray traces represent the 1, 2, 4, 6, and 10 h time points. The bimodal distribution in most traces shows a high MW bottlebrush polymer peak at lower retention time and a lower MW peak at higher retention time representing dead linear polymer.

Table 9.1. Summary of polymers synthesized in this study.

Entry	Monomer	DP Backbone	[M]/[CTA]	[AIBN]/[CTA]	Mn (kDa)[a]	Đ[a]	%Dead[b]	%Conv[c]
1	sty	50	1000	0.02	114	1.03	37	27
2	sty	50	1000	0.2	293	1.01	57	32
3	sty	50	750	0.2	260	1.02	43	44
4	sty	50	500	0.2	216	1.02	41	35
5	sty	50	100	0.2	103	1.04	28	40
6	sty	50	50	0.2	44.0	1.04	24	34
7	sty	100	50	0.2	97.0	1.08	21	29
8	sty	500	50	0.2	753	1.08	36	40
9	sty	750	50	0.2	1110	1.02	30	40
10	sty	1000	50	0.2	1150	1.07	40	33
11	MA	100	50	0.2	400	1.05	14	89
12	ACMO	100	50	0.2	740	1.04	11	82

[a]Measured by SEC using absolute MW determined by light scattering. [b]Determined using peak fitting of SEC RI data. [c]Calculated using relative integrations of monomer and polymer resonances using ^{1}H NMR spectroscopy. These data represent the 6 h time point for each polymerization. All polymerizations were carried out at [Monomer] = 17 v/v%.

9.5.2. Effect of Initial [M]/[CTA] Ratio

An additional factor that we expected to affect RAFT transfer-to polymerization was the initial [M]/[CTA] ratio. Typically, the initial [M]/[CTA] ratio used during RAFT determines the polymer MW.[34] For bottlebrush polymer synthesis by RAFT transfer-to, the MW of the bottlebrush polymer side-chains depends on the [M]/[CTA] ratio, as each repeat unit of the bottlebrush polymer backbone contains a pendant CTA. Holding the DP of **PCTA1** fixed at 50 and using an [AIBN]/[CTA] ratio of 0.2, the [M]/[CTA] ratio was varied between 1000 and 50 over a series of transfer-to polymerizations with styrene as the monomer (Table 9.1, entries 2-6 respectively).

Aliquots were periodically taken from the reaction mixtures and analyzed by SEC (Figure 9.3). It should be noted that the conversions of the polymerizations as measured by ^{1}H NMR spectroscopy varied slightly between experiments due to the different initial conditions employed in each. However, the bottlebrush polymer MWs and dead polymer fractions were less sensitive to conversion than they were to initial reaction conditions, so we chose to compare these parameters as a function of initial conditions for the 6 h time points.

Consistent with traditional RAFT polymerization, decreasing the [M]/[CTA] ratio resulted in lower MW bottlebrushes (293 kDa for [M]/[CTA] = 1000 to 44.0 kDa for [M]/[CTA] = 50). Given that the polymerizations used the same PCTA, this decrease in MW is a result of a decrease in the size of the side-chains. The initial [M]/[CTA] ratio had little effect on the conversion of the polymerizations after 6 h or the Đ values of the resulting bottlebrush polymers.

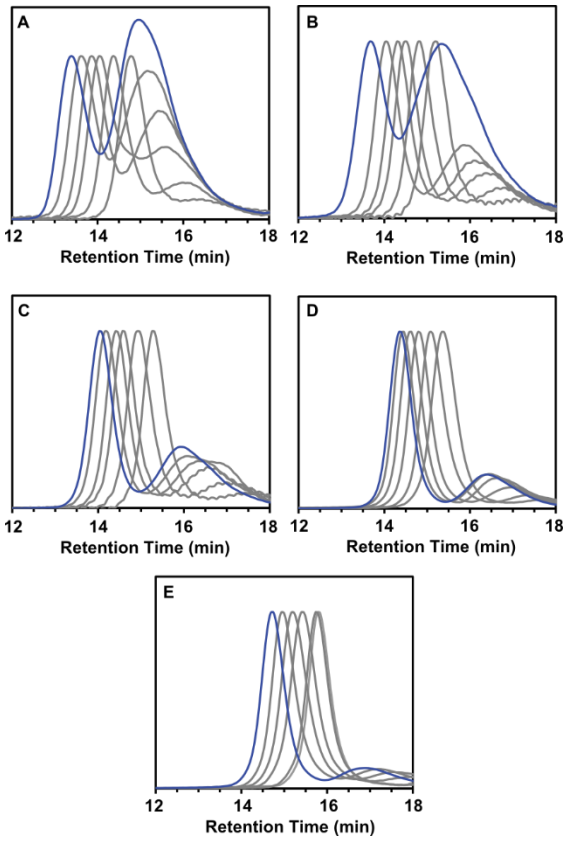

Figure 9.3. Effect of the [M]/[CTA] ratio on RAFT transfer-to polymerization (Table 9.1, entries 2-6), demonstrating that higher [M]/[CTA] ratios lead to higher percentages of dead polymer. Shown above are SEC traces (refractive index detector) at various time points for (A) [M]/[CTA] = 1000, (B) [M]/[CTA] = 750, (C) [M]/[CTA] = 500, (D) [M]/[CTA] = 100, and (E) [M]/[CTA] = 50. The final time point for each sample (blue lines) was taken after 24 h, while the gray traces represent the 1, 2, 4, 6, and 10 h time points. The peak at higher retention time in each trace corresponds to dead linear polymer.

Bottlebrush polymer weight fraction decreased over the course of the polymerizations, with higher [M]/[CTA] ratios yielding more dead polymer impurities (Figure 9S16). The effect of the [M]/[CTA] ratio was visualized by plotting bottlebrush polymer wt fraction as function of initial [M]/[CTA] ratio for the 6 h time points. As shown in Figure 9.4A, bottlebrush polymer weight fraction decreased with increasing [M]/[CTA] ratios. Moreover, the weight fraction of bottlebrush polymer appeared to be negatively correlated with expected side-chain MW (Figure 9S17). We believe that these decreases in bottlebrush polymer weight fraction are likely due to steric factors. Large side-chains have a relatively greater entropic barrier against chain-transfer back to a bottlebrush polymer backbone compared with small chains.[36] Therefore, increasing the [M]/[CTA] ratio led to higher MW side-chains and larger bottlebrush polymers but also resulted a greater percentage of dead chains.

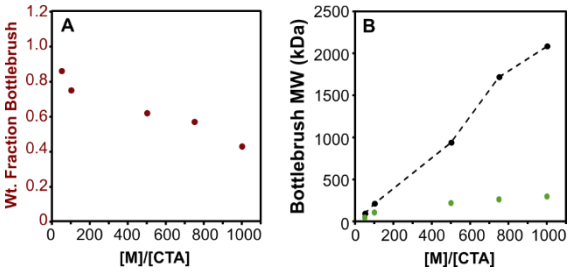

Figure 9.4. Evaluation of bottlebrush polymer weight fraction as a function of [M]/[CTA] ratio at 6 h (Table 9.1, entries 2-6). (A) Bottlebrush polymer weight fraction plotted as a function of [M]/[CTA] ratio. (B) MW of the bottlebrush polymers measured by SEC (green circles) compared to expected MW values calculated using monomer conversions as a function of [M]/[CTA] ratio (black circles).

Bottlebrush polymer MWs were compared to expected values that were calculated using monomer conversions obtained via ^{1}H NMR spectroscopy for the 6 h time points. As shown in Figure 9.4B,

the observed bottlebrush polymer MWs were dramatically lower than expected. This deviation is most apparent at high [M]/[CTA] ratios. Star or bottlebrush polymers prepared by RAFT transfer-to polymerization often possess MWs that are much lower than expected;[37,38] however, the origin of this phenomenon is often attributed to inaccurate determination of MW. Plots of bottlebrush polymer MW vs conversion were linear for each [M]/[CTA] ratio utilized (Figure 9S18); therefore, it is unlikely that the deviations between observed and expected MW values originate from chain-transfer or termination side reactions. Rather, the lower than expected bottlebrush polymer MW values most probably arise as the result of less than perfect grafting densities. For RAFT transfer-to polymerization mediated by **PCTA1**, the grafting density of the bottlebrush polymers likely decreases with increasing [M]/[CTA] ratio, which is consistent with the larger fraction of dead polymers observed at high [M]/[CTA] ratios.

9.5.3. Effect of PCTA Backbone Degree of Polymerization

Next, we investigated the effect of the initial backbone DP of the PCTAs on bottlebrush polymer MW, Đ, and dead polymer quantity. Several different PCTAs were synthesized via ROMP of **CTA1** with backbone DPs of 50, 100, 500, 750, and 1000 (Table 9S1). RAFT transfer-to polymerization was then performed using each of these PCTAs while keeping the [AIBN]/[CTA] ratio constant at 0.2 and the [M]/[CTA] ratio at 50 (Table 9.1, entries 6-10). Time points were taken from each polymerization and analyzed by SEC and ^{1}H NMR spectroscopy. Unsurprisingly, bottlebrush polymer MWs increased as a function of backbone DP, with Đ values remaining low regardless of initial conditions (Figure 9.5). The dead polymer fraction also appeared to increase as a function of backbone DP. For example, RAFT of styrene mediated by a DP = 50 PCTA after 6 h yielded a dead polymer fraction of 24% while the composition of the DP = 1000 sample was 40% dead polymer at a similar conversion. We did not expect a large increase in dead polymer

fraction between these experiments due to the fact that the [M]/[CTA] ratio was held constant at 50 over the series. We observed that the polymerization solutions had become noticeably viscous after ~6 h for the DP = 500, 750, and 1000 samples despite the relatively dilute conditions utilized (17 v/v% monomer). Therefore, we speculate that the observed increase in dead polymer percentage does not arise as a direct result of increasing the backbone DP, but rather due to increased solution viscosity for the higher DP PCTAs.

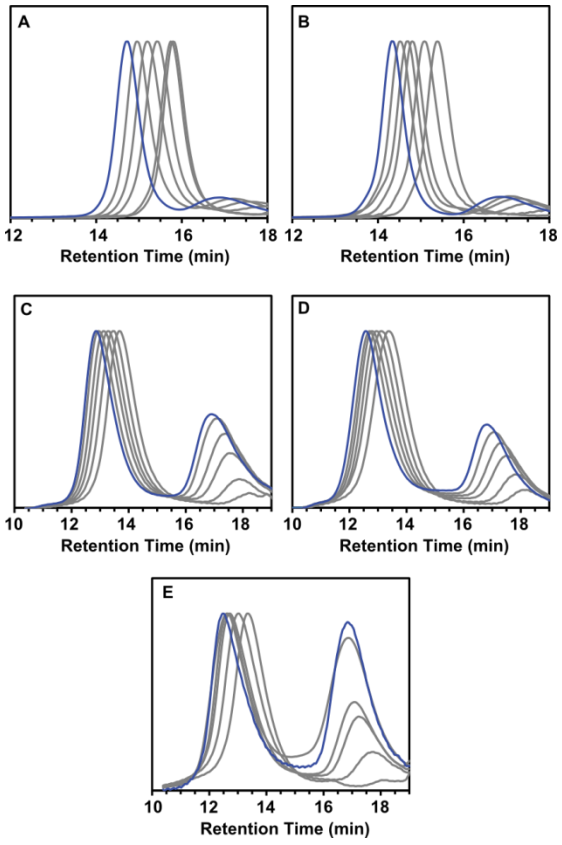

Figure 9.5. Effect of PCTA backbone DP on RAFT transfer-to polymerization (Table 9.1, entries 6-10, demonstrating that higher backbone DPs lead to higher percentages of dead polymer. Shown above are SEC traces (refractive index detector) at various time points for (A) DP = 50, (B) DP = 100, (C) DP = 500, (D) DP = 750, and (E) DP = 1000. The final time point for each sample (blue lines) was taken after 24 h, while the gray traces represent the 1, 2, 4, 6, and 10 h time points. The second population of chains in the traces at lower retention times corresponds to dead polymer.

The weight fraction of bottlebrush polymer decreased with increasing polymerization time, especially for higher DP PCTAs (Figure 9S19). The decrease in bottlebrush polymer wt fraction

observed at longer reaction times may also be the result of increased solution viscosity. An increase in viscosity during RAFT transfer-to polymerization would result in decreased chain transfer efficiency between the polymer radicals and the bottlebrush polymer backbone, leading to uncontrolled polymerization and/or termination of linear polymer chains. However, when comparing the 6 h time points, it appears that the weight fraction of bottlebrush polymer did not depend substantially on the DP of the PCTA backbone (Figure 9.6A).

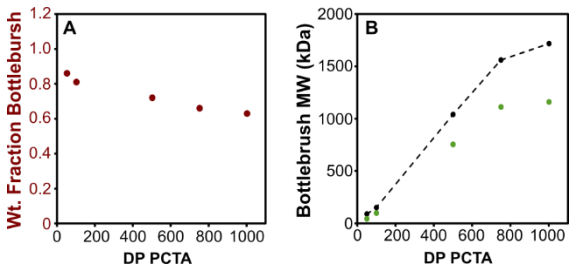

Figure 9.6. Evaluation of bottlebrush polymer sample wt fraction as a function of the DP of the PCTA at 6 h (Table 9.1, entries 6-10). (A) Bottlebrush polymer weight fraction plotted as a function of DP. (B) MW of the bottlebrush polymer measured by SEC (green circles) compared to an expected MW value calculated using monomer conversions as a function of PCTA DP (black circles).

The bottlebrush polymer MWs determined by SEC at the 6 h time points were compared against expected values (Figure 9.6B). In contrast to the experiments in which the [M]/[CTA] ratio was varied (Figure 9.4B), observed and expected MW values were in reasonably good agreement for this data set. Based on these data and the relatively high bottlebrush polymer wt fractions observed for the 6 h time points, we speculate that, in the absence of high viscosity, bottlebrush polymer grafting density does not depend extensively on the DP of the PCTA utilized.

9.5.4. Effect of Monomer Selection

In addition to the parameters above, the choice of vinyl monomer can have a significant influence on how the bottlebrush polymer forms during the transfer-to process. RAFT transfer-to polymerizations were performed on two different monomers—methyl acrylate (MA) and

acryloylmorpholine (ACMO)—using **PCTA1** and similar polymerization conditions (Table 9.1, entries 11 and 12). The rate constants of propagation (k_p) of these monomers are at least an order of magnitude greater than styrene.[35] Given that the addition of a RAFT CTA to a polymerization reaction does not alter the concentration of radicals in solution, this trend in propagation rates is expected to hold regardless of the RAFT agent used or its concentration.[39] Therefore, polymerizations of MA and ACMO should experience fewer termination events than styrene, all other things being equal. Based on this knowledge, we hypothesized that transfer-to polymerization of MA or ACMO would provide bottlebrush polymers with high MW, high bottlebrush polymer purity, and a low quantity of dead polymer chains. Indeed, both of these transfer-to bottlebrush polymer syntheses reached near complete conversion in 6 h. The increase in k_p when using MA or ACMO relative to styrene allowed for the synthesis of large MW bottlebrush polymers (Figure 9.7) with high bottlebrush polymer weight fractions (Figure 9.8), implying high grafting density of the MA and ACMO bottlebrushes. Based on these results, it is clear that bottlebrush polymer synthesis by RAFT transfer-to using **PCTA1** is particularly well suited for polymerizing acrylate or acrylamide monomers.

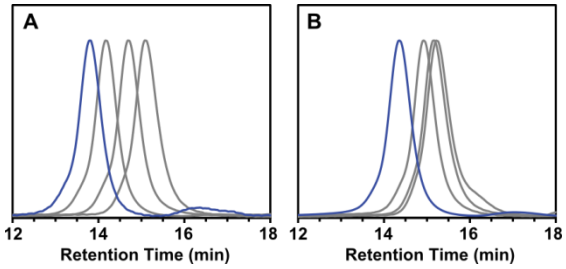

Figure 9.7. Effect of monomer on RAFT transfer-to polymerization (Table 9.1, entries 11 and 12). Shown above are SEC traces (refractive index detector) at various time points for RAFT transfer-to of (A) MA and (B) ACMO. The final time point for each sample (blue lines) was taken after 6 h, while the gray traces represent the 1, 2, and 4 h time points.

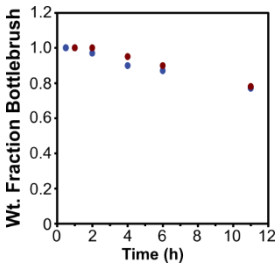

Figure 9.8. Change in bottlebrush polymer weight fraction over time for RAFT transfer-to polymerizations conducted with MA (blue circles) or ACMO (red circles).

9.6. Conclusions

The effect of radical initiator loading, [M]/[CTA] ratio, backbone DP, and monomer type were studied in RAFT transfer-to bottlebrush polymer synthesis with the goal of a polymerization that yielded high MW bottlebrush polymers of narrow dispersity with few dead linear chains. A low initial [M]/[CTA] ratio led to the formation of a bottlebrush polymer with few dead linear chains; however, this also restricted its MW. As the [M]/[CTA] ratio was increased, a greater fraction of dead linear chains was observed. The DP of the PCTA did not directly affect the population of dead linear chains; however, the use of large backbones resulted in high MW polymers but also noticeably viscous reaction mixtures, which eventually led to an increase in the amount of dead linear polymer compared with lower DP PCTAs. The type of monomer had a dramatic effect on RAFT transfer-to polymerization. Compared with styrene, faster polymerizations and lower percentages of dead linear chains were generated when transfer-to polymerizations were carried out with MA or ACMO (high k_p monomers). Based on these results, we propose that for RAFT transfer-to polymerization, monomer choice and the initial [M]/[CTA] ratio are critically important considerations. High k_p monomers are expected to perform well due to reduced termination. The size of the side-chains determines the MW of the final bottlebrush polymer and the dead polymer fraction due to steric factors and likely affects the grafting density of the bottlebrush polymers as

well. These insights may aid efforts toward fully realizing the potential of the transfer-to technique in bottlebrush polymer synthesis.

9.7. References

(1) Pakula, T.; Zhang, Y.; Matyjaszewski, K.; Lee, H.-i.; Boerner, H.; Qin, S.; Berry, G. C. *Polymer* **2006**, *47*, 7198.

(2) Matyjaszewski, K.; Tsarevsky, N. V. *Nat Chem* **2009**, *1*, 276.

(3) Miyake, G. M.; Piunova, V. A.; Weitekamp, R. A.; Grubbs, R. H. *Angew. Chemie. Int. Ed.* **2012**, *51*, 11246.

(4) Sveinbjörnsson, B. R.; Weitekamp, R. A.; Miyake, G. M.; Xia, Y.; Atwater, H. A.; Grubbs, R. H. *PNAS* **2012**, *109*, 14332.

(5) Yu, Y.; Chen, C.-K.; Law, W.-C.; Mok, J.; Zou, J.; Prasad, P. N.; Cheng, C. *Mol. Pharm.* **2013**, *10*, 867.

(6) Johnson, J. A.; Lu, Y. Y.; Burts, A. O.; Lim, Y.-H.; Finn, M. G.; Koberstein, J. T.; Turro, N. J.; Tirrell, D. A.; Grubbs, R. H. *J. Am. Chem. Soc.* **2010**, *133*, 559.

(7) Grigoriadis, C.; Nese, A.; Matyjaszewski, K.; Pakula, T.; Butt, H.-J.; Floudas, G. *Macromol. Chem. Phys.* **2012**, *213*, 1311.

(8) Pietrasik, J.; Sumerlin, B. S.; Lee, H.-i.; Gil, R. R.; Matyjaszewski, K. *Polymer* **2007**, *48*, 496.

(9) Pesek, S. L.; Li, X.; Hammouda, B.; Hong, K.; Verduzco, R. *Macromolecules* **2013**, *46*, 6998.

(10) Sheiko, S. S.; Sumerlin, B. S.; Matyjaszewski, K. *Prog. Polym. Sci.* **2008**, *33*, 759.

(11) Moad, G.; Rizzardo, E.; Thang, S. H. *Acc. Chem. Res.* **2008**, *41*, 1133.

(12) Bielawski, C. W.; Grubbs, R. H. *Prog. Polym. Sci.* **2007**, *32*, 1.

(13) Xia, Y.; Kornfield, J. A.; Grubbs, R. H. *Macromolecules* **2009**, *42*, 3761.

(14) Radzinski, S. C.; Foster, J. C.; Matson, J. B. *Polym. Chem.* **2015**, *6*, 5643.

(15) N'Guyen, D. A.; Leroux, F.; Montembault, V.; Pascual, S.; Fontaine, L. *Polym. Chem.* **2016**, *7*, 1730.

(16) Bolton, J.; Rzayev, J. *ACS Macro Lett.* **2012**, *1*, 15.

(17) Li, Z.; Zhang, K.; Ma, J.; Cheng, C.; Wooley, K. L. *J. Poly. Sci. Part A: Polym. Chem.* **2009**, *47*, 5557.

(18) Dalsin, S. J.; Hillmyer, M. A.; Bates, F. S. *ACS Macro Lett.* **2014**, *3*, 423.

(19) Hernández-Guerrero, M.; Davis, T. P.; Barner-Kowollik, C.; Stenzel, M. H. *Eur. Polym. J.* **2005**, *41*, 2264.

(20) Radzinski, S. C.; Foster, J. C.; Chapleski, R. C.; Troya, D.; Matson, J. B. *J. Am. Chem. Soc.* **2016**, *138*, 6998.

(21) Sumerlin, B. S.; Neugebauer, D.; Matyjaszewski, K. *Macromolecules* **2005**, *38*, 702.

(22) Barner, L.; Davis, T. P.; Stenzel, M. H.; Barner-Kowollik, C. *Macromol. Rapid Commun.* **2007**, *28*, 539.

(23) Sumerlin, B. S. *ACS Macro Letters* **2012**, *1*, 141.

(24) Stenzel, M. H.; Zhang, L.; Huck, W. T. S. *Macromolecular Rapid Communications* **2006**, *27*, 1121.

(25) Stenzel, M. H.; Davis, T. P.; Fane, A. G. *J. Mater. Chem.* **2003**, *13*, 2090.

(26) Barner-Kowollik, C.; Davis, T. P.; Stenzel, M. H. *Aust. J. Chem.* **2006**, *59*, 719.

(27) Boschmann, D.; Mänz, M.; Fröhlich, M. G.; Zifferer, G.; Vana, P. In *Controlled/Living Radical Polymerization: Progress in RAFT, DT, NMP & OMRP*; American Chemical Society: 2009; Vol. 1024, p 217.

(28) Mayadunne, R. T. A.; Jeffery, J.; Moad, G.; Rizzardo, E. *Macromolecules* **2003**, *36*, 1505.

(29) Love, J. A.; Morgan, J. P.; Trnka, T. M.; Grubbs, R. H. *Angew. Chem., Int. Ed.* **2002**, *41*, 4035.

(30) Liu, J.; Gao, A. X.; Johnson, J. A. *J. Vis. Exp.* **2013**, e50874.

(31) Foster, J. C.; Radzinski, S. C.; Lewis, S. E.; Slutzker, M. B.; Matson, J. B. *Polymer* **2015**, *79*, 205.

(32) Arena, J. V.; Leu, T. M. *J. Chem. Ed.* **1999**, *76*, 867.

(33) Arena, J. V.; Mazzarella, C. R.; Gluodenis, R. J. *J. Chem. Ed.* **1994**, *71*, 483.

(34) Keddie, D. J. *Chem. Soc. Rev.* **2014**, *43*, 496.

(35) Odian, G. *Principles of Polymerization*; 4th ed.; John Wiley & Sons, Inc.: New Jersey, 2004.

(36) Fröhlich, M. G.; Vana, P.; Zifferer, G. *Macromol. Theory Simul* **2007**, *16*, 610.

(37) Boschmann, D.; Edam, R.; Schoenmakers, P. J.; Vana, P. *Polymer* **2008**, *49*, 5199.

(38) Jesberger, M.; Barner, L.; Stenzel, M. H.; Malmström, E.; Davis, T. P.; Barner-Kowollik, C. *J. Poly. Sci. Part A: Polym. Chem.* **2003**, *41*, 3847.

(39) Goto, A.; Sato, K.; Tsujii, Y.; Fukuda, T.; Moad, G.; Rizzardo, E.; Thang, S. H. *Macromolecules* **2001**, *34*, 402.

9.8. Appendix

Table 9S1: PCTA characterization data.

PCTA DP	NMR Conv.	Theo. M_n[a]	M_n (GPC)	Đ (GPC)
50	>99	16,500	17,000	1.09
100	>99	32,900	35,600	1.15
250	>99	82,300	-[b]	-[b]
500	>99	165,000	-[b]	-[b]
750	>99	247,000	-[b]	-[b]
1000	>99	329,000	-[b]	-[b]

[a]Based on M_n = (NMR Conv.)/100 * MW CTA*targeted DP [b]Polymer was not soluble in THF.

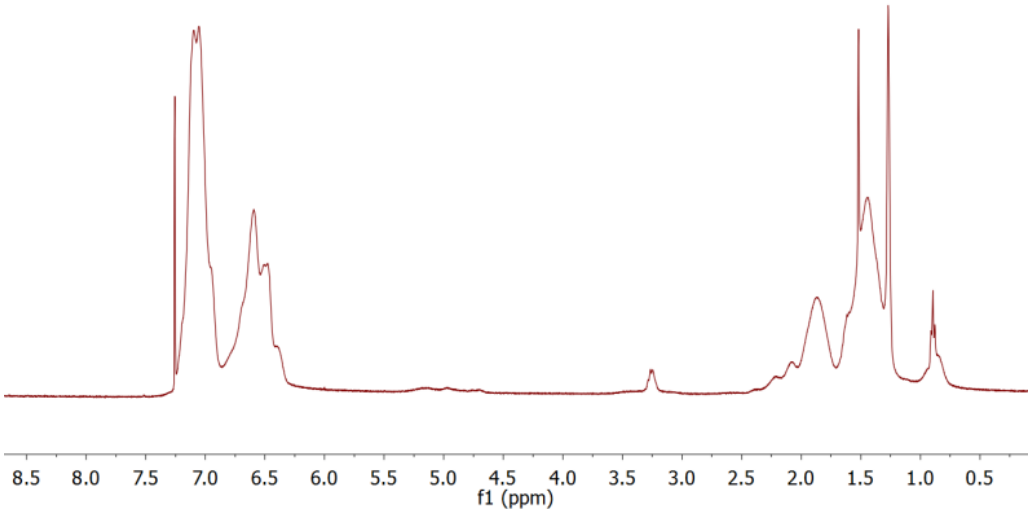

Figure 9S1: Representative ^{1}H NMR spectrum of bottlebrush polymer prepared using styrene as the monomer (Table 9.1, entry 2).

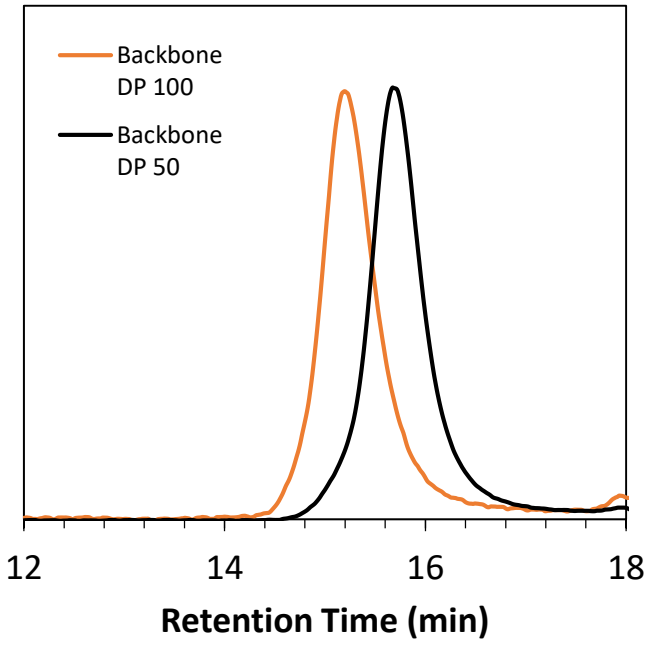

Figure 9S2: SEC traces of backbone PCTA with DP of 50 and 100.

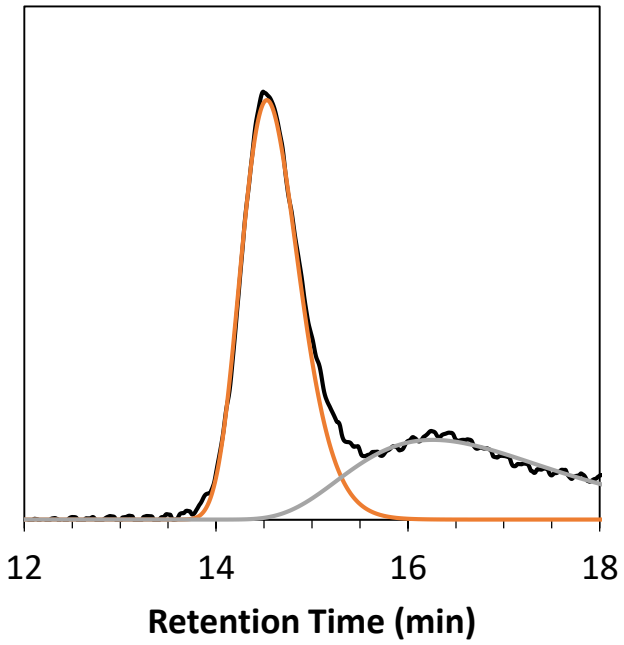

Figure 9S3: SEC trace and peak fit of bottlebrush polymer from Table 9.1, entry 1. The black trace is the raw RI signal obtained via SEC. Red and green traces represent fits of bottlebrush and linear polymer populations, respectively.

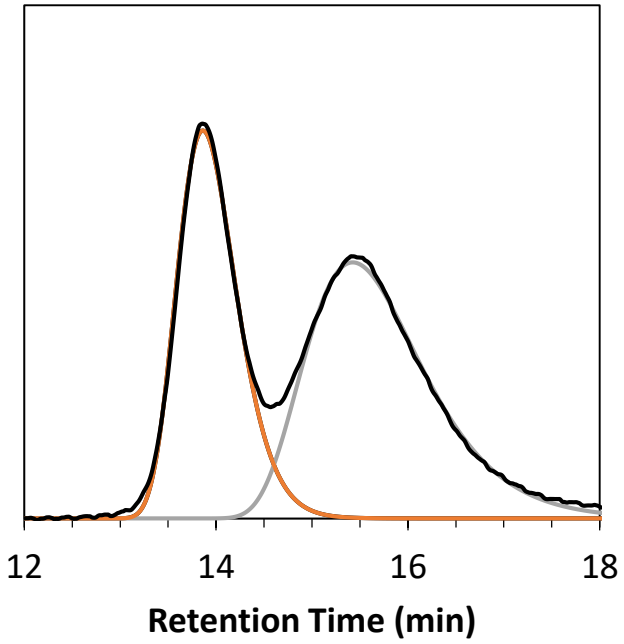

Figure 9S4: SEC trace and peak fit of bottlebrush polymer from Table 9.1, entry 2. The black trace is the raw RI signal obtained via SEC. Red and green traces represent fits of bottlebrush and linear polymer populations, respectively.

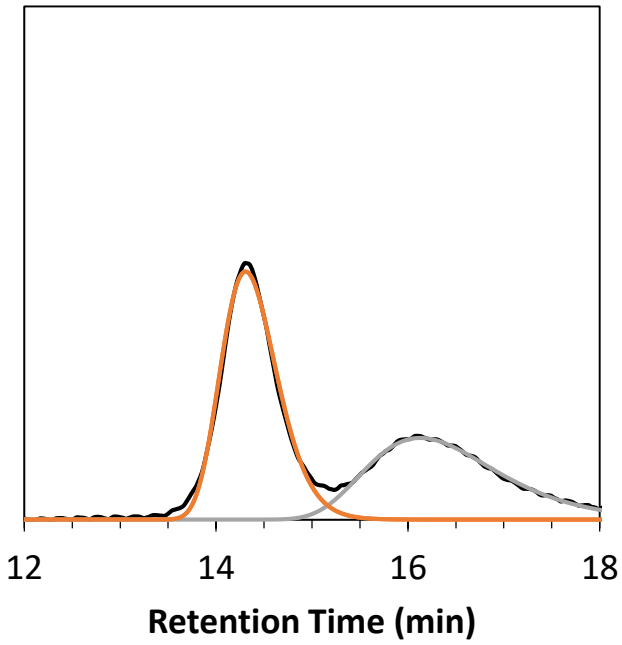

Figure 9S5: SEC trace and peak fit of bottlebrush polymer from Table 9.1, entry 3. The black trace is the raw RI signal obtained via SEC. Red and green traces represent fits of bottlebrush and linear polymer populations, respectively.

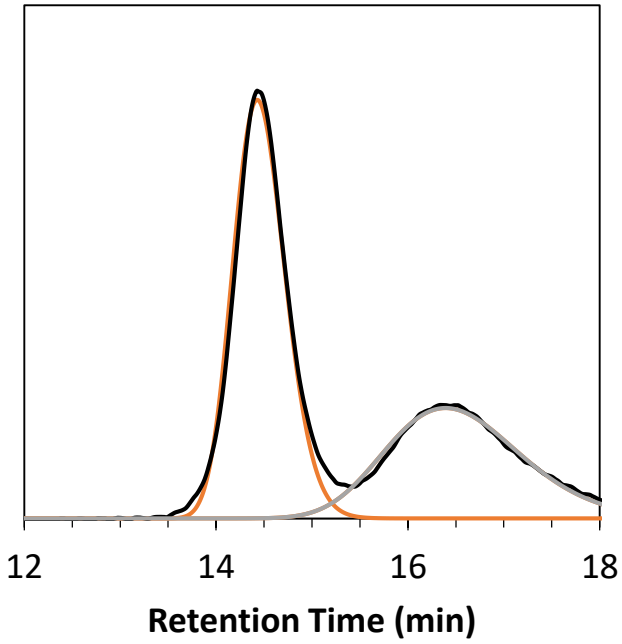

Figure 9S6: SEC trace and peak fit of bottlebrush polymer from Table 9.1, entry 4. The black trace is the raw RI signal obtained via SEC. Red and green traces represent fits of bottlebrush and linear polymer populations, respectively.

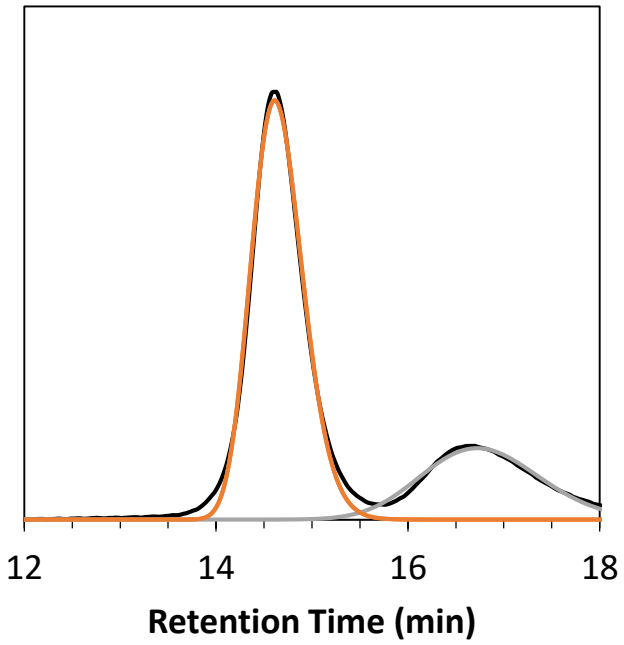

Figure 9S7: SEC trace and peak fit of bottlebrush polymer from Table 9.1, entry 5. The black trace is the raw RI signal obtained via SEC. Red and green traces represent fits of bottlebrush and linear polymer populations, respectively.

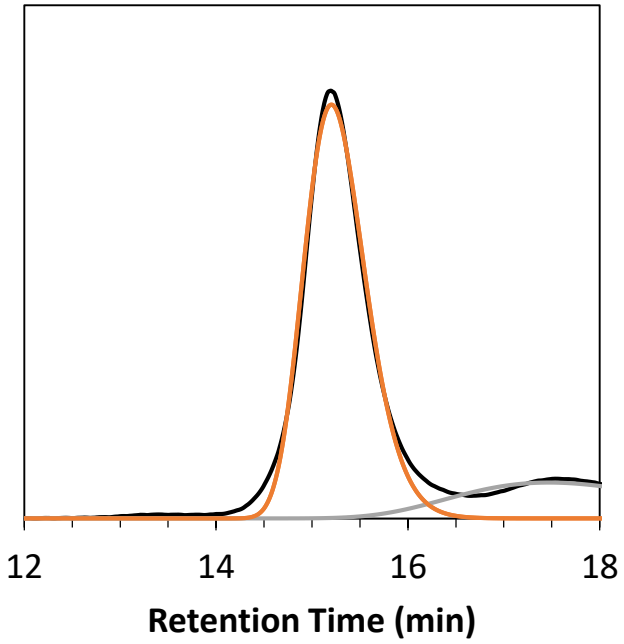

Figure 9S8: SEC trace and peak fit of bottlebrush polymer from Table 9.1, entry 6. The black trace is the raw RI signal obtained via SEC. Red and green traces represent fits of bottlebrush and linear polymer populations, respectively.

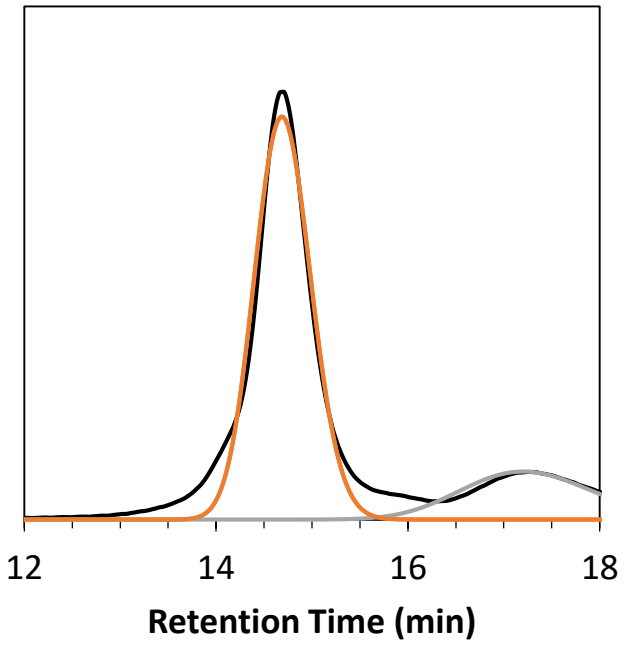

Figure 9S9: SEC trace and peak fit of bottlebrush polymer from Table 9.1, entry 7. The black trace is the raw RI signal obtained via SEC. Red and green traces represent fits of bottlebrush and linear polymer populations, respectively.

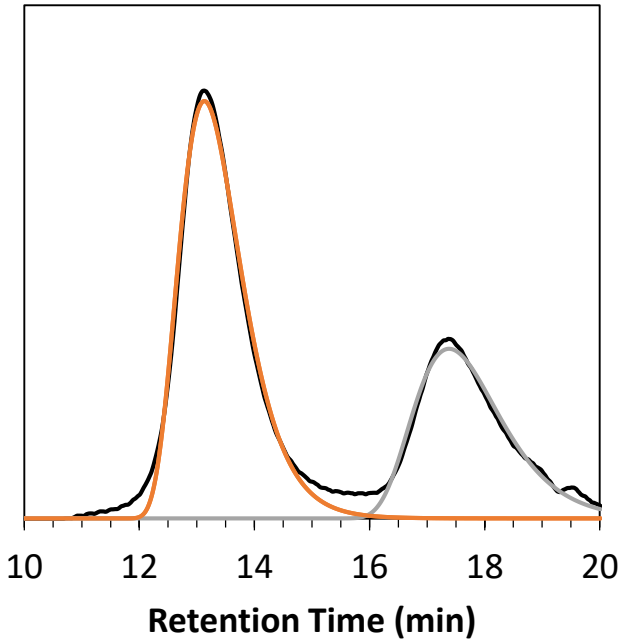

Figure 9S10: SEC trace and peak fit of bottlebrush polymer from Table 9.1, entry 8. The black trace is the raw RI signal obtained via SEC. Red and green traces represent fits of bottlebrush and linear polymer populations, respectively.

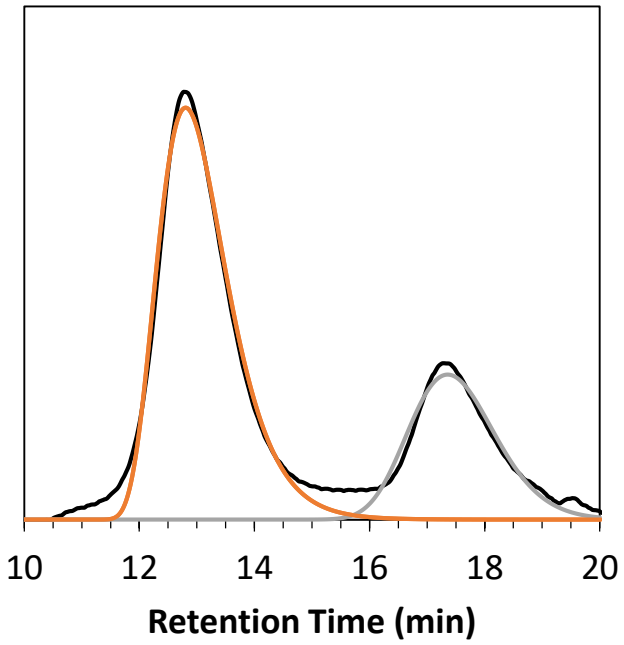

Figure 9S11: SEC trace and peak fit of bottlebrush polymer from Table 9.1, entry 9. The black trace is the raw RI signal obtained via SEC. Red and green traces represent fits of bottlebrush and linear polymer populations, respectively.

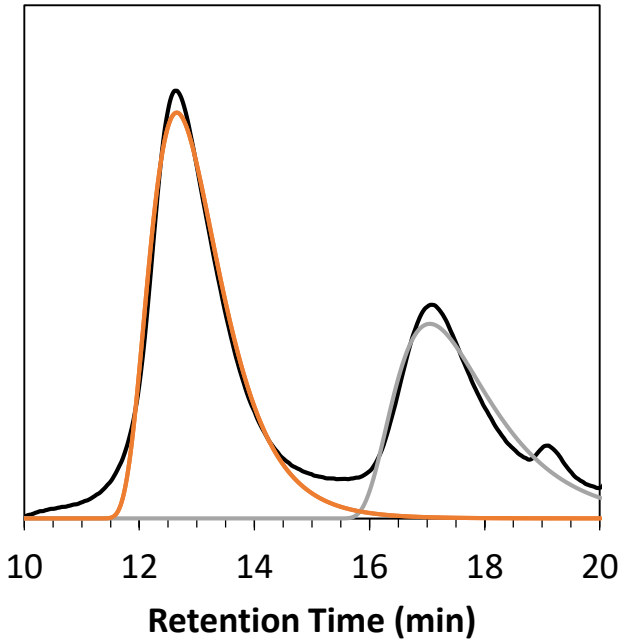

Figure 9S12: SEC trace and peak fit of bottlebrush polymer from Table 9.1, entry 10. The black trace is the raw RI signal obtained via SEC. Red and green traces represent fits of bottlebrush and linear polymer populations, respectively.

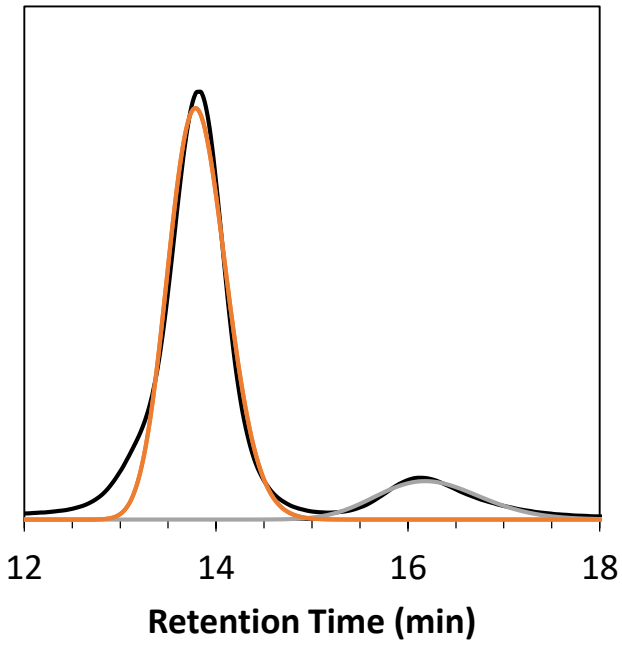

Figure 9S13: SEC trace and peak fit of bottlebrush polymer from Table 9.1, entry 11. The black trace is the raw RI signal obtained via SEC. Red and green traces represent fits of bottlebrush and linear polymer populations, respectively.

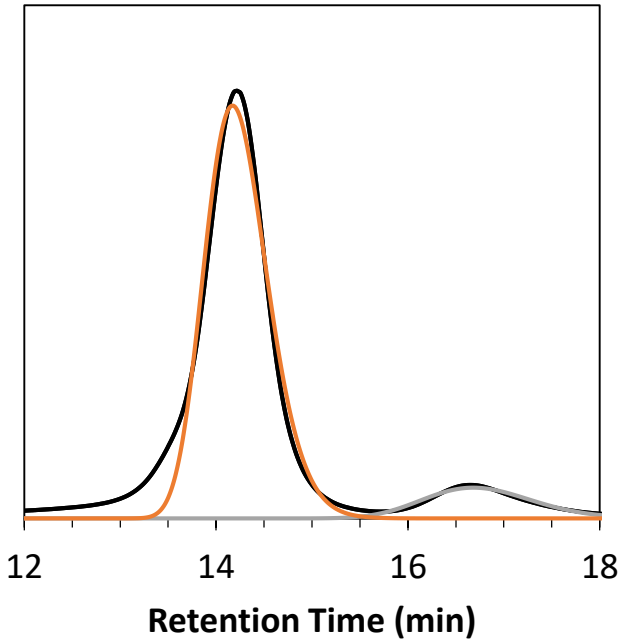

Figure 9S14: SEC trace and peak fit of bottlebrush polymer from Table 9.1, entry 12. The black trace is the raw RI signal obtained via SEC. Red and green traces represent fits of bottlebrush and linear polymer populations, respectively.

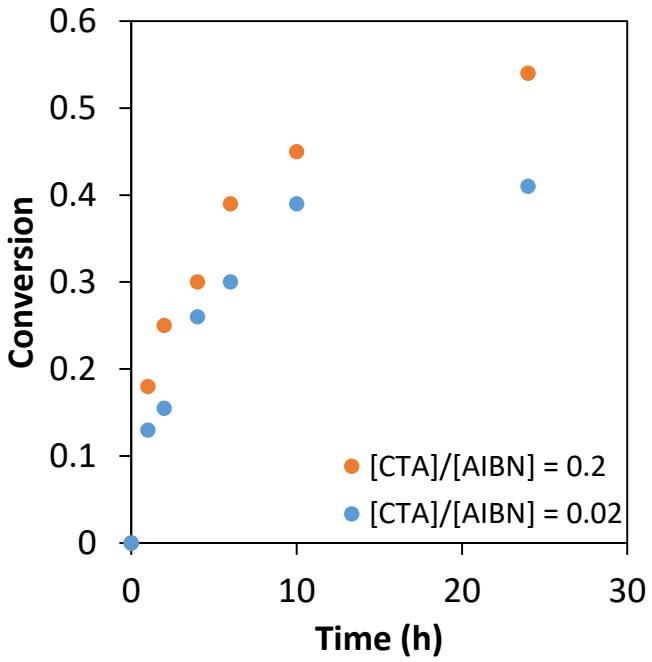

Figure 9S15. Kinetics of RAFT transfer-to polymerization of styrene with different amounts of radical initiator. Polymerizations were conducted at [M]/[CTA] = 1000 with different equivalents of AIBN relative to CTA.

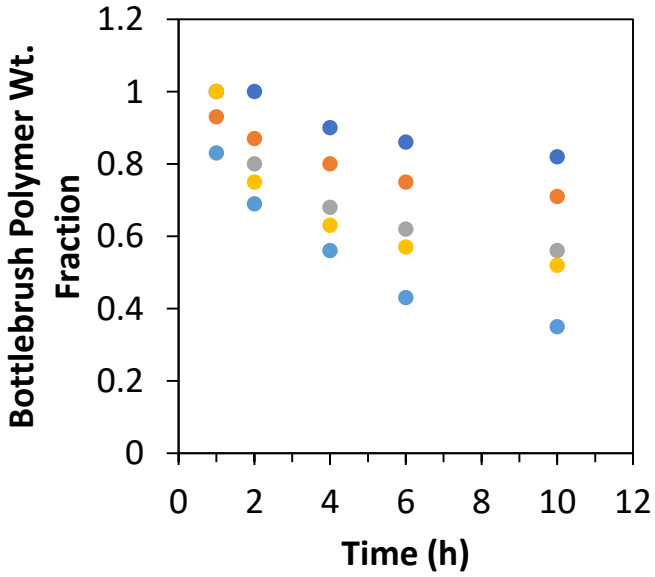

Figure 9S16. Change in bottlebrush weight fraction over time for polymerizations conducted with [M]/[CTA] = 1000 (dark blue circles), 750 (purple circles), 500 (green circles), 100 (red circles), and 50 (light blue circles).

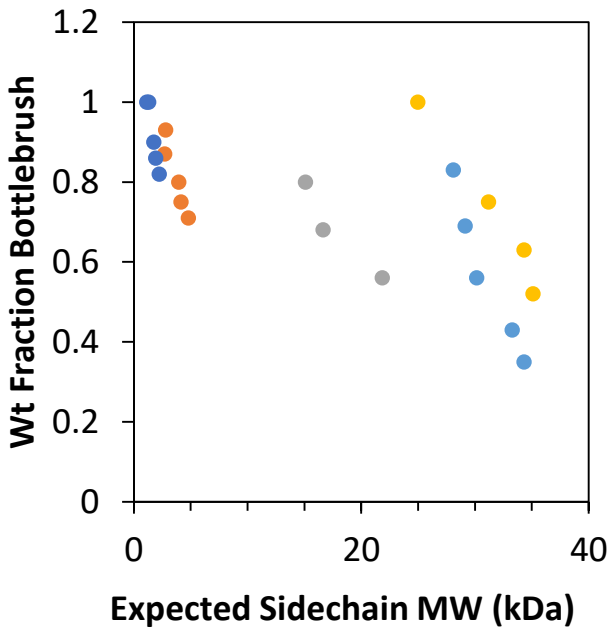

Figure 9S17. Relationship between expected sidechain molecular weight, calculated using the equation $MW_{sidechains} = conv * \frac{[M]}{[CTA]} * MW_{styrene}$, and the bottlebrush polymer sample composition based on area under the curves of the SEC traces at each time point for polymerizations conducted with [M]/[CTA] = 1000 (dark blue circles), 750 (purple circles), 500 (green circles), 100 (red circles), and 50 (light blue circles).

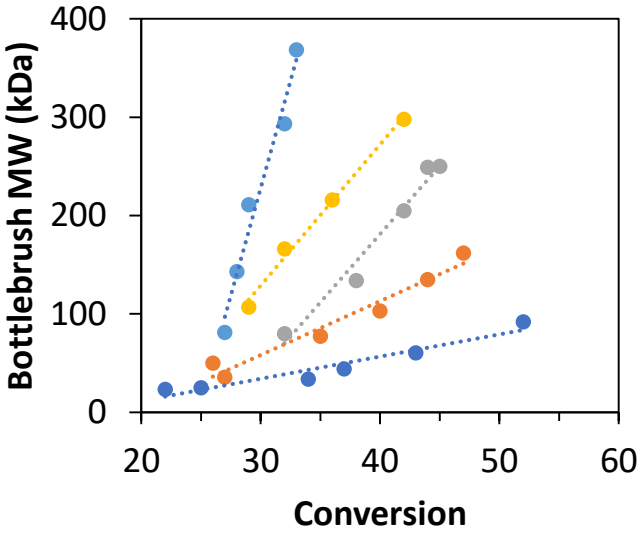

Figure 9S18. MW vs conversion for polymerizations conducted with conducted with [M]/[CTA] = 1000 (dark blue circles), 750 (purple circles), 500 (green circles), 100 (red circles), and 50 (light blue circles). Linear fit lines have been provided as a visual aid.

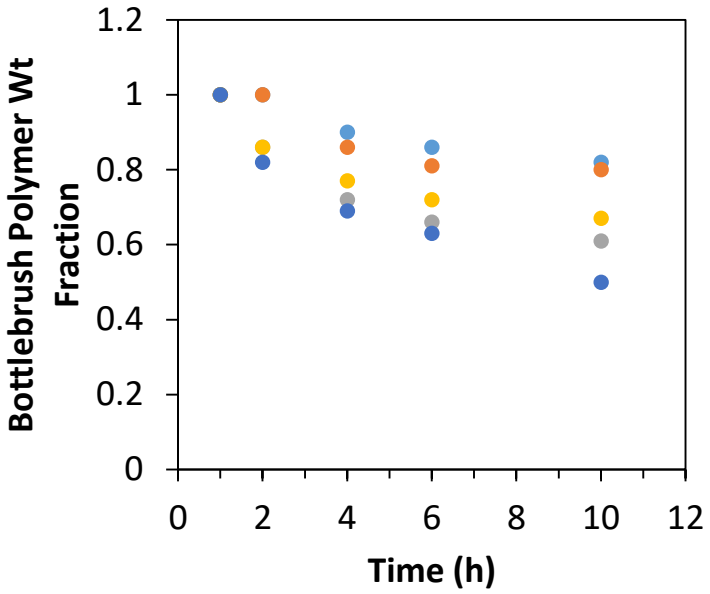

Figure 9S19. Change in bottlebrush polymer weight fraction over time for polymerizations conducted with PCTA DP = 50 (dark blue circles), 100 (purple circles), 500 (green circles), 750 (red circles), and 1000 (light blue circles).

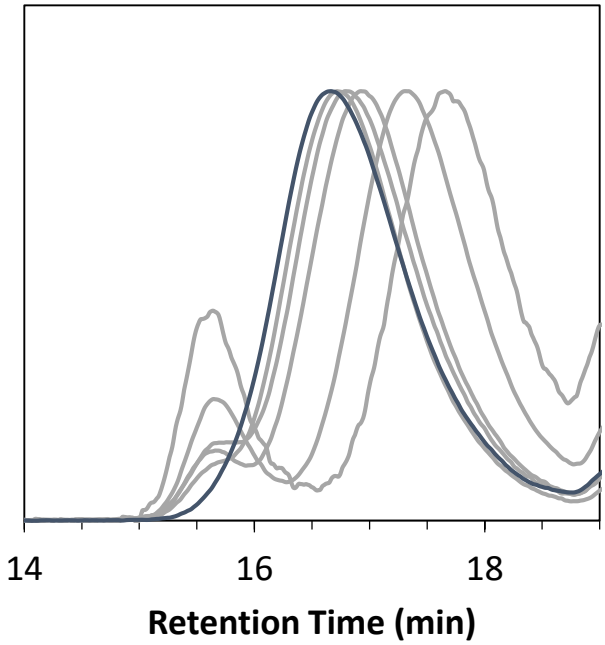

Figure 9S20. SEC traces of aminolyzied bottlebrush polymers from the polymerization denoted as Table 9.1, entry 6 at various time points. The final time point for each run (blue lines) was taken after 24 h. Aminolysis experiments were conducted by adding 0.5 mL of a 40 v/v% solution of methylene in H_2O to a solution of ~100 mg of bottlebrush polymer in 1 mL of THF for each time

point. These mixtures were stirred for a minimum of 48 h under air to ensure complete oxidation of the ω-chain end thiols before the samples were analyzed by SEC.

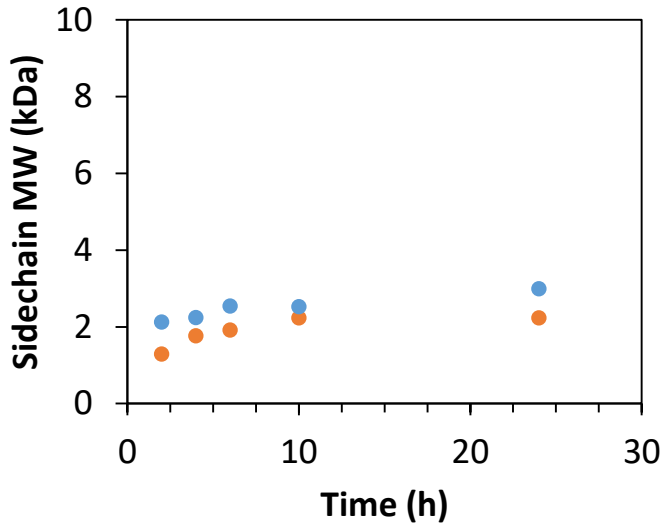

Figure 9S21. Comparison of bottlebrush polymer sidechain MWs calculated from monomer conversions obtained via ^{1}H NMR spectroscopy (red circles) and measured for cleaved sidechains (blue circles) for the polymerization with [M]/[CTA] = 50 and a backbone DP of 50. Sidechains MWs were calculated using the equation $MW_{sidechains} = conv * \frac{[M]}{[CTA]} * MW_{styrene}$.

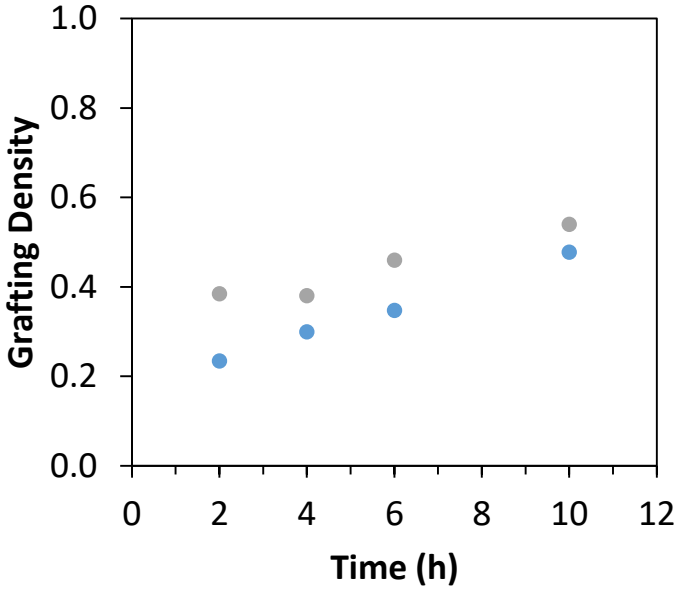

Figure 9S22. Comparison of bottlebrush polymer grafting density calculated by diving the observed MW of the bottlebrush polymer by sidechain MWs calculated from monomer conversions obtained via ^{1}H NMR spectroscopy (green circles) and measured for cleaved sidechains (blue circles) for the polymerization with [M]/[CTA] = 50 and a backbone DP of 50.

Chapter 10. Conclusions and Future Work

A route to synthesizing H_2S-releasing polymeric micelles is described. These H_2S-releasing micelles are selectively toxic to cancer cells and were shown to outperform leading H_2S donor compounds in terms of their cytotoxicity towards cancer cells. The topology of polymers functionalized with H_2S-releasing SATO groups was found to have an impact on the kinetics of H_2S release. Therefore, a study was conducted to optimize the synthesis of bottlebrush polymers using the RAFT transfer-to strategy.

Chapter 3

We synthesized a series of *S*-aroylthiooximes (SATOs) from SATHAs and aldehydes or ketones. We showed that SATOs are relatively hydrolytically stable at pH ~7. We demonstrated that the half-life of H_2S release could be varied between 8–82 min simply by changing the substituent on the SATHA ring.

For future work, we would like to apply thiooxime chemistry to other systems. In preliminary work, we explored additions to the thiooxime bond with allyl bromide to introduce an additional chemical handle for further derivatization. The reduction product was obtained with a conversion (with no optimization) of 73%. The resulting vinyl group could be potentially modified via cross methathesis with a number of internal or pendant olefins using Ru-based catalysts. The success of the allyl bromide addition reaction suggests that additions of other nucleophiles such as Grignard reagents and organ lithium compounds should be possible. These concepts are developed further in Appendix A.

Chapter 4

We demonstrated the RAFT homopolymerization of FBEMA to be a new and effective route toward the preparation of aldehyde-functionalized polymers of controllable M_n and low Đ. The aldehyde functionalities react rapidly and quantitatively with hydroxylamines and hydrazides. For the first time SATOs were formed from polymeric aldehydes. Random copolymers of FBEMA and MEO_2MA were prepared and functionalized via reaction with 3 different SATHAs. These copolymers released H_2S in response to cysteine and glutathione with tunable kinetics consistent with similar small molecule SATOs.

As mentioned in Chapter 4, the kinetics of the H_2S releasing reaction could be controlled by tuning the electronics of the arylthioester ring. Due to the fact that these polymers are water soluble and the kinetics of H_2S release are easily controlled, it would be interesting to evaluate the effect of release rate in a biological capacity.

Chapter 5

We prepared H_2S-releasing micelles based on SATO-functionalized polymer amphiphiles. They were significantly more toxic to HCT116 cells compared to other common H_2S donors. This enhanced toxicity was attributed to the slow H_2S release profile of the micelles. The micelles were well tolerated by healthy NIH/3T3 cells, implying a selectivity in the toxicity of H_2S toward cancer cells.

The micelles released H_2S at a substantially slower rate than the linear SATO-functionalized polymers or small molecule SATOs. In current and future work, we are investigating the effect of polymer glass transition temperature and solution assembly morphology on the rate of diffusion

of the triggering Cys molecules into the SATO micelles as well as how this influences the kinetics of H_2S release.

Chapters 6-8

A novel RAFT CTA with a directly polymerizable Z-group was prepared. This novel CTA controlled polymerization of styrene and nBA. We demonstrated that this CTA could be utilized effectively for transfer-to and grafting-through methodologies. We also prepared two new dithiocarbamate CTAs with Z-groups derived from norbornene imide and the corresponding reduced secondary amine. Based on norbornene imide electronics, it is apparent that only certain alkylating agents can be used to prepare CTAs derived from this Z-group. Reduction of norbornene imide was conducted to prepare a new dithiocarbamate CTA. This CTA provided moderate control over the polymerization of vinyl acetate.

The effect of radical initiator loading, [M]/[CTA] ratio, backbone DP, and monomer type were studied in RAFT transfer-to bottlebrush polymer synthesis. A low initial [M]/[CTA] ratio led to the formation of a bottlebrush polymer with few dead linear chains. As the [M]/[CTA] ratio was increased, a greater fraction of dead linear chains was observed. The DP of the PCTA did not directly affect the population of dead linear chains. The type of monomer had a dramatic effect on RAFT transfer-to polymerization. Compared with styrene, faster polymerizations and lower percentages of dead linear chains were generated when transfer-to polymerizations were carried out with MA or ACMO (high k_p monomers).

Bottlebrush or star polymer synthesis by RAFT transfer-to occurs away from the CTA "core". Due to this fact, new monomer units will always be "inserted" near the CTA core. When making block polymer sidechains/arms, this means that each new block grown will be closer to the CTA core

than the previous. To prepare block polymers using RAFT polymerization, the monomer that forms the most stable radical must be polymerized first (i.e. MMA then MA), otherwise the polymer radical will not add to the monomer. In current and future work, we aim to prepare star-shaped thermoplastic elastomers using n-butyl acrylate (nBA) for the soft block and MMA for the hard block. If MMA is grown first and nBA second using RAFT transfer-to, the star polymers will possess the correct arrangement (with the hard blocks on the outside) to produce a robust TPE.

Appendix A: More Chemistry of Small Molecule Thiooximes

A.1. Effect of Different Acids on Thiooxime Formation

The *S*-aroylthiooxime (SATO) formation reaction was attempted under various conditions using 4-formylbenzoic acid (FBA) as the electrophile, as shown in Scheme A1.

Scheme A1. SATO formation under different conditions.

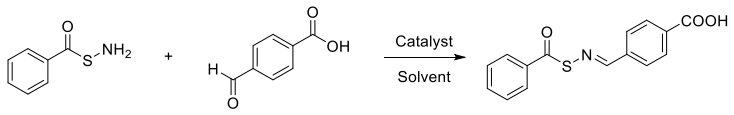

It was found that upon addition of one drop of conc. HCl, a white ppt formed. Moreover, no product formation was observed after 24 h. Addition of HCl to a solution of thiohydroxylamine (THA) alone resulted in immediate precipitation, thus it was concluded that the THA NH_2 became protonoated upon exposure to HCl and that this salt was insoluble in CH_2Cl_2. This same reaction was repeated in DMSO-d_6 and followed by ^{1}H NMR spectroscopy. Product formation was observed, but the product quickly decomposed to starting materials, likely due to hydrolysis. The reaction could also be conducted in the absence of an acid catalyst at 60 °C, though yields were generally lower.

A.2. Reactions of SATOs

A.2.1. Reduction using $NaBH_3CN$

Reduction of SATOs using a reducing agent commonly employed to reduce oximes and hydrazones ($NaBH_3CN$) was attempted as shown in Scheme A2.

Scheme A2. Reduction of SATOs using $NaBH_3CN$.

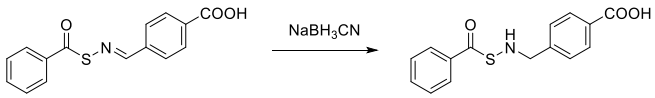

The reaction was conducted according to the following procedure:

Thiooxime (100 mg, 0.35 mmol) was dissolved in 2 mL of a 10% HCl solution in MeOH in a flask. To the flask was added $NaBH_3CN$ (120 mg, 1.9 mmol) in one portion. The reaction mixture was stirred at room temperature for 1 h. The reaction mixture was then rotovapped to remove the excess HCl and MeOH.

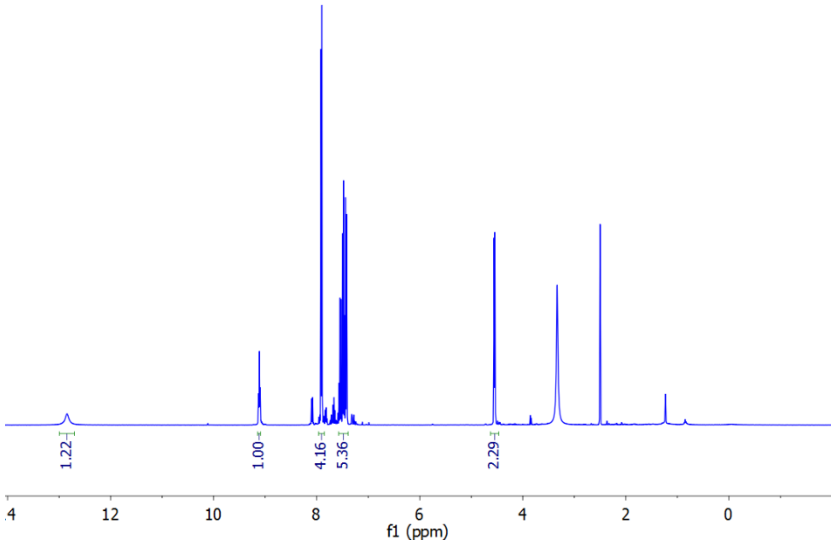

Figure A1. ^{1}H NMR spectrum of crude reaction mixture of reduction of SATO by $NaBH_3CN$.

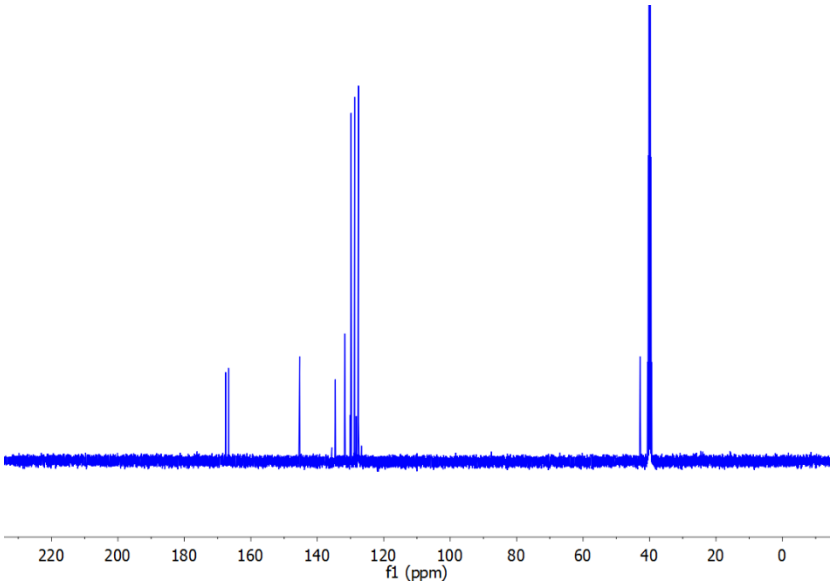

Figure A2. ^{13}C NMR spectrum of crude reaction mixture of reduction of SATO by $NaBH_3CN$.

NMR analysis of the crude reaction mixture does not shown the expected product (Figures A1 and A2). Instead, the NMR spectra indicate that the thioester moiety has been eliminated from the molecule, which has likely been replaced by an amide. Since THAs can undergo an intermolecular reaction with the NH_2 acting as a nucleophile to produce benzamide, it is likely the case that a similar reaction mechanism is in effect here. Indeed, the NMR spectra shown seem to indicate that the following rearrangement has occurred resulting from nucleophilic addition of the NH to the thioester carbonyl:

Scheme A3. Intermolecular rearrangement of reduced SATO.

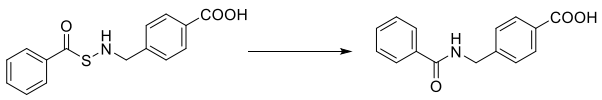

This reaction warrents further investigation. In particular, it would be interesting to investigate the blocking of the rearrangement shown in Scheme A3, perhaps through steric crowing around the nucleophilic NH, or modifications to the thioester ring.

A.2.2. Enolate addition to SATOs.

We also attempted enolate chemistry to modify SATOs. A one-pot, two-step reaction was attempted in which SATO formation was conducted first by mixing THA and FBA in CH_2Cl_2 in the presence of an acid catalyst (Scheme A4). An excess of K_2CO_3 and acetone were then added.

Scheme A4. Addition of acetone enolate to a SATO.

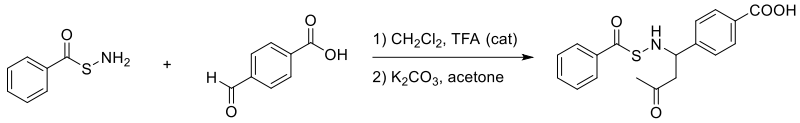

The procedure was as follows:

THA (100 mg, 0.65 mmol) and FBA (99 mg, 0.66 mmol) were dissolved in 2 mL of CH_2Cl_2 in a scintillation vial. A drop of TFA was then added to start the reaction. After 2h, an excess of K_2CO_3 was added in one portion, followed by 2 mL acetone.

NMR analysis of the crude reaction mixture showed promise. In particular, the ^{13}C NMR spectrum showed evidence of the presence of 3 carbonyl resonances with chemical shifts indicative of a ketone, a thioester, and a carboxylic acid (as would be expected for the product shown in Scheme A4) (shown in Figure A3). The ketone was not acetone, as the crude reaction mixture was rotovapped and dried under vacuum. No attempt was made to isolate the product from the crude reaction mixture.

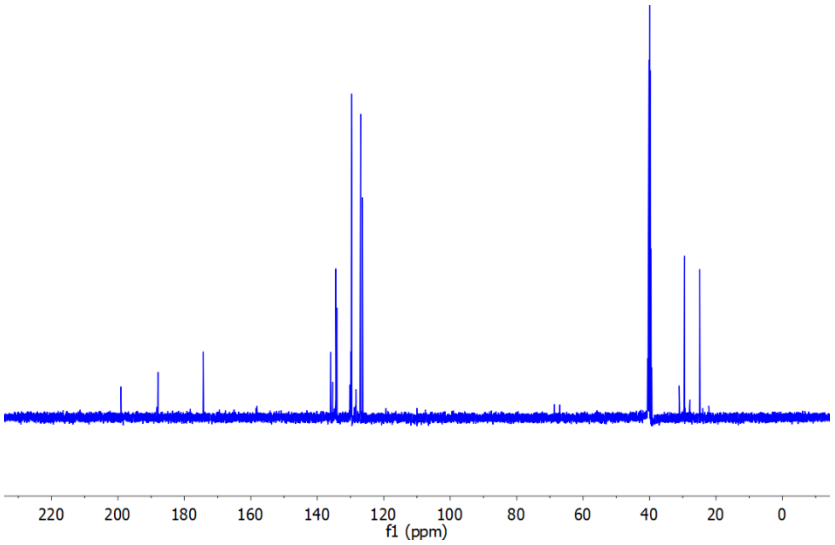

Figure A3. ^{13}C NMR spectrum of crude reaction mixture of reaction between SATO and acetone enolate as depicted in Scheme 11.4.

Further investigation into this reaction and its mechanism are warrented. In addition, the scope of enolate addition to SATOs should be further explored.

A.2.3. Addition of ally bromide to SATOs.

Finally, Zn catalyzed addition of ally bromide to a SATO was carried out. Similar reactions have been reported for oxygen-containing analogues of thiooximes. Toward this end, a SATO was treated with Zn and allyl bromide in the presence of NH_4Cl according to Scheme A5.

Scheme A5. Addition of allyl bromide to a SATO.

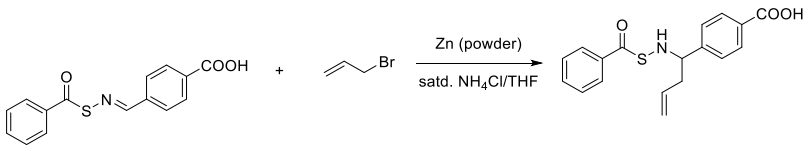

The procedure was as follows:

A vial was charged with SATO (20 mg, 0.083 mmol), zinc powder (19 mg, 0.290 mmol), 300 uL of THF, and 1.5 mL of satd. NH_4Cl soln. Then, 3-bromoprop-1-ene (22 µl, 0.25 mmol) was added

with rapid stirring. The reaction mixture was stirred at rt for 1 h. 3 mL of 2N NaOH and 3 mL of ether were both added to the vial. The organic layer was collected, and the aqueous layer was extracted 2x with ether. The combined ether layers were washed with H_2O and brine, dried over Na_2SO_4, and rotovapped to give the crude product as a colorless oil. ^1H NMR showed a mixutre of the desired product (~85%) and the starting material.

As before, NMR analysis of the crude product showed that the reaction occurred to relatively high conversion, and that the desired product was formed. Resonances at ~40 and ~60, and ~120 ppm in the ^{13}C NMR spectrum correspond to the added methylene and terminal alkene groups (Figure A4). Some starting materials were left over that were not removed from the crude product.

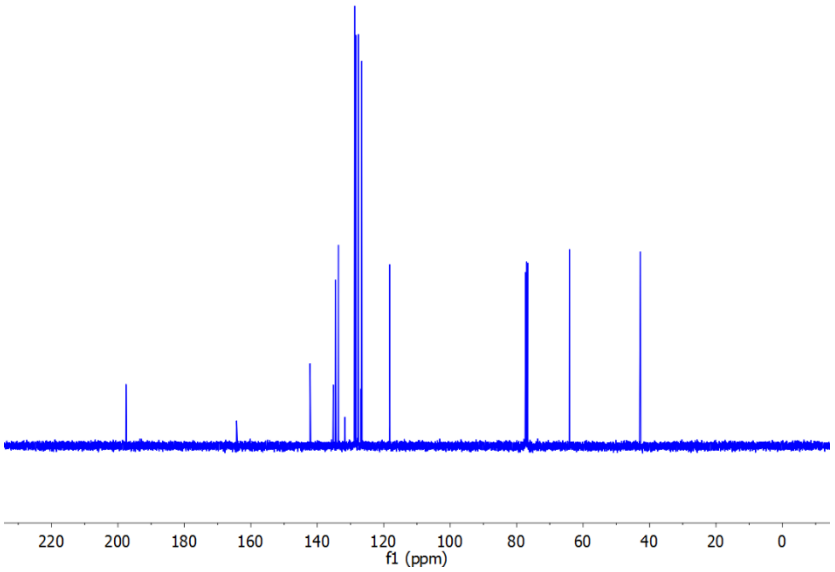

Figure A4. ^{13}C NMR spectrum of the crude reaction mixture following addition of allyl bromide to a SATO.

This reaction should be further investigated. In particular, is the reaction sensitive to the electronics of the aldehyde ring? Can the alkene be utilized in later reactions such as cross metathesis or thiol-ene click? And most importantly, how does this change in structure effect H_2S release?

Appendix B: An Alternative Route to Thiooxime-Functionalized Micelles

S-Aroylthiooxime (SATO)-functionalized micelles prepared by reversible addition-fragmentation chain transfer (RAFT) polymerization were discussed in Chapter 5. We also prepared SATO micelles using other polymerization strategies. One such strategy, in which ring-opening metathesis polymerization (ROMP) is used, is discussed below.

12.1. Synthesis of monomers

SATO-functionalized monomers to be used in ROMP were prepared by two routes that differed in how the SATO functional group was attached to the polymerizable norbornene moiety. Based on this subtle difference, the products of release after reaction of the SATO group with a triggering thiol such as Cys differ. Scheme B1 shows the preparation of a SATO-functionalized ROMP monomer that is attached to the norbornene via the aldehyde. In contrast, the synthesis of a H_2S-releasing ROMP monomer attached via the thiohydroxylamine (THA) is shown in Scheme B2.

Scheme B1. Preparation of ROMP monomer 1.

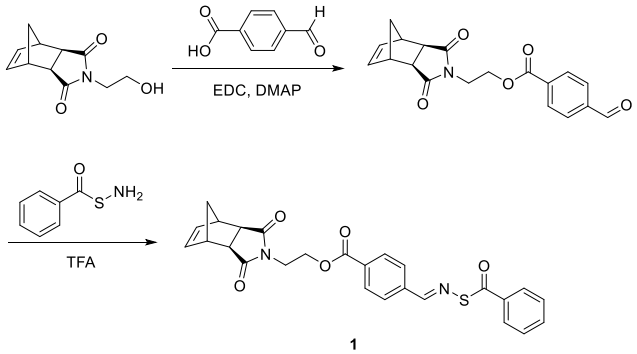

Monomer **1** was prepared according to the following procedures:

Synthesis of NB-Aldehyde

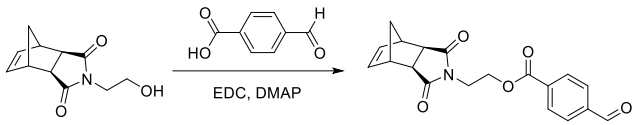

A round bottom flask was charged with NB-OH, FBA, EDC, DMAP, and CH_2Cl_2. The reaction mixture was stirred at rt overnight. The following day, the reaction mixture was washed with 1N HCl (3x), H_2O, satd. $NaHCO_3$ (3x), and brine, dried over Na_2SO_4, and rotovapped. The pure product was obtained as a while solid.

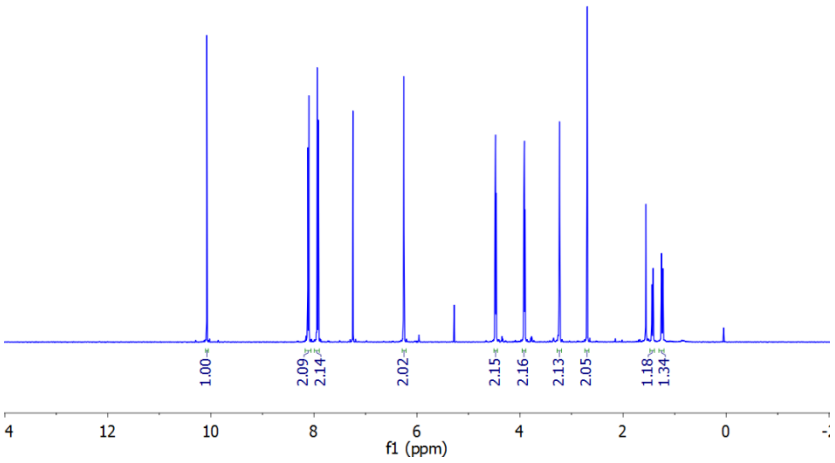

Figure B1. ^{1}H NMR spectrum of NB-Aldehyde.

Synthesis of monomer 1

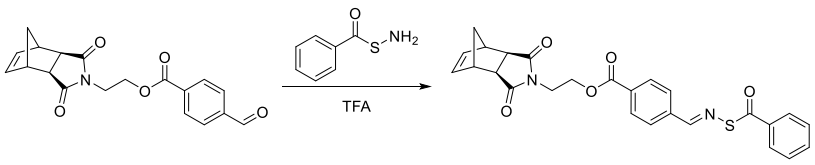

NB-Aldehyde and THA were dissolved in 15 mL of CH_2Cl_2 in a vial. To the vial was added 30 uL of TFA and sieves. The reaction mixture was left to stand at rt for 2 h. The sieves were removed via filtration and the reaction mixture was rotovapped. The pure product was obtained as a white solid.

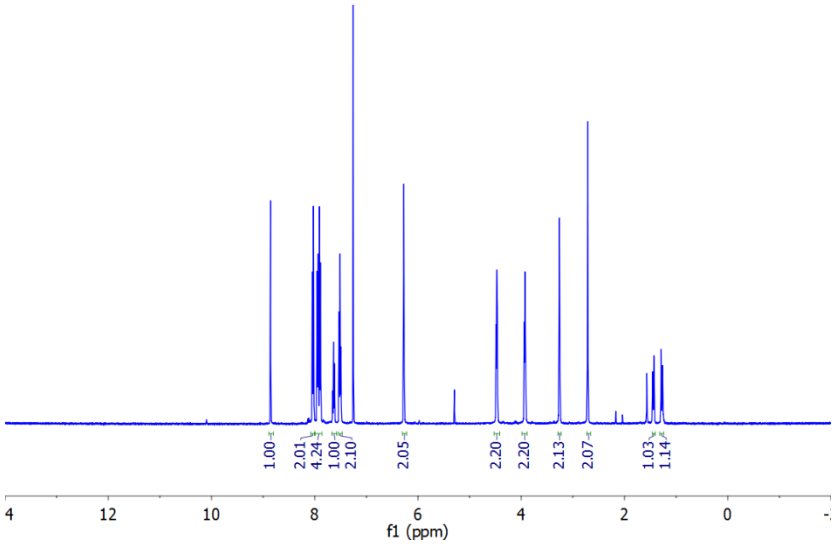

Figure B2. ^{1}H NMR spectrum of monomer 1.

Scheme B2. Preparation of ROMP monomer 2.

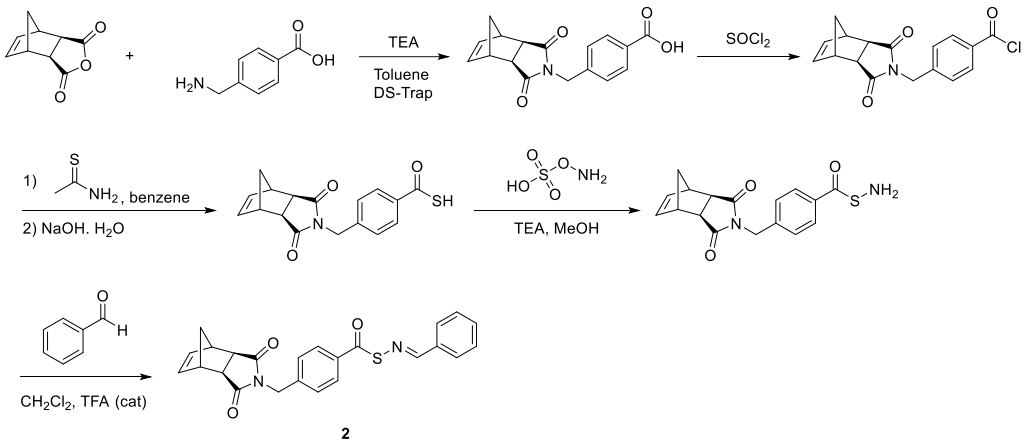

Monomer **2** was prepared according to the following procedures:

Synthesis of NB-COOH

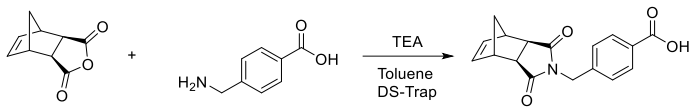

An RBF was charged with NB-anhydride (5.0 g, 31 mmol), 4-aminomethylbenzoic acid (4.8 g, 32 mmol), TEA (0.43 mL, 3.1 mmol), and 60 mL of toluene. The flask was outfitted with a Dean-Stark trap and condenser. The reaction mixture was heated at reflux overnight. The reaction mixture was allowed to cool to rt. It was then concentrated and redissolved in EtOAc. The EtOAc layer was washed with 1N HCl (3x) and brine, dried over Na_2SO4, and rotovapped. The pure product was obtained as a while solid (8.6 g, 95% yield).

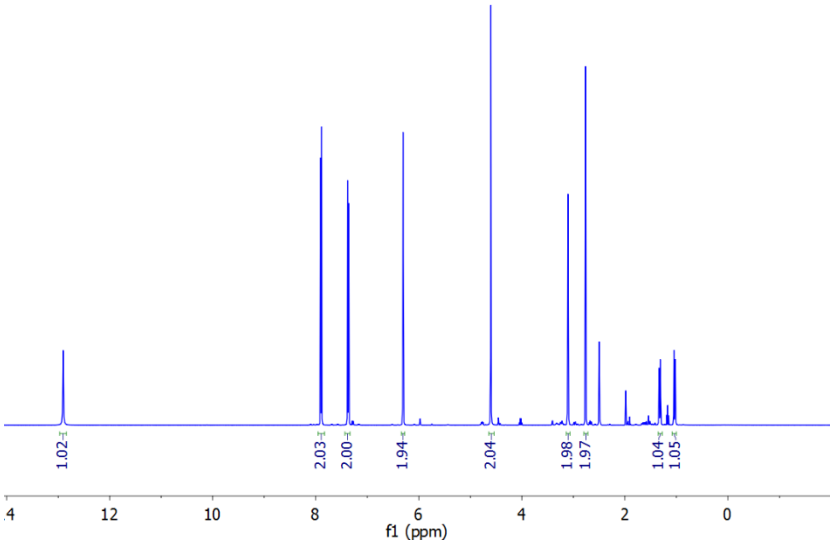

Figure B3. ^{1}H NMR spectrum of NB-COOH.

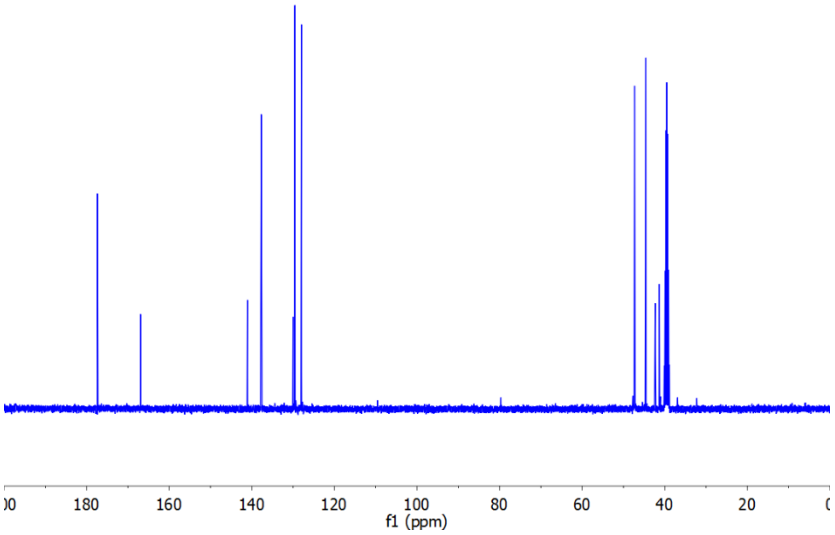

Figure B4. ^{13}C NMR spectrum of NB-COOH.

Synthesis of NB-COCl

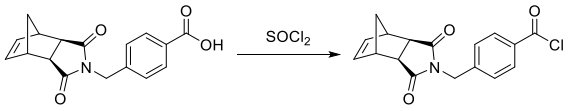

A RBF was charged with NB-COOH (3g, 10.0 mmol) and 12 mL of $SOCl_2$. The flask was fitted with a reflux condenser. The reaction mixture was heated to reflux overnight. The reaction mixture was then cooled to room temperature, and the excess $SOCl_2$ was removed under vacuum. The crude product was used in the next step without further purification.

Synthesis of NB-COSH

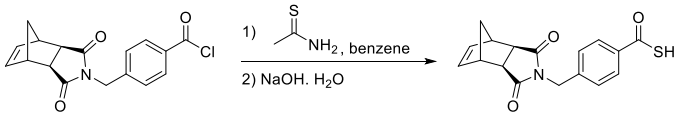

NB-COCl (3.2 g, 11 mmol) was dissolved in 10 mL of benzene with heating. To the flask was added thioacetamide (0.80 g, 11 mmol) in one portion. The reaction mixture was stirred at rt overnight. The following day, 20 mL of 0.5 M NaOH was added, and the reaction mixture was stirred for an

additional 30 min. The precipitating solids were isolated via vacuum filtration and subsequently redissolved in DCM. The DCM soln was washed with satd. $NaHCO_3$ (4x) and brine, dried over Na_2SO_4 and rotovapped to give the pure product as an off-white solid (2.3 g, 71 % yield).

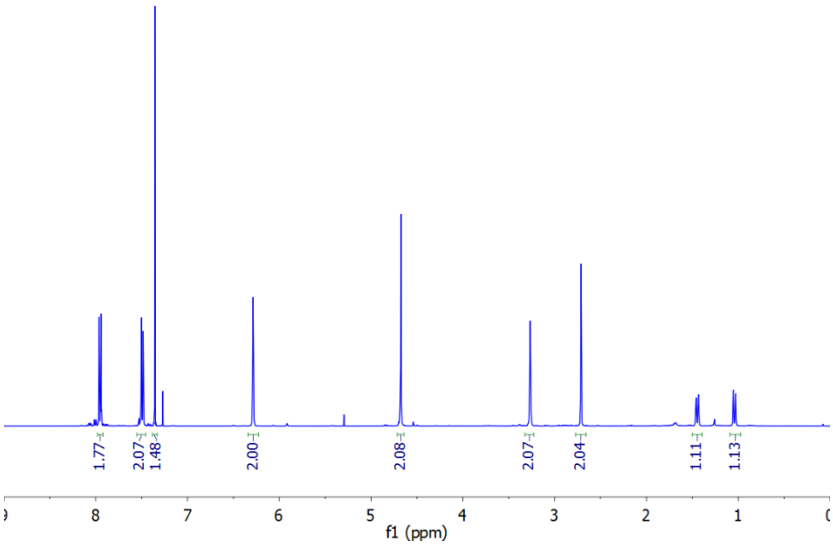

Figure B5. ^{1}H NMR spectrum of NB-COSH.

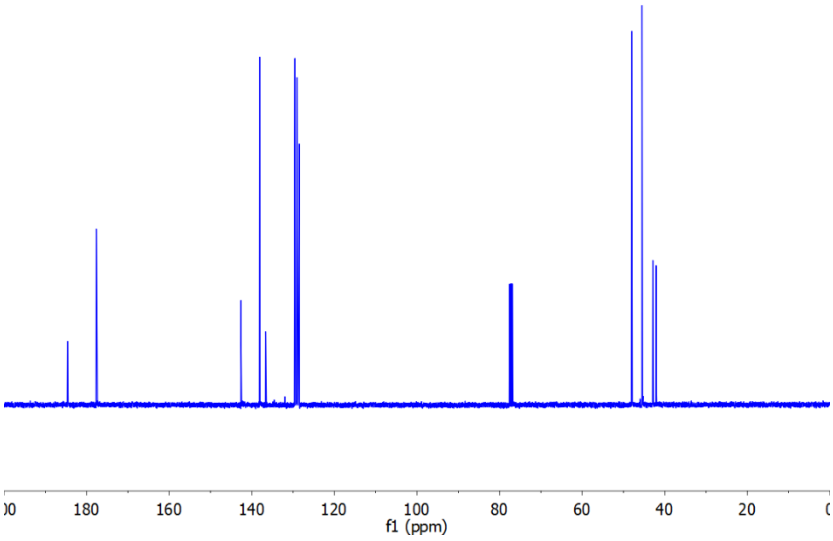

Figure B6. ^{13}C NMR spectrum of NB-COSH.

Syntheis of NB-THA

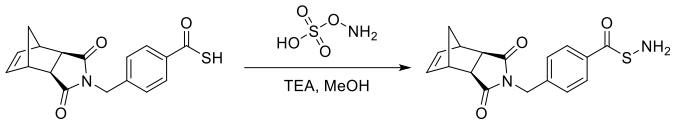

NB-COSH (2.3 g, 7.2 mmol) was dissolved in 20 mL of DCM in a RBF. To the flask was added 2.8 mL of DIEA (2.2 equiv). The flask was submerged in an ice bath. Hydroxylamine-O-sulfonic acid (0.89 g, 7.9 mmol) was then added in one portion at 0 °C. The reaction mixture was stirred at 0 °C for 2 h. The reaction mixture was rotovapped, and the crude product was dry loaded onto a silica column, eluting with 30% EtOAc in hexanes. The pure product was obtained as a white solid (0.57 g, 24% yield).

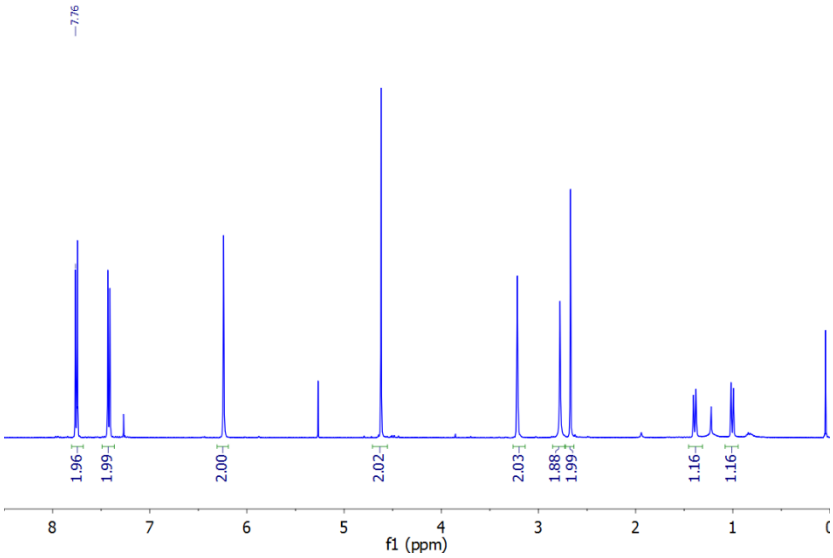

Figure B.7. ^{1}H NMR spectrum of NB-THA.

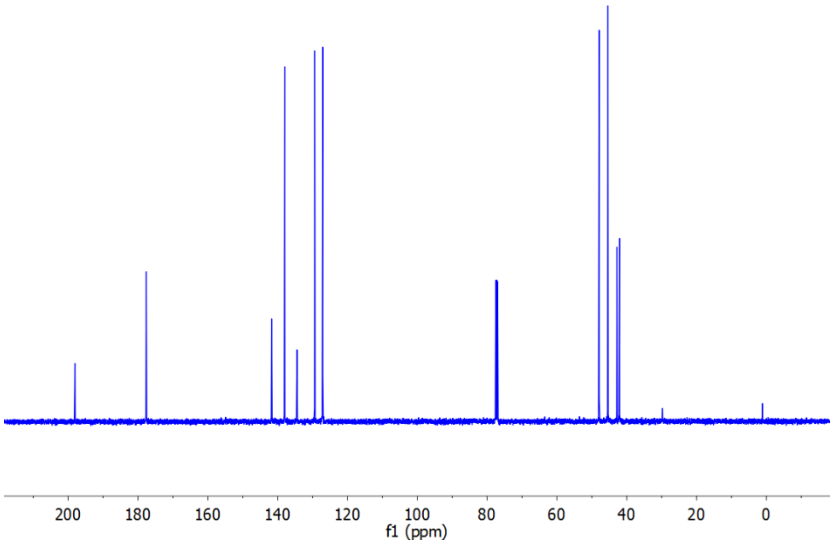

Figure B8. ^{1}H NMR spectrum of NB-THA.

Synthesis of monomer 2

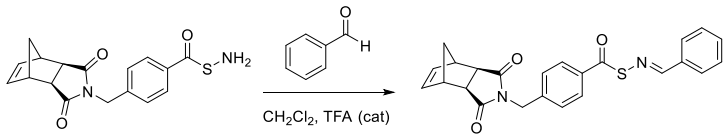

NB-THA (0.23 g, 0.70 mmol) was dissolved in 3 mL of DCM in a scintillation vial. To the vial was added benzaldehyde (0.075 mL, 0.74 mmol) follwed by one drop of TFA and molecular sieves. The reaction mixture was allowed to react for 2 h. The reaction mixture was then filtered and rotovapped. The pure product was obtained as a while solid (0.29 g, 99% yield).

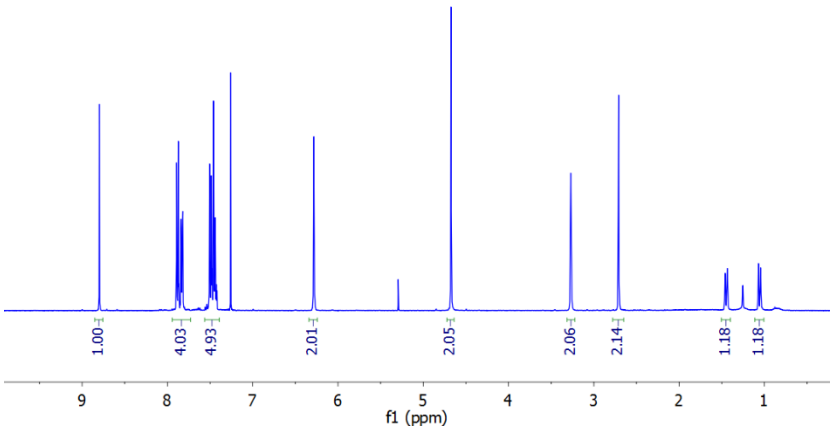

Figure B9. ^{1}H NMR spectrum of monomer 2.

A water-soluble PEG monomer (monomer **3**) was also prepared to be polymerized as the hydrophilic block in the SATO-functionalized polymer amphiphiles. This was prepared in one step via a Mitsunobu reaction according to the following procedure:

Synthesis of monomer 3

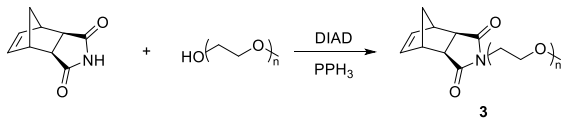

NB-Imide (0.32 g, 1.9 mmol) and PEG (1.1 g, 2.0 mmol, M_n = 550 Da) were dissolved in 10 mL of toluene in a 2-necked RBF. The flask was fitted with a Dean-Stark trap and condenser. The mixture was heated at reflux for 1 h. The reaction mixture was cooled to rt. The Dean-Stark trap was removed and replaced with a rubber septum. To the flask was added 10 mL of dry THF, PPH_3 (0.57 g, 2.2 mmol), and DIAD (0.39 mL, 1.9 mmol) dropwise under N_2 flow. The reaction mixture was stirred at rt overnight. The reaction mixture was then filtered and rotovapped. The crude product was purified on a silica column, eluting with 5% MeOH in CH_2Cl_2. This removed all of

the impurities except Ph_3PO, which co-eluted with the desired product. A second column (gradient from Et_2O to 10% MeOH in CH_2Cl_2) was used to remove this. The pure product was obtained as a colorless oil (0.84 g, 64% yield).

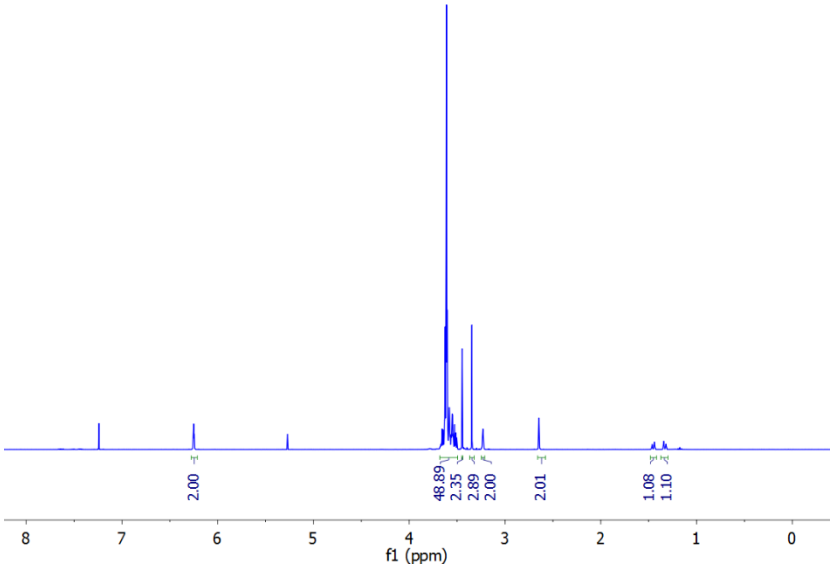

Figure B10. ^{1}H NMR spectrum of monomer 3.

B.2. Polymerization of SATO-functionalized ROMP monomers

With the monomers in hand, amphiphilic block copolymers were prepared using ROMP by adding the monomers sequentially to Grubbs' 3rd generation catalyst in CH_2Cl_2. The polymerizations were terminated with EVE and purified via precipitation from hexanes. The polymers were characterized using NMR and size-exclusion chromatography (SEC). An example polymerization procedure is as follows:

Synthesis of block copolymers

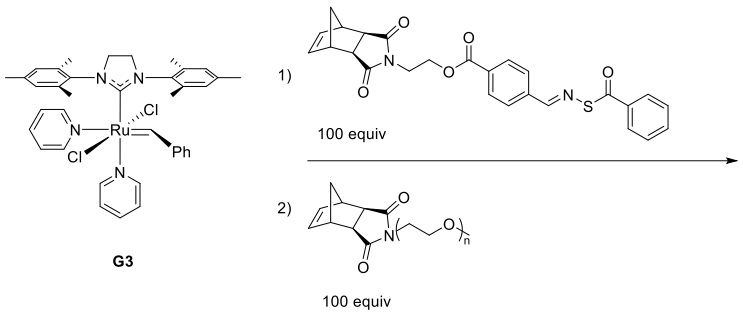

*Monomer **1** (100 equiv) was dissolved in 2 mL of dry CH_2Cl_2 in a vial. To the vial was added a solution of G3 (1 equiv) in 0.5 mL of dry CH_2Cl_2. The reaction mixture was stirred for 20 min at rt. To the vial was added a solution of monomer **3** (1 equiv) in 0.5 mL of dry CH_2Cl_2. The polymerization was then quenched after an additional 40 min via the addition of a few drops of EVE. The polymer was isolated via precipitation from hexanes (91 mg, 76% yield, M_n = 115 kDa, $Đ$ = 1.02).*

B.3. Self-assembly of H_2S-releasing polymers prepared by ROMP

A series of block copolymers were prepared using monomers **1** and **3** with varying hydrophilic to hydrophobic ratios to produce polymers **P1**-**P3**. Micelles were then made using these polymers using the solvent switch method (THF to H_2O) and subsequent dialysis against H_2O. The micelles were characterized using TEM and DLS as shown in Table B1 and Figures B11 and B12.

Table B1. Characterization of polymers P1-P3 and micelles prepared from them.

Polymer	m^a	n^a	$X_m{}^b$	$M_{n,\,theo}{}^c$	$M_{n,}$(kDa)^d	$Đ^d$	d (nm)^e
P1	50	50	0.55	56.8	57.8	1.02	26.1
P2	100	100	0.51	114	115	1.02	54.2
P3	200	200	0.53	227	227	1.03	115

[a]Block DPs were determined from the initial monomer feed ratios assuming full conversion of each block. [b]Weight fraction of PEG monomer. [c]Calculated using the MWs of the monomers and the feed ratio. [d]Absolute MW measured by light scattering. [e]Micelle diameter measured by DLS.

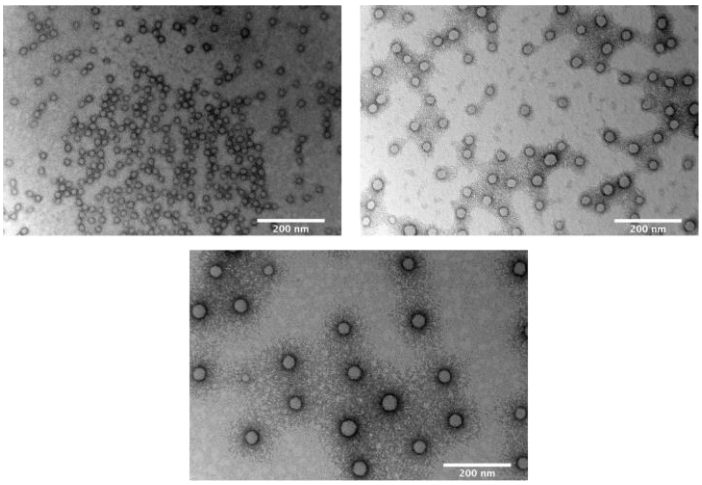

Figure B11. TEM micrographs of micelles prepared from polymers P1 (top left), P2 (top right), and P3 (bottom).

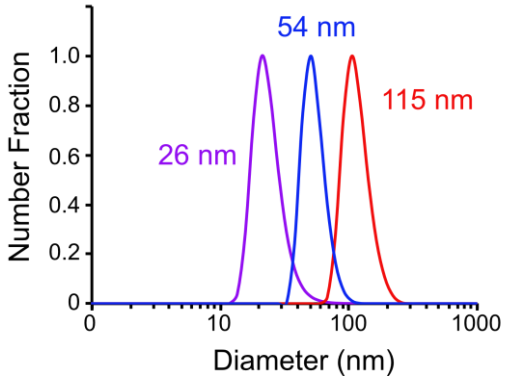

Figure B12. DLS size distributions of micelles prepared from polymers P1 (purple), P2 (blue) and P3 (red).

B.4. H_2S Release from micelles prepared from block polymers synthesized via ROMP

H_2S release from the micelles triggered by Cys was monitored using an H_2S-selective microelectrode. The instantaneous concentration of H_2S was determined from the output current using a calibration curve. As shown in Figure B13, the resulting H_2S concentration profile was compared against a small molecule SATO. It is clear that almost no H_2S is released from the micelles after 60 min. It was hypothesized that, due to the glassy morphology of the micelle cores, the Cys trigger molecules were unable to effectively diffuse into the micelles to trigger H_2S release.

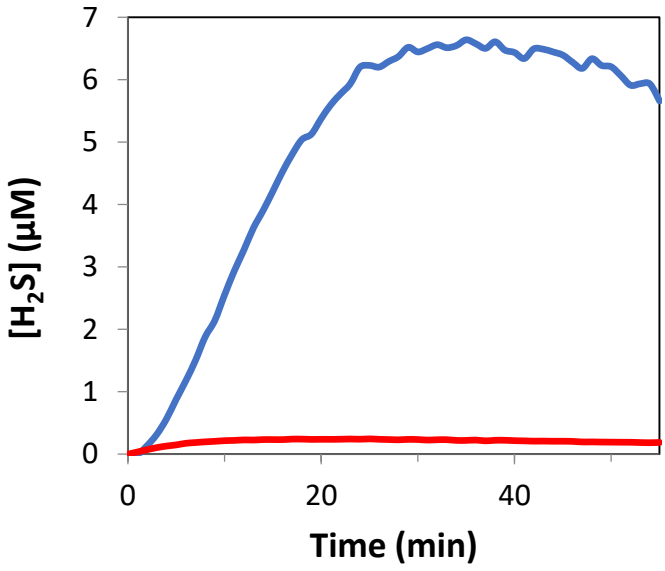

Figure B13. H_2S release from ROMP micelles (red trace) and a small molecule SATO (blue trace) triggered by 1 mM Cys. The SATO concentration was 50 µM for both experiments. The reactions were conducted in 1X PBS buffer (pH = 7.4).

Appendix C: Thiooxime Stars

The optimized chemistry used to prepare the *S*-aroylthiooxime (SATO) functionalized norbornene monomers for use in ring-opening metathesis polymerization (ROMP) discussed in appendix B was exploited to prepare bis-norbornenes that were linked via a SATO bond. We attempted to prepare star polymers via the brush-first technique using this compound. The synthesis of this bis-norbornene crosslinker is described below.

Synthesis of crosslinker

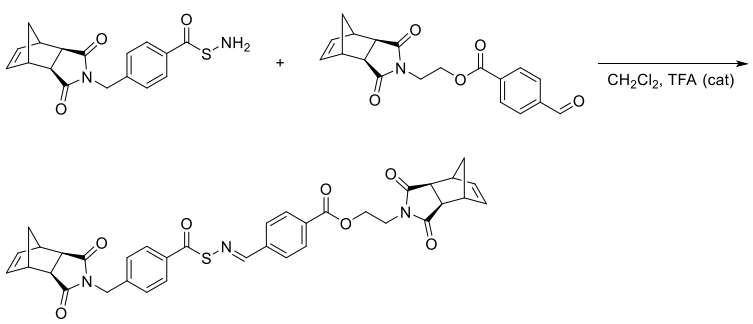

NB-THA (0.14 g, 0.43 mmol) and NB-Aldehyde (0.15 g, 0.43 mmol) were dissolved in 4 mL of CH_2Cl_2 in a vial. To the vial was added 20 uL of TFA followed by molecular sieves. This mixture was allowed to react for 4 h. The reaction mixture was then filtered and rotovapped. The crude product was further purified via recrystallization from hexanes. The pure product was obtained as a white solid (0.19 g, 67% yield).

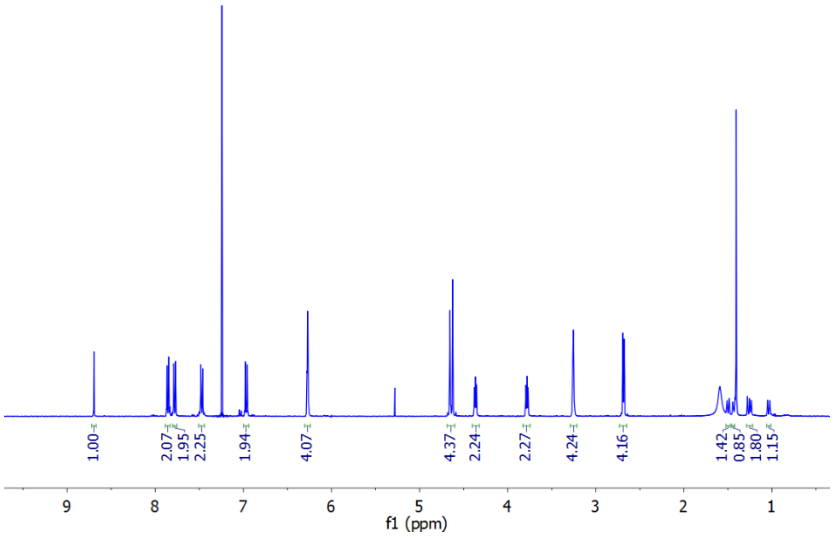

Figure C1. ^{1}H NMR spectrum of crosslinker.

To prepare star polymers by the brush-first method, macromonomers had to be prepared. We chose to use PEGylated norbornene macromonomers. These were synthesized according to the procedure for monomer **3** listed above in Appendix B. Next, star polymer synthesis was carried out by adding a solution of G3 to a solution of monomer **3**, allowing the polymerization to continue until all macromonomer had been consumed, and then adding a solution **crosslinker** to induce star formation. A representative procedure for this method is as follows:

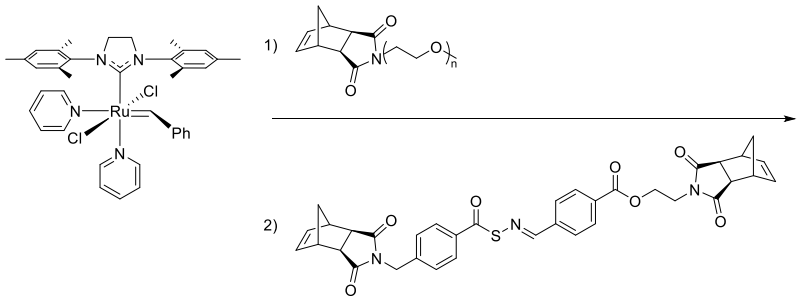

*Monomer **3** (20 mg, 0.03 mmol) was dissolved in 1 mL of CH_2Cl_2 in a vial. To the vial was added 0.5 mL of a solution of G3 (0.73 mg, 1 μmol) with rapid stirring. The reaction mixture was stirred for 20 min. A sample was removed for analysis by SEC. 0.5 mL of a solution of **crosslinker** was*

then added (3.3 mg, 5 μmol) and the polymerization was continued for 40 min before terminating with ethyl vinyl ether.

We conducted a variety of star polymerizations, varying the equivalents of PEG macromonomer and crosslinker. The star polymer synthesis reactions were followed by size-exclusion chromatography (SEC) by taking aliquots of the reaction mixtures over time and adding a few drops of ethyl vinyl ether to quench the reaction. Preliminary data suggested that star polymer synthesis proceeded smoothly, and that increasing the number of equivalents of **crosslinker** increased the size of the resulting star polymers (Table C1). However, polymerizations were conducted in THF, and attempts to remove the THF and redissolve the polymers in H_2O were unsuccessful. Dialysis methods in which H_2O was first added to the polymerization mixtures before transferring to dialysis tubing were similarly ineffective due to the apparent insolubility of the star polymers in H_2O.

Table C1. Star polymer synthesis using SATO crosslinker.

Eqiv X-linker to G3	M_n (kDa)[a]	Đ[a]	Apparent # of Arms[b]
0	19	1.01	---
5	38.4	1.05	2
5	72.6	1.04	4
10	174	1.04	9
20	417	1.08	22

[a]Absolute MW determined by light scattering. [b]Calculated by dividing the MW of the star by the MW of the brush "arm". The [MM]/[G3] ratio used was 30 : 1. Polymerizations were conducted in THF.

Appendix D: Random CTAs

We synthesized a variety of chain transfer agents (CTAs) for use in reversible addition-fragmentation chain transfer (RAFT) polymerization that had unique features such as "switchable" activity or reactivity towards dienes in Diels-Alder reactions. The synthesis and properties of a few of these are described below.

D.1. Preparation of norbornene-containing "switchable" CTA.

The "switchable" Foszinski CTA was meant to mediate the polymerization of both less-activated and more-activated monomers depending on the protonation state of the pyridal nitrogen atom. The CTA also contains a norbornene moiety that can be polymerized using ring-opening metathesis (ROMP) polymerization. Our idea was to utilize this CTA to prepare bottlebrush polymers using the RAFT transfer-to strategy described above. In this fashion, we could prepare bottlebrush polymers with unique sidechain chemistries that were previously inaccessible using alternative methods. The synthesis of the Foszinski CTA was readily achieved according to Scheme D1.

Scheme D1. Synthesis of norbornene-containing "switchable" CTA.

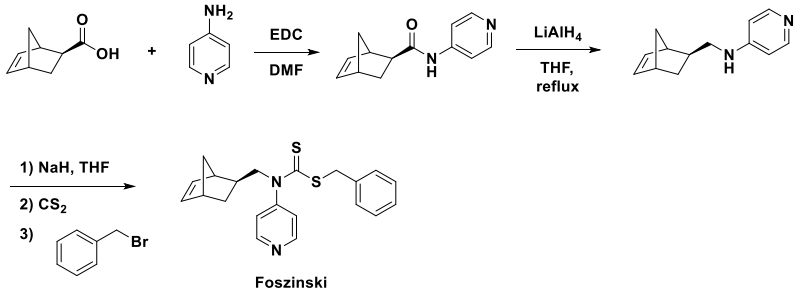

Synthesis of BNI-Py.

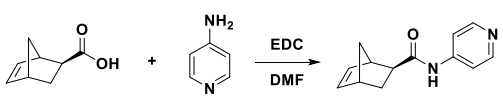

A round bottom flask was charged with BNI, amino pyridine, EDC, and DMF. The reaction mixture was stirred at rt overnight. The following day, the reaction mixture was diluted with H_2O and extracted with EtOAc (2x). The combined EtOAc layers were washed with H_2O (3x) and brine, dried over Na_2SO_4, and rotovapped. The pure product was isolated as a white solid (3.2 g, 41% yield).

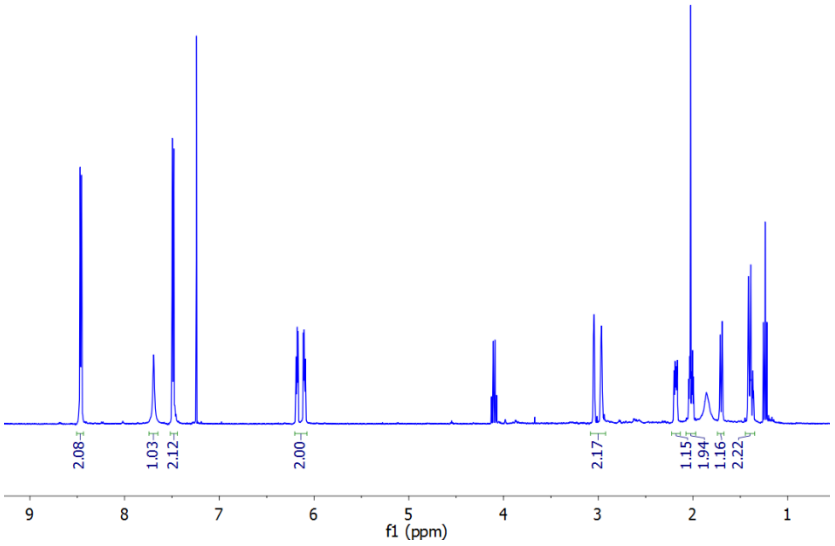

Figure D1. ^{1}H NMR spectrum of BNI-Py. The spectrum also contains EtOAc.

Synthesis of GNI-Py.

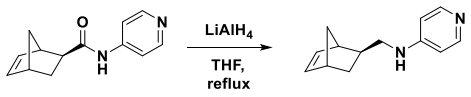

A 2-necked round bottom flask was charged with LAH. The flask was evacuated and back-filled with N_2. To the flask was added dry THF at 0 °C under N_2 flow. A solution of BNI-Py in dry THF was then added. The reaction mixture was allowed to warm to room temperature, and was then heated to reflux overnight. After cooling to 0 °C in an ice bath, excess LAH was quenched via sequential addition of H_2O, 10% NaOH solution, and H_2O. The reaction mixture was then filtered

through celite and rotovapped. The product was obtained as a colorless oil (0.98 g, 93% yield) and was used in the next step without further purification.

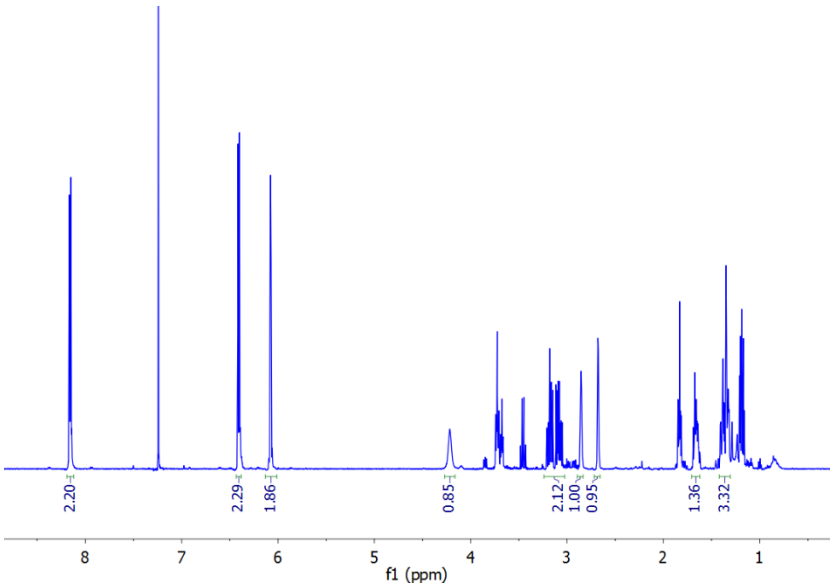

Figure D2. ^{1}H NMR spectrum of GNI-Py. The spectrum also contains THF and other impurities.

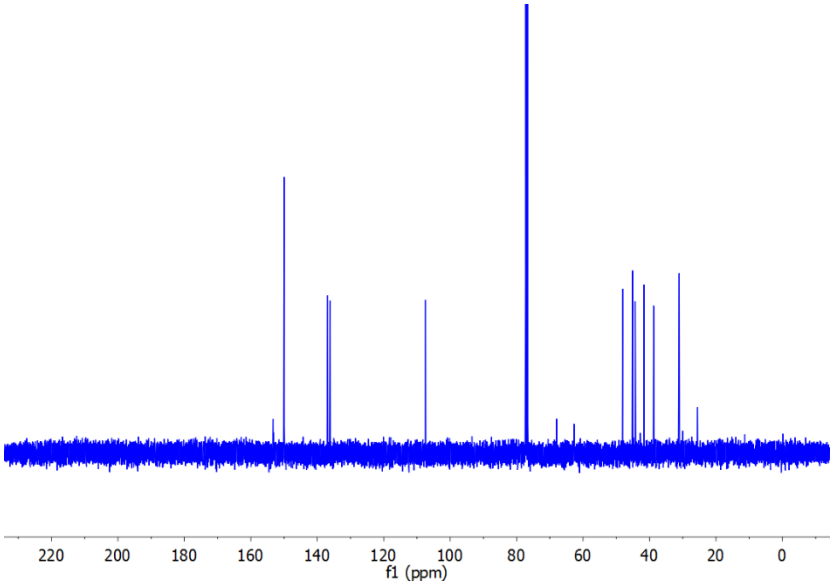

Figure D3. ^{13}C NMR spectrum of GNI-Py. The spectrum also contains THF and other impurities.

Synthesis of "Foszinski"

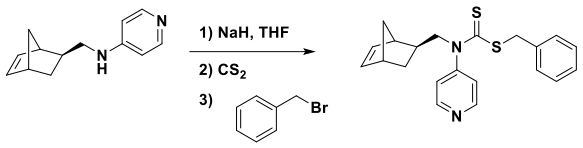

A 2-necked RBF was charged with NaH. The flask was evacuated and back-filled with N_2. To the flask was added dry THF at 0 °C under N_2 flow. A solution of GNI-Py in dry THF was then added. After 5 min, CS_2 was added dropwise. The reaction mixture was stirred for 20 min. Benzyl bromide was then added dropwise, and the reaction mixture was stirred for 1 h at 0 °C and then 4 h at rt. Excess NaH was quenched by adding a few drops of isopropanol. The reaction mixture was rotovapped, and the crude product was purified via trituration from hot $CHCl_3$. The pure product was obtained as a light brown solid (5.4 g, 80% yield).

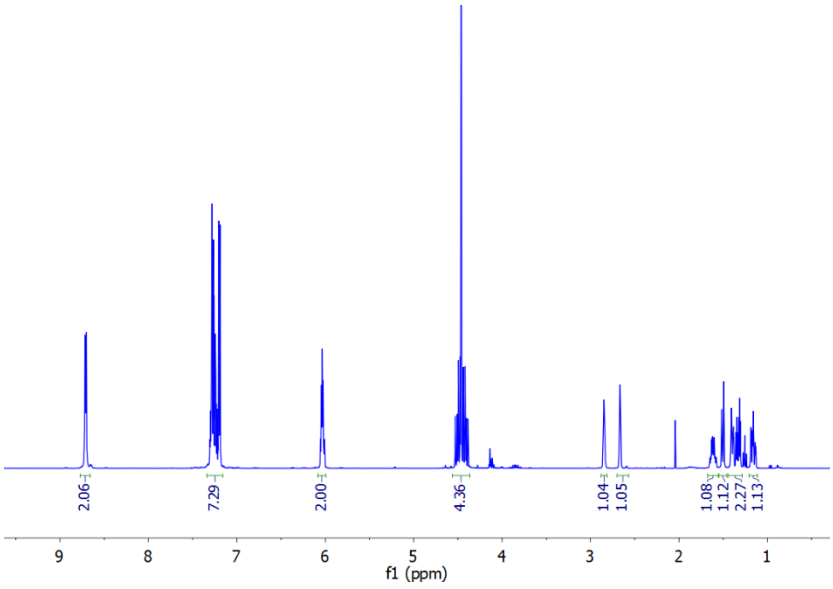

Figure D4. ^{1}H NMR spectrum of Foszinski.

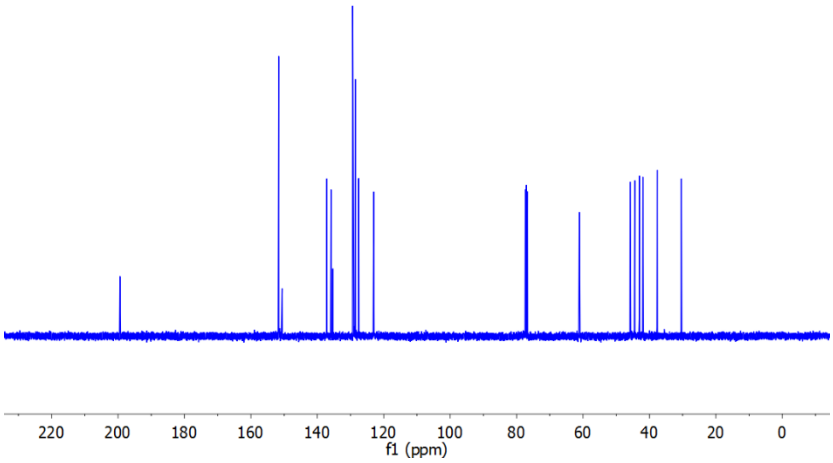

Figure D5. ^{13}C NMR spectrum of Foszinski.

We were able to polymerize Foszinski by ROMP in DMF. This polymerization required long reaction times and rigorous exclusion of both O_2 and H_2O to reach high conversions. RAFT polymerization using Foszinski was attempted, and the type of acid was varied (TsOH being the most promising), along with the solvent and the reaction temperature. It was determined that Foszinski was incapable of mediating polymerization of any monomer other than styrene, despite the reaction conditions utilized. However, the reason for this was not thoroughly explored.

D.2. Diels-Alder active CTAs

There are several reports of RAFT CTAs that are capable of acting as dieneophiles in Diels-Alder (DA) reactions. We were interested in exploiting this chemistry to prepare macromonomers, as the resulting DA adducts are often norbornenes. We envisioned a strategy is which the CTA would first be employed to mediate RAFT polymerization of a given monomer. Then, the CTA group on the chain end could be modified via reaction with cyclopentadiene to produce a macromonomer. ROMP would be used in the final step to produce a bottlebrush polymer via the grafting-through strategy. Scheme D2 shows a generalized scheme for this idea.

Scheme D2. Preparation of bottlebrush polymers via DA chain end modification of poylmers prepared by RAFT polymerization.

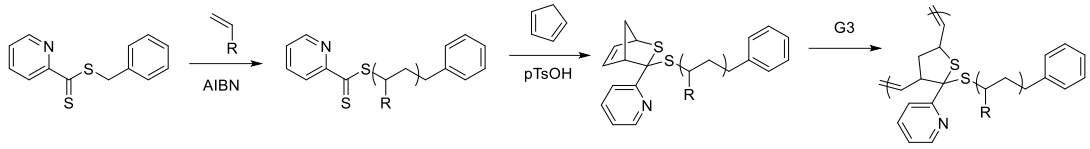

The CTA employed in this study was prepared in 2 steps according to Scheme D3.

Scheme D3. Synthesis of DA active CTA.

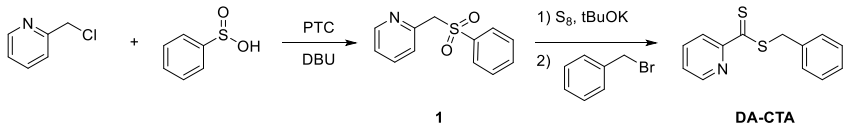

Synthesis of compound 1

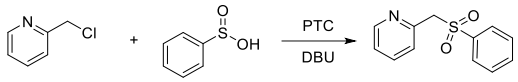

A round bottom flask was charged with 2-(chloromethyl)pyridine hydrochloride (5.0 g, 31 mmol), sodium benzenesulfinate (7.5 g, 46 mmol), tetrapropylammonium bromide (0.81 g, 3.1 mmol), DBU (4.6 ml, 31 mmol), and 50 mL of acetonitrile. The reaction mixture was heated at reflux overnight. The following day, the reaction mixture was diluted with CH_2Cl_2, washed with H_2O (2x) and brine, dried over Na_2SO_4, and rotovapped to give the pure product as a light brown powder (5.8 g, 82% yield).

Synthesis of DA-CTA

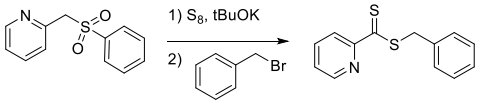

*A round bottom flask was charged with compound **1** (5.8 g, 25 mmol), elemental sulfur (2.4 g, 75 mmol), and 100 mL of THF. Potassium 2-methylpropan-2-olate (8.4 g, 75 mmol) was then added in one portion. The reaction mixture was stirred at rt overnight. The following day,*

(bromomethyl)benzene (8.9 ml, 75 mmol) was added dropwise. The reaction mixture was stirred for an additional 1 h. The reaction mixture was then rotovapped and the residue was redissolved in CH_2Cl_2, washed with H_2O and brine, and dry loaded onto a silica column, eluting with 5% EtOAc in hexanes. The pure product was obtained as light pink solid (1.2 g, 19% yield).

DA-CTA was capable of mediating the polymerization of styrene, yielding polymers will controllable molecular weights and low dispersities. Under acidic conditions, this CTA becomes activated and is capable of participating in DA reactions with dienes. It was treated with TsOH and cyclopentadiene according to the following procedure:

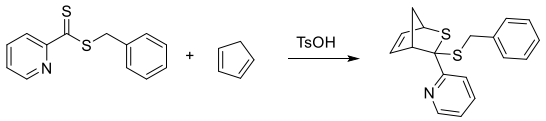

*A vial was charged with **DA-CTA** (50 mg, 0.20 mmol), TsOH (35 mg, 0.21 mmol), cyclopentadiene (0.026 ml, 0.31 mmol), and 2 mL of CH_2Cl_2. The pink color disappeared quickly with vigerous shaking. 15 mL of hexanes was added, and an oil collected on the sides of the vial. The solution was decanted, and the DA adduct was dried under vacuum. The pure product was obtained in quantitative yield.*

Unfortunately, ROMP of either the small molecule DA adduct or the chain-end modified polystyrene macromonomer were unsuccessful, despite multiple efforts. It was suspected that the steric bulk of the DA adducts coupled with the lack of control over the stereohemisry of the DA adduct (endo configurations polymerize slowly during ROMP) led to slow propagation. It may be worth re-investigating these reactions under more forcing ROMP conditions.

Appendix E: Self-Immolative Polymers that Release COS

Coincident with the work of Mike Pluth at the University of Oregon, we focused on the development of COS-releasing small molecules and polymers. COS is a gaseous molecule that is readily metabolized to H_2S and CO_2 by the ubiquitous carbonic anhydrase (CA) enzyme. The biological relevance of H_2S, as well as its therapeutic potential, were discussed in the preceding chapters. COS might also have its own biological activity; however, to date there have been no reports regarding the direct involvement of COS in biological systems.

Scheme E1. Self-immloative COS-releasing small molecules.

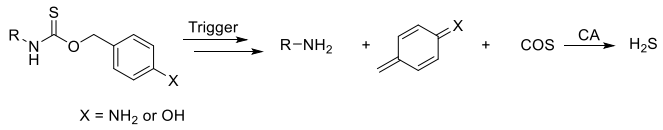

One way that COS is released from small molecules is via the self-immolation of benzyl thiocarbamates. This reaction was first reported by Pluth and coworkers, and could be triggered by a variety of stimuli based on the chemistry of the aniline protecting group (Scheme E1). We envisioned that this chemistry could be extended to prepare self-immolative polymers that could be triggered to decompose and release COS as a byproduct. Our design includes a azide-functionalized end-capper that could be reduced to initiate the depolymerization cascade reaction. This functional group can be reduced by H_2S in addition to other reducing agents such as phosphines. In the presence of CA, COS released during depolymerization would be converted to H_2S, thereby initiating depolymerization of other polymer chains. In this sense, the depolymerizastion reaction acts auto-catalytically and can therefore be triggered by sub stoichiometric quantities of H_2S.

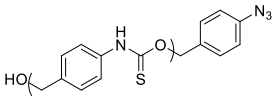

Figure E1. Proposed structure of self-immolative polymer for COS release.

We sought to prepare a reduction-triggered self-immolative thiocarbamate polymer with the structure shown in Figure E1. Upon treatment with a reducing agent such as H_2S, this polymer would depolymerize according to the mechanism shown in Scheme E2 to afford COS and other small molecule byproducts.

Scheme E2. Depolymerization mechanism.

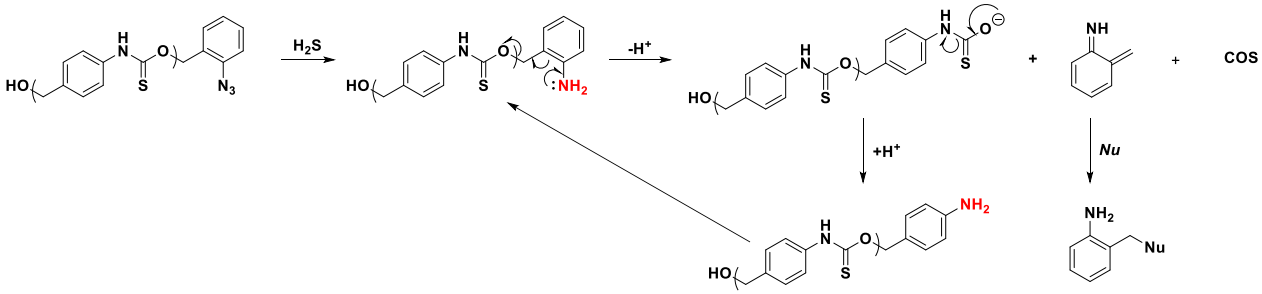

This self-immolative thiocarbamate polymer can be easily prepared in one step from one of the two monomers shown in Figure E2. Polymerization of both monomers proceeds via a step growth mechanism and is catalyzed by strong bases (i.e., DBU, tBuOK, NaH) or Lewis acid compounds such dibutyltin dilaurate (DBTDL).

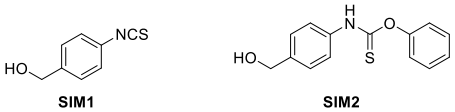

Figure E2. Monomers for preparation of self-immolative thiocarbamate polymers.

E.1. Synthesis of monomers

Monomers **SM1** and **SIM2** can be prepared according to Schemes E3 and E4, respectively.

Scheme E3. Synthesis of monomer SIM1.

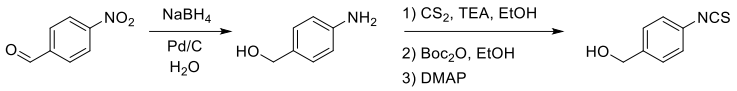

Scheme E4. Synthesis of monomer SIM2.

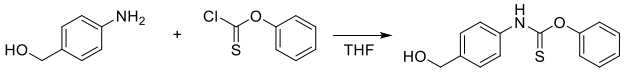

Monomer **SIM1** was prepared in two steps. Synthetic procedures are given below.

Syntheis of 4-aminobenzyl alcohol.

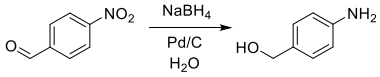

$NaBH_4$ (180 mg, 4.8 mmol) was dissolved in 6 mL of H_2O in a 2-necked round bottom flask under N_2 flow. To the flask was added 4-nitrobenzaldehyde (200 mg, 1.32 mmol) in one portion. Pd/C (0.5 wt%) was then added slowly to the flask (CAUTION: vigerous H_2 gas evolution and sparking). The reaction mixture was stirred at rt until all of the solids dissolved (~ 4 h). The reaction mixture was then filtered through celite. The aqueous solution was extracted with EtOAc (2x), and the combined organic layers were dried over Na_2SO_4 and rotovapped. The pure product was obtained as an off-white solid (140 mg, 86% yield).

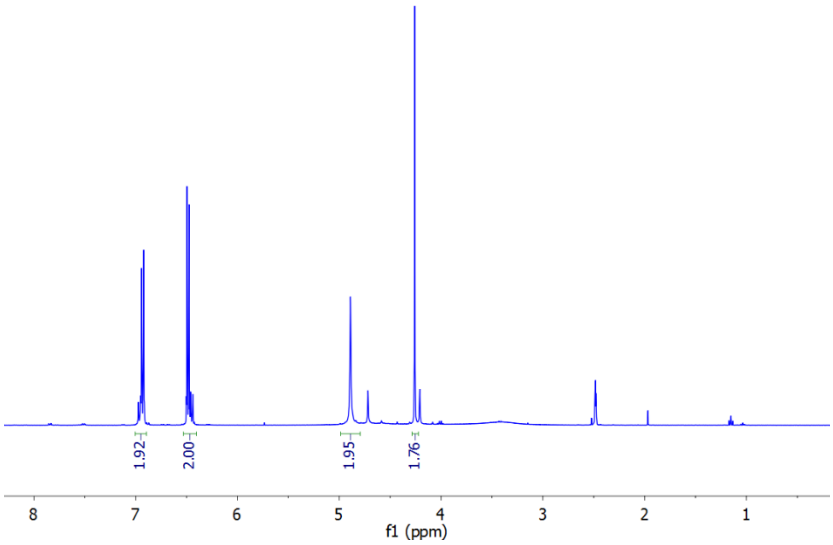

Figure E3. ^{1}H NMR spectrum of amino benzyl alcohol.

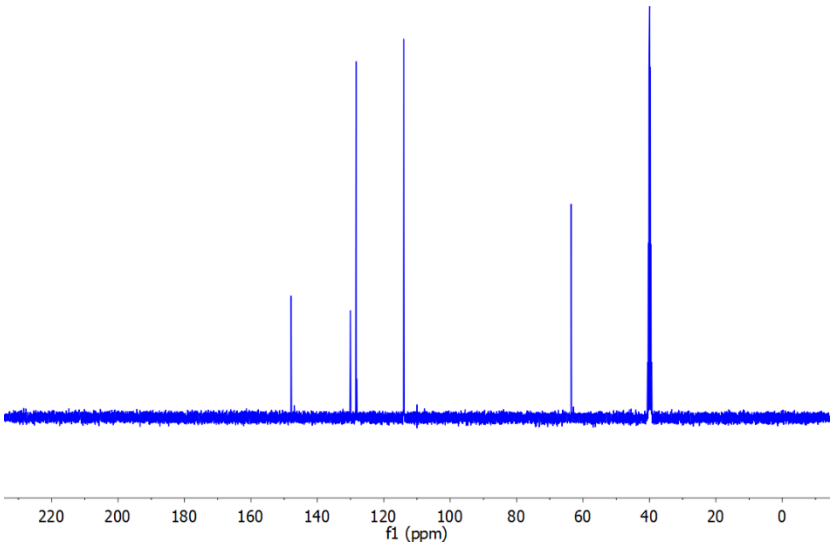

Figure E4. ^{1}H NMR spectrum of amino benzyl alcohol.

Synthesis of SIM1.

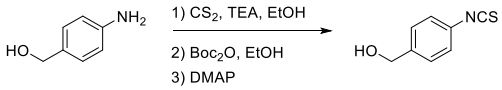

4-Aminobenzyl alcohol(2.0 g, 16 mmol) was dissolved in 40 mL of EtOH in a round bottom flask. To the flask was added CS_2 (10 mL, 170 mmol) followed by TEA (2.3 mL, 17 mmol). The reaction mixture was stirred at rt for 30 min. The flask was placed in an ice bath. A solution of Boc_2O (3.2g,

15 mmol) in 10 mL of EtOH was added at 0 °C. A few crystals of DMAP were added, and the reaction was allowed to warm to rt and was stirred for an additional 30 min. The reaction mixture was diluted with CH_2Cl_2, washed with H_2O and brine, dried over Na_2SO_4, and rotovapped. The crude product was dry-loaded onto a silica column, eluting with CH_2Cl_2. The pure product was obtained as a white solid (1.5 g, 56% yield).

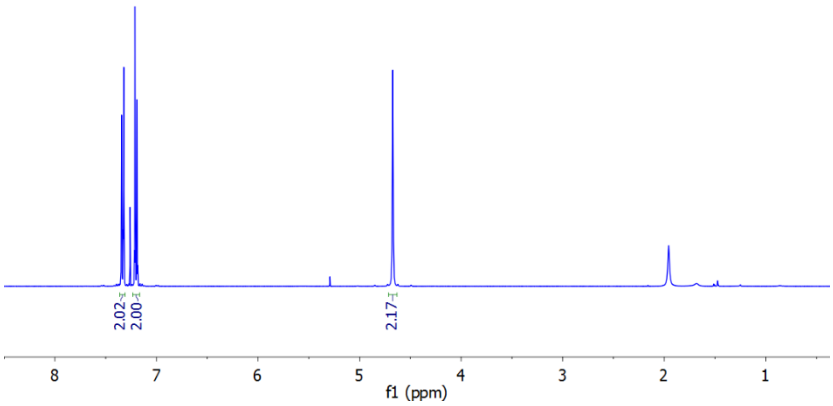

Figure E5. ^{1}H NMR spectrum of SIM1.

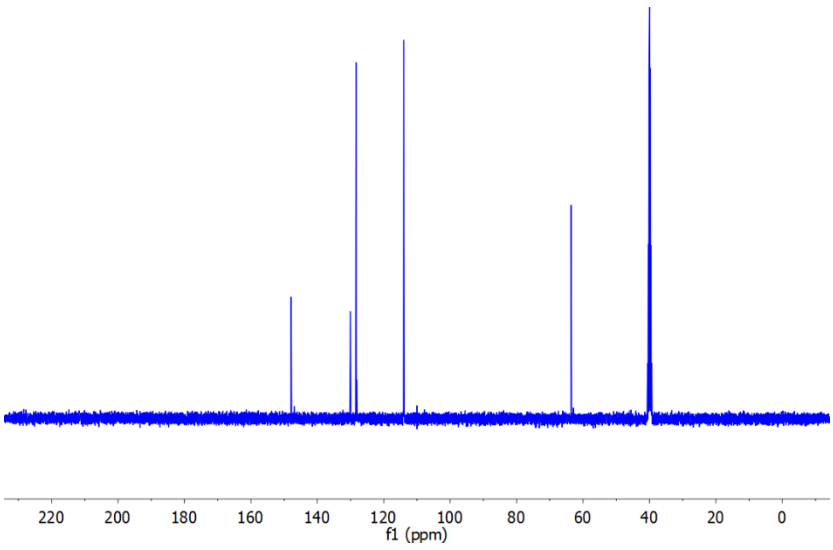

Figure E6. ^{13}C NMR spectrum of SIM1.

Monomer **SIM2** was synthesized in 1 step starting from *4*-aminobenzyl alcohol.

Synthesis of SIM2

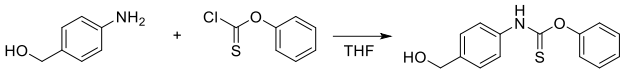

4-Aminobenzyl alcohol (1.8 h, 14 mmol) was dissolved in 40 mL of dry THF in a round bottom flask. To the flask was added phenylthiochloroformate (1.0 mL, 7.2 mmol) dropwise. The reaction mixture was stirred at rt for 30 min. The reaction mixture was filtered to remove the precipitating solids and then rotovapped. The crude product was purified via recrystallization from benzene. The pure product was obtained as a white solid (1.4 g, 75% yield).

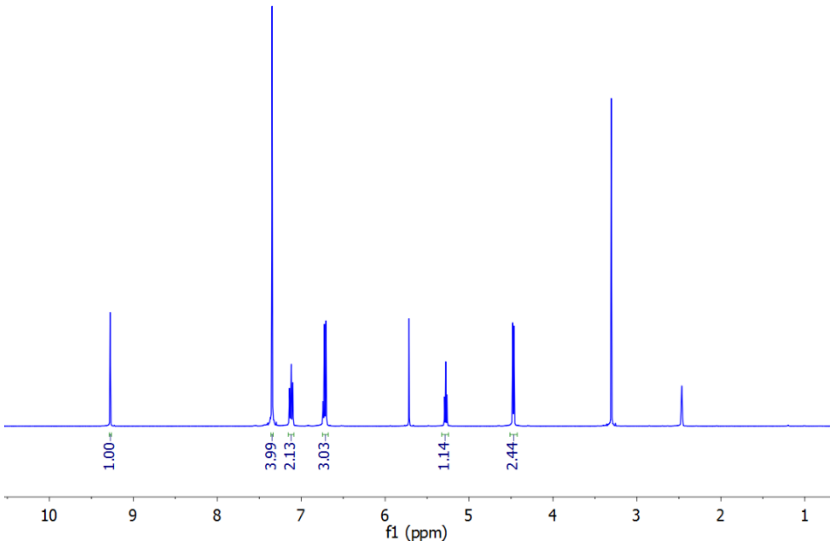

Figure E7. ^{1}H NMR spectrum of SIM2.

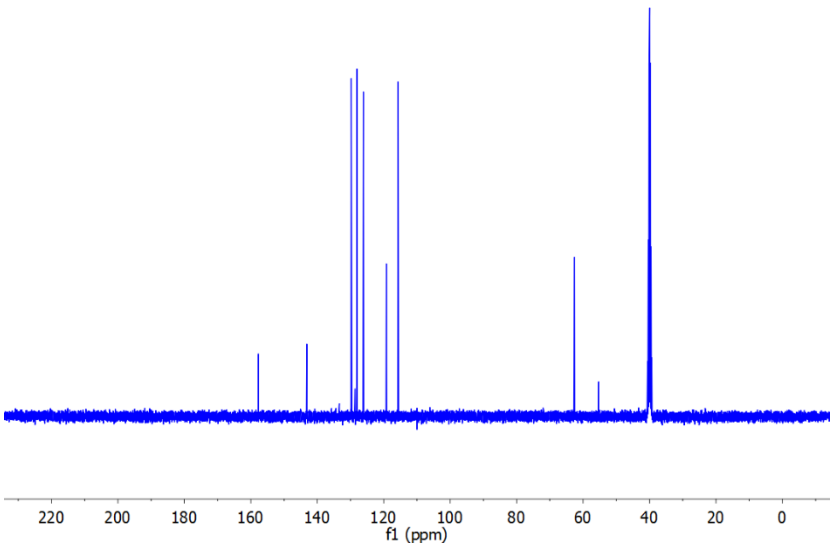

Figure E8. ^{13}C NMR spectrum of SIM2.

E.2. Polymerization of SIM1 and SIM2 to give self-immolative polymers

With monomers **SIM1** and **SIM2** in hand, polymerizaitons were conducted under a variety of conditions. First, **SIM1** was polymerized in the presence of a base or DBTDL, the latter of which required heating. Figure E9 shows compares the spectra of the crude polymerization mixtures in the presence of various bases.

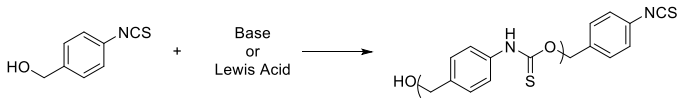

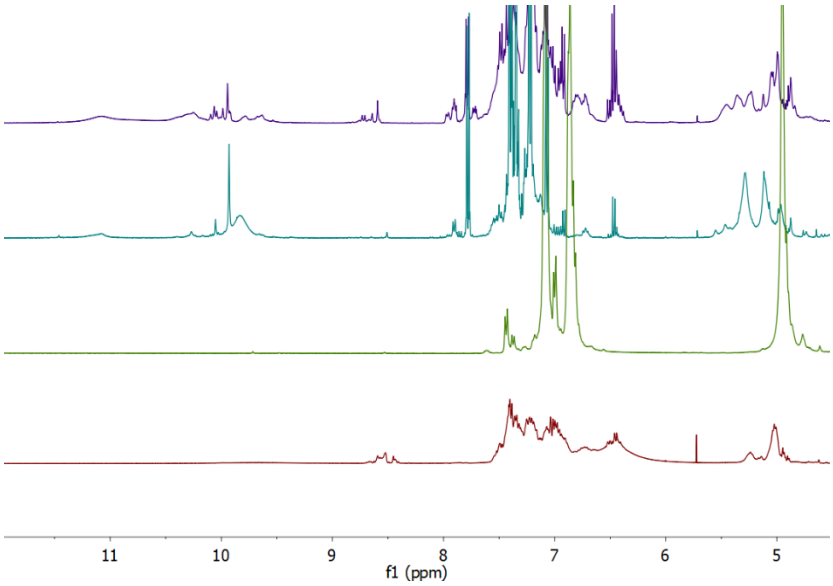

Figure E9. Polymerizaiton of SIM1 under various conditions. Shown above are polymerizations conducted in the presence of 1 eqivalent of NaH (purple trace), tBuOK (teal trace), $CsCO_3$ (green trace), and DBU (red trace).

It is clear from Figure E9 that using DBU as the base resulted in the cleanest polymerization reaction. However, end group analysis of the the polymer showed a relatively low degree of polymerization (DP ~ 7). Therefore, we invesitated the use of DBTDL to catalyze addition to the isothiocyanate in **SIM1** instead of using a base additive. Using this method, polymers with DPs of up to 15 were acquired. Polymerizaion of **SIM2** catalyzed by DBTDL was also conducted. ^{1}H NMR spectra of the crude polymerization mixtures were almost identical (Figure E10). Therefore, **SIM1** was used in to prepare polyemrs in future studies. A representative polymerization procedure of **SIM1** using DBTDL is as follows:

Polymerization of SIM1

*A 2-necked round bottom flask equipped with a stir bar was flame dried under vacuum and back-filled with N_2. To the flask was added **SIM1** (200 mg) under N_2 flow followd by 0.4 mL of dry DMF. The flask was placed in an oil bath set to 60 °C. DBTDL (5 mol%) was then added to the*

flask to initiate polymerization. After 4 h, a solution of end-capper (1 equiv) in 0.4 mL of dry DMF was added, and the reaction mixture was stirred at 60 °C overnight. The polymer was isolated via precipitation from MeOH.

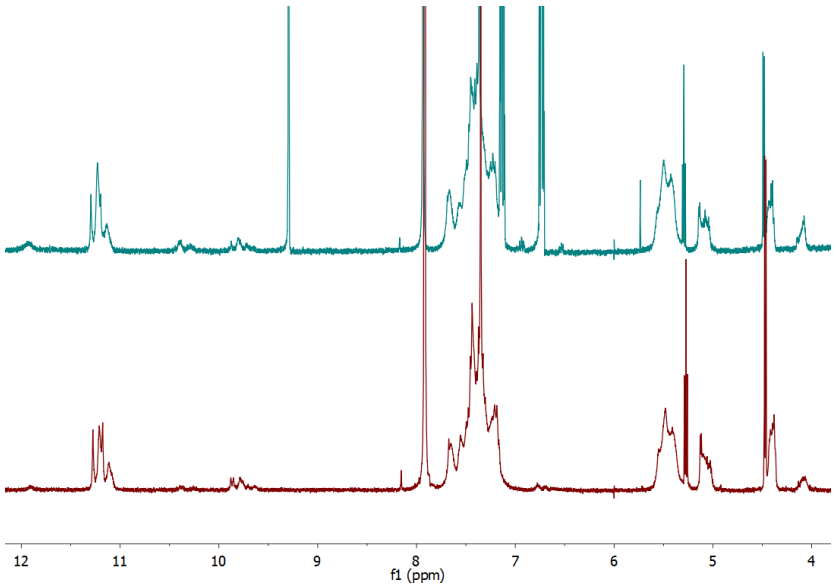

Figure E10. Comparison of ^{1}H NMR spectra of polymers prepared from SIM1 (bottom), and SIM2 (top). The top spectrum containes phenol, a byproduct of the polymerization of SIM2.

Azide incorprotation was confirmed by FTIR spectroscopy, and polymer molecular weights were determined via end group analysis.

E.3. Depolymerization reactions and kinetics

Depolymerization reactions were first attempted by treating the polymers with reducing agents such as Na_2S and TCEP. However, despite multiple attepts, no depolymerization was observed. We then investigated the use of acid (AcOH) and base additives (TEA and *4*-methylpipiridine) as well as DMAP—a catalyst utilized in many reactions involing an amine or alcohol. Of these additives, TEA was found to be most efficatious in faciliting depolymerization. A kinetic experiment was then conducted using TCEP as the reducing agent and TEA as the base in DMSO-d_6. The disappearance of polymer was quantified using ^{1}H NMR spectroscopy by integrating the

polymer peaks relative to those from the breakdown products. A representative procedure for the depolymerization reaction is as follows:

Depolymerization of self-immolative polymer

A vial was charged with polymer (2 mg), TEA (1 equiv), and 1 mL of DMSO-d_6. TCEP (1 equiv) was added in one portion to start the reaction. ^{1}H NMR spectra were then collected at various time points.

The results of this depolymerization experiment are shown in Figures E11 and E12.

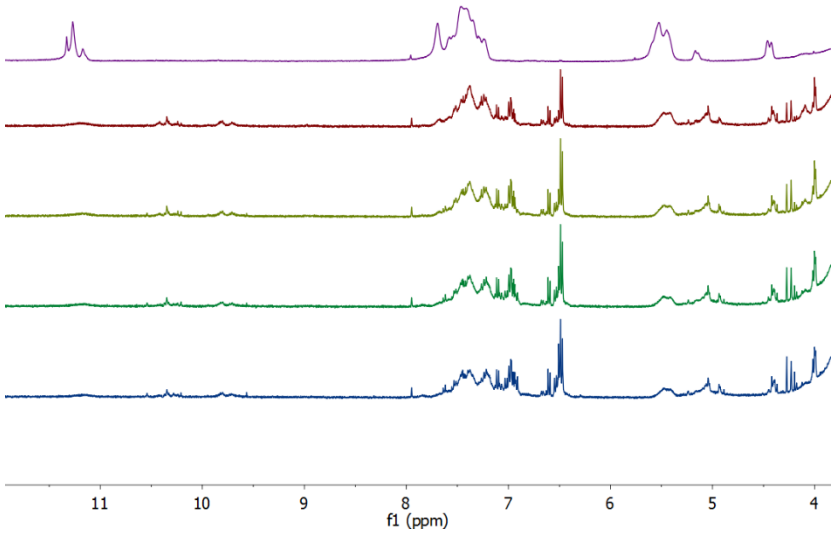

Figure E11. Depolymerization of self-immolative polymer over time. Shown are the 0 h (purple trace), 24 h (red trace), 48 h (green trace), 72 h (green trace), and 96 h (blue trace) time points. Peaks at ~6.5 ppm correspond to aniline-containing breakdown products.

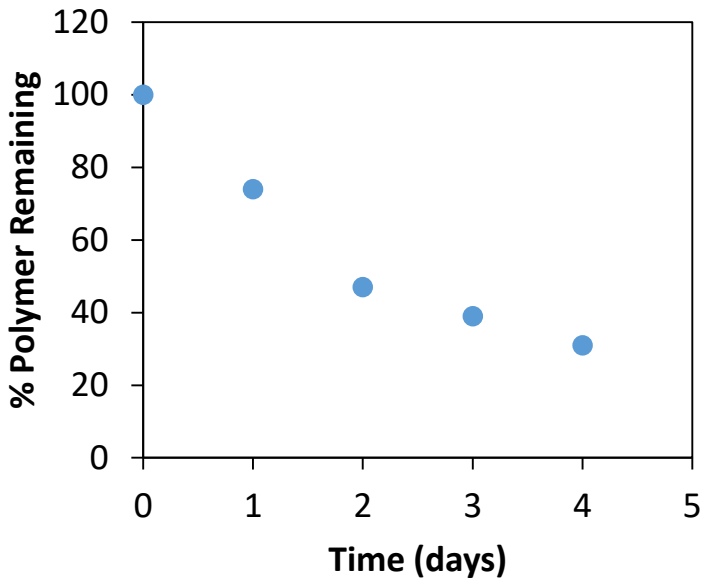

Figure E12. Kinetics of depolymerization.

Depolymerization was initially considered to be too slow to be useful. Various other self-immolative systems were invesitated but ultimately "Hawkered", either due to the complexity of monomer synthesis, or the inability to polymerize the monomers once they had been synthesized. Upon further reflection, the chemistry contained in this appendix can be exploited under optimized conditions. Future studies will focus on detection of COS/H_2S release from the immolative polymers. In addition, experiments will be conducted to prove the autocatalytic nature of the depolymerization reaction by triggering breakdown with sub-stoichiometric quantities of reducing agent in the precence of CA.